Less is more: the efficacy of gene therapy to treat Fabry disease

Jonathan Richard Albert Lambert

Great Ormond Street Institute of Child Health

University College London

A thesis submitted for the degree of Doctor of Philosophy

January 2018

Declaration

I, Jonathan Richard Albert Lambert, confirm that the work presented in this thesis is my own. Where information has been derived from other sources, I confirm that this has been indicated in the thesis.

Signed ……..

Date ……..

Abstract

Fabry disease (FD) is caused by mutation in *GLA* that encodes lysosomal α-galactosidase-A (α-gal-A). Loss of α-gal-A leads to glycosphingolipid storage in cells. Symptoms are life-threatening and current treatment is often enzyme replacement with variable therapeutic benefit. Alternative therapies are required. The world's first clinical gene therapy trial was recently approved using lentivirus to integrate *GLA* into target cells for long-term enzyme expression. This thesis examined the efficacy of a previously engineered lenti-vector which may inform design of future trials.

Endogenous α-galA activity was characterised in human and murine tissues. The Jurkat lymphoblastic leukaemia cell-line exhibited low α-gal-A activity. Transduction of Jurkats resulted in dose-dependent increase of α-galA expression, without apparent toxicity. The enzyme produced by cells with 0.4 transgene copies per cell (vg/cell) had comparable kinetic properties to wild type. Increasing exposure to 1.8vg/cell resulted in an apparent increase in Michaelis Constant when compared to wild type. Therefore less virus dosage may be more therapeutically efficient.

Increasing intracellular α-galA activity was accompanied by increased enzyme secretion and uptake of the extracellular enzyme into wild-type Jurkats, indicating cross-correction between cells. Previous research found deficits in mitochondrial function in FD. Here, inhibition of respiratory chain complex I appeared not to effect either lentivirus transduction efficiency or uptake of extracellular α-galA, but inhibited enzyme secretion. So FD may impede cross-correction. Extending the work into patient fibroblasts, this thesis found suggestion of reduced growth rate and impaired transduction efficiency. If correct these results may indicate the metabolic deficiencies in FD extend beyond complex I deficiency.

In conclusion, lentivirus-mediated gene delivery is a promising therapeutic option for FD. However, excessive enzyme generation could result in a protein that has inferior kinetic properties, so dosage requires optimisation. Therapeutic strategies to support mitochondrial function may promote efficacy of treatment.

Table of contents

List of figures

List of tables

Acknowledgements

I would first of all like to give heartfelt thanks to my main supervisor Professor Simon Heales from whom I have learnt so much. His clarity of thought and enquiring mind have greatly inspired me in doing the research for this thesis. Simon was a marvelous support through the Three Minute Thesis competition 2016; without his support I would not have got so far. Thank you for believing in me and being proud of me Simon. Your positivity, enthusiasm, kindness and patience kept me going, especially throughout the last year when I was writing-up. You deserve a medal for regularly spurring me on and shoring me up when I was close to pieces. I am deeply thankful to you for being a wonderful supervisor.

I also want to thank Dr Derek Burke who was until recently a fellow student and now, as always, is a good friend. It was invaluable to have his wise support, the benefit of his experience and the comfort of sharing the ups and downs of the PhD journey with someone in a similar life-situation to myself. It was a much-needed stress-reliever to talk about plans and aspirations beyond PhD during evenings in the lab. Derek's general knowledge, and zeal for travel and learning meant there was never a dull conversation. I deeply value those times that were a refreshment and encouragement. Together with Aziza Khabbush, Carmen De La Fuente Barrigon, Dr Mesfer Al Shahrani and Dr Michael Orford, we enjoyed social events and support as part of the great Healesy Family. Thank you to all of you. Mesfer was particular help with mitochondrial assays.

Everyone in the Enzymes Section of Camelia Botnor Labs, Great Ormond Street Hospital, where I have done much of the practical work for this thesis, has been an invaluable support too. Listening to the lab banter was more entertaining and interesting than the best of radio stations. I especially want to thank Matt for looking out for me, giving down-to-earth practical perspective that helped calm me down when anxious and encouraged me when down; Sabia for her quiet kindness; Emmy for her friendliness, advice and support; and Umma for teaching me fibroblast culture and, together with Biljana, for attempting to grow patient fibroblasts from archives.

Also I want to thank Dr Ralph Wigley for his interest in my project and for sharing his knowledge.

All my cell culture and preparation of lentivirus was carried out in Molecular Cellular Immunology (MCI) Section of the UCL Great Ormond Street Institute of Child Health where I was officially based throughout my training. I owe a debt of gratitude to Dr Steve Howe who was initially my primary supervisor and was a great help to me finding my feet and getting settled into the project. His kindness, support and willingness to help and advise were vital in those early days. Big thanks also go to Dr. John Estridge, Sue Ballard and Patricia Cheng whose sterling work keep MCI running. Their warm smiles every day made me feel welcome and cared for, and I can't imagine MCI without them. Thank you for being so consistently kind, friendly and supportive. I am also deeply thankful for the good friends made in MCI. Especially I wish to thank Dr. Giuseppa Piras, Agnes Chan, Andrea Schejtman, Marta Zinicola, Dr Sameer Syad and Annie Etuk whose support, care and friendship have made the last four years special with great memories. You are all super stars.

My sincere thanks goes to Dr Ahad Rahim who was my secondary supervisor during the latter half of my project. Thank you also to Professor Bryan Winchester and Dr Iain Hargreaves who were valuable sources of advice and guidance during the project, and Dr Simon Waddington who kindly provided the murine tissues used in Chapter 3. I gratefully acknowledge Srinath Rajaraman and Dr Conrad Vink who provided the pRRLSIN.cPPT.hPGKGLA.WPRE and pRRLSIN.cPPT.hPGKGFP.WPRE lentivirus vector plasmids used in Chapters 4, 5 and 6. The project was funded jointly by University College London (UCL) and Sanofi Genzyme Ltd. through the UCL Impact Scheme and was supported by the National Institute of Health Research (NIHR) Great Ormond Street Hospital Biomedical Research Centre. The views expressed are those of the author and not necessarily those of the NHS, the NIHR or the Department of Health.

Finally my deepest gratitude goes to my Mum. She is my constant support, encouragement and best friend. Thank you Mum. This thesis is for you.

List of abbreviations

3MT	Three Minute Thesis competition
4MU	4-methylumbelliferone
4MUG	4-methylumbelliferyl-α-D-galactopyranoside
AAV	adeno-associated virus
ADP	adenosine di-phosphate
A-gal A / α-gal A	α-galactosidase A
A-gal B / α-gal B	α-galactosidase B
α-GalNAc	α- linked terminal N-acetylated saccharides
α-GlcNAc	α-N-acetylglucosamine
AMP	adenosine mono-phosphate
ANOVA	analysis of variance
APC	antigen presenting cell
ATP	adenosine tri-phosphate
BCA	bicinchoninic acid
BH4	tetrahydobiopterin
BSA	bovine serum albumin
Cav1	caveolin-1
CMV	cytomegalovirus promoter region
CR	creatine phosphate

DGJ	1-deoxy-galactonojirimycin
DPBS	Dulbecco's phosphate buffer solution
DTNB	5,5' dithiobis (2-nitrobenzoic acid)
eNOS	endothelial nitric oxide synthase
ER	endoplasmic reticulum
ERAD	endoplasmic reticulum-associated degradation
ERT	enzyme replacement therapy
FD	Fabry disease
Ga2	galabiosylceramide / digalactosylceramide
Gb3	globotriaosylceramide / ceramidetrihexoside
GFP	green fluorescent protein
GFP	gene encoding green fluorescent protein
GLA	gene encoding α-gal A
GOSH	Great Ormond Street Hospital
GOSICH	Great Ormond Street Institute of Child Health
GSL	glycosphingolipid
HIF	hypoxia inducible factor
hPGK	human phosphoglycerate kinase promoter region
HRP	horseradish peroxidase
HSA	human serum albumin
HSC	haematopoietic stem cell

iPS	inducible pluripotent stem cells
LAMPs	lysosomal associated membrane proteins
LC	liquid chromatography
LC3	microtubule-associated protein 1 light chain 3
LIMPs	lysosomal integrated membrane proteins
LSD	lysosomal storage disease
LTR	long terminal repeats
LysoGb3	globotriaosylsphingosine
M6P	mannose-6-phosphate
M6PR	mannose-6-phosphate receptor
MOI	multiplicity of infection
MPS	mucopolysaccharides
MS	mass spectrometry
MS/MS	tandem mass spectrometry
mTORC1	mechanistic target of rapamycin complex 1
n	number of independent replicates measured in an experiment
NADH	nicotinamide adenine dinucleotide
NAGA	N-acetyl-D-galactosamine
NIHR	National Institute of Health Research
NO	nitric oxide
PBS	phosphate buffered saline

PEI	polyethylenimine
pfu/ml	plaque forming units per ml
PI	protease inhibitor cocktail
qPCR	quantitative polymerase chain reaction
ROS	reactive oxygen species
RPMI	cell culture media used for growing Jurkats
RSV	rous sarcoma virus promoter region
S1P	sphingosine-1-phosphate
SD	standard deviation
SRT	substrate reduction therapy
TFEB	transcription factor E box
TGN	trans-golgi network
TIL	tumour infiltrating lymphocytes
TNB	thionitrobenzoic acid
TPER	tissue protein extraction reagent
UCL	University College London
UCLH	University College London hospital
UPLC	ultra performance liquid chromatography
vg/cell	viral genomes per cell
WPRE	woodchuck hepatitis post-transcription regulatory element

Chapter 1 Introduction

1.1 The lysosome

The lysosome was first discovered by Christian de Duve in 1955. Based upon early experiments measuring acid phosphatase activity in rat liver homogenate following centrifugal fractionation, he theorised with others that the enzyme functioned within a selectively permeable membrane sac (Berthet et al., 1951). Later de Duve et al (1955) discovered these sac-like particles contained multiple acid hydrolases, each one displaying enzymatic activity on its own specific substrate. Hence he named the particles lysosomes, meaning "lytic body" (Duve et al., 1955). The biochemical concept of the lysosome was supported structurally by electron microscopy of the mitochondrial fraction of rat liver homogenate by Novikoff et al (1956) (Novikoff et al., 1956). They observed acid phosphatase activity located within lipid membrane-bound bodies which contained electron-opaque granules that were morphologically distinct from mitochondria (Essner and Novikoff, 1961). The lysosome concept is summarised in Figure 1-1.

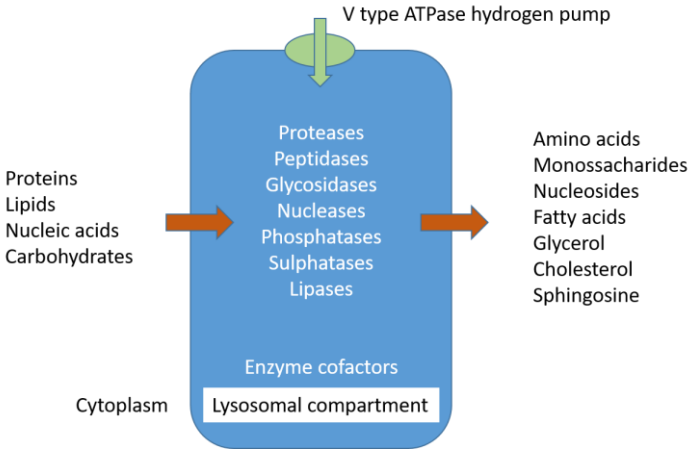

Figure 1-1: Lysosomes receive macromolecules for catalysis by a plethora of enzymes to recycle basic building-block molecules to the cytoplasm

The hydrolytic activity of lysosomal enzymes is optimum at an acidic pH, an environment that is maintained within lysosomes by the V type ATPase proton pump integrated within the lysosomal membrane (Saftig and Klumperman, 2009). Macromolecules include redundant, old or damaged cellular components for recycling. Precursor molecules may also be sent to the lysosome for activation by one of the hydrolytic enzymes (Settembre and Ballabio, 2014b). Lysosomal associated membrane proteins (LAMPs) and lysosomal integrated membrane proteins (LIMPs) are important for transport of substrates, hydrolytic enzymes and cofactors to the lysosome.

Functional studies discovered that the acid hydrolases within lysosomes digest extracellular material by the process of endocytosis via fusion with late endosomes, and intracellular material by the process of autophagy (de Duve, 1963, de Duve, 2005). The major autophagic mechanism is macroautophagy which commences with two molecular ubiquitin-like conjugation systems that initiate encasement of cytoplasm and redundant organelles in a double-membrane bound autophagosome. The outer membrane fuses with the lysosome to form an autophagolysosome containing the inner-membrane bound autophagic body that undergoes lysosomal degradation. A marker of autophagosomes in mammalian cells is microtubule-associated protein 1 light chain 3 (LC3) (Yang et al., 2005). The products of reactions catalysed by hydrolases acting on material within the lysosome are released through the lysosomal membrane into the cytoplasm for use in biosynthesis (Settembre and Ballabio, 2014a). Lysosomes can also fuse with the plasma membrane to repair damage to lipid bilayer components, recycle signalling receptors, membrane channels and adhesion molecules, and secrete material into interstitial space by lysosomal exocytosis (Settembre et al., 2013).

All three interactions are regulated by the Ca^{2+}-dependent E box transcription factor called TFEB in response to substrate concentrations in the lumen of the lysosome (Medina et al., 2011, Sardiello et al., 2009, Settembre et al., 2011, Settembre et al., 2012, Song et al., 2013). Amino acids are sensed by V-ATPase and sufficient levels activate assembly of the mechanistic target of rapamycin complex one (mTORC1) on the lysosomal surface. The membrane complex phosphorylates TFEB to prevent its translocation to the nucleus. Conversely depleted amino acid levels allow mTORC1 to dissociate from the lysosomal membrane which allows TFEB to dephosphorylate and translocate to the nucleus where it facilitates transcription of genes that promote lysosomal activity and autophagic pathways which mediate lipid catabolism (Settembre and Ballabio, 2014b). Together these interactions comprise the endosomal-lysosomal system and are summarised in Figure 1-2.

Lysosomal exocytosis: enzyme release, surface receptor expression, transmitter release, antigen presentation and cellular clearance. This mechanism is also involved in phagocytosis, neurite outgrowth and cell motility (Samie and Xu, 2014).

Lysosomal activity and biogenesis is regulated by the TFEB transcription factor. Translocation of TFEB to the nucleus in response to amino acid, carbohydrate and lipid concentrations within the lysosomal lumen is mediated by mTORC1 (Settembre and Ballabio, 2014).

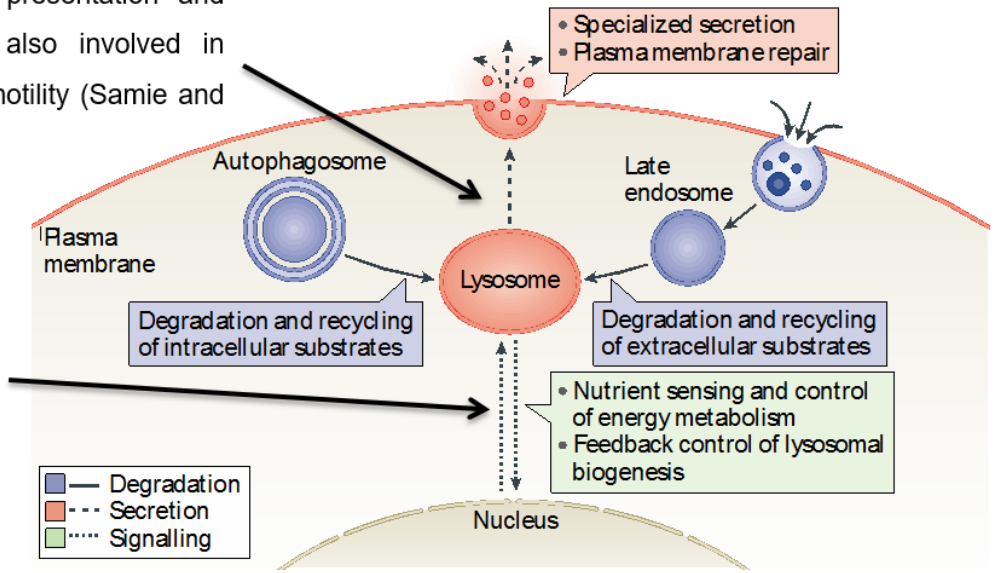

Figure 1-2: Interactions of the lysosome with other cellular organelles including the nucleus

The lysosome co-ordinates homeostasis between energy demand and supply, and cellular clearance. It fuses with the plasma membrane in order to repair damage to lipid bilayer components, recycle signalling receptors, membrane channels and adhesion molecules, and secrete material into interstitial space by lysosomal exocytosis. The lysosome receives extracellular material by the process of endocytosis via fusion with late endosomes, and receives intracellular material by the process of autophagy. A signalling pathway between nucleus and lysosome regulates these three interactions. These interactions form the endosomal-lysosomal system which positions the lysosome as the central hub of cellular metabolic homeostasis (Samie and Xu, 2014, Settembre and Ballabio, 2014b). Picture adapted from (Settembre et al., 2013).

The essential roles of the lysosome in degrading and recycling intra- and extra-cellular components place it central to regulating intracellular signal transduction, cellular clearance, antigen presentation at the cell surface, immunity against pathogens, and cholesterol homeostasis. The lysosome even signals cell death through release of cathepsin (Saftig and Klumperman, 2009). Through receiving cytoplasmic material and aged, damaged or redundant organelles that have been segregated into autophagosomes, the lysosome samples the nutrient level and health of the cell, and regulates energy metabolism accordingly (Rabinowitz and White, 2010). Lysosomal biogenesis and activity are regulated by a coordinated gene network under the control of TFEB allowing the lysosome to sense the cellular and extracellular environment and adjust its function accordingly (Settembre and Ballabio, 2014b).

Central to the roles of the lysosome are the 60 acid hydrolases it contains (Penati et al., 2017). The most common pathway by which both newly synthesised endogenous enzyme and exogenous extracellular enzyme are trafficked to the lysosome is by a mannose-6-phosphate receptor (M6PR)-dependent pathway (Marchesan et al., 2012). This pathway is illustrated in Figure 1-3. On their synthesis by ribosomes attached to the endoplasmic reticulum (ER) membrane, both secretory and lysosomal proteins undergo co-translational N-linked glycosylation of certain asparagine residues within the ER lumen (Kornfeld, 1986). In the golgi apparatus (GA) post-translational modification of the glycoproteins determine their final destination. Addition of sialic acid groups target enzymes for secretion; but in most cases, precursor enzymes destined for lysosomes acquire phosphomannosyl residues in a two-step process illustrated in Figure 1-4. This process is essential for glycoproteins to be recognised by the M6PR-dependent pathway (Kornfeld, 1986).

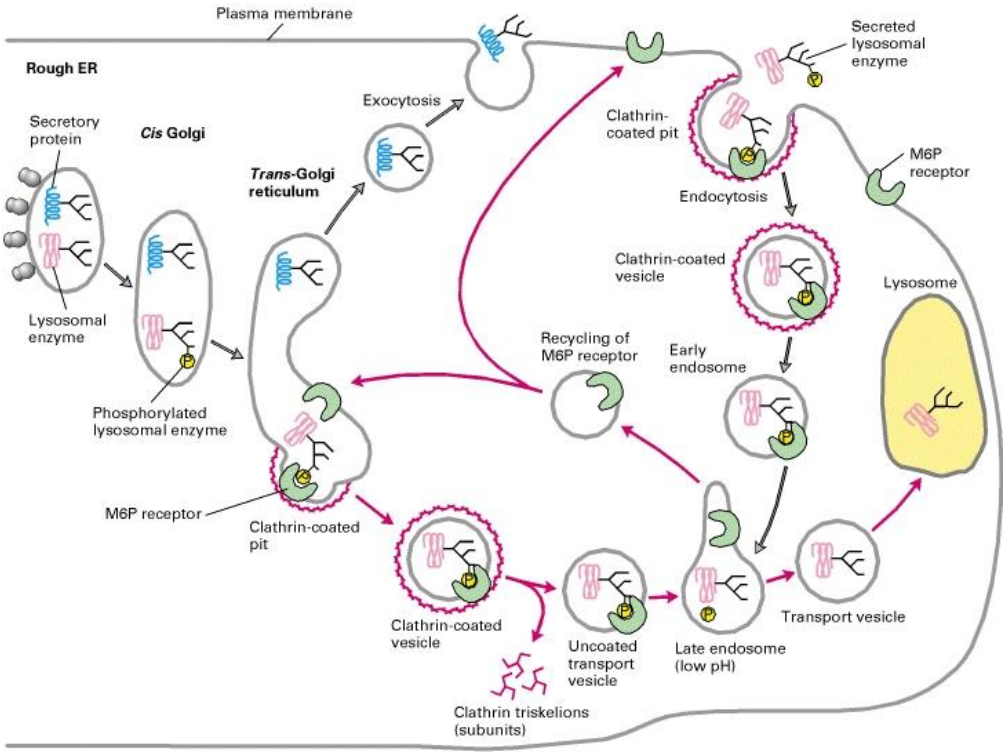

Figure 1-3: Lysosomal trafficking pathways

Precursor lysosomal enzymes undergoes co- and post-translational modification including N-linked glycosylation. Within the golgi apparatus most lysosomal enzymes are recognised by signal recognition sites on phosphotransferase which results in phosphorylation of high mannose residues essential for the enzyme's trafficking from the trans-golgi network (TGN) to the lysosome via a manose-6-phosphate-dependent pathway (Hrebicek and Ledvinova, 2010). Once within the lysosome, the enzyme is clipped by proteases into mature α-gal A (46kDa) that forms a homodimer with optimum catalytic activity at pH 3.8-4.6 (Gal et al., 2011). Overexpression of α-gal A may lead to saturation of available mannose-6-phosphate receptors (M6PRs) in the TGN, leading to secretion of enzyme expressing the M6P moiety. Such enzymes may then be taken up by other cells by M6PRs on their plasma membrane. Image sourced from (Lodish et al., 2000).

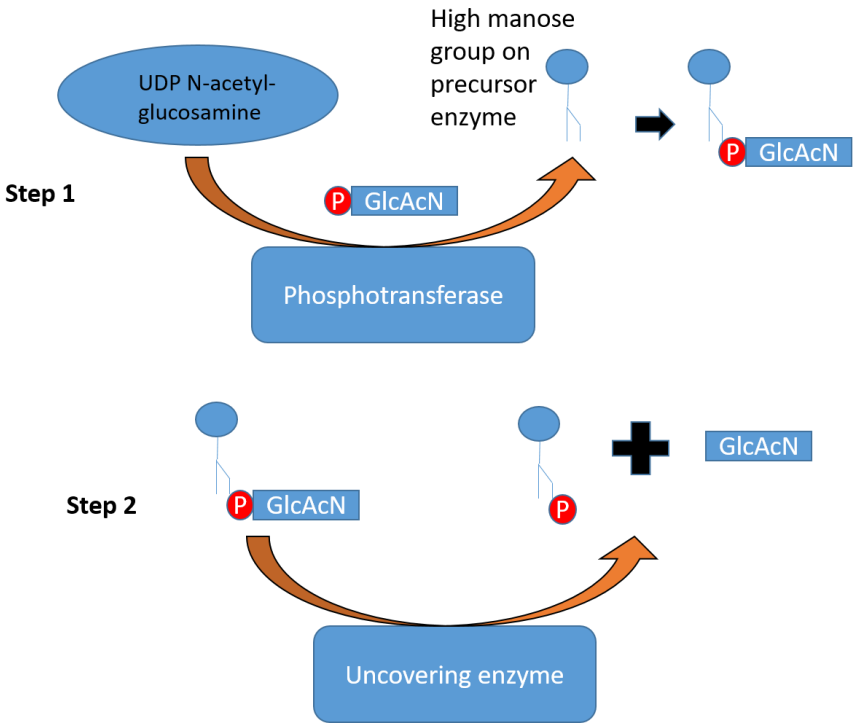

Figure 1-4: The two-step enzymatic addition of phosphomannosyl residues to pre-enzymes essential for M6PR-dependent trafficking to the lysosome

Phosphomannosyl residues are added to selected mannose residues on glycoproteins by a two-step process within the golgi apparatus. Firstly a phosphotransferase transfers N-acetylglucosamine-1-phosphate from uridine diphosphate N-aceylglucsomaine to mannose residues on precursor enzymes destined for the lysosomes. This golgi enzyme exhibits high affinity with lysosomal glycoproteins, possibly due to protein-protein interaction at signal sequences that are not present in secretory or plasma membrane proteins. Secondly, the N-acetylglucosamine is removed from the phosphodiester residue by N-acetylglucosamine-l-phosphodiester α-N-acetylglucosaminidase to expose mannose-6-phosphate signalling moities (Kornfeld, 1986). This has more recently termed the uncovering enzyme (Coutinho et al., 2012). GlcAcN: N-acetylglucosamine. UDP: urine diphosphate.

Lysosomal enzymes processed in this way are subsequently detected by M6PRs expressed in the trans-golgi-network (TGN). M6PR may also be expressed at the cell surface, enabling the recapture of secreted enzyme that escaped the lysosomal trafficking pathway. The ligand-receptor complex is packaged into clathrin-coated transport vesicles that bud from the TGN and merge with the late endosome. A low pH microenvironment within late endosomes allows the enzyme to dissociate from M6PR. The enzymes enter the lysosomes where they are clipped by proteases into their mature, active form (Coutinho et al., 2012, Desnick et al., 2001).

Other lysosomal trafficking pathways exist which are M6PR-independent, depending upon cell-type and hydrolytic enzyme (Prabakaran et al., 2012). For example lysosomal integral membrane protein LIMP2 acts as a receptor for localising β-glucocerebrosidase to the lysosome in various tissues, especially within liver (Reczek et al., 2007). Endocytosis of portions of the plasma membrane to the lysosome is essential for import of certain lysosomal hydrolytic enzymes that have bypassed the intracellular route of newly synthesised lysosomal proteins. Acid phosphatase provides an example of a lysosomal protein which is trafficked to the lysosome via clathrin-mediated endocytosis at the plasma membrane (Pryor and Luzio, 2009).

1.2 Lysosomal storage disorders

The lysosome concept introduced by de Duve (1963) first postulated the existence of congenital disorders due to enzymatic deficiencies effecting lysosomal function (de Duve, 1963). In the same year Hers (1963) showed that a type of α-glucosidase called acid maltase was deficient in Pompe disease, a glycogen storage disorder (Hers, 1963), and LeJeune et al (1963) showed that acid maltase was collocated with acid phosphatase which was recognised at the time as a lysosome marker (de Duve, 1963, Lejeune et al., 1963). In this light, Hers (1963) hypothesised that the symptoms of Pompe disease were due not only to the enzyme deficiency itself, but to the wider implications of lysosomal dysfunction, giving rise to the idea of the Lysosomal storage disorder (LSD) (Hers, 1963).

LSDs impair breakdown, salvage and secretion of cellular components essential for membrane integrity, cell-cell signalling, energy metabolism, autophagy, immune response and lysosomal biogenesis (Settembre et al., 2013, Das and Naim, 2009). The number of identified LSDs has since expanded into a group of approximately 70 genetically distinct diseases due to mutation in genes which effect the function of one or more of the elements of the endosomal-lysosomal system. Although individually rare, LSDs have a collective incidence of one in 7,500 live births (Cox and Cachon-Gonzalez, 2012).

LSDs may be classified according to the type of primary storage material which accumulates within effected cells (Futerman and van Meer, 2004). This classification is most appropriate for disease categories such as sphingolipidosis and mucopolyssacharidosis. In these groups a defect in any of the lysosomal enzymes involved in sequential catalysis of glycosphingolipids and glucoaminoglycans (GAGs) respectively, directly result in storage of the relevant undigested material. However there are many LSDs caused not by direct defects in any lysosomal acid hydrolase but defects in the wider endosomal-lysosomal system which result in accumulation of multiple types of storage material (Winchester, 2012). So another classification system was developed according to the molecular defect causing the disorder (Filocamo and Morrone, 2011). Both classification systems are utilised to develop the framework currently in use which is summarised in Table 1-1. The main basic mechanisms underlying LSDs are illustrated in Figure 1-5 to help interpret Table 1-1.

Table 1-1: Classification of Lysosomal Storage Disorders based upon the type of material stored and the molecular basis of diseases

Lysosomal storage disorders may be classified according to the type of storage material that accumulates in effected cells. This applies to the first four classifications in the table. Where this order is not appropriate, diseases may be subdivided according to whether the underlying pathological mechanism is a genetic defect in acid hydrolases, or some other factor effecting lysosome function. This applies to the remaining classifications in the table. GAGs: glycoaminoglycans. M6PR: mannose-6-phosphate receptor. SUMF1: formylglycine generative enzyme which activates lysosomal sulfatases. LIMP: lysosomal integral membrane protein. LAMP: lysosomal-associated membrane protein. (Cox and Cachon-Gonzalez, 2012, Winchester, 2012).

Classification:	*Molecular basis of disease class and type of material accumulated in storage cells*	*Mechanism expanded in Figure 1.5*
Muco-polyssacharidoses	Defects in any of 11 lysosomal enzymes involved in systematic catalysis of GAGs.	1, 4
Sphingolipidoses	A group of diseases caused by defects in any of 9 lysosomal enzymes involved in systematic catalysis of glycosphingolipids, or defects in any of four sphingolipid activator proteins (saposins A, B, C & D) for these enzymes or their precursor (prosasposin).	1, 3, 4
Glycoproteinoses	Defects in lysosomal enzymes relating to catalysis of glycopeptides, glycolipids and oligo-saccharides.	1, 4
Neuronal Ceroid Lipofuscinoses (NCLs)	This class comprises diverse defects of the endosomal-lysosomal system that result in the accumulation of an auto-fluorescent deposit called lipofuscin within lysosomes.	-
Defects in lysosomal enzymes for glycogen and lipid catalysis, and lysosomal proteases		1, 4
Defects in post-translational processing of lysosomal enzymes, including defects in phosphotransferase and the uncovering enzyme required for proteins to follow the M6PR-dependent pathway which causes stuttering. Post-translational modifications can also take place within the lysosome itself by activator enzymes such as SUMF1 which is defective in multiple sulfatase deficiency.		2, 3
Defects in specific transporters, receptors and channels within the lysosomal membrane essential for correct function, as well as LIMP receptor proteins necessary for ingress of certain hydrolytic enzymes, and LAMP glycoproteins responsible for fusion with autophagosomes.		2, 5
Defects in the biogenesis of lysosomes and their related organelles		-

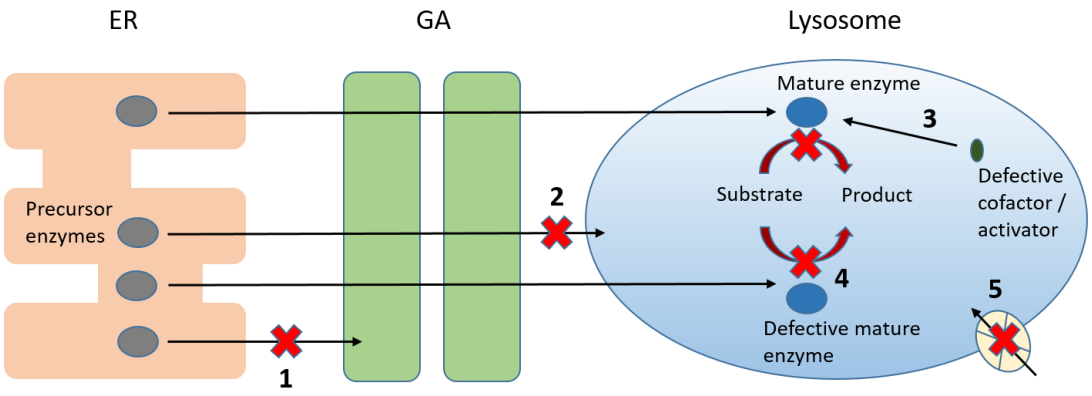

Figure 1-5: Classification of LSDs according to their underlying molecular basis

Lysosomal storage disorders may be due to a wide variety of pathological molecular mechanisms where their root causes may extend beyond the lysosome itself to implicate the wider endosomal-lysosomal system. **1.** Misfolded mutant precursor enzymes may fail quality control checks with the ER leading to ERAD. Even if ERAD is avoided, misfolding may prevent formation of multi-enzyme complexes required in some cases for transport out of the ER. **2**. Once within the GA, mutant precursor enzymes may not be correctly glycosylated, resulting in aberrant trafficking to the lysosome by the M6PR-dependent pathway. Defects in other pathways may prevent transport to the lysosome necessary for function. **3**. Activator proteins or cofactors may be defective leading to reduced enzyme activity in the lysosome. **4**. Glycosylation defects within the GA, or defects within the enzyme itself, may lead to reduced enzyme activity in the lysosome. **5**. Defects in lysosomal membrane proteins or other regulatory molecules may prevent enzyme transport to the lysosome or interaction with endosomes, autophagosomes or the plasma membrane. ERAD: Endoplasmic Reticulum-associated degradation. ER: Endoplasmic reticulum. GA: Golgi apparatus. M6PR: Mannose-6-Phosphate receptor. (Futerman and van Meer, 2004).

1.3 Sphingolipidosis

Glycosphingolipids (GSLs) are a family of complex biological macromolecules composed of a lipid root which is embedded within the phospholipid bilayer of the plasma membrane of all eukaryotic cells. This anchor is most commonly ceramide which is a long chain amino alcohol called sphingosine in amide linkage with a fatty acid. Alternatively, the anchor may be sphingosine. Attached to the anchor may be a glycan moiety. The composition of the glycan moiety, together with the length, saturation and hydroxylation of the long chains of the root confer considerable variation in structure, and consequently function, of members of the GSL family. As a major component of the glycocalix, GSLs have important roles in cell-cell interaction, cell surface receptor-mediated signal transduction, immunity, and providing a water permeability barrier for skin (Kolter and Sandhoff, 1999, Lingwood, 2011).

The GSL family of macromolecule in humans are divided into two main categories: those based upon lactosylceramide, and galactosylceramide. Each is further subdivided into series according to the content and order of carbohydrate in the glycan moiety as shown in Figure 1-6. Sequential catabolism commences from the terminal carbohydrate of GSLs by specific acid hydrolases within lysosomes until sphingosine remains. Deficient activity of any one enzyme or its activating cofactor will result in accumulation of substrate and deficiency in the bioavailability of product, leading to sphingolipidosis (Cox and Cachon-Gonzalez, 2012). Figure 1-6Figure 1-5 shows the enzyme responsible for each catabolic step in the degradation of GSL, and the sphingolipidosis which results from its deficiency.

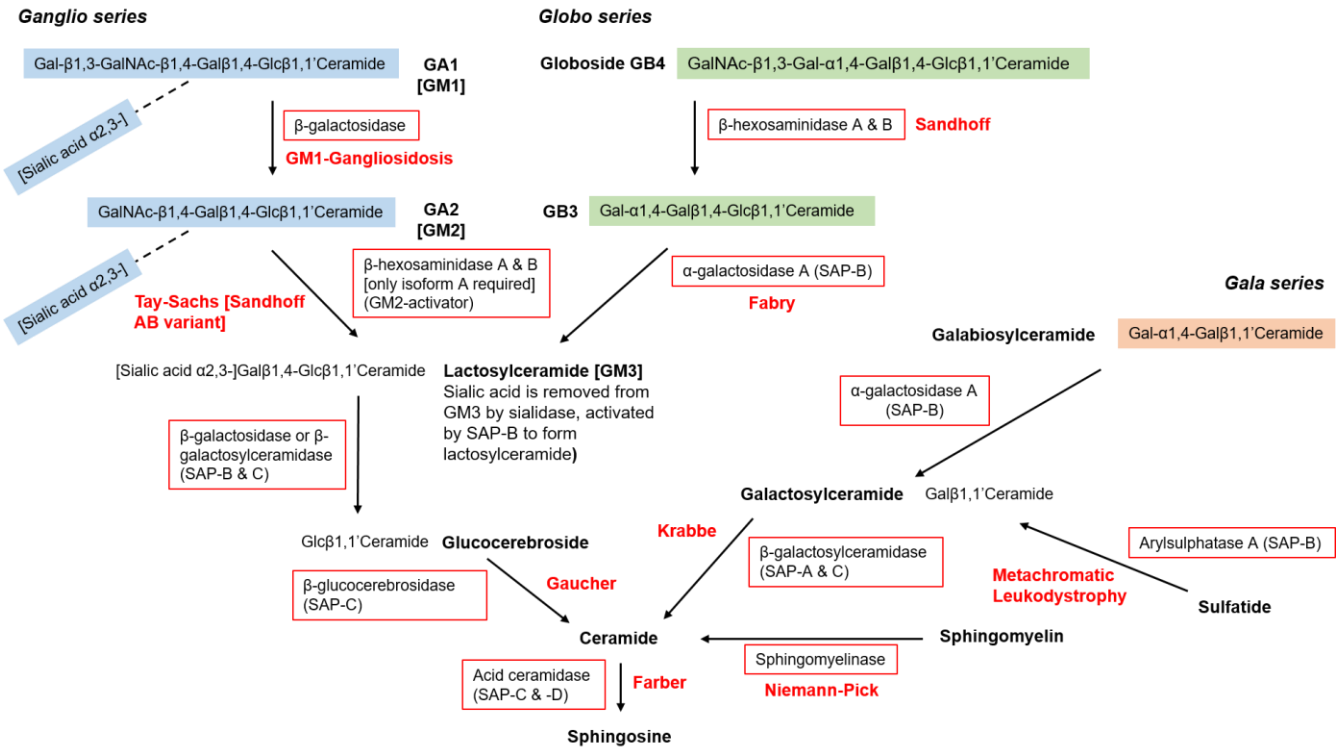

Figure 1-6: Catabolic pathway for sphingolipids within lysosomes, and the sphingolipidoses caused by deficiencies in specific enzymes

The highly diverse family of glycosphingolipids (GSLs) are organised, according to the order of the glycan moiety attached to the ceramide membrane anchor, into ganglio, globo and gala series. The sphingolipid sphingomyelin is highly abundant within lipid membranes. Lysosomal hydrolytic enzymes degrade GSLs sequentially from the glycan moiety terminal end. Each enzyme catalyses a specific step in the pathway. Deficiency in either an enzyme, or a prerequisite activing cofactor, results in a blockage in the pathway at the relevant step or steps. Boxed in red is the enzyme responsible for catalysing each step in the pathway, and emboldened in red is the disease caused by blockage at that step. SAP-A, B or C: Saposin A, B or C required for activating enzyme. GM1, 2 & 3 contains [sialic acid]. Breakdown of GM2 to GM3 requires β-hexosaminidase A and GM2 activator; deficiency leads to AB-variant Sandhoff disease. (Kolter and Sandhoff, 1999, Winchester, 2012).

1.4 Fabry disease

1.4.1 History

In 1897 the German dermatologist Johannes Fabry and the British clinician William Anderson reported independently the first observed cases of "angiokeratoma corporis diffusum" (Anderson, 1898, Fabry, 2002, Fabry, 1898). Their patients presented with red-purple maculopapular skin lesions focused in the upper thigh and trunk regions. Johannes Fabry went on to monitor his patient who developed respiratory disease, albuminuria and increased incidence of cutaneous eruptions, leading him to suggest the patient was presenting a systemic vasculopathy and kidney dysfunction. His theory was supported by others who reported accumulation of lipids in vasculature and glomeruli smooth muscle, together with gastroenteritis, in patients presenting similar characteristics (Karr, 1959). The condition subsequently became known as Fabry's disease (FD) (OMIM no. 301500).

Sweeley and Klionsky (1963) identified the biochemical nature of the disease. They examined kidney tissue from a FD patient who died following renal failure aged 28 and found abnormally high concentrations of two glycosphingolipids: globotriaocylceramide (Gb3) and, to a lesser extent, galabiocylceramide. Thus FD was shown to be a sphingolipidosis (Sweeley and Klionsky, 1963). Examination of seventeen FD families by Opitz et al (1965) showed the disease was inherited through the maternal line and predominantly effected males. Female carriers were usually either asymptomatic or only mildly affected; rarely were females found to present symptoms as severely as in males. Sons of effected fathers were asymptomatic. Together the data collected suggested an X-linked genetic cause for the accumulation of Gb3 in patients (Opitz et al., 1965).

Through analysing samples of small intestinal mucosa collected from two affected brothers and their minimally affected mother with FD, Brady et al (1967) found deficient activity of α-galactosidase A (α-gal A), otherwise known as ceramidetrihexodase (EC 3.2.1.22), in all three subjects. The acid hydrolase is responsible for removal of the terminal galactose from the glycan moiety of Gb3. Other enzymes involved in the systematic breakdown of globoside to ceramide

within lysosomes were unaffected (Brady et al., 1967). The gene encoding α-gal A, identified as *GLA*, was mapped to the long arm of the X chromosome (Xq21-22) (Fox et al., 1984), and the coding regions of the gene was sequenced for the mature lysosomal form of the human enzyme (Bishop et al., 1986).

Today, FD is only partially understood as a highly progressive, multi-systemic and heterogeneous lysosomal storage disease due to inborn error of glycosphingolipid metabolism. The *GLA* genotype does not correlate with disease phenotype observed in patients because of the extreme variability in severity and presentation, even within families. This complexity is enhanced by the effect of genetic modifiers, partial penetrance of *GLA* mutations in females due to X-inactivation and the central role of the lysosome in controlling cellular metabolic homeostasis (Desnick et al., 2001, Germain, 2010). So the history of FD is still in the making.

1.4.2 Clinical symptoms and epidemiology

FD is a complex multi-systemic condition presenting non-specific symptoms that are extremely challenging for clinicians to correctly diagnose. Patients may experience delay of over ten years from first reporting symptoms to confirmed diagnosis (Thomas and Mehta, 2013).

Early or childhood symptoms of classical FD may include angiokeratoma (skin lesions), acroparaethesia (burning discomfort in extremities), anhydrosis (deficient or excessive sweating) and proteinuria. Later, or by adulthood, substrate accumulation causes worsening of symptoms that may progress to include gastrointestinal dysfunction, respiratory disorders, cardiomyopathies, renal disease, neuropathic pain and fatigue with a commensurate reduction in quality of life. Patients often present cornea verticilata (asymptomatic corneal clouding), vascular ectasia and tortuosity (pathological changes to the retina), and may report hearing loss (Brady, 2010).

Heterozygous females are not only genetic carriers of a pathogenic mutation in *GLA* but may show signs of disease that in exceptional cases may be as severe as classical FD (Pinto et al., 2010, Wang et al., 2007). Classical FD reduces life span by up to twenty years in males and fifteen years in females (Mehta and Hughes, 2002); cause of death is usually renal failure, myocardial infarction or stroke (Thomas and Mehta, 2013).

In a study of seven affected males and five heterozygous females, Morgan et al (1990) found numerous cases of abnormal thermal sensation, especially impaired electrophysiological response to cold, indicating small myelinated fibre neuropathy. The study also revealed occurrence of abnormal brain scans by magnetic resonance imaging, even in the absence of obvious neurological/behavioural changes in patients (Morgan et al., 1990). Recently FD has also been associated with the neurodegenerative disorders (Nelson et al., 2014, Plotegher and Duchen, 2017, Stoka et al., 2016). For example, α-gal A-deficiency was found in post-mortem brains from late-stage Parkinson's disease patients, and level of enzyme deficiency correlated with α-synuclein accumulation (Nelson et al., 2017).

Diagnosis is complicated by non-classical, atypical variants of FD that present later in life in milder, mono- or oligo-symptomatic forms (Ko et al., 1996, Sachdev and Elliott, 2002). The recorded incidence of FD is between 1:117,000 (Meikle et al., 1999) and 1:4,000 (Spada et al., 2006) in males, suggesting diagnosis is inconsistent. A screening study of 171,977 consecutive new-borns in Taiwan reported an incidence of 1:1,250 and 1:40,000 FD cases amongst males and females respectively (Hwu et al., 2009). A systematic review suggested that screening of new-born and high risk populations identified individuals with *GLA* mutation or genetic variants that were of unknown significance with regards to FD, highlighting that until diagnostic criteria are improved, identifying true incidence of the disease will remain very difficult (van der Tol et al., 2014). So there is an urgent need to improve understanding of the pathological biochemistry of FD in order to improve early diagnosis.

1.4.3 Biochemistry

Human *GLA* codes for the 50kDa precursor α-gal A protein. Newly synthesised pre-enzyme incorporates a 31 residue signal sequence essential for the translocation of enzyme from the membrane of the ER into the lumen (Bishop et al., 1986). Subsequently it undergoes co- and post-translational modification including N-linked glycosylation essential for the enzyme's trafficking from ER to the lysosome (Hrebicek and Ledvinova, 2010). Fibroblasts, but not endothelial cells, appear to predominantly use M6PR-dependent trafficking for α-gal A (Marchesan et al., 2012), but podocytes use megalin and sortilin receptors as well as M6PR receptors (Prabakaran et al., 2011) and renal endothelial cells use sortilin receptors to endocytose extracellular α-gal A via LIMP2 lysosomal membrane proteins (Prabakaran et al., 2012).

On entering the lysosome, the enzyme is clipped by proteases into the mature, active form which is 46kDa and organises into homodimers with optimum catalytic activity at pH 3.8-4.6 on neutral or synthetic α-galactosyl substrates (Desnick et al., 2001, Gal et al., 2011). The structure of a lysosomal α-gal A monomer with α-galactose bound to the active site is shown in Figure 1-7. The enzyme is glycosylated at three aspartate residues (Hrebicek and Ledvinova, 2010).

Hydrolysis of substrate is by a double displacement mechanism in which D170 executes nucleophilic attack upon the anomeric carbon (C1) of α-galactose, cleaving its glycosidic linkage with the substrate and creating a covalently bound α-galactose-enzyme intermediate (Figure 1-7). Then a water molecule deprotonated by D231 executes a second nucleophilic attack on C1, liberating α-galactose from the active site and regenerating the enzyme. So α-gal A allows the anomeric configuration of the terminal saccharide molecule of substrate to be retained in the product and is called an α-retaining exoglycosidase (Garman and Garboczi, 2004).

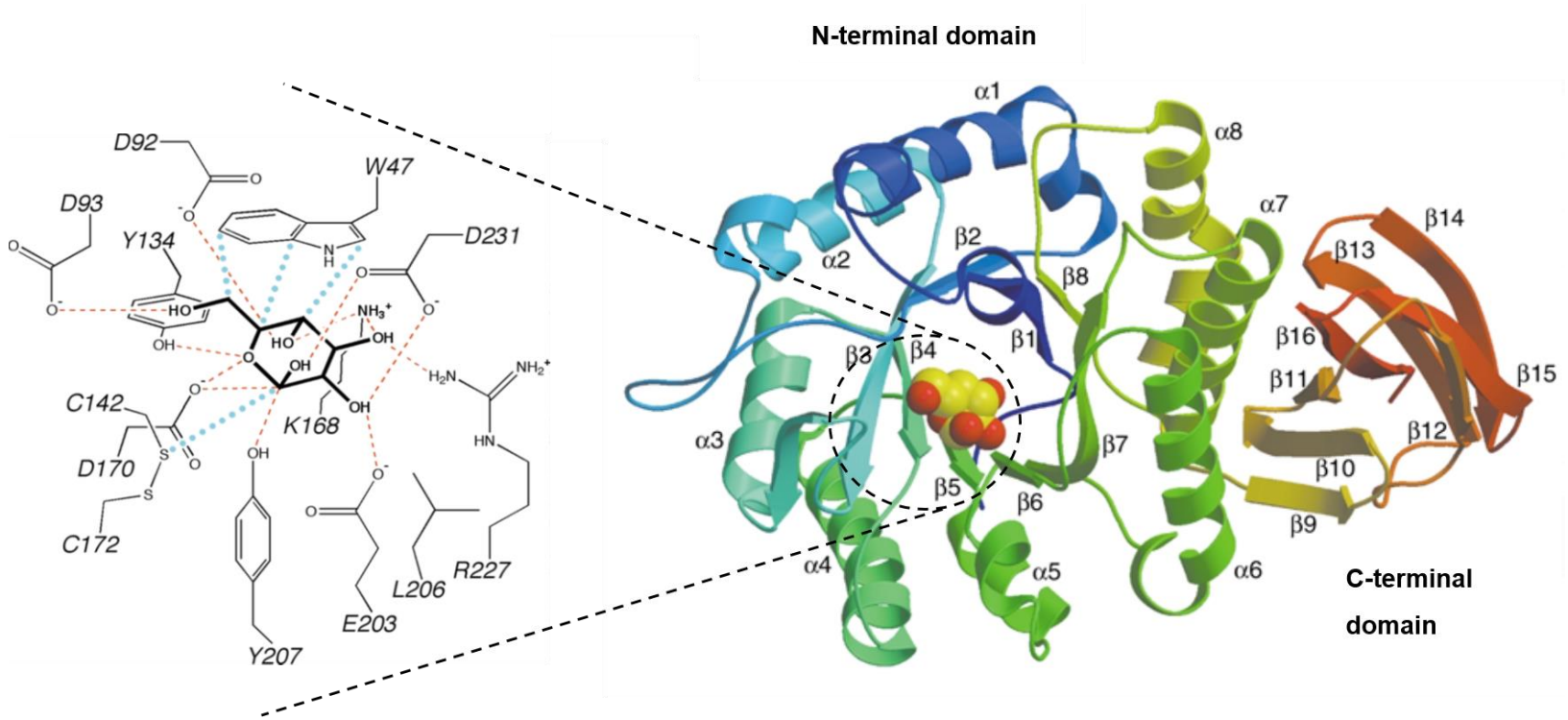

Figure 1-7: The ribbon structure of monomeric α-gal A with details of its active site with α-galactose bound

Peptide is illustrated in colours graded from red at the C-terminus to blue at the N-terminus. The C-terminal domains of two monomers interact to form a homodimer in the lysosome. The active site of each monomer is located within the N-terminal domain and is shown with bound α-galactose. The active site comprises of 15 remote residues that co-localise by protein folding and interact with the substrate's terminal α-galactose molecule as shown: hydrogen bonds and polar interactions are indicated in red, and van de Waal forces are shown in blue dashed lines. Adapted from (Garman and Garboczi, 2004).

The *in vivo* substrates of α-gal A are glycosphingolipids, shown in Figure 1-8, which comprise of a hydrophilic glycosidic tail linked to a hydrophobic ceramide head. This general structure suits substrates for inclusion within the lipid membranes of cells and subcellular structures. Gb3 is the predominant substrate and has been shown to be a diagnostic and prognostic marker for FD (Mills et al., 2002, Young et al., 2005). Gb3 is a major component of membrane-bound organelles, vesicles and the outer-leaflet of plasma membrane where it localises within caveolar-associated lipid rafts that are rich in cholesterol and receptor signalling complexes (Das and Naim, 2009).

The α-gal A substrate Gb3 is named P blood group antigen p_k (Marcus et al., 1981) and cell surface marker CD77. It has widespread baseline expression in human tissues (Table 1-2). Within the haematopoietic system Gb3 expression is restricted to germinal centre B lymphocytes (Mangeney et al., 1991); and is an important marker for Burkitt lymphoma cells (Nudelman et al., 1983) and megakaryoblastic leukaemia cells (Furukawa et al., 2002). Verotoxins released by *Escherichia coli* are ligands for Gb3; ligation triggers endocytosis of the verotoxin that subsequently exerts a cytotoxic effect by inhibiting protein synthesis, suggesting that Gb3 is involved in signal transduction (Endo et al., 1988). There is evidence that CD77 associates with CD19 at the cell surface to induce retrograde transport of CD19 to the nuclear membrane to signal apoptosis (Khine et al., 1998), and inhibit growth in response to interferon-α (Maloney et al., 1999).

There is interesting evidence that α-gal A activity may be an essential regulator of invariant natural killer T (iNKT) cell response to glycosphingolipids, preventing overstimulation to endogenous Gb3 yet, in the presence of exogenous Gb3, enhancing iNKT cell stimulation to reach threshold for release of cytokines. The presence of microbes appears to inhibit α-gal A activity in antigen presenting cells (APC) by a toll-like receptor-induced mechanism, increasing Gb3 expression. Gb3 may be trafficked from the lysosome on CD1 for presentation at the APC surface to amplify iNKT activity (Darmoise et al., 2010). Thus α-gal A dysfunction may impact iNKT cell roles in immunity, autoimmunity and cancer. Gb3 has been shown to inhibit iNKT-cell activation in a CD1-dependent manner (Pereira et al., 2016).

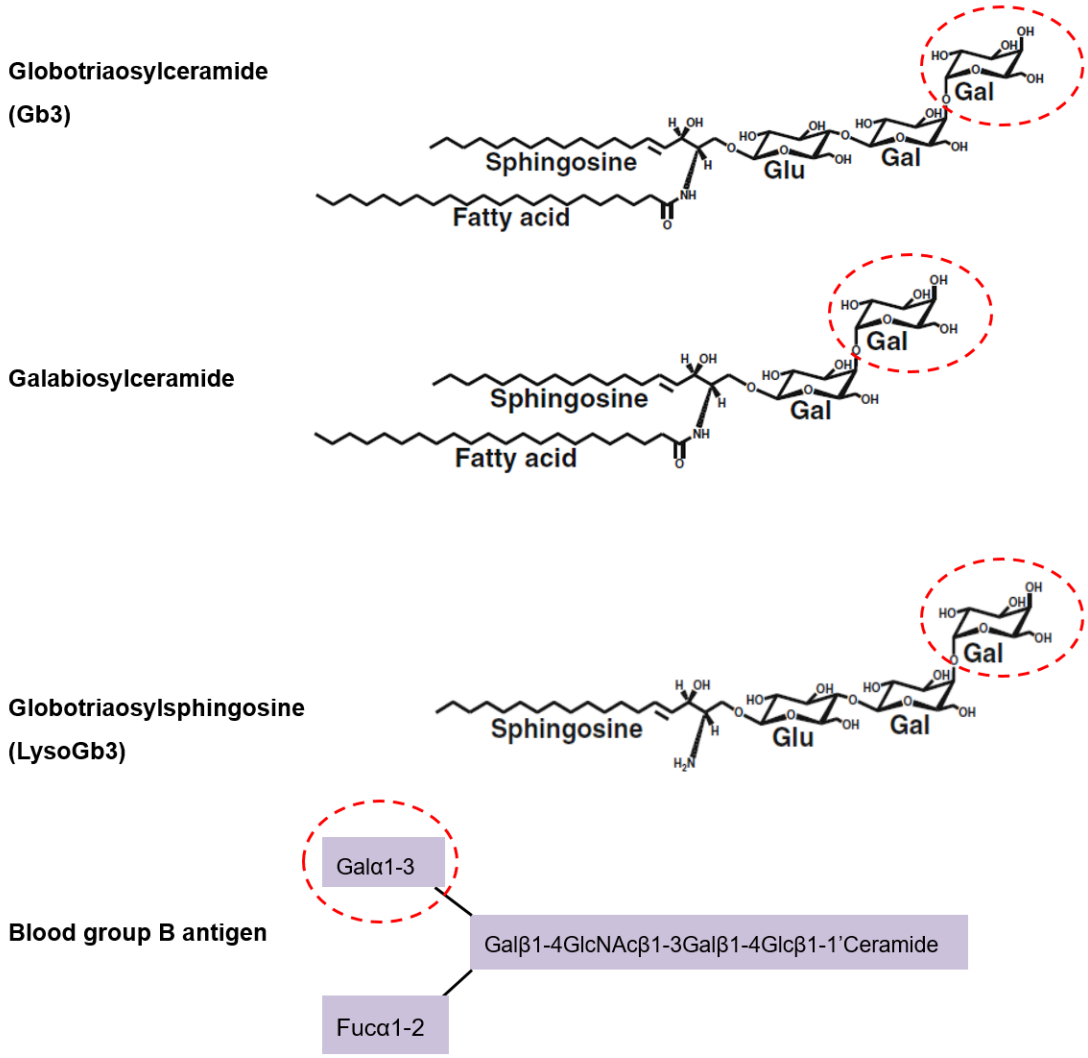

Figure 1-8: *In vivo* substrates for α-gal A are neutral glycosphingolipids, predominantly globotriaosylceramide (Gb3) and, to a lesser extent, digalactosylceramide (Ga2), blood group B antigen and globotriaosylsphingosine (lysoGb3).

Hydrolysis of terminal α-galactose, highlighted in red, requires the activator glycoprotein saposin B which increases solubility of the substrate and accessibility by the enzyme (Hrebicek and Ledvinova, 2010). A-gal A can also hydrolyse lysoGb3, a de-acylated metabolite of Gb3 which is increased in plasma of FD patients, but with 50-fold less efficiency than Gb3 (Aerts et al., 2008).

The major sites of glycosphingolipid storage and subsequent cellular pathology in humans with FD are also listed in Table 1-2. Histological hallmarks of progressive disease include zebra-like lipid aggregates in storage lysosomes and autofluorescent ceroid deposition in long-living cell types such as smooth muscle or post-mitotic cardiomyocytes. Ceroid is thought to be an indicator of irreversible cellular damage (Elleder, 2010).

Table 1-2: The distribution of Gb3 in human health and disease

The glycosphingolipid globotriaosylceramide (Gb3) is normally found in the cellular membranes of a diverse range of tissue types and organs, all of which are highly vascular (Pallesen and Zeuthen, 1987, Hughes et al., 2002, Kojima et al., 2000). The distribution reflects the sites of storage observed in Fabry disease (FD) (Desnick et al., 2001, Elleder, 2010, Hozumi et al., 1990).

Human tissues with high baseline amount of Gb3	Major sites of Gb3 storage in Fabry disease
Vascular endothelial & smooth muscle cells Kidney Liver Pancreas Lungs Neurons of CNS Gastrointestinal system Male reproductive system Heart Placenta	Vasculature: endothelium; underlying perivascular and smooth muscle cells; Renal glomeruli and distal tubules; Cardiomyocytes; Neurons; Fibroblasts of skin and heart; Macrophages; Epithelial cells lining bronchioles.

1.4.4 Genetics

Human *GLA*, located within the long arm of the X chromosome at position Xq22, contains seven exons comprising 1418 nucleotides (NCBI: NM_000169.2). Within the non-coding intronic regions between exons are located 12 *Alu* transposable repeat elements. The International Human Genome Sequencing Consortium (2001) found that these elements are common locations for mutations (Lander et al., 2001). It is not surprising therefore that the Human Gene Mutation Database (Stenson et al., 2009) details approximately 900 FD-causing mutations identified within *GLA*, and the number is increasing. These mutations can be categorised as shown in Table 1-3.

Table 1-3: Categories of *GLA* variants

Gene rearrangements involving large deletions and insertions usually translate to a severe disease phenotype for patients. Small insertions or deletions that were often frame-shift mutations leading to premature termination of transcripts frequently result in the classical disease phenotype in males. The most common point mutations include N215S, R227Q, R227X, R342Q, and R342X (Eng and Desnick, 1994). A new born screening study in Taiwan found a very high incidence of mutation c.639+919G>A (Hwu et al., 2009), which results in alternative transcriptional splicing and reduced α-gal A activity (Ishii et al., 2002).

Category of *GLA* mutation	Example Genotype
Large gene rearrangements	Partial gene deletions or insertions involving multiple introns and exons
Small deletions and insertions	Usually within exons
Mutations causing defects in transcript processing	Mutations at splice sites usually located within introns or at the edge of exons
Point mutations	Missence and nonsence mutations within exons

No clear correlation between genotype and phenotype has yet been discerned. Generally, missense mutations result in residual enzyme activity and are associated with non-classical FD. This is because these mutations may cause the tertiary structure of α-gal A to be unstable, leading to protein misfolding and subsequent degradation by ERAD quality control, or failure to be trafficked to the lysosomal, or reduced substrate affinity. Nonsense, splice or frame-shift mutations, and missense mutations at functionally significant sites, are associated with classical FD and less than 10% normal α-gal A activity (Gal, 2010). For example, N215S was a common

missense mutation linked with non-classical variant FD effecting mainly the heart. R227X was the most common nonsense mutation linked with the classical phenotype (Eng et al., 1993).

One of the challenges posed by the heterogeneous nature of FD is differentiating between mutations resulting in non-classical disease phenotypes and non-disease causing polymorphisms (Schiffmann et al., 2016). The relationship between *GLA* variants and α-gal A activity is shown in Figure 1-9, which illustrates that there are two groups of variants with enzyme activity above 20%, and 40%, of normal presenting highly variable phenotypes. For example, the *GLA* variant R118C is associated with over 30% residual α-gal A and no Gb3 storage within tissues, yet reports vary regarding the clinical presentation. The mutation was associated with a cerebrovascular disease (Rolfs et al., 2013), cardiac hypertrophy (Caetano et al., 2014) and non-FD phenotypes (Ferreira et al., 2015).

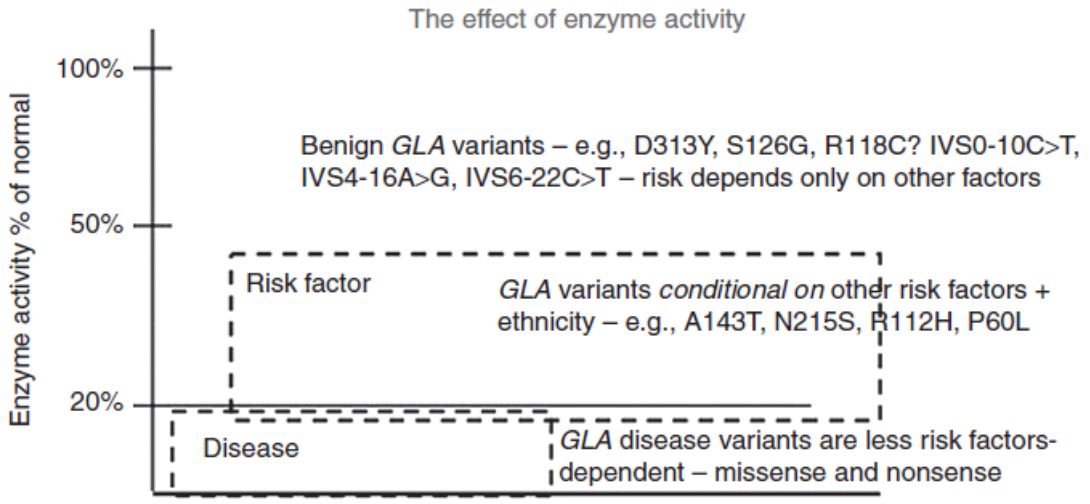

Figure 1-9: The relationship between *GLA* genotype and phenotype

The relationship between *GLA* genotype and phenotype is dependent upon various risk factors including the genetic/epigenetic background, gender and environment to which the individual is exposed. The influence of these factors increase with increasing residual α-gal A activity. Image sourced from (Schiffmann et al., 2016).

The phenotype resulting from *GLA* genotypes within these groups is variably influenced by epigenetic factors and modifier-genes such as those coding for interleukin-6, endothelial nitric oxide synthase (eNOS), factor V and protein Z (Schiffmann et al., 2016, Heltianu et al., 2002). For example, the Factor V Leiden mutation is associated with thromboembolic events in FD patients (Lenders et al., 2015), and polymorphisms in the gene for eNOS are associated with increased cardiac hypertrophy in FD patients (Rohard et al., 2008).

1.4.5 Pathophysiology

From the nature of FD discussed so far, it is logical to propose several pathophysiological mechanisms cascading from the primary enzyme deficiency to impair global cellular function. Identification and understanding of these mechanisms may lead to explanations for the extreme variability observed between patients and across tissue-types within patients (Germain, 2010). Pathological processes evidenced in FD are summarised in Figure 1-10 and will be discussed here.

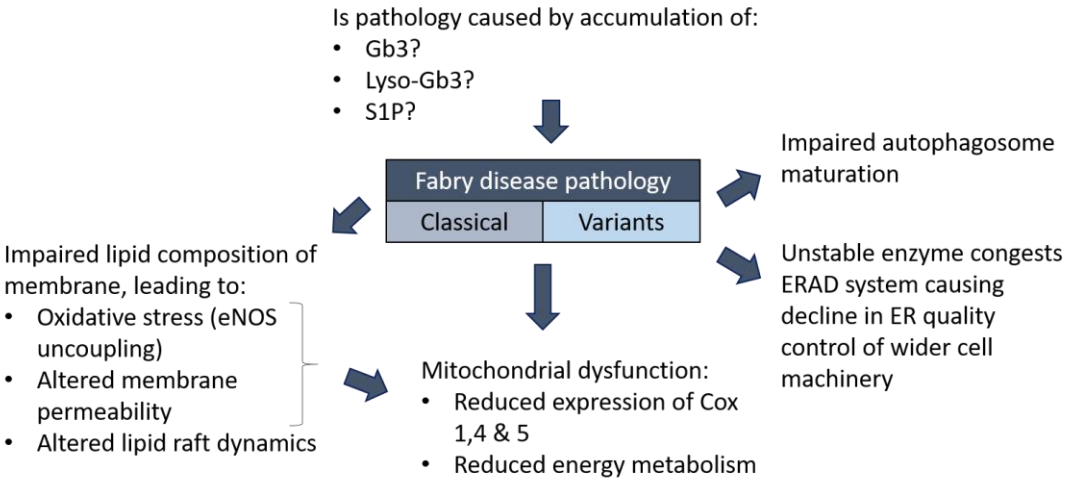

Figure 1-10: Pathophysiological mechanisms involved in the clinical manifestations of Fabry disease

The major substrate of α-gal A is globotriaosylceramide (Gb3). Fabry disease causes accumulation of Gb3 which alters lipid composition of cell membranes leading to metabolic deficits. Secondary metabolites globotriaosylsphingosine (lyso-Gb3) and sphingosine-1-phosphate (S1P) also increase and signal pathological processes. Lyso-Gb3 appears to be a better biomarker than Gb3 for differentiating classical from variant phenotypes in patient plasma. Storage of material in lysosomes may effect functions including autophagy. Increased pressure on endoplasmic reticulum associated degradation (ERAD) due to misfolded or unstable α-gal A mutants may cause wider implications for cellular quality control.

Firstly there are the effects of impaired recycling of glycosphingolipids Gb3 and galabiosylceramide (Ga2) on membrane dynamics, cell-cell interactions including immune response, and general receptor-mediated signal transduction. In patient fibroblasts, impaired lipid raft dynamics prevented the co-localisation of α-gal A with LAMP2 at the plasma membrane resulting in impaired trafficking of α-gal A to the lysosome, further exaggerating the accumulation of Gb3 (Maalouf et al., 2010).

Accumulation of Gb3 in the lysosomal-endosomal compartments of cultured *GLA*-deficient vascular endothelial cell-lines increases production of reactive oxygen species (ROS) which cause oxidative stress (Shen et al., 2008). Gb3 also accumulates within plasma membrane lipid rafts where it displaces cholesterol, and cholesterol-associated caveolin-1 (cav1) (Shu and Shayman, 2007). Cav1 is an essential regulator of eNOS that converts arginine to nitric oxide (NO) and citruline, dependent upon the cofactor of eNOS, tetrahydrobiopterin (BH4). Reduced cav1 content within lipid rafts may lead to eNOS:BH4 imbalance and eNOS uncoupling, resulting in production of superoxide instead of NO. Superoxide converts NO to peroxynitrite, a potent ROS which destabilises BH4 leading to enhanced eNOS uncoupling (Kietadisorn et al., 2012, Shayman, 2010). Reduced NO bioavailability will impair vasoresponse, promoting a pro-thrombotic and pro-atherosclerotic state and endothelial dysfunction (Shen et al., 2008, Forstermann and Munzel, 2006, Kang et al., 2014).

Accumulation of Gb3 will also disrupt the lipid and cholesterol composition of cellular membranes which is important for membrane permeability, integrity and key membrane associated processes such as the mitochondrial respiratory chain (Das and Naim, 2009). Lucke et al (2004) observed reduction in the activity of respiratory chain complexes I, IV and V in skin fibroblasts from FD patients compared to controls. Cellular content of ADP, AMP and creatine phosphate (CR) also reduced, but ATP only fell marginally. The authors attributed this to ATP replenishment by CR (Lucke et al., 2004).

Oxidative stress and eNOS uncoupling are probable further contributors to reduced energy metabolism. Increased ROS production will exert a deleterious effect on mitochondrial respiration by damaging enzymes, transporters, receptors, and mitochondrial DNA (Ventura et al., 2002, Heales et al., 1996, Lenaz et al., 2002, Shen et al., 2008). Consistent with this, cardiac energy metabolism was reduced in patients (Machann et al., 2011), and associated with increased rate of left ventricular hypertrophy over an eight year follow-up period following diagnosis (Palecek et al., 2010). Significantly reduced glucose consumption was found in the brains of α-gal A knock-out mice compared with controls, suggesting that cerebral energy metabolism also may be impaired in FD (Itoh et al., 2001).

The mitochondria is the site of cellular respiration and regulates cell growth, division and death (Osellame et al., 2012). In their paper reporting autopsy results in three patients having undergone varying lengths of treatment, Negano et al discovered mitochondrial content in myocardial tissue inversely correlated with Gb3 deposition in the cytoplasm of cardiomyocytes. There was a significant decrease in mitochondrial content in the patients who received two years therapy or none at all compared with patient who received fourteen years of therapy (Nagano et al., 2016).

Next, since plasma Gb3 do not correlate well with severity, especially in females, and clearance of stored Gb3 from cells resulting from treatment do not always result in remission, there is evidence that other factors besides the predominant substrate contribute to pathophysiology (Togawa et al., 2010, Young et al., 2005). Failure of cells to catabolise Gb3 by the systematic process described earlier, leads to employment of alternative pathways available to cells to rectify accumulated substrate. Acid ceramidase de-acylates the ceramide anchor to release fatty acid and globotriaosylsphingosine (lysoGb3). LysoGb3 is less polarised and therefore more soluble than Gb3 (Hrebicek and Ledvinova, 2010). Aerts et al (2008) discovered that lysoGb3 levels were increased in plasma of FD male patients by over ten-times that of Gb3, but this increase did not correlate with severity (Aerts et al., 2008). In females, lysoGb3 levels correlated with disease severity. LysoGb3 may present a suitable biomarker for assessment of clinical significance of genetic variants of *GLA*: whether they are pathological mutations or non-pathological variants (Niemann et al., 2014). LysoGb3 competitively inhibits α-gal A, and promotes proliferation of cultured smooth muscle cells (Aerts et al., 2008). In cultured human podocytes lysoGb3 increased expression of secondary mediators of tissue injury, inflammation and fibrosis (Sanchez-Nino et al., 2011). Fibrosis indicates poor prognosis for response to treatment and may explain the link between lysoGb3 and disease progression (Weidemann et al., 2013). Lyso-Gb3 is also linked to increased sensitivity to pain in C57/BL6 mice. Murine cells in culture exposed to lyso-Gb3 at concentrations equivalent to those found in plasma of pre-treated FD patients, showed ingress of calcium via voltage-gated calcium channels in nociceptors. Lyso-Gb3 may therefore

be the causative factor of neuropathic pain experienced by FD patients (Choi et al., 2015).

Another sphingolipid metabolite associate with FD is Sphingosine-1-phosphate (S1P). S1P is formed from phosphorylation of sphingosine and predominantly is bound to circulating high density lipoproteins. Plasma S1P was significantly increased in male patients compared with healthy subjects and may be a potential biomarker of cardiovascular remodelling associated with FD (Brakch et al., 2010). S1P stabilises hypoxia inducible factor (HIF) 1α, the oxygen sensing subunit of HIF1 transcription factor which is also increased in patients (Hadjimichael et al., 2013). There is cross talk between HIF1 and mitochondria to co-regulate cellular energy metabolism and oxygen availability; HIF1 regulates transcription of complex IV of the respiratory chain (Semenza, 2011).

Thirdly, accumulation of substrates within lysosomes leads to lysosomal dysfunction. The lysosome degrades and recycles cellular and extracellular components, and regulates energy metabolism in response to nutrient levels by sampling cytoplasmic and organelle content isolated by autophagy. Cultured fibroblasts from untreated FD patients expressed the autophagolysosome marker LC3 more than controls, suggesting blockage in autophagy (Yang et al., 2013), and impaired autophagosome maturation (Chevrier et al., 2010). There is evidence that increased biogenesis of dysfunctional lysosomes and autophagosomes cause lysosomal lipid accumulation secondary to the main storage material. This may lead to disrupted energy metabolism and membrane permeability, and reduced expression of lysosomal membrane proteins which are important for catabolite export and maintenance of low pH within the lysosome (Samie and Xu, 2014). Finally there is the potential effect of accumulation of misfolded α-gal A protein leading to saturation of ERAD-associated quality control and widespread pathology due to unfolded protein response (Thomas and Mehta, 2013).

To help in the investigation of FD pathophysiology a mouse model was developed in 1997 by Ohshima and colleagues. The model contained a large deletion within murine *GLA* resulting in total inactivation of α-gal A in liver, kidney and fibroblast cells. By 10

weeks of age, Gb3 accumulation was observed in lysosomes of renal tubular, liver and fibroblast cells of these mice, as in FD patients (Desnick et al., 2001, Ohshima et al., 1997). Substrate accumulation plateaued in liver and kidney tissues at 20 weeks age. Histological examination of tissues at 60 weeks found lipid inclusions in skin; and by 80 weeks Gb3 was stored in cardiac connective tissue macrophages, cerebrovascular endothelium and smooth muscle cells. However no clinical symptoms associated with human FD were observed in these mice, possibly because globoside is absent from murine erythrocytes preventing significant accumulation in vascular endothelium and smooth muscle (Ohshima et al., 1999). Globoside is a major component of erythrocyte plasma membranes in humans (Brady, 2010).

1.4.6 Diagnosis

The diagnosis of FD is made based upon the clinical picture and α-gal A activity in plasma and leucocytes (Gal et al., 2011) or dried blood spots (Gasparotto et al., 2009). Concentrations of the enzyme's substrate, Gb3 in urine and plasma can be used to monitor disease progression using tandem mass spectrometry (MS/MS) using appropriate internal standards (Mills et al., 2002, Young et al., 2005). However, in non-classical FD in hemizygote males and heterozygous females, enzyme activity and/or substrate levels may be within normal range (Winchester, 2014). In this context Gb3 concentration in urine was found to be a more useful diagnostic biomarker than in plasma in heterozygous females (Young et al., 2005).

Lyso-Gb3 may be used as a biomarker in plasma (Aerts et al., 2008, Rombach et al., 2010, Togawa et al., 2010). An ultra-performance liquid chromatography (UPLC) MS/MS assay was developed and validated for measuring lyso-Gb3 concentration in plasma (Boutin et al., 2016). A recent study showed that plasma lyso-Gb3 can identify heterozygote patients confirmed by *GLA*-mutation analysis, despite normal leukocyte α-gal A activity, using highly-sensitive electrospray ionisation liquid chromatography together with MS/MS (Nowak et al., 2017). Lyso-Gb3 is detectable in urine from FD patients using time of flight MS, but absent in controls. Urinary concentrations of the metabolite correlates with urine Gb3 levels, gender, treatment status and disease severity assessed by mutation analysis (Auray-Blais et al., 2010).

Figure 1-11 shows that lysoGb3 levels in plasma clearly differentiates between classic Fabry in males, heterozygous females and healthy controls, however this is not the case for Gb3 in plasma, especially between either non-classical variant of FD in males or female carriers and controls (Rombach et al., 2010, Togawa et al., 2010, Young et al., 2005). In light of the apparent usefulness of plasma lyso-Gb3 in diagnosis, a multiplexed UPLC-MS/MS assay has been developed for quantitation of lyso-Gb3 in dried blood spots (Sirka et al., 2015). In urine, the sensitivity of lyso-Gb3 levels as a biomarker of disease in children is lower than for Gb3 levels, especially in females (Auray-Blais et al., 2015).

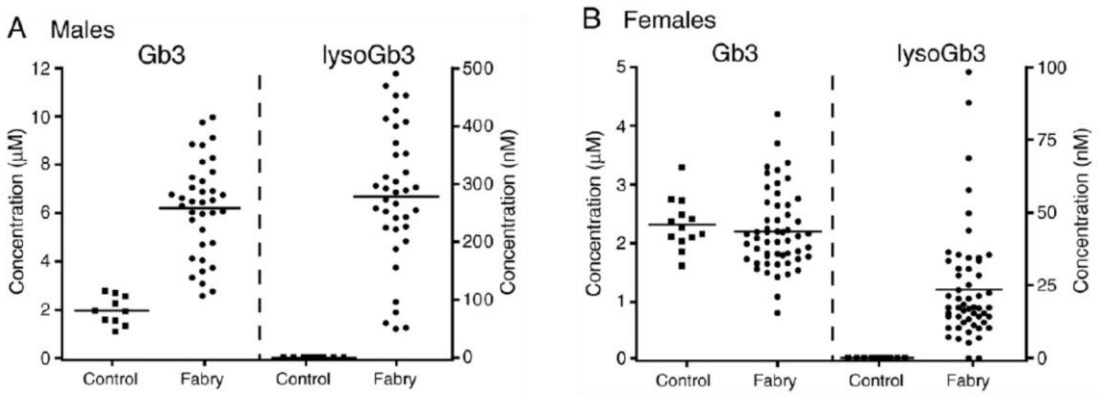

Figure 1-11: Concentrations of Gb3 and deacylated metabolite lyso-Gb3 in human plasma

Gb3 and lyso-Gb3 concentration in plasma is shown for males (**A**), and females (**B**). Plasma lyso-Gb3 concentration is able to distinguish FD patients from controls amongst male hemizygotes and most female heterozygotes. The concentration of plasma Gb3 is high in the majority of male patients, but in female there is no difference in plasma Gb3 levels between carriers and controls. Plasma lyso-Gb3 therefore represents a good biomarker for diagnosis (Source: Rombach et al., 2010).

The chemical structures of Gb3 and lyso-Gb3 cater for a potentially wide variety of analogues because of the long carbon chains of fatty acid and sphingosine. Variation in length and non-saturation give rise to analogues which may have significance as biomarkers for FD. The predominant Gb3 analogue detected in human plasma was C16:0, i.e. 16 carbon, fully saturated fatty acid tail; but human urine contained C22:0, C24:0 or C24:1, i.e. 24 carbon fatty acid tail with a single double bond. The urinary analogues were also found in liver, spleen, brain, heart, kidney and urine of the *GLA*-knock out mouse model (Mills et al., 2002, Young et al., 2005). This information illustrates that analogues of Gb3 and lyso-Gb3 may indicate the source, and thus scale of tissue involvement. A study by Manwaring et al (2013) identified seventeen Gb3 analogues in plasma that were previously found by the same group to be excreted in urine at different relative concentrations. The excretion of these plasma biomarkers varied between FD patients and controls (Manwaring et al., 2013). Similarly, modifications in the sphingosine tail of lyso-Gb3 were detected in urine from patients but not controls. Furthermore, levels of secretion correlated with gender. In males, levels also correlated with treatment (Lavoie et al., 2013). Specific analogues of lysoGb3 in urine have higher sensitivity than Gb3 as a whole, highlighting the importance of MS in biomarker discovery for both diagnosis and treatment

monitoring (Auray-Blais et al., 2015). Metabolomics has also identified analogues of lyso-Gb3 which appeared in patient plasma but which were absent in controls (Dupont et al., 2013). Analogues of Ga2 were identified as potential novel biomarkers in urine for FD (Boutin and Auray-Blais, 2015), and most recently, analogues of Gb3 accumulated in kidney persisted in young *GLA* knockout mice despite treatment (Kodama et al., 2017). Substrate analogues may therefore have important utility not only in diagnosis but also in optimising and monitoring treatment.

The clinical picture is dependent upon the genotype of *GLA* and the modulating effects of epigenetics and interacting genes, and environmental factors. Nonetheless genetic analysis of *GLA* may provide useful confirmation for diagnostic purposes (Gal et al., 2011). Heterozygous carrier females may be asymptomatic or present organ-specific symptoms possibly due to skewed or random X-inactivation (Whybra et al., 2001, Pinto et al., 2010); so diagnosis must be confirmed by *GLA* genotyping (Gal et al., 2011). Genetic analysis may also be helpful in prognosis and disease classification (Lukas et al., 2013).

1.4.7 Treatment

On diagnosis, there are currently two forms of treatment available to patients: enzyme replacement therapy (ERT) (Schiffmann et al., 2001, Eng et al., 2001) and small molecule chaperone therapy (Markham, 2016). Since 2001 ERT was available to FD patients by intravenous administration biweekly (Schiffmann et al., 2001, Eng et al., 2001). Two preparations are currently approved for marketing within the EU: agalsidase alfa (Replagal, Shire Human Genetic Therapies) manufactured in a human cell line by gene activation technology; and agalsidase beta (Fabrazyme, Genzyme Corporation, a Sanofi company) manufactured within Chinese hamster ovary cells using recombinant technology (Motabar et al., 2010b, Hughes et al., 2013). Clinical response to ERT display considerable variation across patients, tissue-types, age and disease severity (El Dib et al., 2016, Ortiz et al., 2016, Rombach et al., 2013).

A recent trial compared the efficacy of long-term (median five year) ERT in patients with and without prior history of FD-associated cardiac, cerebrovascular and renal symptoms. The research showed that patients who commenced treatment with no prior history of major symptoms were at lower risk of developing life-threatening complications during their treatment (Rombach et al., 2013). This suggests therapeutic benefit of ERT is significantly reduced in patients whose disease has progressed, which is currently when the majority of FD cases are diagnosed (Meikle et al., 1999). In some cases, but not all, this is a poor return for the psycho-social and physical burden of biweekly intravenous administration of recombinant protein that ERT imposes on patients.

The second treatment option is currently available only to certain patients with missense and other mutations in *GLA* that result in unstable protein folding. Consequently α-gal A is not effectively trafficked to the lysosome but degraded by ERAD. Research found that a potent competitive inhibitor of α-gal A called 1-deoxy-galactonojirimycin (DGJ), when administered at concentrations lower than necessary to inhibit the enzyme, was able to enhance α-gal A activity in cultured lymphoblasts with the *GLA* mutation R301Q (Fan et al., 1999). R301Q translates to a later-onset, mild cardiac variant of FD (Sakuraba et al., 1990). Further investigation found that the

reason for the enhanced activity was that DGJ stabilised the protein synthesised from mutated *GLA* by binding to the active site, rescuing enzyme from degradation and increasing its transport to the lysosome. At low pH the enzyme is activated and showed higher affinity to natural substrates than DJG, so the inhibitor was released from the active site. Oral administration of DJG to R301Q mutant mice resulted in enhanced α-gal A activity, especially in the heart (Fan et al., 1999).

Chaperone treatment using DJG is limited to patients with compatible mutations, so a cell-based assay has been developed to test amenability (Benjamin et al., 2017, Wu et al., 2011). The small molecule, marketed as migalastat (Galafold, Amicus Therapeutics) was recently granted approval for use in treating FD caused by amenable mutations (Markham, 2016). In phase 3 clinical trials in ERT-naive male patients, migalastat produced clinical benefit in those with amenable mutations in terms of kidney function, left ventricular mass and gastrointestinal symptoms (Feldt-Rasmussen et al., 2017, Germain et al., 2017a, Germain et al., 2017b, Germain et al., 2016). Liquid chromatography-tandem mass spectrometry was used to show that plasma lyso-Gb3 concentration fell in both male and female patients in response to migalastat and remained low for the subsequent 18 months, independent of whether they were previously on ERT (Hamler et al., 2015). There was also evidence of Gb3 clearance from renal podocytes of male patients following 6 months of migalastat treatment (Mauer et al., 2017). However amenable mutations only account for 35% - 50% of pathogenic mutations in *GLA* (Hughes et al., 2016). So, at least half of all Fabry disease patients will not benefit from this mode of treatment.

Alternative therapies are therefore urgently required to treat Fabry disease. Substrate reduction therapy (SRT), an orally administered glucosylceramide synthase inhibitor called lucerastat, has recently completed its first early-stage clinical trial in patients receiving ERT (Guerard et al., 2017). Glucosylceramide synthase catalyses the formation of glucocerebroside and is the initial reaction in the synthesis of both ganglio- and globo- series glycosphingolipids. So lucerastat has potential applications as an SRT for numerous other LSDs including Gaucher disease and Sandhoff disease (Arenz, 2017). Preliminary results in FD patients receiving ERT showed that plasma Gb3, lactosylceramide and glucocerebroside concentrations reduced significantly

over a 12 weeks course of lucerastat. There was no change in plasma concentration of lyso-Gb3, but this may be due to levels already being rapidly reduced by ERT. Furthermore, the lucerastat study was of insufficient duration to observe any clinical benefits of reduction of Gb3 levels in plasma (Guerard et al., 2017).

Biomarkers play a vital role in monitoring patient response to treatment (Beirao et al., 2017, Young et al., 2005). Within Great Ormond Street Hospital (GOSH) (London, UK), both urine Gb3 and plasma lyso-Gb3 are measured for this purpose by Dr Kevin Mill's laboratory at Great Ormond Street Institute of Child Health (GOSICH) (London, UK). Figure 1-12, Figure 1-13 and Figure 1-14 show the biomarker profiles collated and graphed for four male patients with confirmed FD, two of whom were brothers (Figure 1-14). The profiles demonstrate that the concentration of lyso-Gb3 in plasma appears to be a more exacting parameter of treatment efficacy. This is shown in both Figure 1-13 and Figure 1-14B where plasma lyso-Gb3 remains very high and urine Gb3 is beneath normal threshold. The reason for the inconsistency between the two biomarkers remains to be resolved. The second point that Figure 1-14 show is the absence of correlation between both biomarkers and genotype. The profiles of two siblings with presumably the same *GLA* genotype are quite different. The younger brother (Figure 1-14A) shows declining concentrations of both plasma lyso-Gb3 and urine Gb3 from a very elevated starting point at diagnosis and commencement of treatment. The older brother (Figure 1-14B) started with comparably high levels of plasma lyso-Gb3, but in contrast, normal urine Gb3 concentration. In this patient, treatment resulted in decline in plasma lyso-Gb3, similar to his brother. Perhaps specific analogues of these biomarkers may reveal closer correlation with genotype.

Since FD is due to monogenic loss-of-function mutations, it is a good candidate for gene therapy (Friedmann and Roblin, 1972). Recently a clinical trial application for a "first in the world" gene therapy trial for FD using *ex vivo* lentivirus-mediated transgene delivery to haematopoietic stem cells (HSCs) was recently accepted (Huang et al., 2017). So the next section will introduce this form of treatment in more detail.

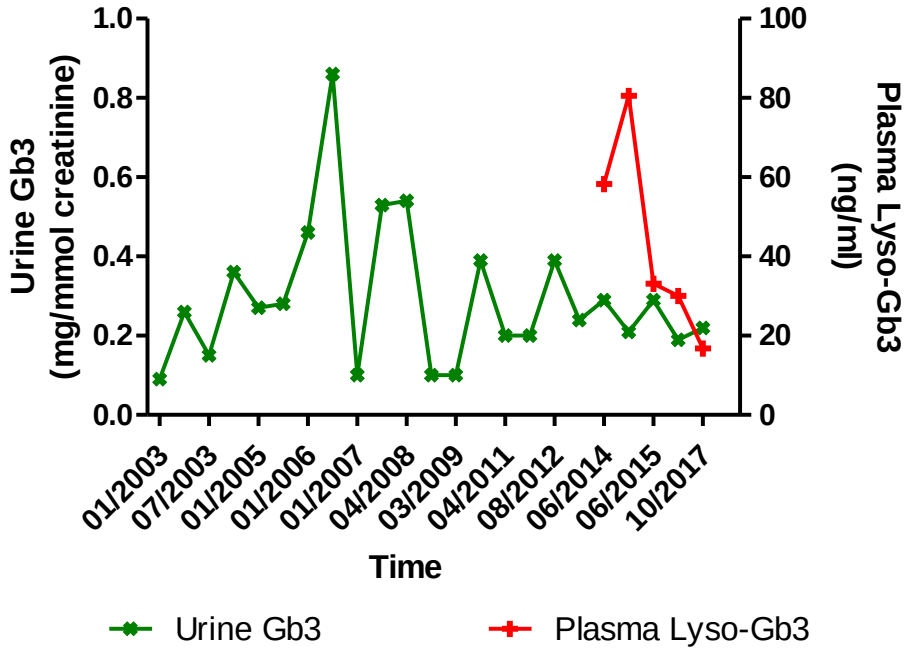

Figure 1-12: Biomarker profile over a 15 year period in a male patient aged 22 years old on diagnosis

The patient was diagnosed biochemically in October 2002 with α-gal A activity in leucocytes of 0.35 nmol/hr/mg protein, and in plasma of 0.03 nmol/hr/ml, both within the affected range. Urine Gb3 gradually increased over four years from 0.09 to 0.86 mg/mmol creatinine. In June 2006 the patient commenced ERT. Over the subsequent 11 years urine Gb3 fluctuates but gradually declines. However, as of October 2017 the urine Gb3 concentration is above normal. Plasma Gb3 monitoring did not commence until June 2014. Despite a considerable spike in concentration in December 2014, the plasma lyso-Gb3 level markedly declined, but remained above the normal threshold. Time as shown on the x axis is not linear and shows dates of sampling in month and year. Data courtesy of Dr Kevin Mills, GOSICH, London, UK.

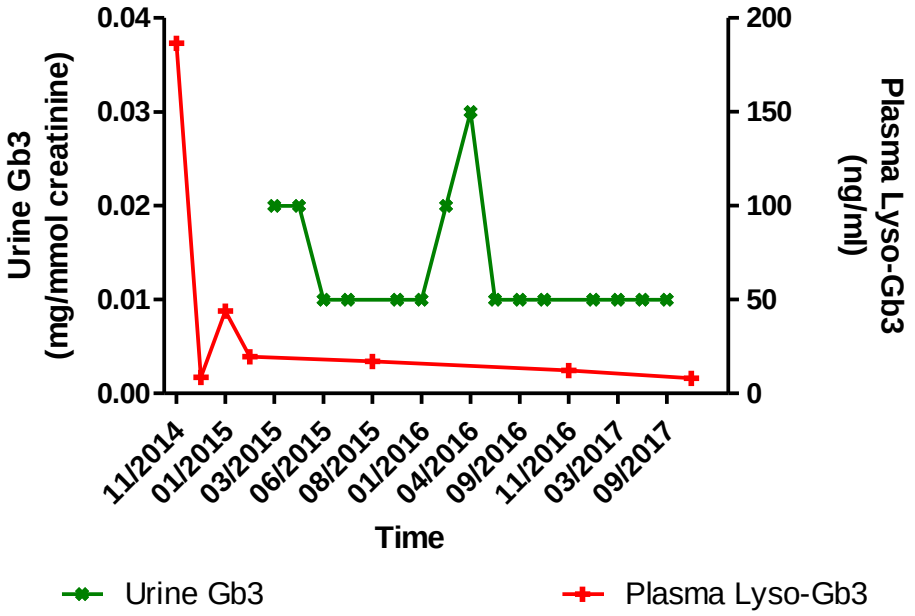

Figure 1-13: Biomarker profile over a 3 year period in a male patient aged 11 years old on diagnosis

The patient was diagnosed biochemically at close of 2014 with α-gal A activity in leucocytes of 1.8 nmol/hr/mg protein, and in plasma of 0.04 nmol/hr/ml, both within the affected range. Genotyping found mutation c.401A>C (Y134S) in *GLA*. ERT appeared to markedly reduce plasma lyso-Gb3 concentration in the first month, after which levels gradually settled but remained above the normal threshold. Over this latter period, urine Gb3 remained consistently within the normal threshold. Time as shown on the x axis is not linear and shows sampling dates as month and year. Data courtesy of Dr Kevin Mills, GOSICH, London, UK.

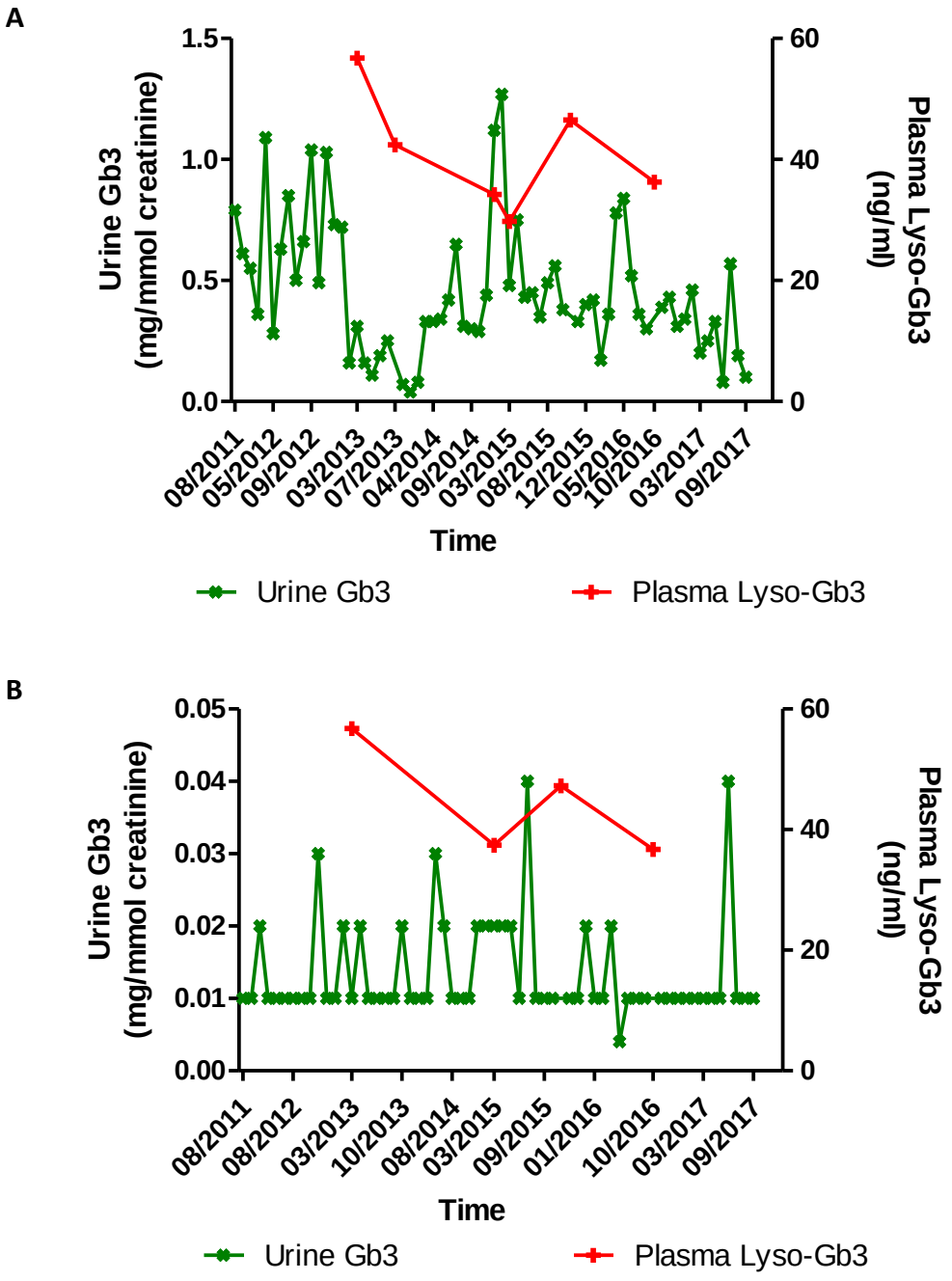

Figure 1-14: Biomarker profiles for two brothers diagnosed with Fabry disease

The brothers were aged 1 (A) and 2 (B) on biochemical diagnosis early 2002. The younger brother (A) was identified first with α-gal A activity in leucocytes of 0.85 nmol/hr/mg protein, and in plasma of 0.03 nmol/hr/ml, both parameters within the affected range for FD. Subsequently the older brother (B) was diagnosed with α-gal A activity in leucocytes of 2.5 nmol/hr/mg protein, and in plasma of 0.04 nmol/hr/ml, both within the affected range. **A.** Urine Gb3 fluctuated considerably with a slight downward trend. Concentration remains above the normal threshold. Plasma lyso-Gb3 levels show clearer general decline, but concentration remains very high. **B.** Urine Gb3 concentration was below the normal threshold on diagnosis and remained so except occasional spikes. In marked contrast in this patient, plasma Gb3 was very high despite a general decline. Time as shown on the x axis is not linear and shows dates of sampling in month and year. Data courtesy of Dr Kevin Mills, GOSICH, London, UK.

1.5 Gene therapy

1.5.1 Background

In 1928 the Griffith's experiment reported the first genetic transformation of pneumococcal bacteria from a non-virulent to virulent type. He mixed living non-virulent bacteria with virulent bacteria that had been killed by heat inactivation and inoculated mice with the mixture. Subsequently the mice died of pneumonia and virulent bacteria was cultured from their blood. He concluded that the living non-virulent bacteria was transformed into a virulent type by an unknown agent from the dead virulent bacteria (Griffith, 1928). It was not until 1944 that Avery, MacLeod and McCarty discovered that the transforming agent was DNA (Avery et al., 1944). This genetic transfer phenomenon was later applied to a human bone marrow-derived cell line. A metabolic defect in a mutant strain was corrected by transformation with wild type DNA from wild type cells. Furthermore, the correction was inherited by daughters of the transformed cells, demonstrating the potential therapeutic benefit of gene transfer to treat hereditary disorders in humans (Szybalska and Szybalski, 1962, Wirth et al., 2013).

The utility of viruses as vehicles for transfer of DNA was first demonstrated in Salmonella. Zinder and Lederberg discovered that transfer of hereditary traits occurred between bacterial strains when separated by a glass filter that prevented direct cell-cell interaction. When examining the filterable agent they found it did not contain DNA but particles identified by electron microscopy, which they argued were bacteriophages. They termed this virus-mediated genetic transfer, transduction (Wirth et al., 2013, Zinder and Lederberg, 1952).

The first evidence that DNA within a virus may correct an enzyme deficiency in human cells was made by Rogers et al, 1973. Skin fibroblasts cultures derived from a patient with hyperarginaemia, due to deficient arginase activity, were grown in media with Shope rabbit papilloma virus. This virus was shown previously to induce viral arginase activity in rabbit skin and human cells (Rogers, 1966). Seven months after inoculation, the cells showed increased arginase activity, and increased ornithine levels following addition of arginine to culture media (Rogers et al., 1973). Furthermore,

immunofluorescence microscopy showed increased expression of viral arginase in the treated cells compared with controls, addressing concerns raised by Friedmann and Roblin, (1972) that virus infection only stimulated endogenous arginase activity in humans (Rogers et al., 1973). Together this suggested that virus mediated gene transfer may have long term therapeutic benefit for metabolic disorders.

Later, recombinant DNA technology enabled transfer of a foreign gene into human cells. The first gene transfer experiments in humans were approved in December 1988 for patients with metastatic melanoma (Wirth et al., 2013). A proof of principle trial was carried out using retrovirus to deliver a neomycin resistance gene into tumour infiltrating lymphocytes (TILs) extracted from patients *ex vivo*. The modified TILs were re-introduced to the patients. Neomycin resistance gene expression was found in TILs from all patients up to three weeks after delivery without any adverse events, which demonstrated the feasibility and safety of retrovirus-mediated gene therapy (Rosenberg et al., 1990). Encouraged by this, Rosenberg et al used the same method to deliver the human tumour necrosis factor (TNF) gene to TILs *ex vivo* (Rosenberg et al., 1993). Three weeks after re-introduction of the modified cells to patients there was no detectable tumour around the injection site (Wirth et al., 2013).

The above evidence that virus-mediated gene transfer may be used to reprogram human cells by introducing a therapeutic gene *ex vivo* for autologous transplantation raises the question whether this can be applied as a potential therapy for FD. The rationale behind this form of treatment, and the progress made towards gene therapy for FD is discussed next.

1.5.2 Rationale behind gene therapy for Fabry disease

Since FD is due to a loss of function, single gene mutation, it is a good candidate for gene therapy (Penati et al., 2017, Ruiz de Garibay et al., 2013). The major classes of virus recently used as vectors for gene delivery include retrovirus (Medin et al., 1996, Sugimoto et al., 1995, Takenaka et al., 1999a, Takenaka et al., 2000, Takenaka et al., 1999b, Takiyama et al., 1999) and lentivirus (Yoshimitsu et al., 2006, Yoshimitsu et al., 2007, D'Costa et al., 2003, Lee et al., 2011, Yoshimitsu et al., 2004), both single-stranded RNA viruses containing reverse transcriptase and capable of inserting pro-viral DNA into the host cell genome for long term, stable expression of a therapeutic transgene (Sakuma et al., 2012); and adeno associated virus (AAV) which are non-enveloped, single-stranded DNA viruses (Ruiz de Garibay et al., 2013, Jung et al., 2001). AAV is usually non-integrating so that the viral genome may persist transiently as episomal DNA (Flotte et al., 1994) within host liver and muscle cells (Goncalves, 2005). AAV therefore carries reduced risk of mutagenesis developing in transduced cells, but high viral titres are required for clinically significant transgene expression (Ruiz de Garibay et al., 2013). Non-viral gene delivery strategies, which generally offer improved clinical safety with limited transduction efficiency, have also been explored but with limited success (Ruiz de Garibay et al., 2013). In all cases, vector delivery may be either intra-parenchymal, or systemic *in vivo* or *ex vivo* (Ruiz de Garibay et al., 2013).

Gb3 accumulation impacts nearly all cell types, so pluripotent haematopoietic stem cells (HSCs) that give rise to all the cell types of blood and tissue macrophages including microglial are a potential target for gene delivery (Huang et al., 2017). The therapeutic potential of healthy HSCs was shown when Gb3 storage was reduced in a murine model of α-gal A deficiency following transplantation of bone marrow from healthy control mice (Ohshima et al., 1999). Virus-mediated gene transfer to HSCs was first demonstrated in mice by Williams et al, (1984). The bacterial neomycin resistance gene was successfully delivered into murine HSCs from bone marrow *ex vivo* using retrovirus. Subsequently the transduced cells were transplanted into lethally irradiated mice, resulting in engraftment as shown by pro-viral sequences

found within DNA from spleen, an important site of haematopoiesis in transplant mice (Williams et al., 1984).

Since 1999, virus-mediated gene transfer to HSCs as the route and means of *ex vivo* gene delivery of *GLA* to treat FD has been explored using retrovirus (Takenaka et al., 1999a, Takenaka et al., 2000, Takenaka et al., 1999b, Takiyama et al., 1999), and then lentivirus (Yoshimitsu et al., 2007). Later it was reported, using lentivirus, that transplant of HSCs transduced with *GLA* resulted in greater reduction in Gb3 storage within heart and kidney of α-gal A-deficient mice than HSCs transduced with the green fluorescent protein gene *GFP* (Pacienza et al., 2012). This suggests lentivirus-mediated *ex vivo* HSC-targeted gene therapy may be more effective than allogeneic bone marrow transplant (Ruiz de Garibay et al., 2013).

Research suggests only 5% of enzyme activity is required for a therapeutic benefit (Biffi, 2016), suggesting a low level of transduction may be sufficient for a clinically relevant benefit. Lentivirus is able to transduce both dividing and non-dividing cells with high transduction efficiency for long-term stable expression (Sakuma et al., 2012), and is the vector of choice for the first and only clinical trial to date of gene therapy for FD (Huang et al., 2017). So lentivirus vector technology will be discussed in more depth.

1.5.3 Lentivirus vector technology

Lentivirus offers a potent method of gene delivery to both dividing and non-dividing cells with high transduction efficiency. This type of virus is a member of the retrovirus family: viruses that consist of an enveloped capsid containing double-stranded RNA. The general structure is shown in Figure 1-15. On entering a target cell, the virus mRNA is reverse-transcribed and integrated into the cell's chromosomal DNA for long-term stable integration. Host cell machinery transcribes the viral genome and synthesises lentivirus which buds from the cell surface to repeat the life cycle as shown in Figure 1-16 (Byrne et al., 2012).

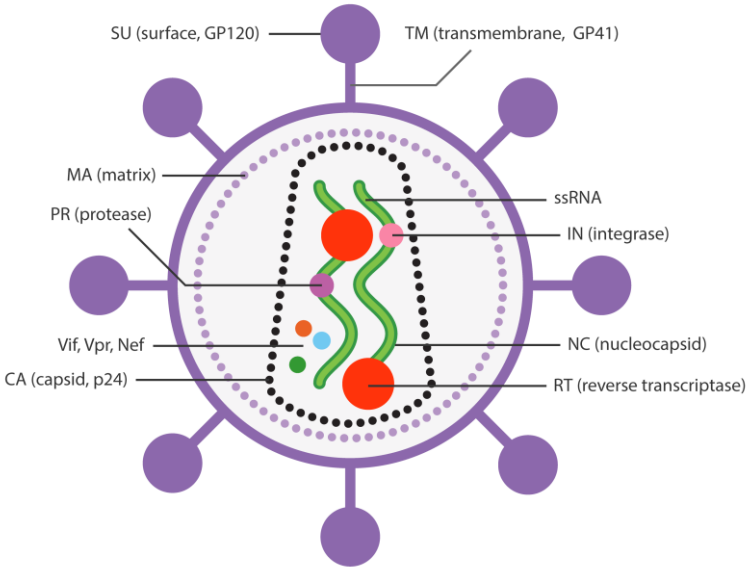

Figure 1-15: Schematic showing the basic structure of lentivirus

Lentivirus is an enveloped retrovirus that expresses transmembrane and surface glycoproteins that confer tissue tropism. The capsid contains two macromolecules of single stranded RNA containing the virus transcriptome, viral proteins Vif, Vpr and Nef, integrase, protease and reverse transcriptase to enable the virus to integrate the genetic instructions for itself within a host cell genome (Sakuma et al., 2012). Image sourced from (ABM, 2015).

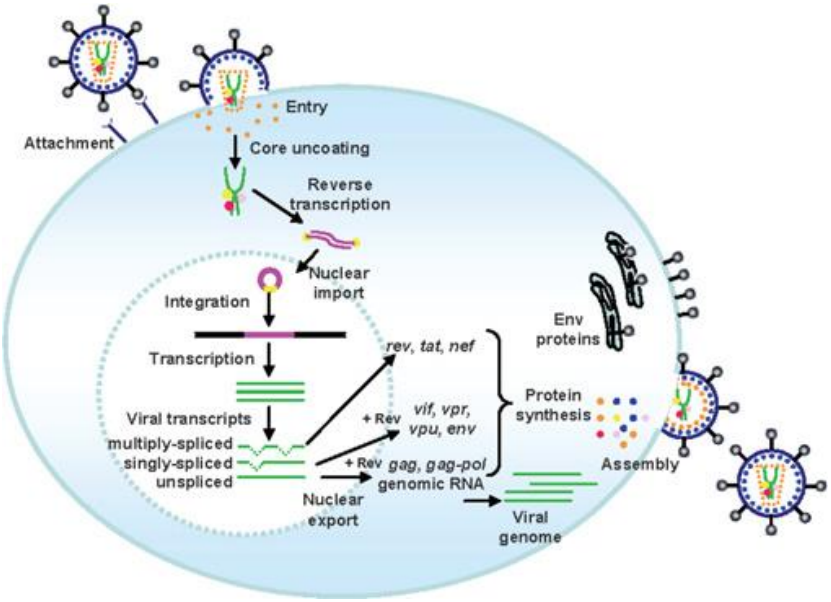

Figure 1-16: Self-replication of lentivirus within host cells

Host cell infection is mediated by glycoproteins expressed on the surface of lentivirus which confer broad tissue tropism. Within the cell, reverse transcriptase synthesises the provirus genome from the viral RNA, and integrase integrates it into the host cell genome. Integration is at long terminal repeat (LTR) regions either end of the provirus genome: The 5'LTR contains an enhancer/promoter site to which host cell RNA polymerase II binds and transcribes the provirus genome; and the 3'LTR R region is a polyadenylation signal to stabilise transcripts. Between the LTRs the provirus genome contains structural, regulatory and accessory genes which are expressed in multiply spliced transcript variants by the host cell machinery. The first genes to be transcribed are expressed in multiply-spliced transcripts and are regulatory: *tat* and *rev*. Tat protein trans-activates the 5'LTR for enhanced transcription of *rev*. Once cytoplasmic Rev protein levels reach threshold it promotes expression of single- and un-spliced transcript variants that encode envelop and structural proteins respectively. The virus assembles at the cell surface and buds from the host cell (Sakuma et al., 2012). Image sourced from (Sakuma et al., 2012).

As shown in Figure 1-16, the singly-spliced transcripts translate into envelop surface proteins which determine the target cell population of the virus. Broad tissue tropism is enabled by the G glycoprotein which is expressed on the surface of the vesicular stomatitis virus and encoded by *vsv-g*. Structural genes are *gag* and *pol* which are expressed through un-spliced transcripts as core and functional proteins respectively. Core proteins include components for the matrix, capsid and nuclear capsid of the virus; and functional proteins include reverse transcriptase and integrase necessary for stable replication and integration of the viral genome into target cells. The un-spliced transcript includes a packaging sequence (ψ) that promotes inclusion of complete single-stranded RNA sequence within the virus assembly at the cell surface. Once the daughter virus buds from the host cell it is able to transduce other cells and repeat the life cycle described (Sakuma et al., 2012).

To utilise the potential of lentivirus to integrate a transgene into the genome of target cells, the ability of virus to self-replicate and to transduce other cells must be controlled (Wirth et al., 2013). Disease-causing accessory genes which are not necessary for target cell transduction, but confer pathogenicity on the virus particle, are removed. The virus genome is split over three separate plasmids, as shown in Figure 1-17. The plasmids are co-transfected into 293T cell line “producer cells” that subsequently synthesise replication-incompetent lentivirus. Only the vector plasmid, which contains the transgene, expresses the packaging sequence Ψ which signals packaging of the vector transcript within the lentivirus capsid. The packaging plasmids contain structural, functional, regulatory and envelop genes necessary to synthesise infectious lentivirus capsid. So lentivirus manufactured by the “producer cells” contains only the transcript for the transgene flanked by LTRs; no further life cycles are possible. If random recombination within the producer cell genome were to align the DNA sequences of vector and packaging plasmids to enable synthesis of replication competent virus, then the self-inactivating long terminal repeats (LTR) illustrated in Figure 1-17 prevent transcriptional activation (Sakuma et al., 2012).

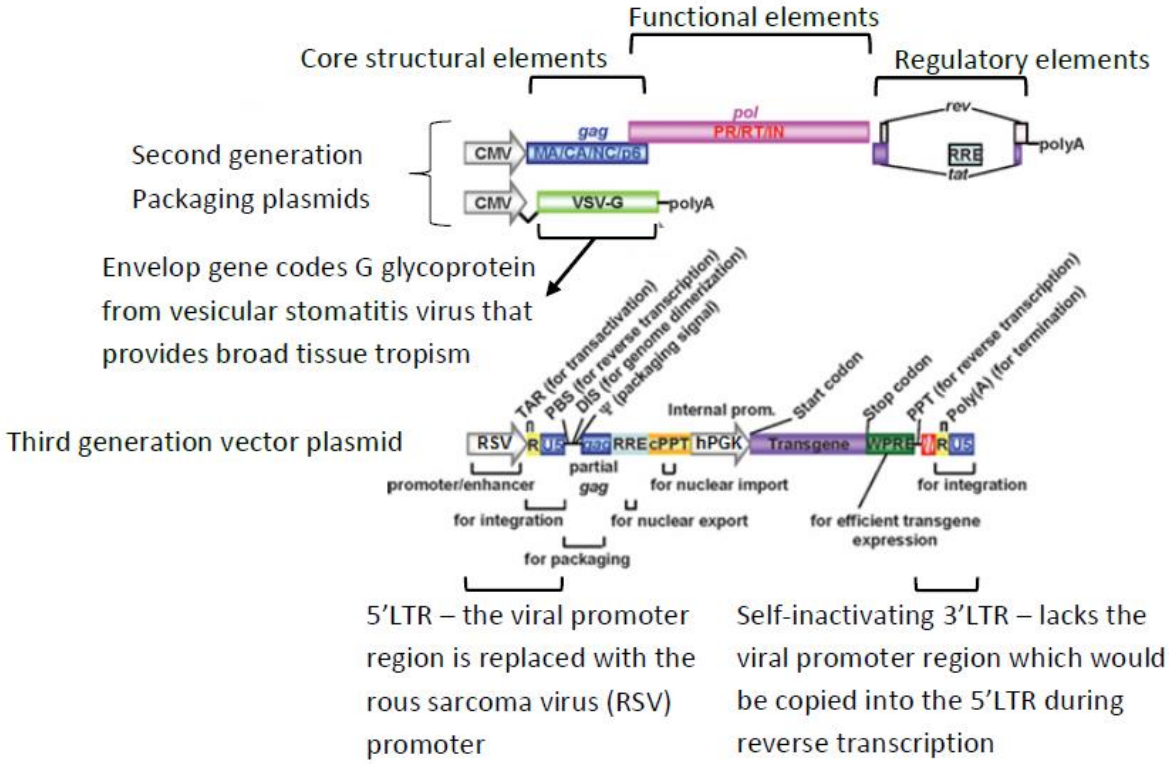

Figure 1-17: Typical structural configuration packaging and vector plasmids used for generating lentivirus capable of transducing target cells to express a transgene such as *GLA* used in this project

Plasmids used to co-transfect cells to produce replication-incompetent lentivirus containing a transgene. Second generation packaging plasmids lack HIV-1 associated accessory genes to prevent pathogenicity. After transfection, the vector plasmid expression is driven by the rous sarcoma virus (RSV) promoter. The transgene is expressed by an internal promoter such as the human phosphoglycerate kinase (hPGK) promoter within transduced cells (Sakuma et al., 2012). Adapted from (Sakuma et al., 2012).

The third generation lentivirus vector plasmid shown in Figure 1-17 contains two additional elements that improve transduction efficiency. The central polypurine tract (*cPPT*), together with PPT, allow reverse transcription and formation of a central overlap of DNA that increases transduction efficiency and may promote nuclear import. The woodchuck hepatitis virus post-transcriptional regulatory element (*WPRE*) increases transcription of unspliced RNA and transgene expression (Sakuma et al., 2012); but contains a truncated gene for woodchuck hepatitis virus protein X (WHX) that is a transcriptional activator of peptides associated with hepatocellular carcinoma in mice. To mitigate risk of functional WHX activity and tumourigenesis, six point-mutations were inserted into the WHX promoter region of the WPRE element. Research showed the mutation reduced WHX expression without abrogating transgene delivery and expression (Zanta-Boussif et al., 2009).

1.5.4 Design of a lentivirus vector to treat Fabry disease

A third generation *pRRLSIN.cPPT.PGK-GLA.WPRE* lentivirus vector plasmid, containing a transgene encoding mature human α-gal A regulated by the human phosphoglycerate kinase (hPGK) promoter, was constructed at UCL GOSICH (Bishop et al., 1986, Rajaraman, 2013). The transgene contains a 93 base pair sequence which translates into the 31 amino acid pro-peptide signalling sequence necessary for trafficking the enzyme from the ER, followed by the 1194 base pair complementary DNA sequence identified by Bishop et al, 1986. This vector plasmid is compatible with second generation packaging plasmids *pMDG.2* and *pCMV-dR8.74* that contain lentiviral envelop, and regulatory, functional and structural genes respectively. Together the vectors provide a safe method for overexpressing *GLA* in target cells (Sakuma et al., 2012). The plasmids are shown in Figure 1-18.

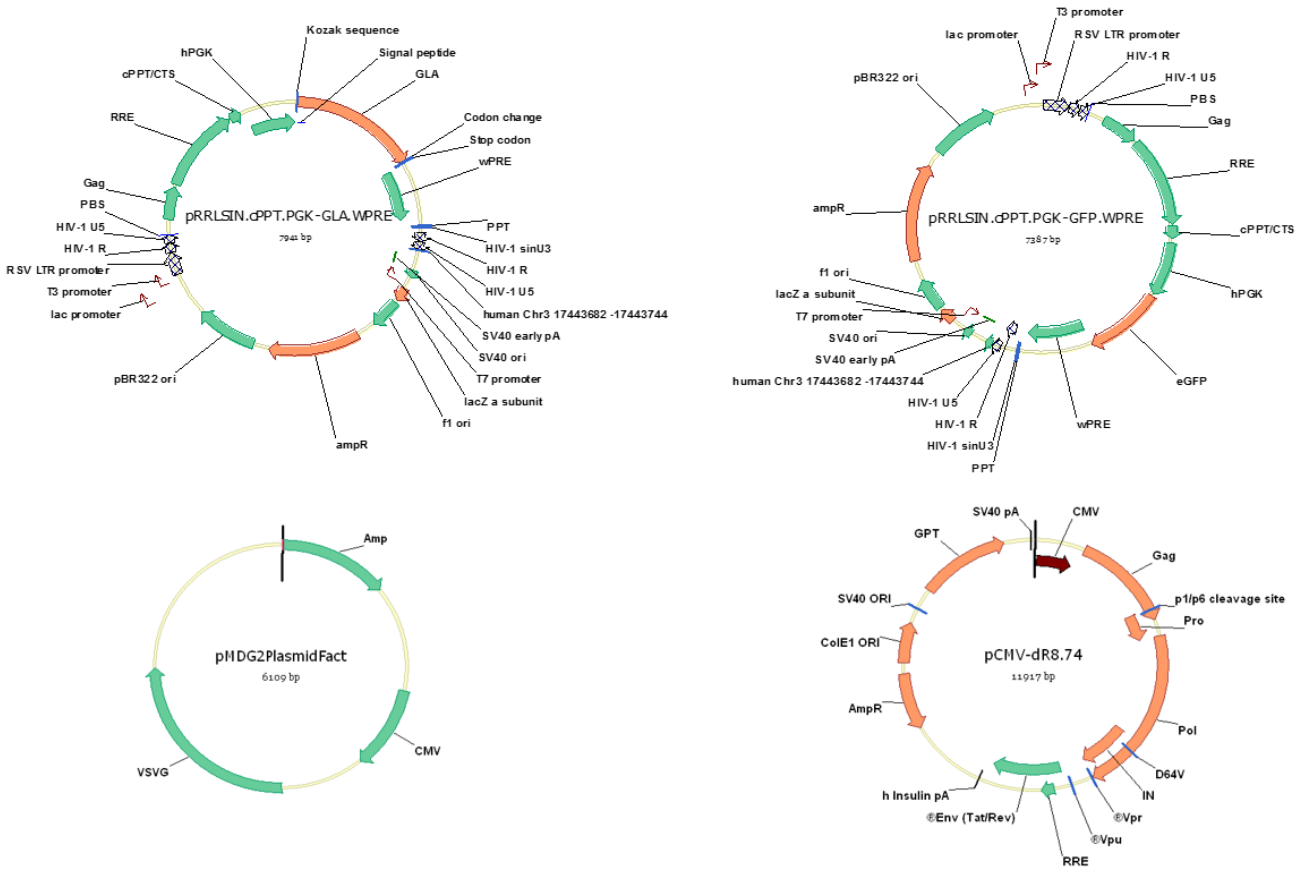

Figure 1-18: Schematics of packaging and vector plasmids used to produce lentivirus in this project

(A) Vector plasmid containing the transgene *GLA* encoding mature human α-gal A called *GLA*; (B) Same as A except the transgene is GFP (green fluorescent protein gene); (C) & (D) Packaging plasmids pMDG.2 and pCMV-dR8.74 respectively which are compatible with the vector plasmids (Rajaraman, 2013).

1.6 Project aims and thesis outline

The overall aim of the project was to examine the effectiveness of lentivirus-mediated *GLA* gene transfer to overexpress α-gal A in human cells. The thesis commences in Chapter 3 with characterisation of α-galactosidase in human fibroblasts and cell-lines, CD1 murine tissues and plasma samples from patients. The α-gal A assay was established, relative contributions of A and B isozymes to total α-galactosidase activity studied, and prognostic value in standardising α-gal A for lysosomal content in different cell types examined.

Utilising a previously constructed lentivirus vector containing the cDNA sequence for mature human α-gal A, Chapter 4 reports the manufacture, harvest and use of lentivirus to transduce Jurkats. The effect on various lysosomal hydrolases and cell toxicity was explored. Enyzme kinetic studies on α-gal A from wild type and transduced Jurkats were used to explore their relative affinity with synthetic substrate 4-methylumbelliferyl-α-D-galactopyranoside (4MUG), revealing that enzyme produced by higher virus doses may clear substrate less effectively.

Manifestations of the disorder are multi-systemic, so the efficacy of gene therapy depends upon ability of cells to cross-correct. Chapter 5 shows transduced Jurkat cells release α-gal A into culture media, and wild type Jurkats take-up α-gal A from media. Fabry disease is associated with reduction in the activity of respiratory chain enzymes, raising the research question: do mitochondrial deficits effect the ability of cells to cross-correct? This was addressed by inhibiting respiratory chain complex I of Jurkats and measuring the effect on lentivirus transduction efficiency, enzyme release and uptake. The results suggest potential therapeutic options may enhance cross correction.

Finally the work was extended to primary skin fibroblasts in Chapter 6. Patient cells showed reduced α-gal A activity. Transduction resulted in supra-physiological overexpression, albeit with apparently reduced transduction efficiency compared with controls. These results raise important questions which pave the way for future research.

Chapter 2 Materials and Methods

2.1 Materials

2.1.1 DNA Plasmids

pRRLSIN.cPPT.PGK-GLA.WPRE: Competent E. coli Stbl3 cells transformed with 3rd generation HIV-1 SIN lentiviral plasmid expressing *GLA* driven by the human PGK promoter, and the ampicillin resistance gene. Stored in glycerol at -80°C and provided by Srinath Rajaraman (UCL GOSICH, London, UK) (Rajaraman, 2013).

pMDG.2: Second generation packaging construct expressing VSV envelope glycoprotein for broad tissue tropism, driven by the CMV promoter. Purchased from Addgene plasmid repository (Cambridge, MA, USA).

pCMVdR8.74: Second generation packaging construct expressing lentivirus structural proteins gag-pol-tat-rev, driven by the CMV promoter. Purchased from Addgene plasmid repository (Cambridge, MA, USA).

pRRLSIN.cPPT.PGK-GFP.WPRE (Addgene plasmid #12252, gifted by D. Trono, unpublished): Competent E. coli Stbl3 cells transformed with 3rd generation HIV-1 SIN lentiviral plasmid expressing *GFP* driven by the human *PGK* promoter, and the ampicillin resistance gene. Stored in glycerol at -80°C and provided by Dr Conrad Vink (UCL GOSICH, London, UK).

2.1.2 Human cells

The human cell-lines and primary cells used are shown in Table 2-1.

Table 2-1: The source for human cells used to generate this thesis

Cell ID	Tissue of origin	Cell type	Source
HEK-293T (CRL-3216)	Embryonic kidney	Cell-line	American Type Culture Collection (ATCC, Teddington, UK)
SH-SY5Y	Neuroblastoma	Cell-line	Kindly donated by Derek Burke, Chief Biomedical Scientist (Department of Chemical Pathology, GOSH, London, UK)
Hu-H7	Hepato-carcinoma	Cell-line	Kindly donated by Miguel Calero, PhD student (UCL GOSICH, London, UK)
Jurkat (TIB-152)	T-lymphoblastoid	Cell-line	American Type Culture Collection (ATCC, Teddington, UK)
Fibroblast	Fibroblasts cultured from non-Fabry disease patients	Primary	Derek Burke (Department of Chemical Pathology, GOSH, London, UK)

2.1.3 Cell culture reagents

LB broth — Sigma (Poole, UK)

Ampicillin — GOSICH (London, UK)

Dulbecco's Modified Eagle Medium with Glutamax (DMEM); Life (Paisley, UK)

RPMI 1640 medium with Glutamax (RPMI) — Life (Paisley, UK)

Fetal bovine serum (FBS) — Sigma (Poole, UK)

Penicillin streptomycin (pen-strep) — Life (Paisley, UK)

0.05% trypsin in EDTA — Life (Paisley, UK)

Dulbecco's phosphate buffered saline (DPBS) — Life (Paisley, UK)

Trypan blue solution	Sigma (Poole, UK)

2.1.4 Murine Tissue Samples

Four adult male wild type CD-1 mice, non-inbred to International Genetic Standards to prevent genetic drift and ensure genetic standardization between colonies, kindly provided by Dr Simon Waddington, UCL Institute of Women's Health (London, UK).

2.1.5 Plasmid preparation

QIAprep Spin Miniprep kit	Qiagen (Manchester, UK)
QIAGEN plasmid maxi kit	Qiagen (Manchester, UK)

2.1.6 Lentivirus production

Reduced serum medium (Opti-MEM)	Life (Paisley, UK)
Polyethylenimine (PEI)	Sigma (Poole, UK)

2.1.7 Quantitative polymerase chain reaction (qPCR)

DNEasy blood and tissue kit	Qiagen (Manchester, UK)

Platinum qPCR Supermix-UDG with ROX universal mastermix; Life (Paisley, UK)

Standard (plasmid pBTW2L), kindly donated by Dr Steven Howe, GOSICH (London, UK)

The primers and probes used for qPCR are shown in Table 2-2.

Table 2-2: Primers and probes used for quantitative PCR

Target	Identity	Sequence	Source
WPRE	Forward primer	TGG ATT CTG CGC GGG A	Kindly donated by Dr Steven Howe, GOSICH (London, UK)
	Reverse primer	GAA GGA AGG TCC GCT GGA TT	
	Probe (5' FAM reporter and 3' TAMRA quencher)	CTT CTG CTA CGT CCC TTC GGC CCT	
Beta-actin	Forward primer	TGA GGA TCT TCA TGA GGT AGT CAG	
	Reverse primer	TCA CCC ACA CTG TGC CCA TCT ACG A	
	Probe (5' FAM reporter and 3' TAMRA quencher)	ATG CCC TCC CCC ATG CCA TCC TGC GT	

2.1.8 Reagents

Solvent used in preparation of all reagents was distilled H2O, unless otherwise stated.

2.1.8.1 Reagents for the BCA Protein assay

Bovine serum albumin (BSA) 1mg/ml standard	Sigma (Poole, UK)
Bicinchoninic acid (BCA), pH 11.25	Sigma (Poole, UK)
4% (w/v) copper (II) sulphate solution	Sigma (Poole, UK)

2.1.8.2 Reagents for α-galactosidase A activity assays

4-methylumbelliferyl-α-D-galactopyranoside (4MUG), MWt 356.3	Melford (Ipswich, UK)
Concentrated (18M) Acetic acid, MWt 60	VWR (Lutterworth, UK)
Sodium acetate trihydrate, MWt 136.08	VWR (Lutterworth, UK)
Sodium dihydrogen phosphate, MWt 156	VWR (Lutterworth, UK)

Di-sodium hydrogen phosphate, MWt 141.96	VWR (Lutterworth, UK)
N-acetyl-D-galactosamine (NAGA), MWt 221.2	Sigma (Poole, UK)

2.1.8.3 Reagents for β-galactosidase and total β-hexosaminidase activity assays

4-methylumbelliferyl-2-acetaminido-2-deoxy -β-D-glucopyranoside, MWt 379	Melford (Ipswich, UK)
4-methylumbelliferyl-β-D-galactopyranoside, MWt 338	Sigma (Poole, UK)
Human serum albumin (HSA)	Sigma (Poole, UK)
Sodium chloride (NaCl), MWt 58.4	VWR (Lutterworth, UK)
Di-sodium hydrogen phosphate, MWt 141.96	VWR (Lutterworth, UK)
Citric acid (monohydrate), MWt 210.14	VWR (Lutterworth, UK)

2.1.8.4 Reagents for citrate synthase activity assay

All reagents were kindly donated by Dr Mesfer Al Shahrani, Neurometabolic Unit, University College London Hospital (UCLH) (London, UK):

100mM Tris/0.1%v/v Triton; pH 8 (assay buffer)

10mM acetyl-CoA

20mM 5,5’ dithio-bis (2-nitrobenzoic acid) (DTNB)

20mM oxaloacetate

2.1.8.5 Reagents for mitochondrial respiratory chain complex I activity assay

All reagents were kindly donated by Dr Mesfer Al Shahrani, Neurometabolic Unit, UCLH (London, UK):

Potassium dihydrogen phosphate

Di-potassium hydrogen phosphate

Magnesium chloride hexahydrate

100mM potassium cyanide (KCN)

50mg/mL bovine serum albumin, fatty acid free (BSA)

5mM ubiquinone

1mM rotenone in ethanol

5mM nicotinamide adenine dinucleotide (NADH), pH>7

2.1.9 Solutions

The solutions used throughout this thesis are shown in Table 2-3.

Table 2-3: The content of assay solutions

Solution	Content	Used in assay
0.1M acetate buffer	0.1M acetic acid, 0.1M sodium acetate trihydrate, pH 4.5	Intracellular α-galactosidase A activity assay
20mM sodium phosphate buffer	20mM sodium dihydrogen phosphate, 20mM di-sodium hydrogen phosphate, pH 6.4	
0.5M acetate buffer	0.5M acetic acid, 0.5M sodium acetate trihydrate, pH 4.8	Extracellular α-galactosidase A activity assay
HSA/NaCl solution	0.4% (w/v) HSA in 0.4M NaCl	Intracellular β-galactosidase activity assay
McIlvaine 4.1 buffer (MV4.1)	0.1M citric acid, 0.2M di-sodium hydrogen phosphate, dilute 1:1 in H2O, pH 4.1	
McIlvaine 4.5 buffer (MV4.5)	0.1M citric acid, 0.2M di-sodium hydrogen phosphate, pH 4.5	Total β-hexosaminidase activity assays
25mM potassium phosphate buffer	25mM potassium dihydrogen phosphate, 25mM di-potassium hydrogen phosphate, pH 7.2	Mitochondrial respiratory chain complex I activity assay
Complex I buffer	10mM magnesium chloride hexahydrate in 25mM potassium phosphate buffer, pH 7.2	
1M stopping buffer	1.6mol glycine, 2mol sodium hydroxide, in 2L H2O, pH 10.2-10.4	Lysosomal enzyme activity assays
0.25M stopping buffer	IM stopping buffer diluted 1 in 4 with H2O, pH 10.2-10.4	
4MU standard	1nmol 4-methylumbelliferone (4MU), MWt 176, in 200µL H2O	

2.1.10 Western blotting

M-Per lysis buffer	Fisher (Loughborough, UK)
Halt protease inhibitor cocktail	Life (Paisley, UK)
Laemmli loading buffer	Sigma (Poole, UK)
4-12% Bis-Tris NuPage polyacrylamide gel	Life (Paisley, UK)
MOPS SDS running buffer	Life (Paisley, UK)
NuPage transfer buffer	Life (Paisley, UK)
PVDF membrane	Fisher (Loughborough, UK)
Methanol	Fisher (Loughborough, UK)
Tween 20	Sigma (Poole, UK)
Skimmed milk powder	Fisher (Loughborough, UK)
Phosphate buffer saline tablets	Fisher (Loughborough, UK)
Super signal West Pico chemiluminescent substrate;	Life (Paisley, UK)
Re-blot plus strong solution (stripping buffer)	Fisher (Loughborough, UK)

2.1.11 Antibodies

The antibodies used in this thesis are detailed in Table 2-4.

Table 2-4: Details of antibodies used

IgG antibody	Function	Raised in:	Dilution	Source
α-gal A (sc-25823)	Primary	Rabbit	1/200	Santa Cruz Biotechnology (Santa Cruz, USA)
NAGA (sc-367199)	Primary	Rabbit	1/200	
GAPDH (sc-25778)	Primary	Rabbit	1/600	
Anti-rabbit (sc-2313)	HRP-conjugated secondary	Donkey	1/7000	

2.2 Methods

2.2.1 Purification and measurement of plasmid DNA

A starter-culture of competent E. coli Stbl3 cells transformed with DNA plasmid *pRRLSIN.cPPT.PGK-GLA.WPRE* or *pRRLSIN.cPPT.PGK-GFP.WPRE* was incubated overnight on a shaker at 250rpm (Innova 44) at 37°C in 10mL LB broth, 0.1% ampicillin. Plasmid DNA was subsequently purified from 1mL starter-culture, using the QIAprep Spin Miniprep kit according to manufacturer's instructions, for approximate plasmid DNA yields of 100ng/µL H_2O. For larger-scale purification of plasmid DNA (approximately 1µg/µL H_2O), 5ml starter-culture was seeded into 500mL LB broth, 0.1% ampicillin, and incubated overnight as above. Plasmid DNA was extracted from the entire culture using the QIAGEN Plasmid Maxiprep kit according to manufacturer's instructions. The purity and yield of harvested DNA was measured using NanoDrop ND1000 spectrophotometer (LifeTech International).

2.2.2 Restriction enzyme digestion and gel electrophoresis

Approximately 1µg purified plasmid DNA, 1µL restriction enzyme and 10x restriction buffer were made up to 20µL with RNase-free water on ice and incubated at 37°C for 2 hours. The resulting DNA fragments were applied with 5x loading dye to 1% (w/v) agarose gel in TAE, 0.01% Sybr Safe DNA gel stain, and electrophoresed alongside 10µL 1kb Plus DNA ladder at 75volts for 1 hour. DNA fragments were visualised by exposure to ultraviolet light using the UVITech system. Fragment lengths were compared with those calculated from the theoretical nucleotide sequences using Vector NTI software (Invitrogen).

2.2.3 Sanger Sequencing

The complete DNA sequence of *pRRLSIN.cPPT.PGK-GLA.WPRE* was analysed by Sanger sequencing carried out by Source Biosciences (Cambridge, UK). The forward

and reverse primers were designed to ensure the entire length of the vector plasmid was accurately sequenced. The primer binding-sites were approximately located as shown in Figure 2-1. Table 2-5 details the sequence of primers which were ordered from Life Technology (Paisley, UK).

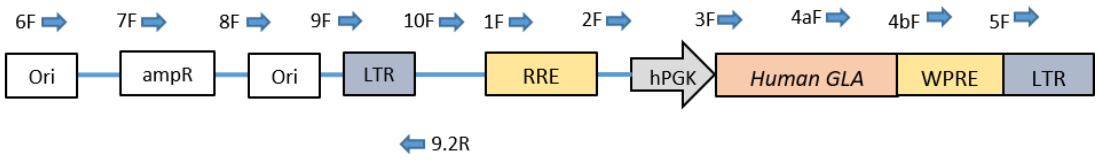

Figure 2-1: Primers and primer binding sites used for sequencing the lentivirus vector plasmid *pRRLSIN.cPPT.PGK-GLA.WPRE*

Table 2-5: Primer sequences used for sequencing the lentivirus vector plasmid *pRRLSIN.cPPT.PGK-GLA.WPRE*

Symbol	Primer Name	Oligo Sequence (5' – 3')	Designer
1F	pT7_01F	GTAAGACCACCGCACAGCA	Dr C Vink
2F	pT7_02F	AGGCAGGGATATTCACCATT	Dr C Vink
3F	pT7_03F	GTTCCGCATTCTGCAAGC	Dr C Vink
4aF	pRRL-gla4a	TGTGTACTCCTGTGAGTGGCCTC	J Lambert
4bF	pRRL-gla4b	ATGAGGAGTTGTGGCCCGTTG	J Lambert
5F	pT7_05F	GGCTAATTCACTCCCAACGA	Dr C Vink
6F	pT7_06F	GTAATAGCGAAGAGGCCCG	Dr C Vink
7F	pT7_07F	TGCTGAAGATCAGTTGGGTG	Dr C Vink
8F	pT7_08F	GCATTGGTAACTGTCAGACCAA	Dr C Vink
9F	pT7_09F	GAGCCTATGGAAAAACGCC	Dr C Vink
10F	pRRL-gla10	CCACTGAATTGCCGCATTGCAG	J Lambert
9.2R	pRRL-gla rev primer 9.2	CTCTCCTTCTAGCCTCCGCTAGTC	J Lambert

2.2.4 Cell Culture

HEK-293T and Hu-H7 cell-lines were grown in DMEM,10% FBS, 1% pen-strep. The cells formed an adherent monolayer so 0.05% trypsin in EDTA was used to dissociate the cells for passaging 1:10 whenever the cells were confluent. Jurkats were cultured in suspension in RPMI, 10% FBS, 1% pen-strep; and passaged 1:10 whenever the cells were confluent. All cells were grown by incubation in their relevant media at 37°C, 5% CO2.

2.2.5 Transfection of HEK-293T cells

HEK-293T cells were cultured to 80% confluence in T125 flasks. Vector plasmid DNA (*pRRLSIN.cPPT.PGK-GLA.WPRE* or *pRRLSIN.cPPT.PGK-GFP.WPRE*) and second-generation packaging constructs *pMDG.2* and *pCMVdR8.74,* were added to Opti-MEM in a 50mL centrifuge tube labelled solution A in the proportions shown in Table 2-6.

Table 2-6: Volumes required in solution A for transfection of HEK-293T cells

Content of solution A	Amount per T175 flask
Opti-MEM	5mL
Vector Plasmid DNA	40µg
pMDG.2	10µg
pCMVdR8.74	30µg

In a second 50mL tube labelled solution B: 5.5µl 10mM PEI was added to 27.5mL Opti-MEM. Both solutions A and B were passed through a separate 0.22µm filter and then combined and incubated at room temperature for 20 minutes to allow PEI-DNA complexes to form. To the culture media of each T125 flask, 10mL PEI-DNA complex was added and the HEK-293T cells incubated for 4 hours. The media was then removed from each flask and replaced with 18mL fresh culture media, and the cells

were incubated for 48 hours to produce lentivirus containing either *GLA* or *GFP*, depending on the vector plasmid co-transfected.

2.2.6 Harvesting of lentivirus

Culture media was collected from HEK-293T cells 48 hours post-transfection and centrifuged at 3,345 g for five minutes to remove cell debris, and the supernatant passed through 0.22µm filter. The filtrate was centrifuged at 71,793 g for 2 hours and supernatant removed and excess allowed to drain from the virus pellet. The virus pellet was suspended in 150µl Opti-MEM, incubated on ice for 20 minutes, and re-suspended before 30µl aliquots were prepared for storage at -80°C. Fresh culture media was added to the transfected HEK-293T cells before incubation for a further 24 hours to obtain a second harvest using the same protocol.

2.2.7 Cell counting

Cells in media suspension were stained with trypan blue solution at 1:1. A haemocytometer was loaded with 10µl cell-stain mixture and live and dead cells in four 0.1mm^3 grids were counted and labelled X. The number of cells per mL of suspension was calculated as:

$$= \frac{X}{4} \times 2 \times 10^4$$

2.2.8 Transduction of cells with lentivirus

Jurkats were transduced as follows: To each well of a 12-well plate 200,000 Jurkats were seeded in 1.5mL culture media with (10µL-1µL) lentivirus containing either *GLA* or *GFP*. The well plates were incubated for three days; after one day, a further 1.5mL fresh culture media was added to each well.

Human primary fibroblasts were transduced as follows: To each well of a 6-well plate 300,000 fibroblasts were seeded in 3mL culture media and incubated overnight to adhere to well base. Media was replaced with 1.5mL fresh media with (5µL-1µL) lentivirus containing *GLA*; after one day, a further 1.5mL fresh culture media was added to each well.

All cells were washed three times in DPBS to thoroughly remove virus before reseeding in fresh flasks for expansion before experiments.

2.2.9 Multiplicity of Infection

If the titre of the lentivirus suspension, defined as the number of infective plaque forming units (pfu)/mL, was already know, the exact volume of virus used, and the number of cells transduced, was chosen based upon the required multiplicity of infection (MOI) which is defined as the predicted pfu/cell:

$$MOI = \frac{virus\ titre \times volume\ of\ virus}{number\ of\ cells\ transduced}$$

2.2.10 Cell and media harvesting

When sufficient estimated cell volume for experiments was expanded in culture, media and cells were collected centrifuged at 832g for 10 minutes at 4°C. Media was harvested and placed on dry ice, and cells were washed in DPBS on ice three times. After final wash the cells were aliquoted in 200µL DPBS and placed on dry ice. Media and cells were stored at -20°C for experiments.

2.2.11 Quantitative polymerase chain reaction (qPCR)

Genomic DNA was extracted from cells transduced with lentivirus containing either *GLA* or *GFP* using the QIAGEN DNEasy blood and tissue kit according to manufacturer's instructions for cultured cells. Absolute quantification of lentivirus WPRE and genomic β-actin sequences were measured against a plasmid pBTW2L standard curve using the Bio-Rad c1000 Touch thermo-cycler. Amplification of β-actin and WPRE sequences were used to calculate cell number and viral copy number respectively using Bio-Rad CFX manager software. The reaction mixture in Table 2-7 was made in a 96-well plate and exposed to the following thermal cycle:

- 50°C for 2 minutes prevents carryover contamination using uracil-DNA glycosylase (UDG)
- 95°C for 10 minutes deactivates UDG;
- 95°C for 15 seconds double strand melt;
- 60°C for 1 minute primer annealing and DNA extension;
- Repeat 3-4 for forty cycles.

This method was used to measure the titre of virus suspensions and the actual number of viral genomes (vg) per cell in transduced cells, which may be different to the predicted MOI.

Table 2-7: Preparation of reaction mixture for real time PCR

	TaqMan Universal Master-mix (x2)	Fwd Primer	Rvs Primer	Probe (FAM reporter; TAMRA quencher)	Water	DNA Template	Total reaction mixture
Volume per reaction well (µL)	12.5	0.23	0.23	0.05	7.00	5.00	25.00

2.2.12 Cell lysis

Cells were thawed on ice, centrifuged at 600g for 10 minutes at 4°C. For Western blot, cells were re-suspended in 100µl M-Per lysis buffer containing Halt protease inhibitor cocktail (10µL/mL). Lysate was vortexed for 10 minutes, centrifuged at 16,200g for 15 minutes at 4°C, and supernatant collected and kept on ice. For lysosomal enzyme activity assays, cells were re-suspended in distilled H_2O and lysed by sonication using a Soniprep 150 for 10 seconds at 6µm amplitude. For mitochondrial enzyme activity assays, cells were exposed to three fast freeze-thaw cycles using dry ice in liquid nitrogen and 37°C water bath. Samples were vortexed between cycles.

2.2.13 Murine tissue homogenisation

Heart, kidney, liver, spleen, lung, brain and skeletal muscle organs were removed from four adult male wild type CD-1 mice. Organs were diced on ice and immediately stored at -20°C. Samples were homogenized in cold distilled H_2O using pre-chilled glass pestle and mortar, followed by three fast freeze-thaw cycles using dry ice in liquid nitrogen and 37°C water bath.

2.2.14 Measurement of protein concentration

Protein concentration in cell lysate or tissue homogenate were measured using the BCA method (Smith et al., 1985). Samples were diluted to two concentrations between 1/10 and 1/5 in distilled H_2O, final volume was 50µL. The protein standard (1mg/mL) was diluted to five concentrations between 1/10 and 1/1 in distilled H_2O up to 50µL final volume. Samples and standards were incubated with 1mL BCA at 37°C for ten minutes, and 20µL copper (II) sulphate solution for a further twenty minutes. The biuret reaction between protein and Cu2+ to form Cu1+ in alkaline solution was detected by absorbance of light at 562nm wavelength, due to interaction between BCA and Cu1+, using the Cecil 2040 spectrophotometer. An example standard curve is shown in Figure 2-2: Example calibration curve for the BCA protein assay.

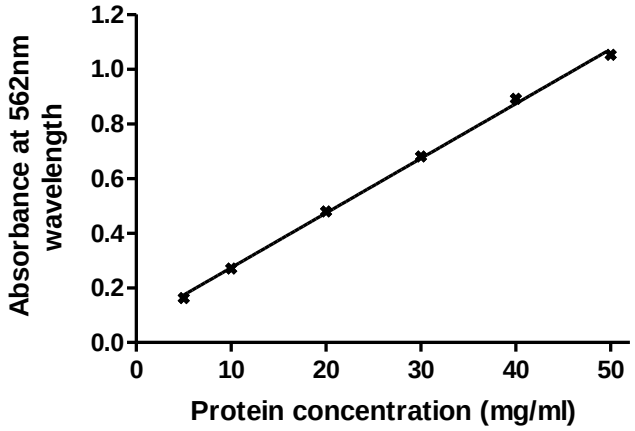

Figure 2-2: Example calibration curve for the BCA protein assay.
The curve was obtained using a standard containing 1mg/mL bovine serum albumin in water supplied by Sigma (Poole, UK). Absorbance of light at 562nm wavelength was detected using the Cecil 2040 spectrophotometer.

2.2.15 Western blot

2.2.15.1 SDS PAGE gel electrophoresis

A volume of supernatant containing 20µg protein was made to 20µl with H_2O and 5µl Laemmli loading buffer (x4) was added before incubating for 5 minutes at 95°C. The

sample proteins were electrophoresed in 4-12% Bis-Tris NuPAGE polyacrylamide gel with MOPS SDS (x20) running buffer at 150V for 1.5 hours.

2.2.15.2 Western blot

Phosphate buffered solution (PBS) was made up using PBS tablets according to manufacturer's instructions. Proteins were transferred onto PVDF blotting membrane with 5% NuPAGE transfer buffer, 10% methanol in H_2O at 25V for 1 hour. The membrane was blocked for 1 hour in milk solution (PBS, 5% milk powder, 0.1% Tween 20), washed in PBS, 0.1% Tween 20 three times for 10 minutes, and incubated overnight at 4°C in milk solution with primary antibody at relevant dilution (see 2.1.11). After further washing, the membrane was incubated at room temperature for 2 hours in milk solution with 0.014% anti-rabbit IgG horse radish peroxidase (HRP)-linked secondary antibody. Following further washing, target expression on the membrane was measured by detection of HRP using Pierce enhanced chemiluminescent Western blot substrate. The signal was detected photographically using UVI Chem software with wide aperture over a range of exposure times.

2.2.16 Total α-galactosidase and α-galactosidase A activity assays

2.2.16.1 In cultured cell lysate and tissue homogenate

Total α-galactosidase activity was measured using the synthetic substrate 4MUG (Donnai et al., 1981). Sample protein was diluted 1:1 with 20mM phosphate buffer pH 6.4, final protein concentration 0.3-0.4mg/mL. The sample solution (50µL) was mixed with 50µL 10mM 4MUG in 0.1M acetate buffer pH 4.5 (substrate solution) and incubated for 30 minutes at 37°C. The reaction products were galactose and 4-methylumbelliferone (4MU). Catalysis was stopped by addition of 1.1mL 0.25M stopping buffer which causes 4MU to fluoresce at 450nm following excitation at 365nm. Fluorescence was quantified using the Perkin Elmer LS55 fluorimeter calibrated against a 1nmol 4MU standard made up to 1.2mL with 0.25M stopping buffer. Enzyme activity was reported in nmol/hr/mg total protein.

The activity of α-galactosidase A was determined by two methods:

- The residual α-galactosidase activity of the B isoform was measured by incubating the sample solution for one hour at 50°C to heat-inactivate the A isoform prior to measuring enzyme activity as above (Beutler et al., 1973). Subtracting α-galactosidase B from total α-galactosidase activity determined α-galactosidase A activity.
- Activity of α-galactosidase A was measured directly by competitively inhibiting the B isoform with 200mM NAGA in the 4MUG substrate solution as above (Mayes et al., 1981)

2.2.16.2 In cell culture supernatant

Total α-galactosidase activity was measured using the method described by Morgan et al., 1990 for plasma α-galA (Morgan et al., 1990). Accordingly 100µL substrate solution (10mM 4MUG in 0.5M acetate buffer, pH 4.8) was added to100µL supernatant. To measure α-galactosidase A activity, the B isoform was competitively inhibited by adding 200mM NAGA to the substrate solution (Mayes et al., 1981). The supernatant/substrate mixture was incubated at 30°C for 2 hours and hydrolysis of 4MUG was stopped by addition of 1mL 1M stopping buffer which causes 4MU to fluoresce at 450nm following excitation at 365nm. Fluorescence was quantified using the Perkin Elmer LS55 fluorimeter calibrated against a 1nmol 4MU standard made up to 1.2mL with 0.25M stopping buffer. Enzyme activity was reported in nmol/hr/mL supernatant.

2.2.17 β-galactosidase activity assay in cultured cells

β-galactosidase activity was measured in cultured cells based upon the method described by (Young et al., 1987). Approximately 4-7µg sample protein was made up to 50µL with HSA/NaCl solution. The sample solution was added to 150µL 1mM 4-methylumbelliferyl-β-D-galactopyranoside dissolved in MV4.1 substrate solution. The mixture was incubated at 37°C for 15 minutes and hydrolysis was terminated immediately by adding 1mL 0.25M stopping buffer which causes 4MU to fluoresce at 450nm following excitation at 365nm. Fluorescence was quantified using the Perkin Elmer LS55 fluorimeter calibrated against a 1nmol 4MU standard made up to 1.2mL

with 0.25M stopping buffer. Enzyme activity was reported in nmol/hr/mg total protein.

2.2.18 Total β-Hexosaminidase activity assays

2.2.18.1 In cultured cell lysate and tissue homogenate

The method to measure total β-hexosaminidase activity was modified from (Brett et al., 1973). Sample containing 5µg protein was diluted in 500µL 0.2% (w/v) HSA in MV4.5. A substrate solution containing 3mM 4-methylumbelliferyl-2-acetamido-2-deoxy-β-D-glucopyranoside in MV4.5 was prepared. 100µL sample solution and 100µL substrate solution were mixed and incubated at 37°C for ten minutes. Hydrolysis was terminated immediately by adding 1mL 0.25M stopping buffer which causes 4MU to fluoresce at 450nm following excitation at 365nm. Fluorescence was quantified using the Perkin Elmer LS55 fluorimeter calibrated against a 1nmol 4MU standard made up to 1.2mL with 0.25M stopping buffer. Enzyme activity was reported in nmol/hr/mg total protein.

2.2.18.2 In cell culture supernatant

The method to measure total β-hexosaminidase activity was modified from (O'Brien et al., 1970). A reaction mixture containing 5µL supernatant, 95µL MV4.5 and 100µL 3mM 4-methylumbelliferyl-2-acetamido-2-deoxy-β-D-glucopyranoside in MV4.5 was incubated at 37°C for twenty minutes. The reaction was terminated by adding 1mL 0.25M stopping buffer which causes 4MU to fluoresce at 450nm following excitation at 365nm. Fluorescence was quantified using the Perkin Elmer LS55 fluorimeter calibrated against a 1nmol 4MU standard made up to 1.2mL with 0.25M stopping buffer. Enzyme activities were reported in nmol/hr/mL supernatant.

2.2.19 Citrate synthase activity assay

Citrate synthase activity was determined according to the method of Shepherd and Garland (1969) (Shepherd and Garland, 1969). The assay buffer was pre-warmed to 30°C. The volumes shown in Table 2-8 were added to spectrophotometer cuvettes.

Table 2-8: Volumes of reagents used in the citrate synthase assay

	Sample cuvette volume (µL)	Reference cuvette volume (µL)
Assay buffer	950	960
Sample cell lysate	20	20
Acetyl CoA	10	10
DTNB	10	10
Oxaloacetate	10	-

Citrate synthase in the sample protein catalyses:

acetyl coenzyme A + oxaloacetate → citric acid + CoA-SH

DTNB + CoA-SH → Thionitrobenzoic acid (TNB) + CoA-S-S-TNB

The reaction product TNB absorbs light at 412nm wavelength, so increase in absorbance per minute was measured using the Kontron Uvikon XL spectrophotometer over 5 minutes once reaction rate settled at 30°C. Enzyme activity (nmole/min/mL lysate) was calculated by Beer-Lambert's law using coefficient of absorption = 13.6 x 103 and light path length through sample = 1cm.

2.2.20 Respiratory chain complex I (NADH-ubiquinone oxidoreductase) activity assay

Complex I activity was assessed as described previously by Schapira et al. (1990) (Schapira et al., 1990). The assay buffer was pre-warm to 30°C. The volumes shown in Table 2-9 were added to spectrophotometer cuvettes.

Complex I oxidizes NADH and delivers an electron pair via iron-sulphur clusters to reduce ubiquinone. KCN inhibits complex IV, thereby preventing oxidation of ubiquinol by complex III. The cuvettes were warmed to 30°C in the Kontron Uvikon XL spectrophotometer before adding 10µL ubiquinone to the sample cuvette. Absorbance of light at 340nm wavelength was measured over five minutes once reaction rate settled. Non-complex I-catalyzed NADH oxidation was then isolated by addition of 20µL rotenone to the sample cuvette to inhibit reduction of ubiquinone. Absorbance at 340nm wavelength was subsequently measured over a further five minutes, after allowing 2-3 minutes for the rotenone to take effect. The difference between change in absorbance min-1 before and after rotenone treatment was proportional to NADH oxidation rate in the sample lysate. Enzyme activity (nmole/min/mL lysate) was calculated by Beer-Lambert's law using coefficient of absorption = 6.81 x 103 and light path length through sample = 1cm.

Table 2-9: Volumes of reagents used in the respiratory chain complex I activity assay

	Sample cuvette volume (µL)	Reference cuvette volume (µL)
Assay buffer	800	800
BSA	50	50
NADH	30	30
KCN	10	10
Sample cell lysate	20	20
H2O	80	90

2.2.21 Software

Electrophoresis gel images were processed with ImageJ 1.47v (National Institute of Health, USA). Statistical testing was performed using Prism 5.01v (GraphPad Software, USA).

2.2.22 Statistical analysis

Bar charts show mean value of replicates (n), with standard deviation (SD) indicated by error bars. Dot plots show mean value of n as horizontal lines. Scatter plots show single data-points unless otherwise stated. The n value is defined as the number of repeat, independent cell culture preparations analysed. In cell-toxicity experiments, the number of live and dead cells in each preparation was counted in duplicate. In enzyme assays, each preparation was measured in duplicate. Virus copy number of each preparation was measured in triplicate. Difference between two data-sets was analysed by Student's t-test; difference between three or more data-sets was measured by one-way analysis of variance (ANOVA) and Bonferroni's post hoc tests. Cell toxicity data was analysed by two-way ANOVA to take account of both duration of incubation and virus dosage. Scatter plots were analysed by linear regression (R^2) if significant correlation was found. In method comparison work, the mean linear regression slope and SD was reported. The effect of rotenone in cell cultures was analysed by comparison of mean linear regression slope and standard deviation using the Student's t-test. In all cases $P<0.05$ was considered to be significant. Before statistical analysis of percentage and ratio data, values were transformed:

$$\sin^{-1}\sqrt{\frac{percentage\ data}{100}}$$

Chapter 3 Characterisation of α galactosidase A

3.1 Introduction

3.1.1 Overall aim

The hallmark of Fabry disease is deficient activity of the lysosomal acid hydrolase α-gal A. Treatment is currently available, predominantly in the form of ERT but clinical response displays considerable variation across patients, tissue-types, age and disease severity (El Dib et al., 2016, Ortiz et al., 2016, Rombach et al., 2013). Alternative therapies are therefore urgently required. Since the condition is due to a loss of function, single gene mutation, it is a good candidate for gene therapy (Biffi, 2016, Friedmann and Roblin, 1972). Before the efficacy of *GLA* delivery to human cells can be explored, it is essential to baseline the characteristics of α-gal A activity in a range of wild-type cells and tissues. The enzyme distribution across tissue types may correlate with regions of substrate accumulation, clinical symptoms or response to ERT. This work will also enable identification of a suitable cell type in which to overexpress *GLA* in future experiment.

3.1.2 Laboratory methods

In vitro α-gal A hydrolyses synthetic substrates without the activator glycoprotein saposin B present (Hrebicek and Ledvinova, 2010). At least two synthetic substrates are available to measure α-gal A activity: a chromogenic assay is available using 4-Nitrophenyl α-D-galactopyranoside (4NPαGal); and a fluorometric assay using 4-methylumbelliferyl-α-D-galactopyranoside (4MUG). Absorbance-based assays are generally less sensitive compared with assays based on fluorescence (Motabar et al., 2010a), so here 4MUG was used according to the protocol described in Chapter 2 Materials and Methods (Donnai et al., 1981). Hydrolysis of 4MUG by α-gal A releases 4-methylumbelliferone (4MU) that fluoresces at a significantly different wavelength from the un-hydrolysed substrate after addition of alkaline buffer to stop the reaction. This allows the amount of 4MU produced to be measured in the presence of excess 4MUG; excess substrate is essential to ensure the enzyme operates at optimum activity over the period of time the assay is run. Fluorescence was measured relative to a 1nmol 4MU standard, and protein concentration of sample preparations determined by the BCA method, allowing enzyme activity to be reported in nmol/hr/mg total protein.

A-gal A shares residual α-galactosidase activity with the hydrolytic lysosomal enzyme α-N-acetyl-galactosaminidase (α-gal B). A-gal B is considered an isoenzyme of α-gal A because both are α-retaining galactosidases; but the primary function of α-gal B is hydrolysis of terminal N-acetylated saccharides (α-GalNAc) from glycolipids and glycoproteins such as N-acetyl-galactosamine (NAGA), and has distinct thermo-stability (Beutler et al., 1973, Dean and Sweeley, 1979a). There are at least two methods to distinguish α-gal A activity from total α-galacotosidase activity. Firstly, heat inactivation of α-gal A allows α-gal B activity to be measured and subtracted from total α-galactosidase activity to determine α-gal A activity for the following reason. Figure 3-1A shows the effect of incubation time at 45°C on α-galactosidase activity in human leucocytes. Fabry disease patients who lack functional α-gal A show no change in α-galactosidase activity, whereas healthy controls show a sharp drop in activity after one hour to the same level as in Fabry disease patients (Beutler and Kuhl, 1972). This illustrates that α-gal A is thermolabile and α-gal B is thermostable

after one hour at 45°C. Secondly, α-gal A activity can be measured directly by competitively inhibiting α-gal B using NAGA (Mayes et al., 1981). Figure 3-1B shows that α-galactosidase activity of isoform A is uninhibited, but that of isoform B is 94% inhibited, when assayed with 0.1M NAGA.

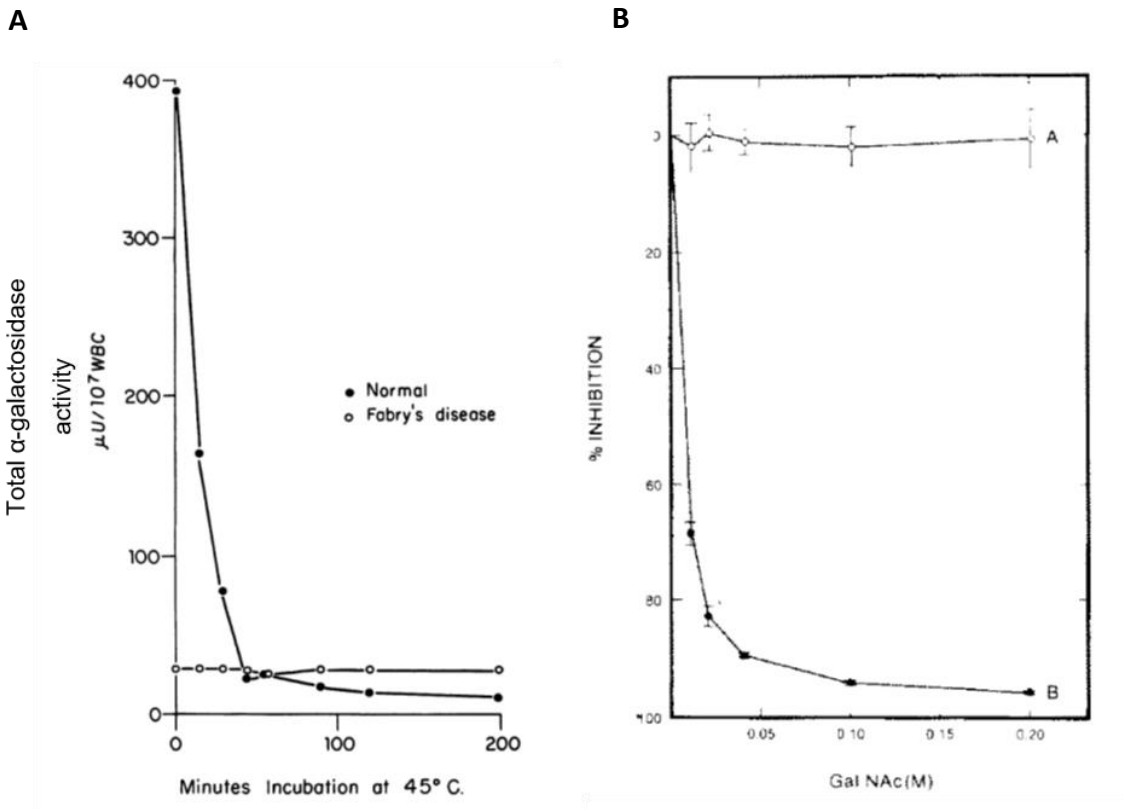

Figure 3-1: Evidence for two methods for distinguishing alpha galactosidase activity due to A and B isoforms

A. Total α-galactosidase activity in leucocytes of classic FD patient and normal control subject following incubation over a range of durations at 45°C, pH7. Enzyme activity in leucocytes from normal subjects fall to the level measured in FD patients after 45 minutes incubation, demonstrating that the deficient enzyme in FD, α-gal A, is thermolabile and that α-gal B, which exhibits the residual α-galactosidase activity, is thermostable at 45°C, pH7 (Beutler and Kuhl, 1972). **B.** Competitive inhibition of α-galactosidase activity in α-gal B (line B) by N-acetyl galactosamine (GalNAc). Optimum GalNAc concentration (0.1M) inhibits 94% of α-galactosidase activity in α-gal B. GalNAc does not inhibit α-gal A activity (line A) (Mayes et al., 1981).

Although α-gal B is unable to compensate for deficient α-gal A activity in patients, it is feasible that they may share in a common regulatory network, especially since they are thought to share a common ancestral gene (Tomasic et al., 2010). However, research to date does not typically report the contribution of α-gal B to total α-galactosidase activity; potentially overlooking valuable information that may throw light on the apparent lack of correlation between α-gal A activity, substrate accumulation, clinical picture and response to ERT.

In an attempt to take account of variation in lysosomal content between cell and tissue types, the ratio of activity of α-gal A was calculated against the activity of at least one other hydrolytic lysosomal enzyme. This is a similar concept to that used for measuring mitochondrial respiratory chain enzyme activities; values are usually reported as a ratio with citrate synthase activity for comparison across samples that may have different mitochondrial content.

The enzymes used were β-galactosidase and total β-hexosamindase. The normalised ratio of α-gal A activity was calculated as:

$$\frac{\text{α galactosidase A activity}}{activity\ of\ \beta galactosidase\ or\ total\ \beta\ hexosaminidase}$$

3.1.3 Human cells and plasma

The human cells listed in Table 3-1 were analysed for α-galactosidase and β-galactosidase activities. Cell-lines were selected for their potential susceptibility to pathology resulting from α-gal A deficiency, based upon their tissue of origin. Peripheral neurons, renal cells and both skin and heart fibroblasts are important sites of Gb3 accumulation in humans (Desnick et al., 2001). Only a low degree of storage is observed in hepatocytes, and liver involvement in symptoms is often absent (Elleder, 2010). Leucocyte α-gal A activity is commonly used for laboratory diagnosis (Gal et al., 2011). These cells are a potential target for therapeutic *GLA* delivered via *ex-vivo* HSC-based gene therapy, and may subsequently act as a factory for production and delivery of functional α-gal A to tissues via the vascular system (Medin et al., 1996, Takenaka et al., 1999a, Takenaka et al., 1999b). Plasma α-gal A is also used for laboratory diagnosis. In the present study, plasma was analysed from patients at GOSH (London, UK), with and without confirmed Fabry disease. This was in order to identify any difference between the two patient groups with regards to α-galactosidase activity of both A and B isoforms.

Table 3-1: Cell-line tissue of origin

Identity	Tissue of origin	Morphology
SH-SY5Y	Neuroblastoma cell line	Epithelial
293T	Adenovirus-transformed embryonic kidney cell line	Epithelial
Fibroblasts	Primary culture	Fibroblast
Jurkat	Lymphoblastic T cell leukaemia cell line	Lymphoblast
Hu-H7	Hepatocarcinoma cell line	Epithelial

3.1.4 Murine tissue

Human tissues other than skin fibroblasts are difficult to acquire, so in the present study samples of heart, kidney, liver, spleen, lung, brain and skeletal muscle were isolated from four adult male wild-type CD1 mice in order to characterise tissue distribution of α-gal A activity. These organs were selected based upon their differential involvement in the pathophysiology of Fabry disease. Cardiovascular, renal and cerebrovascular symptoms predominate, but respiratory disease and substrate accumulation in spleen and liver are also reported. In contrast skeletal muscle appears to have little if any involvement (Elleder, 2010, Germain, 2010).

3.1.5 Objectives

This chapter characterises α-galactosidase activity in human cells, murine tissues and human plasma through the following objectives:

- To establish and validate the α-gal A assay. Linearity of the assay was demonstrated over a range of incubation times and total protein content of samples. This defines the parameters within which subsequent experiments were conducted to ensure consistency of laboratory results;
- To validate the method to accurately distinguish the activity of α-gal A from total α-galactosidase activity in human cells. A-gal A activity measured over a range of concentrations by competitive inhibition was compared with α-gal A activity measured using heat inactivation;
- To check the α-gal A assay for murine tissues. A method to prepare murine tissue homogenate was optimised, and the level of agreement between heat inactivation and competitive inhibition methods to determine α-gal A activity was examined using murine heart tissue;
- To characterise α-galactosidase activity of A and B isoforms in a variety of human cells in order to baseline activity and select the cell type with the lowest α-gal A activity for future overexpression studies;
- To characterise the distribution of α-galactosidase activity of A and B isoforms in murine tissues. This work may help correlate the activity of these enzymes with disease phenotype;
- To characterise the endogenous α-galactosidase activity of α-gal A and B in human plasma from unaffected (control) patients and patients with Fabry disease.

3.2 Methods

The methods are as described in Chapter 2 Materials and Methods.

3.3 Validation of the α galactosidase A assay

3.3.1 Linearity over incubation time and sample protein content

The total α-galactosidase and α-gal A activity assays were as used in the diagnostic chemical pathology laboratory at GOSH, London, UK, and are fully validated according to UK Accreditation Service standard ISO 15189: 2012. It was necessary however to confirm a range of linearity of the assays with respect to incubation time at 37°C and total protein content of the enzymatic reaction for the specific purposes of this project. The source of protein chosen for this was the human T lymphoblastic leukaemia cell-line called Jurkat. Cells were lysed in water by sonication. The results showed that the amount of reaction product (4MUG) formed by a reaction mixture containing 20µg total protein increased linearly with incubation times from 20 to 50 minutes (Figure 3-2A). Similarly the amount of 4MUG formed in 20 minutes increased linearly in reaction mixtures containing 5 to 25µg total protein (Figure 3-2B). These data demonstrate the ranges over which the assay provides consistent results and are valid for all future investigations.

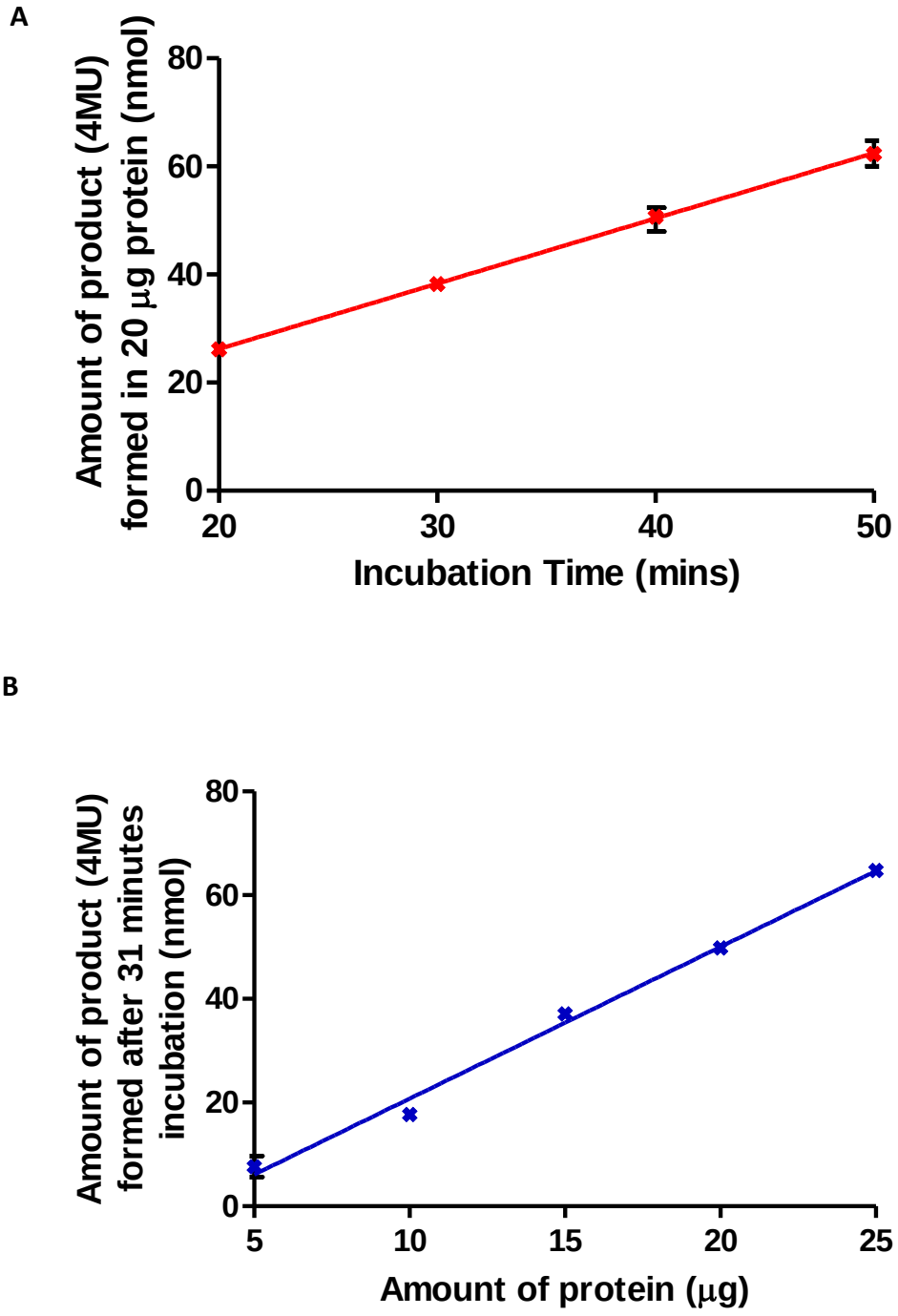

Figure 3-2: Linearity of alpha galactosidase assay determined using Jurkat homogenate

The linearity of the α-galactosidase assay was assessed in order to determine the range of total protein amount and incubation time that may be used in later experiments. Linearity was confirmed over a range of: (**A**) incubation times carried out in 20μg total protein, R^2=0.990 (P<0.0001, n=4); (**B**) amounts of total protein that were incubated for 31 minutes, R^2=0.991 (P<0.0001, n=4).

3.3.2 Limits of agreement between heat inactivation and competitive inhibition in human cells

A-gal A activity was distinguished from total α-galactosidase activity in Jurkat cells using the heat inactivation method at 50°C for 1 hour. A-gal A activity of the same samples were then measured directly by using the competitive inhibitor of α-gal B called N-acetyl-galactosamine (NAGA) at 0.05M, 0.1M and 0.5M concentrations. These concentrations were chosen based on the range over which α-gal B was at least 90% inhibited according to Figure 3-1. This was firstly to ascertain whether heat at 50°C for 1 hours was sufficient to fully inactivate α-gal A over a range of activity. Secondly it was important to confirm the concentration of inhibitor which best agreed with heat inactivation method. Figure 3-3A shows that, over the range of α-gal A activity measured, the relationship between methods is linear, suggesting that the heating protocol is sufficient to fully inactivate α-gal A. The slope with 95% confidence interval and linear regression R^2 values for all inhibitor concentrations assessed is shown in Figure 3-3B. Best agreement between methods is shown with 0.1M NAGA because the linear slope is closest to unity. Since assay pH is an important factor effecting enzyme activity, the effect of NAGA concentration was found not to influence the pH of the reaction mixture from 0.0 to 1.0M NAGA (n=4).

To confirm that competitive inhibition using 0.1M NAGA gave comparable α-gal A activity to the heat inactivation method, Figure 3-4 shows the level of agreement between the two methods using 0.05M, 0.1M and 0.5M competitive inhibitor concentrations by Bland and Altman plots. The dotted lines show ±2SD of the mean difference in α-gal A activity measured by the two methods. At 0.1M inhibitor concentration there is no bias between methods because the average difference in activity measured is close to zero, and there is no evidence of skewing of measurement below 2.5µmol/hr/mg protein. In comparison, at both 0.05M and 0.5M NAGA, the difference with heat inactivation increases with enzyme activity. Therefore competitive inhibition with 0.1M NAGA and heat inactivation methods provide comparable results for α-gal A activity in human Jurkat cells. Since Jurkat is a human cell-line, this result will be applied to all human cell types considered in future work.

A

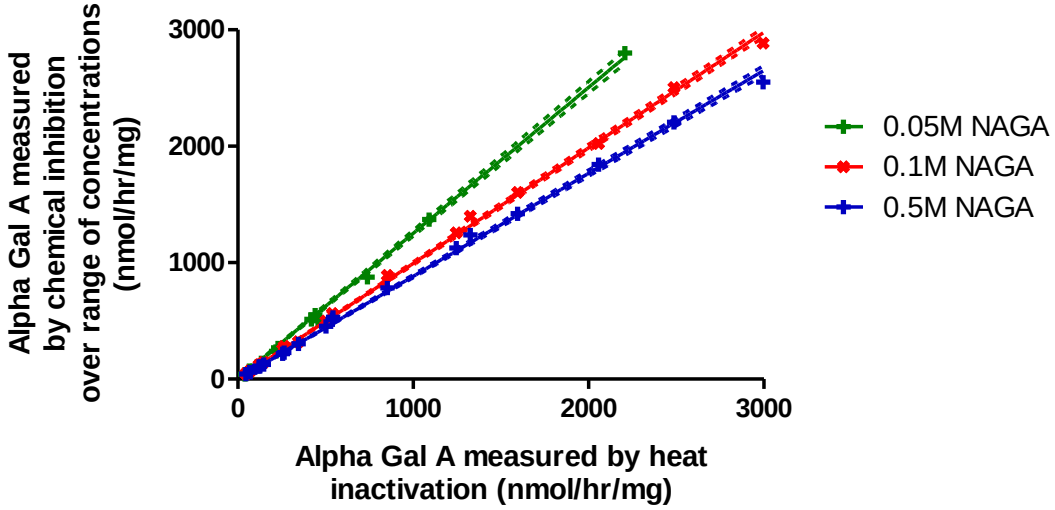

B

NAGA concentration (M)	Slope	R^2	95% confidence interval of slope
0.05M	1.252	0.999	1.227 to 1.278
0.1M	0.993	0.998	0.980 to 1.007
0.5M	0.884	0.998	0.870 to 0.897

C

Concentration of competitive inhibitor NAGA	0.0M	0.1M	1.0M
Alpha galactosidase assay pH	4.47±0.05	4.51±0.01	4.50±0.05

Figure 3-3: Comparison of methods to measure α-galactosidase A activity in human Jurkat cells

A range of enzyme activities were measured using both heat inactivation and competitive inhibition methods in order to confirm agreement over between methods. To check that inhibitor concentration over the range assessed did not affect assay pH and therefore enzyme activity, the pH of the assay was also measured. **(A)** Heat inactivation at 50°C for one hour was compared with competitive inhibition using N-acetylgalactosamine (NAGA) over a range of concentrations. Dotted lines show 95% confidence intervals. **(B)** Linear regression analysis was used to determine the slope of the line comparing heat inactivation with different inhibitor concentrations. The 95% confidence intervals show that the slope of the line comparing competitive inhibition method using 0.1M inhibitor with heat inactivation method crosses unity and therefore shows closest agreement ($P<0.0001$). **(C)** There was no statistical difference in assay pH with a range of competitive inhibitor concentrations (n=4)

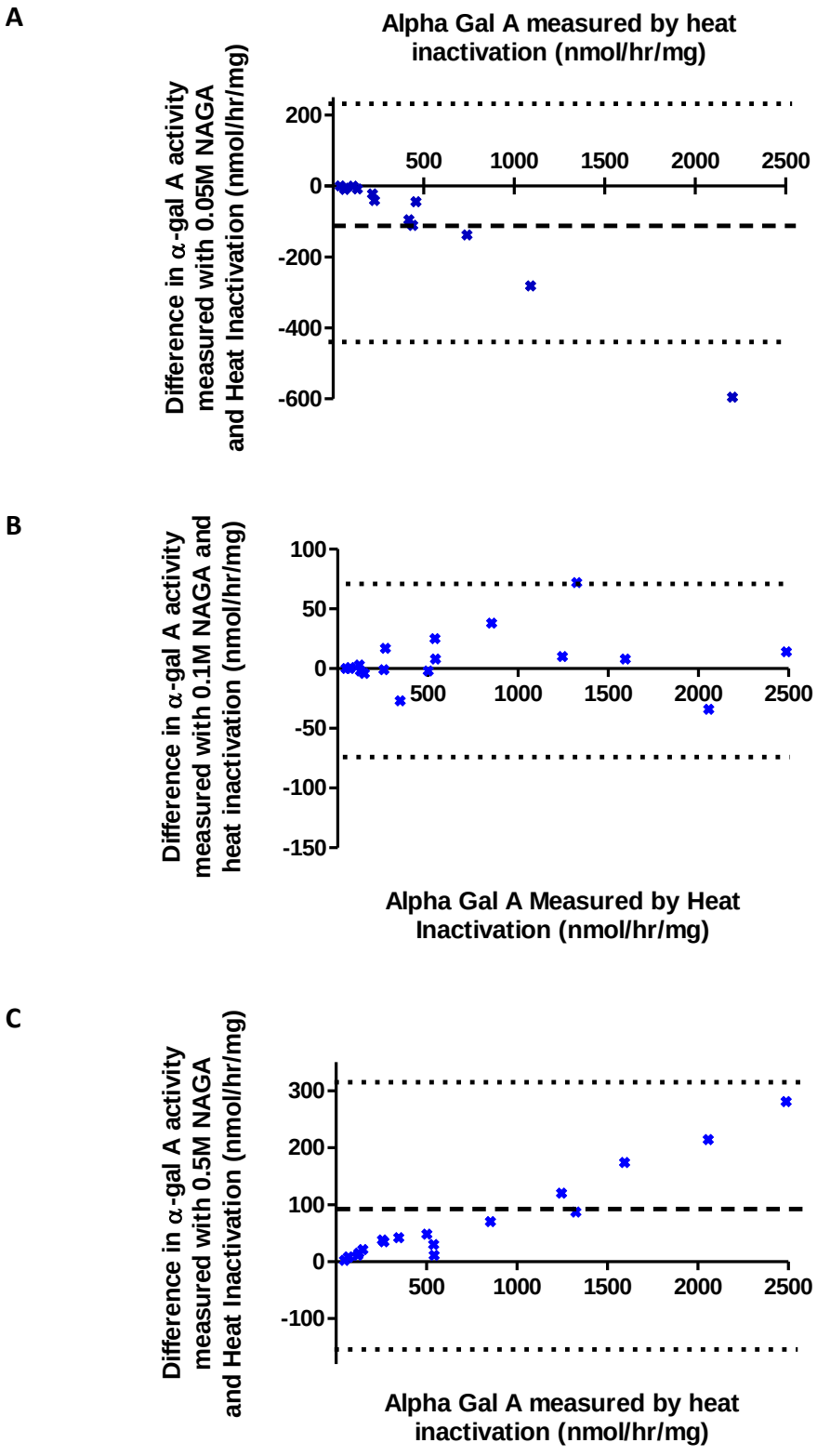

Figure 3-4: Levels of agreement between methods to determine alpha galactosidase A activity in human Jurkat cells.

Bland and Altman plots comparing heat inactivation and competitive inhibition over a range of inhibitor concentrations: **(A)** 0.05M; **(B)** 0.1M; **(C)** 0.5M. The wide dotted lines show mean difference, and the short dotted lines show 2SDs either side of mean.

3.3.3 Assessment of methods to homogenate murine tissues

The method of murine tissue homogenisation was selected based upon a preliminary experiment comparing total α-galactosidase activity measured in murine heart tissue. To be as consistent as possible between human cells and murine tissues, water was used in all tissue homogenisation methods considered as shown in the table within Figure 6. Manual grinding of samples using pestle and mortar followed by three cycles of fast freeze-thaw using dry-ice in methanol and 37°C water-bath released the highest total α-galactosidase activity (Figure 3-5A). This method was selected for preparation of all murine tissue samples.

To ensure that, in tissues with high enzyme content, total enzyme activity was not limited by substrate concentration at high protein concentrations, α-galactosidase activity was measured in 5% and 1% w/v homogenates of murine spleen samples. Previous research showed murine spleen had especially high α-galactosidase activity (Ohshima et al., 1999). Figure 3-5B shows there was no difference in enzyme activity measured in the two preparations, suggesting substrate concentration was not limiting activity in 5% compared with 1% w/v homogenates. So, it was decided to carry out all murine tissue analysis using homogenate with 5% w/v tissue in water in future experiments.

A.

Method	Detail
Water (man)	Grinding samples in H2O using glass pestle and mortar
Water (man) with PI	Grinding samples in H2O and protease inhibitor cocktail (Complete-mini, Roche) using glass pestle and mortar
Water (man) with fast freeze-thaw cycles	Grinding samples in H2O using glass pestle and mortar, followed by three fast freeze-thaw cycles

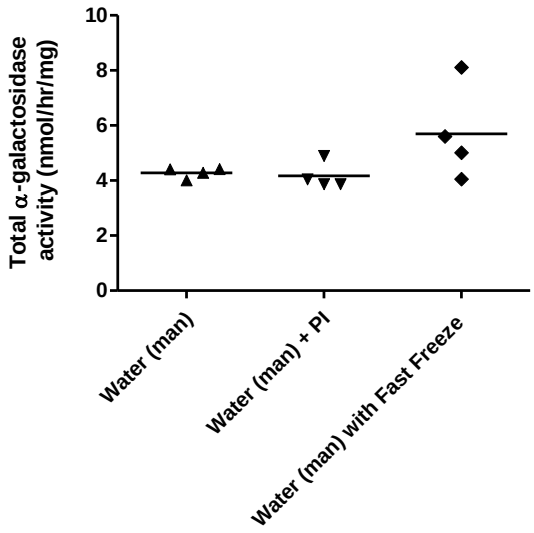

B.

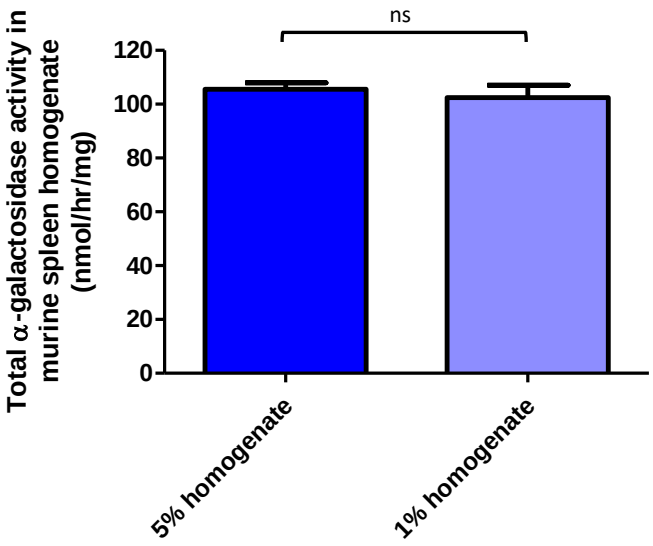

Figure 3-5: Optimisation of protein isolation for measurement of α-gal A activities in murine tissue samples.

(**A**) Total α-gal activity in murine heart using various tissue homogenisation methods detailed in table. PI: protease inhibitor. One-way ANOVA showed no statistical difference between methods, but water (man) with Fast freeze thaw cycles gave the highest yield of enzyme activity. (**B**) Mean total α-galactosidase activity measured in murine spleen using 5% and 1% w/v tissue homogenate in water. There was no statistical difference in mean enzyme activity between homogenates. Bar charts shown mean of four samples; error bars show SD.

3.3.4 Limits of agreement between heat inactivation and competitive inhibition in murine tissues

So far agreement was demonstrated between methods to distinguish α-gal A from total α-galactosidase activity in human cells only. To check whether agreement between competitive inhibition with 0.1M NAGA and heat inactivation holds true in murine tissue, both methods were used to determine α-gal A in murine tissues. Samples from all tissue types listed above were homogenised using the method established in the previous section. The results are compared in Figure 3-6, showing that they are inconsistent because the slope of the linear regression line in Figure 3-6A is considerably above unity. The Bland and Altman plot at Figure 3-6B shows competitive inhibition method directly measured α-gal A activity on average 16nmol/hr/mg higher than heat inactivation. At higher α-gal A activity the difference between methods increased above 2SD of the mean. Since competitive inhibition measures α-gal A activity directly, is therefore more accurate, and is the method predominantly used in the literature, murine tissues will be analysed using 0.1M NAGA.

In summary, the validation work gives license to use either heat inactivation or inhibition to measure α-gal A in human cells lysed by sonication in water, and human plasma. Consequently characterisation of α-gal A in a range of human cell types was carried out using the heat inactivation method. To be consistent, characterisation of α-gal A activity in murine tissues was measured using 0.1M NAGA to inhibit α-gal B using a water-based homogenisation protocol. All future assays used an amount of protein and incubation period within the linear range established herein.

A

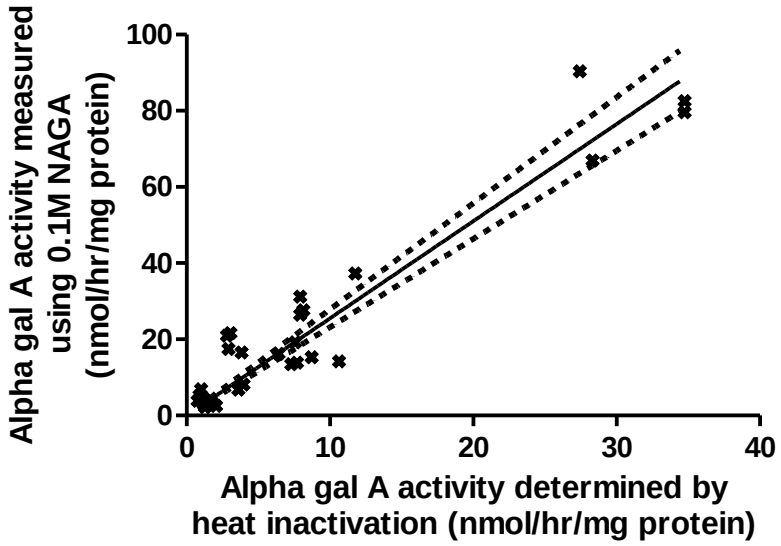

NAGA concentration (M)	Slope	95% confidence interval of slope
0.1M	2.551	2.317 to 2.785

B

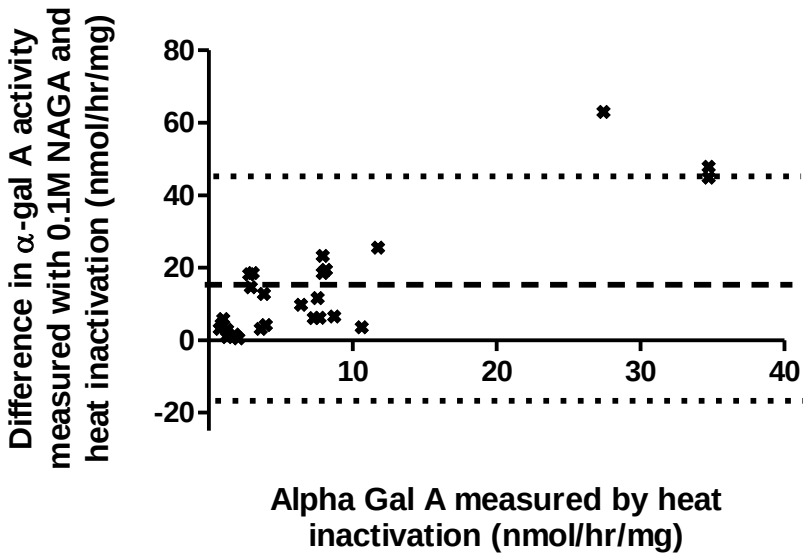

Figure 3-6: Comparison of methods to distinguish alpha galactosidase activity in murine tissues.

Comparison of methods to distinguish α-gal A from total α-galactosidase activity in murine tissues. (**A**) Dot plot of α-gal A activity measured using competitive inhibition (0.1M NAGA) against α-gal A calculated using the heat inactivation method. Table shows slope is significantly above unity. Linear regression R^2=0.911. Dotted lines show 95% confidence interval. (**B**) Bland and Altman plot shows level of agreement. Dotted lines show mean difference between methods ± 2SD.

3.4 Characterisation of α-gal A in human cell lines

The α-galactosidase activity in A and B isoforms were characterised in human cells listed in Table 3-1, using the heat inactivation method validated in the previous section. The purpose was to baseline activity and select the cell type with the lowest α-gal A activity for future overexpression studies. Figure 3-7A shows the distribution of α-gal A and α-gal B, and Jurkat (human T lymphoblastic leukaemia) cells display the lowest absolute α-gal A activity of all cell types examined. The inset table in Figure 3-7A shows mean and standard deviation of the percentage of total α-galactosidase activity due to isoform A. One-way analysis of variance performed on transformed percentage data identified that fibroblasts exhibit a significantly lower proportion of α-galactosidase activity due to isoform A compared with all other cell-lines tested ($P<0.0001$).

To correct α-gal A activity for variation in lysosomal content, β-galactosidase activity was also measured in all cell-lines (Figure 3-7B), and the normalised ratio of α-gal A to β-galactosidase activity was reported in Figure 3-8. Embryonic kidney 293Ts were the only cells exhibiting mean ratio of α-gal A to β-galactosidase activity greater than one; a statistical difference was observed in the transformed ratio across all the cell-lines ($P<0.05$).

The transformation applied to percentage and ratio data is given in Chapter 2 Materials and Methods.

A

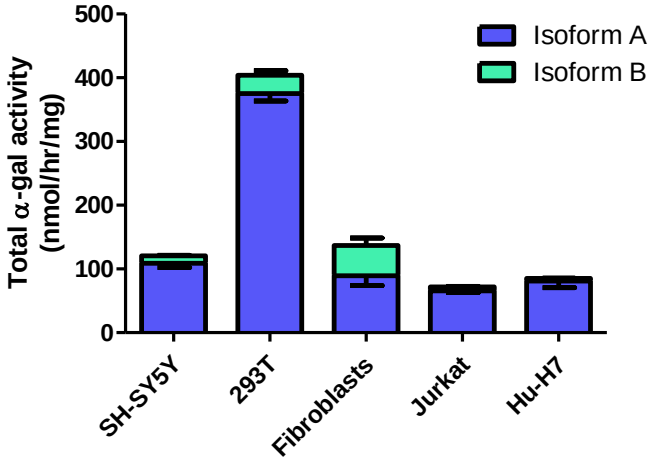

Cultured Cell Line	Mean percentage of total α-gal activity due to A isoform	
SH-SY5Y	90.4 ± 1.0	
293T	92.8 ± 1.5	
Fibroblasts	65.6 ± 3.4	***
Jurkat	91.2 ± 1.3	
Hu-H7	94.9 ± 0.5	

B

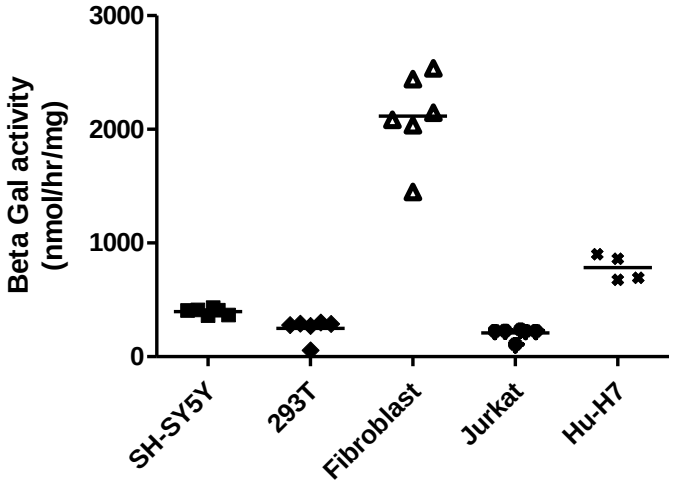

Figure 3-7: Activity of α-galactosidase A and B isoforms, and β-galactosidase, in a range of cultured human cell-lines (n=6)

A. Characterisation of α-galactosidase activity show the contribution of A and B isoforms to total α-galactosidase activity. Primary fibroblasts show significantly lower percentage contribution of A isoform compared to all other cell types measured after data was transformed (P<0.0001) (table inset). Survey of α-gal A activity showed 293T cells exhibit higher activity than all other cell types (P<0.0001). **B.** Survey of β-galactosidase activity in cell-lines.

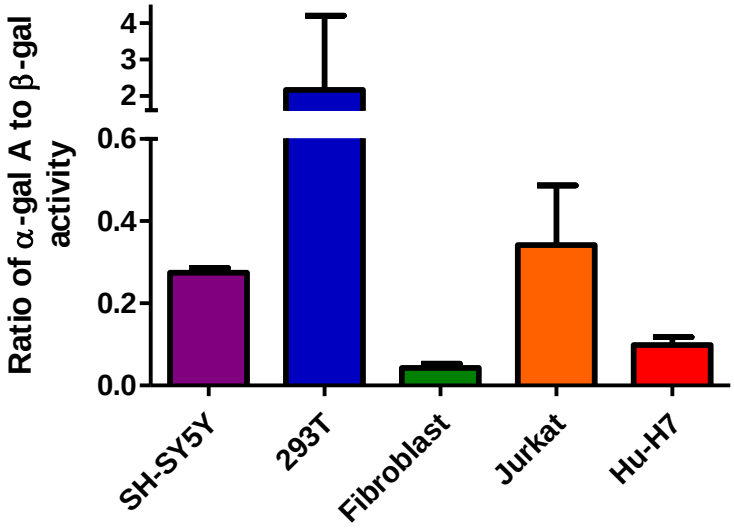

Figure 3-8: Alpha galactosidase A activity standardised for variation in lysosomal content using Beta galactosidase (n=6)

Ratio of α-gal A activity to β-galactosidase activity was calculated in an attempt to standardise α-gal A activity for variation in lysosomal content within the various cell-lines. The resulting survey showed significant difference in standardised activity between 293T and all other cell types assessed after data was transformed ($P<0.05$).

3.5 Characterisation of alpha gal A in murine tissues

To investigate any differences in activity between α-gal A and B isoforms in different tissues, heart, kidney, liver, spleen, lung, brain and skeletal muscle were isolated from four adult male CD1 wild type mice. The organs were selected based upon their differential involvement in the pathophysiology of Fabry disease. Consistent with the optimisation studies reported above, collected tissues were homogenised (5%w/v) in water using pestle and mortar and three fast freeze-thaw cycles. In line with previous research (Ohshima et al., 1999), the α-galactosidase activity of A and B isoforms was analysed using 0.1M NAGA to competitively inhibit α-gal B. The activity of two other lysosomal hydrolytic enzymes β-galactosidase and total β-hexosaminidase were also measured to confirm sample protein viability and to standardise α-gal A activity for variation in lysosomal size and content across samples and tissue types.

For each tissue type, the mean and standard deviation in enzyme activities of four mice are shown in Figure 3-9 and Figure 3-10. Up to three samples were measured from each mouse in duplicate and standard deviation was calculated from the mean of each mouse; variations within mice are not shown. In spleen, both α-gal A and B activity was significantly higher than in all other tissues analysed ($P<0.0001$). The percentage contribution of the A isoform to total α-galactosidase activity was highest in skeletal muscle ($P<0.0001$). The ratios of α-gal A activity against β-galactosidase and total β-hexosaminidase activity are shown in Figure 3-11. The ratio in skeletal muscle is significantly higher than in brain, liver, kidney and spleen using either of the standardising enzymes chosen. However, with β-galactosidase, the ratio in skeletal muscle is significantly higher than in all the other tissue types examined ($P<0.01$). Previous studies found skeletal muscle accumulate very little if any Gb3 resulting from α-gal A deficiency and display little, if any, pathological involvement in Fabry disease.

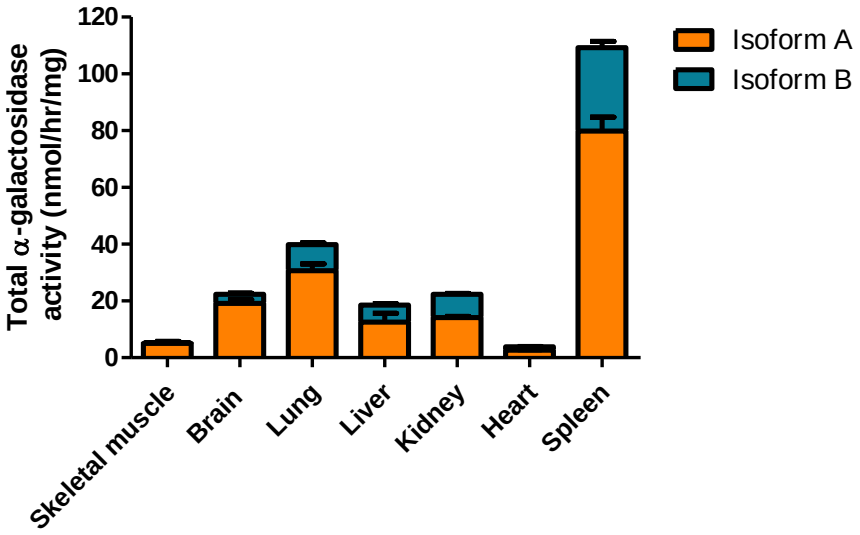

Murine Tissue	Mean percentage of total alpha gal activity due to A isoform	
Skeletal muscle	94 ± 3	
Brain	86 ± 4	
Lung	77 ± 2	***
Liver	68 ± 13	
Kidney	64 ± 2	
Heart	69 ± 6	
Spleen	73 ± 4	

Figure 3-9: Alpha-galactosidase activity in murine tissues (n=4)

The contributions of α-gal A and α-gal B to total α-galactosidase activity are shown. The heat inactivation method was used to distinguish the relative activity of A and B isoforms. One way ANOVA of activity of A and B isoforms across all the tissues analysed suggested that activity in spleen was significantly high ($P<0.0001$). The table inset shows the mean percentage of total activity due to the A isoform. One way ANOVA of transformed percentages showed that skeletal muscle contained significantly higher isoform A contribution to total α-galactosidase activity than in lung, liver, kidney, heart and spleen ($P<0.0001$).

A

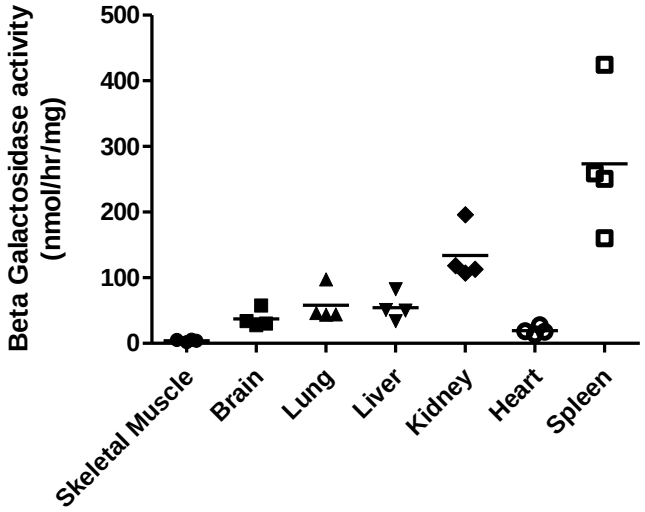

B

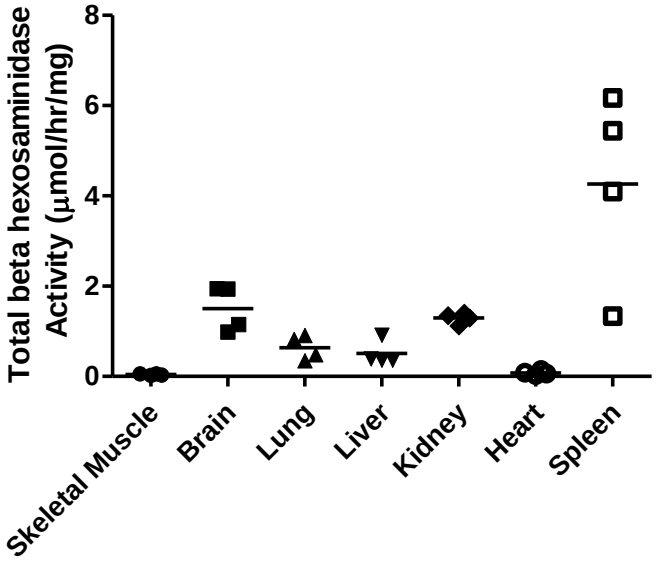

Figure 3-10: Activity of two additional hydrolytic lysosomal control enzymes in various murine tissues (n=4).

Two other enzymes involved in glycosphingolipid catabolism were measured in order to verify murine tissue sample viability and to standardise α-gal A activity for variations in lysosomal content of tissues. **(A)** β-galactosidase activity. **(B)** Total β-hexosaminidase activity.

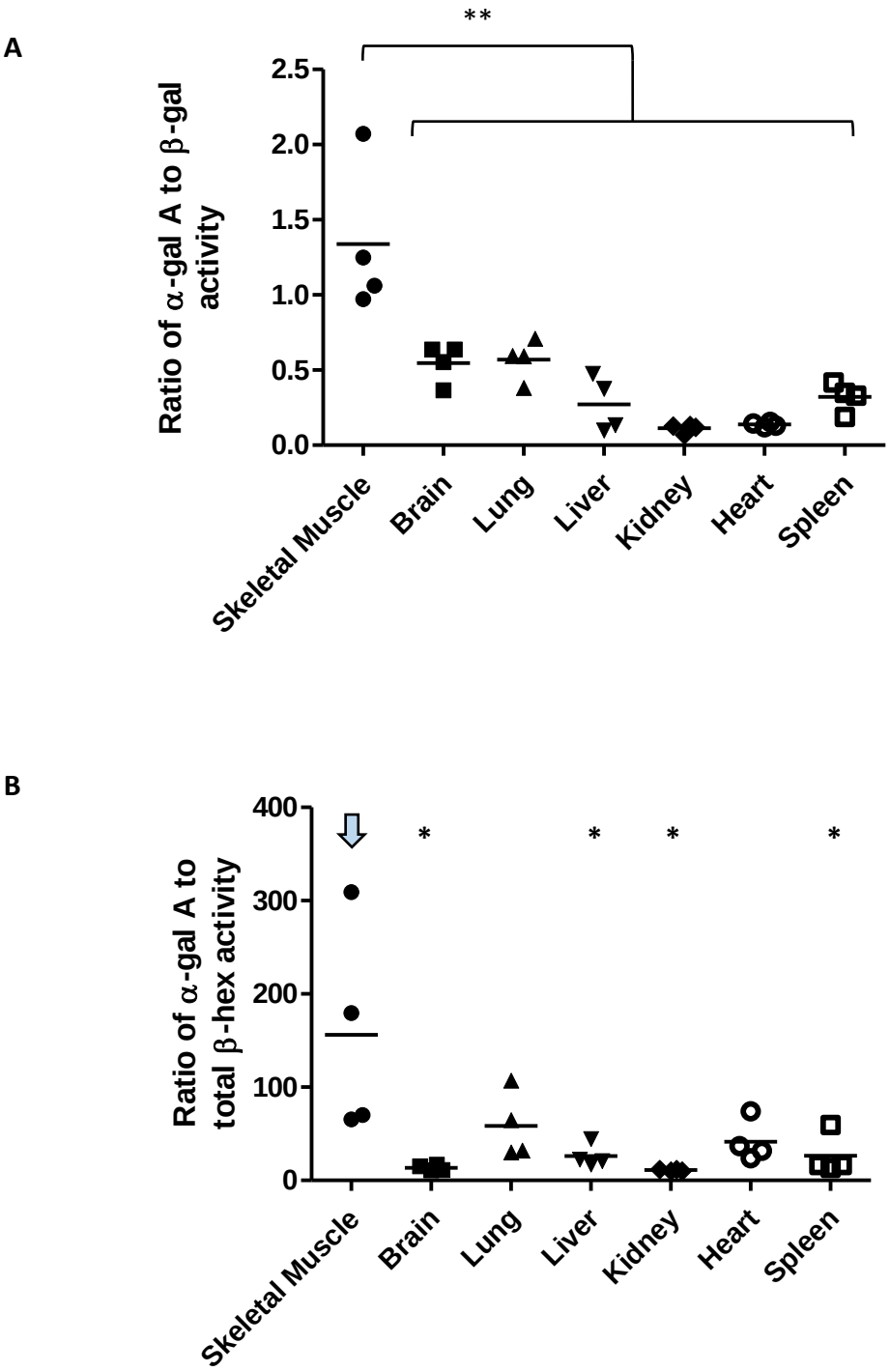

Figure 3-11: Ratio of α-gal A activity against the activity of two other lysosomal hydrolytic enzymes in various murine tissues (n=4)

Ratios were transformed before statistical analysis was performed. **(A)** β-galactosidase. There was significant difference between skeletal muscle and all other tissues types ($P<0.01$). **(B)** Total β-hexosaminidase. There was significant difference between skeletal muscle and brain, liver, kidney and spleen ($P<0.05$).

3.6 Characterisation of α-gal A in human plasma

To assess whether the α-galactosidase activity was able to differentiate between humans affected and unaffected by Fabry disease, α-gal A activity was measured in plasma from male patients at Great Ormond Street Hospital, London, UK, with and without Fabry disease. The α-galactosidase activity of A and B isoforms was determined using 0.1M NAGA to competitively inhibit α-gal B. This is consistent with the standard operational procedure employed within the ISO15189:2012 accredited Department of Chemical Pathology, GOSH (London, UK). Furthermore the validation work above showed this method gave α-gal A activity results comparable with the heat inactivation method, demonstrating a consistent approach across human cells and plasma.

Results in Figure 3-12 show a significant reduction in α-gal A activity, and a slight but significant reduction in α-gal B activity, in affected patients compared with unaffected patients. The inset table in Figure 3-12 compares the contribution of α-gal A to total α-galactosidase activity in affected and unaffected patients. Figure 3-13A shows there was no difference in total β-hexosaminidase activity between the two groups. Figure 3-14 show the standardised ratios of α-gal A and B against total β-hexosaminidase respectively.

To examine whether the observed drop in α-galactosidase activity of the B isoform was due to a change in enzyme expression or functionality, N-acetylgalactosaminidase activity was measured in the plasma samples. N-acetylgalactosaminidase is the dominant activity belonging to α-gal B, and Figure 3-13B shows no difference between the patient groups.

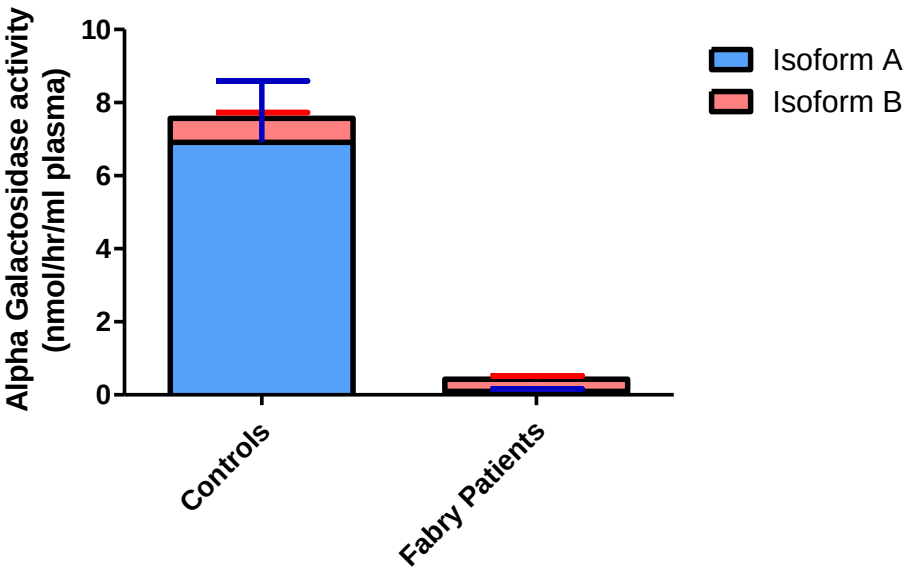

Cultured Cell Line	Mean percentage of total α-gal activity due to A isoform	
Fabry patients (n=5)	22.4 ± 12.5	***
Controls (n=10)	91.0 ± 2.0	

Figure 3-12: Characterisation of α-gal A in plasma of male Fabry patients naive to treatment and non-Fabry control patients.

Activity of isoforms A and B of α-galactosidase. Alpha gal A activity was significantly reduced in Fabry disease patients compared with controls (P<0.0001); isoform B activity reduced slightly but significantly (P<0.001). The table inset shows the mean percentage contribution of α-gal A to total α-galactosidase activity. There is a significant drop in the contribution of the A isoform in Fabry patients compared with controls (P<0.0001).

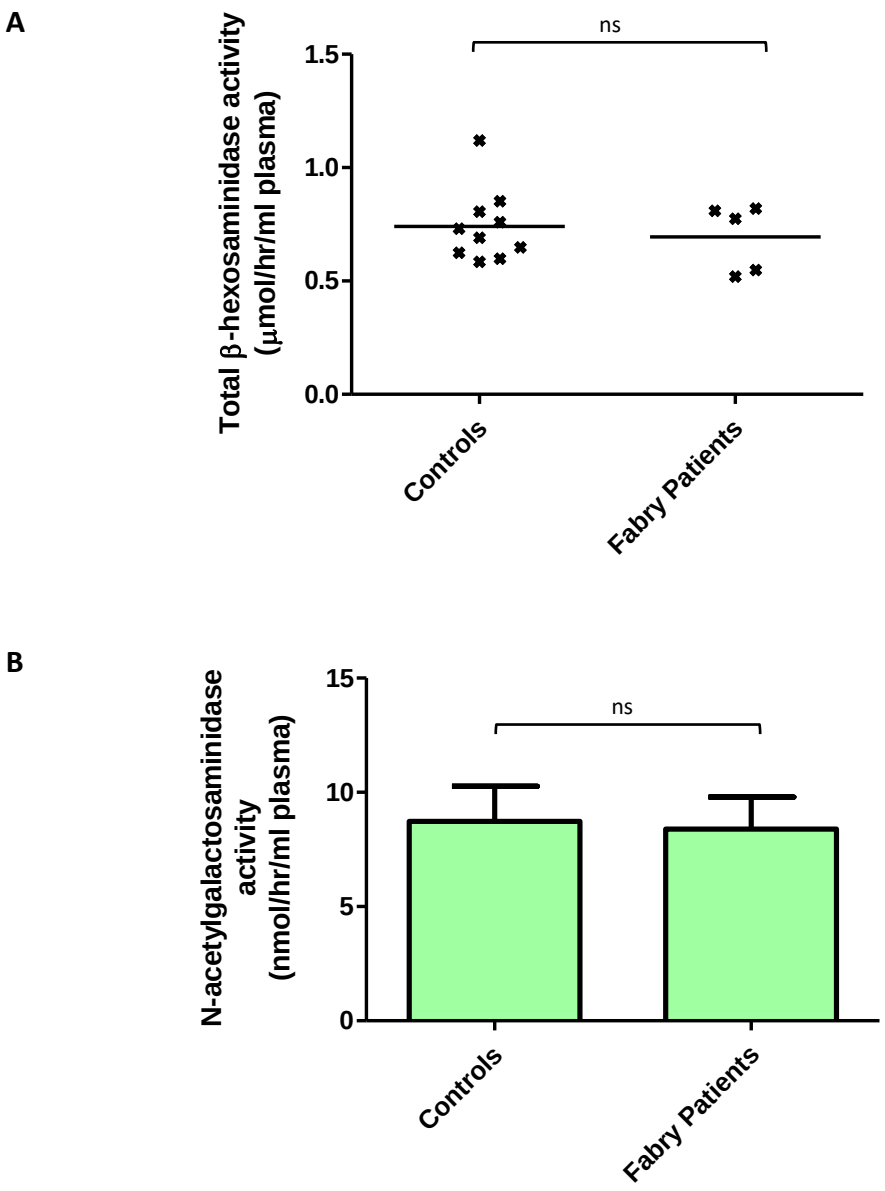

Figure 3-13: Characterisation of control lysosomal enzymes in plasma of Fabry patients naive to treatment.

The activity of two lysosomal hydrolytic enzymes were measured in order to confirm sample viability and to take account of variation in lysosomal content between patients and controls. There was no difference detected in either total β-hexosaminidase (**A**) or N-acetylgalactosaminidase (**B**) activity between the sample groups.

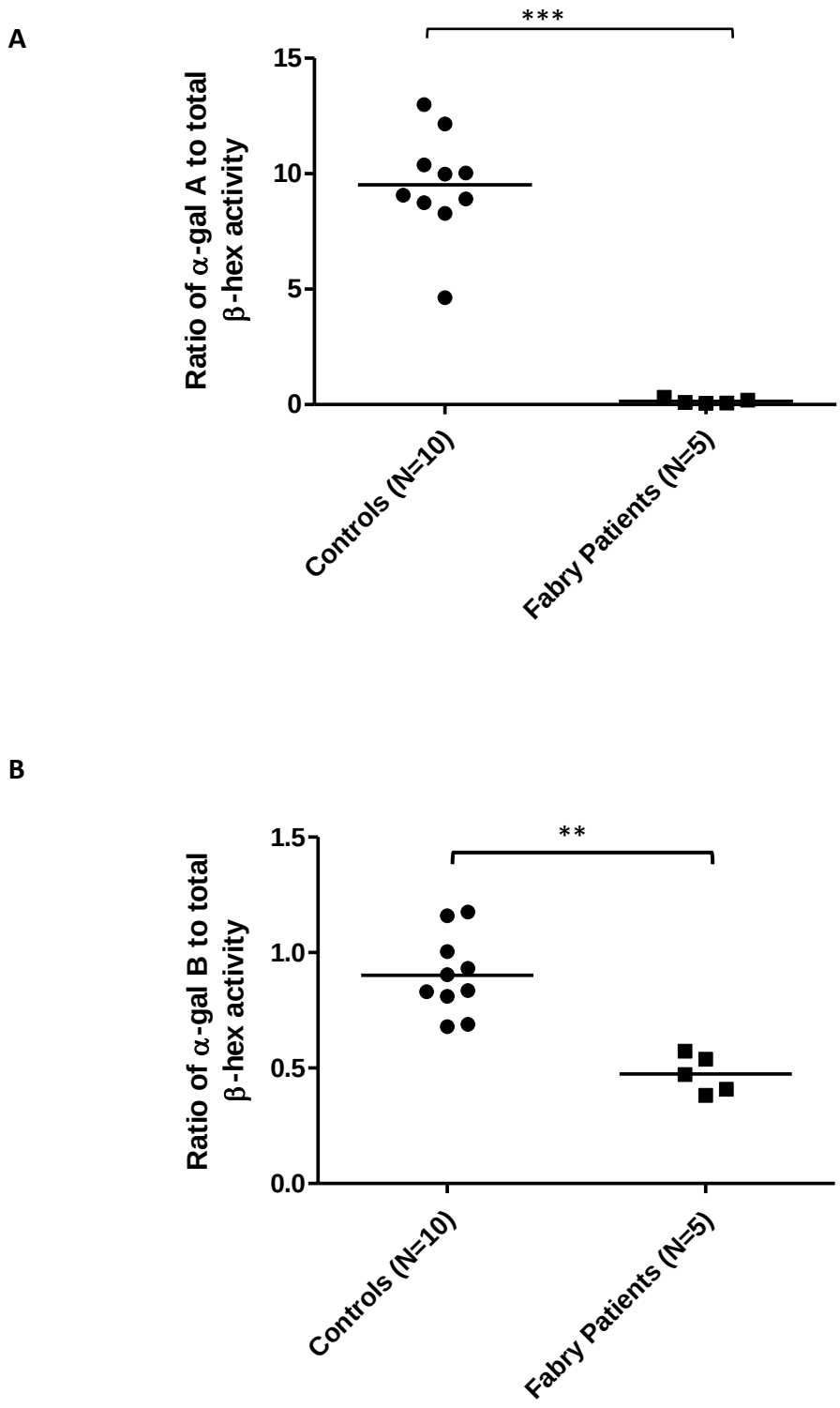

Figure 3-14: Characterisation of α-gal A standardised for variation in lysosomal content in plasma of Fabry patient naive to treatment.

Ratio of α-gal A and α-gal B activity to total β-hexosaminidase activity was calculated in an attempt to standardise α-gal A activity for variation in lysosomal content within patient and control plasma samples. **A**. There was highly significant difference in standardised α-gal A activity between patients and controls (P<0.0001). **B.** There was a significant difference in standardised α-gal B activity between patients and controls (P<0.001)

3.7 Conclusions

In this chapter, an α-gal A activity assay method was established and validated which is consistent across human cell and murine tissue types. Consistent with the range of linearity demonstrated in Figure 3-2 using human Jurkat cells as a source of protein, all measurements of enzyme activity in this thesis were carried out using 15µg total protein and 30 minutes incubation at 37°C. To differentiate α-gal A activity from total α-galactosidase activity, competitive inhibition (using 0.1M NAGA) and heat inactivation methods were compared. In human cells the methods gave consistent α-gal A results, using the Jurkat cell-line as a model (Figure 3-3 & Figure 3-4). However the methods were not consistent in murine tissues taken from wild type male CD1 adult mice (Figure 3-6). Consequently the heat inactivation method was used to determine α-gal A activity in all human cell types in this chapter, but in future chapters the competitive inhibition method using 0.1M NAGA was employed because the methods are consistent. In murine tissues the competitive inhibition method was used because it is the more accurate method and consistent with previous literature. Manual homogenisation of 5% (w/v) tissue in water with pestle and mortar, followed by three fast freeze-thaw cycles, was selected as the optimal sample preparation method prior to enzymatic assays (Figure 3-5).

Using the above established methods the activity of α-gal A and B enzymes were measured in human cell-lines originating from tissues known previously to have differential involvement in the pathophysiology of Fabry disease (Table 3-1). There was significant variation in α-gal A activity across the cell-lines (Figure 3-7A): lymphoblastic Jurkat cells exhibit low α-gal A activity relative to all other human cell-lines tested; and embryonic kidney 293T cells show significantly high α-gal A activity compared with Jurkat activity. The table within Figure 3-7A shows that the percentage of α-galactosidase activity due to the A isoform is significantly lower in primary fibroblasts than in all the other cell-lines tested. The relatively high contribution of the B isoform to total α-galactosidase activity in fibroblasts may be expected to result in resilience to Fabry disease in this cell type because α-gal B possesses some residual α-galactosidase activity and may be able to compensate for α-gal A deficiency. However there is no apparent evidence of resilience since

fibroblasts of both skin and heart accumulate Gb3 in Fabry disease patients (Elleder, 2010).

The inability of α-gal B to compensate for α-gal A deficiency is consistent with the literature (Hrebicek and Ledvinova, 2010). Alpha-gal B shares 49% sequence homology with α-gal A, with complete agreement in active site residues except within the 2-position recognition loop shown in Figure 3-15 (Garman and Garboczi, 2004). The enlarged space created by serine and alanine in α-gal B reduces its affinity with α-galactose (20-fold higher Km) compared with α-GalNAc. The smaller active site created by glutamate and leucine in α-gal A provides no affinity to α-GalNAc (Clark and Garman, 2009). (Tomasic et al., 2010), showed that through interconverting these active site residues they were able to increase enzyme specificity of α-gal B and α-gal A to α-galactose and α-GalNAc substrates respectively. So molecular engineering of autologous α-gal B within fibroblasts may represent an effective source of non-immunogenic ERT for Fabry disease patients (Germain, 2010)

The ratio of α-gal A activity against a second lysosomal enzyme, β-galactosidase, was used to standardise cell-line samples for variations in lysosomal content (Figure 3-8). Embryonic kidney 293T cells exhibited a significantly high ratio, and both neuroblastoma SH-SY5Y and lymphoblastic Jurkat cells were also raised compared with primary fibroblasts and hepatocarcinoma Hu-H7 cells. Possibly a high standardised ratio for α-gal A in tissues is a risk indicator for involvement in Fabry pathophysiology. One of the major organs effected by the disease is kidney (Lee et al., 2012, Sanchez-Nino et al., 2011, Thomaidis et al., 2009, Germain, 2010, Park et al., 2008, Shayman, 2010, Shu and Shayman, 2007); alterations in peripheral neurons due to lysoGb3 accumulation cause pain (Choi et al., 2015, Germain, 2010); and vascular involvement may be exacerbated by release of the accumulated substrate Gb3 from leukocytes (Germain, 2010, Park et al., 2008, Shayman, 2010, Shu and Shayman, 2007). In contrast fibroblasts and hepatocytes are less involved (Elleder, 2010). This hypothesis is limited because cell-lines often possess morphology different to that expected for the tissue of origin (Table 3-1).

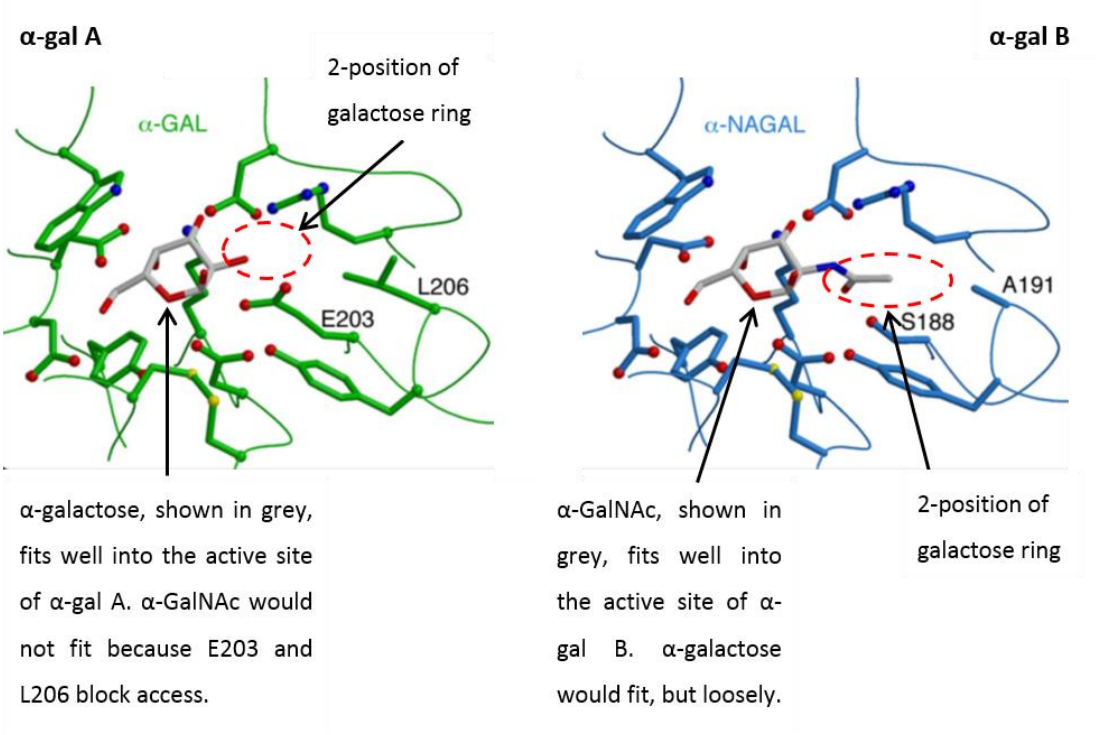

Figure 3-15: Topology of α-gal A and B active sites are designed for ligation with α-galactose and α-GalNAc respectively.

The two amino acids within the 2-position recognition loop are ringed by red dotted lines. Serine and alanine in α-gal B accommodate the N-acetyl group of α-GalNAc. They are replaced by the larger residues glutamate and leucine respectively in α-gal A which reach the hydroxyl group of α-galactose (Adapted from Tomasic et al, 2010).

To examine whether α-gal A activity in tissues is associated with their potential susceptibility to pathological processes involved in Fabry disease, various organs were removed from four wild type CD1 mice, processed and analysed according to the methods established above. The distribution across the tissues analysed was similar for all three lysosomal hydrolytic enzyme activities measured: total α-galactosidase, β-galactosidase and total β-hexosaminidase (Figure 3-9 and Figure 3-10). The spleen showed the highest activity, and the heart and skeletal muscle showed the lowest activities which is consistent with previous research (Ohshima et al., 1999). The relative percentage contribution of α-galA to total α-galactosidase activity does not correlate with absolute α-gal A: skeletal muscle shows the highest and heart, kidney and liver show the lowest percentage contributions. The ratio of α-gal A activity against β-galactosidase or total β-hexosaminidase was calculated to

standardise results for variation in lysosomal content. Results showed with both standardising enzymes that the highest ratio was observed in skeletal muscle (Figure 3-11) which is relatively unaffected by Gb3 accumulation compared with the other tissues assessed (Germain, 2010, Ohshima et al., 1999, Elleder, 2010). This suggests the ratio of α-gal A activity to either β-galactosidase or total β-hexosaminidase activity may be an important parameter correlated with tissue susceptibility to disease-associated pathological mechanisms. The results here appear to be the first evidence that normalisation of α-gal A activity for lysosomal content in tissues is necessary to assess risk of clinical involvement in Fabry disease.

Finally α-galactosidase activity was measured in male human plasma samples from Fabry disease and non-Fabry disease patient controls using the competitive inhibition method (0.1M NAGA). Alpha-gal A activity was almost absent in Fabry disease patients, significantly reduced from 7nmol/hr/mL plasma in controls (Figure 3-12 and Figure 3-14). The normal reference range used at GOSH (London, UK), is 4.0 – 21.9 nmol/hr/ml plasma. Alpha-gal B was significantly reduced by a small amount in Fabry disease patients compared with controls (Figure 3-12 and Figure 3-14), but only 22% of total α-galactosidase activity was due to α-gal A in disease patients compared to 91% in controls. Since only α-gal A and total α-galactosidase activities were actually measured, the result for α-gal B in the control group may be relatively inaccurate. Furthermore there was no difference in NAGA activity between Fabry disease patients and controls, suggesting the observed reduction in α-gal B was an artefact of experimental method (Figure 3-13B).

Together, the work in this chapter establishes the α-gal A activity assay and baselines the activity in a range of murine tissues, human cell-lines and plasma. Key findings suggest firstly that, whilst heat inactivation method is valid in human cell-lines, it is not valid in murine tissues; and secondly that the use of a second hydrolytic lysosomal enzyme against which to standardise α-gal A activity across tissue and cell types may provide data that correlates with involvement in the pathophysiology of Fabry disease. In murine tissues, the ratio of α-gal A to β-galactosidase activity was lower in brain, kidney and heart, relative to skeletal muscle, suggesting low ratio correlates with high risk of pathology in the event of α-gal A deficiency. In the human embryonic

kidney 293T cell-line, the standardised ratio was significantly high compared with other cell-lines assessed, suggesting high ratio correlates with high risk. Possibly the reversal in correlation explains why there is an absence of clinical symptoms of Fabry disease in *GLA*-deficient mice.

This chapter has shown that human T lymphoblastic Jurkat cells contain a relatively low baseline α-gal A activity. Looking forward, this cell-line will be used to overexpress *GLA* using a self-inactivating, third generation lentivirus vector, in order to explore the potential efficacy of gene delivery to treat Fabry disease.

Chapter 4 Efficacy of lentivirus-mediated *GLA* gene transfer on α-gal A activity in the Jurkat human cell line

4.1 Introduction

The work presented so far in this thesis establishes the methods for measuring α-gal A activity in various cell and tissue types and shows, amongst other findings, that in human plasma the activity of the enzyme is significantly reduced in patients with Fabry disease compared with controls. The underlying cause of this disorder is loss of function mutation affecting the single gene called *GLA*, leading to deficient α-gal A activity in nearly all cell types and extracellular space (Desnick et al., 2001). One potentially curative mode of treatment is delivery of the correct gene to patient cells, equipping them to manufacture endogenous α-gal A that may be subsequently trafficked to the lysosome to complete maturation and activation of the functional enzyme (Friedmann and Roblin, 1972, Ruiz de Garibay et al., 2013).

Lentivirus is a retrovirus able to integrate proviral DNA into a host cell genome for long term stable expression. The virus can target both dividing and non-dividing cells with high transduction efficiency. So lentivirus offers a potent method of gene delivery (Sakuma et al., 2012). Previously a lentivirus vector containing the cDNA sequence encoding mature human α-gal A was engineered and denoted *pRRL.cPPT.PGK-GLA.WPRE* (Rajaraman, 2013). The overall aim of this chapter is therefore to assess the potential catalytic efficacy of the viral α-gal A manufactured by cells transduced by the lentivirus produced by this vector. This is important because the ability of any future gene therapy regime for Fabry disease depends upon optimisation of gene dosage for maximal clearance of storage material (Huang et al., 2017).

In this chapter the structure of *pRRL.cPPT.PGK-GLA.WPRE* (Rajaraman, 2013) and the green fluorescent protein (GFP) control vector *pRRL.cPPT.PGK-GFP.WPRE* (UCL GOSICH, London, UK) were inspected using gel electrophoresis and sanger sequencing. Results were compared with the reference plasmid DNA sequence used in the Vector NTI software model built by Dr Conrad Vink (UCL GOSICH, London, UK).

The *GLA* transgene sequence included in this model was identical to that discovered by Bishop et al (1986) that codes for mature human α-gal A (Bishop et al., 1986).

The human lymphoblastic leukaemia cell line Jurkat contained the lowest α-gal A activity of cell types surveyed in the previous chapter and consequently may be considered a representative model of Fabry disease patient cells. Furthermore, patient leukocytes are routinely used to diagnose Fabry disease (Winchester, 2014), and represents the final target of *ex vivo* HSC-directed gene therapy (Penati et al., 2017). So Jurkat was selected as the target cell line on which to assess the functional effect of lentivirus-mediated *GLA* delivery by the structurally validated vector plasmids on lysosomal enzyme expression, activity and cell survival. Jurkats transduced with various doses of lentivirus throughout this thesis are termed as *GLA*-Jurkats.

The catalytic performance of α-gal A produced by both wild type and *GLA*-Jurkats are dependent upon the enzyme's structure and the identity of its substrate, given constant physiological temperature and pH. In investigating the efficacy of lentivirus-mediated gene delivery to overexpress α-gal A, it is therefore important to assess the enzymes performance through studying its kinetic characteristics. By comparing the kinetics of α-gal A from wild type and treated Jurkats the efficiency of gene therapy may be investigated (Voet et al., 2006).

The enzymatic reaction catalysed by enzyme *E* on substrate *S,* releasing product *P,* is shown below:

$$E + S \leftrightarrow ES \rightarrow E + P$$

The initial rate for this reaction (v_o) is described by the Michaelis-Menten equation:

$$v_o = \frac{v_{max}[S]}{K_m + [S]}$$

The equation assumes the enzyme kinetics are steady state such that the concentration of the enzyme-substrate intermediate (*ES*) is constant with respect to time. This assumption holds true only when there is a vast excess of substrate

compared with enzyme. Initial reaction rate applies until 10% of the substrate is hydrolysed, at which point the enzyme kinetics may be influenced by enzyme inactivation due to limited substrate, enzyme inhibition by the product or reversal of the reaction. The maximum initial rate of reaction (v_{max}) for a given amount of enzyme occurs when all active sites are occupied such that further increases in substrate concentration do not increase rate of product formation. Michaelis Constant (K_m) equates to the substrate concentration at which the initial reaction rate is half v_{max}. It is therefore indicative of the affinity of the enzyme to its substrate and a good measure of enzymatic efficiency. The lower the K_m the higher the affinity (Voet et al., 2006).

So to assess the efficiency of α-gal A to hydrolyse the synthetic substrate 4MUG, substrate saturation was analysed by plotting reaction rate against substrate concentration. The Michaelis-Menten equation was applied to the data points by the least-square best fit function, and v_{max} and K_m values were computed, using Prism 5 software, by extrapolation. However, due to the difficulty of accurately determining Vmax as substrate concentration tends to infinity, three different linear transformations were applied to the substrate saturation curve measured from wild type Jurkat cells to confirm the Km and Vmax values measured by Prism 5. These transformations are described under the methods section of this chapter.

In summary, the objectives of this chapter were to:

- Validate the genetic structure of the third generation lentivirus vector plasmids *pRRLSIN.cPPT.PGK-GLA.WPRE* and *pRRLSIN.cPPT.PGK-GFP.WPRE*.
- Harvest self-inactivating lentiviruses produced by a cell line containing the vector plasmids. Observe the functional effect of transduction by the viruses into Jurkat cells on α-gal A expression and activity.
- Explore the kinetic characteristics of intracellular α-gal A from wild type Jurkats and *GLA*-Jurkats for any differences in their affinity to the synthetic substrate 4MUG.

4.2 Methods

The materials and methods used were as described in Chapter 2 Materials and methods of this thesis with the following additions.

As established in the previous chapter, the intracellular activity of α-gal A was measured in human tissues with competitive inhibition using NAGA to isolate α-galactosidase activity of the A isoform from that of α-gal B. As in the previous chapter, β-galactosidase and total β-hexosaminidase activity were also measured in Jurkats as control lysosomal enzymes to confirm that infection of cells by engineered lentivirus was not causing pan-overexpression of lysosomal enzymes. In addition, intracellular N-acetyl galactosaminidase activity of α-gal B was also measured because of its residual ability to hydrolyse α-linked galactose from globo-series glycosphingolipids (Dean and Sweeley, 1979b). It was therefore necessary to check that over-activity of α-galactosidase was specifically due to increased α-gal A expression in response to *GLA* gene delivery alone, and not contributed to by α-gal B.

4.2.1 Protocol for intracellular N-acetyl galactosaminidase activity

N-acetyl galactosaminidase activity was measured in cultured Jukat cells using the synthetic substrate 4-methylumbelliferyl-α-N-acetyl-galactosaminide (4MU-α-GalNAc) (Chabas et al., 1994). Sample protein (1-3mg/mL in 10µL) was mixed with 20µL 6mM 4MU-α-GalNAc in McIlvaine citrate-phosphate pH 4.5 (MV4.5) and incubated for 30 minutes at 37°C. Catalysis was stopped by addition of 1.170mL 0.25M stopping buffer (see Chapter 2: Materials and Methods), which causes 4MU to fluoresce at 450nm following excitation at 365nm. Fluorescence was quantified using the Perkin Elmer LS55 fluorimeter calibrated against a 1nmol 4MU standard made up to 1.2mL with 0.25M stopping buffer. Enzyme activity was reported in nmol/hr/mg total protein.

4.2.2 Substrate saturation curve methodology

Firstly the double reciprocal of the Michaelis-Menten equation gave the Lineweaver-Burk plot:

$$\frac{1}{v_o} = \frac{1}{v_{max}} + \frac{K_m}{v_{max}}\left(\frac{1}{[S]}\right)$$

The linear slope equals K_m/v_{max} and the line intersects the y axis at $1/v_{max}$. The limitation of this plot is that it places more weight on lower substrate concentrations and reaction rates which are inherently less accurate (Voet et al., 2006). The second transformation produces the Eadie-Hofstee plot:

$$v_o = v_{max} - K_m\left(\frac{v_o}{[S]}\right)$$

The linear slope equals $-K_m$ and the y axis intersect equals v_{max}, but the method enhances error in reaction rate (Voet et al., 2006). The last transformation produces the Hanes plot:

$$\frac{[S]}{v_o} = \frac{K_m}{v_{max}} + \left(\frac{1}{v_{max}}\right)[S]$$

Since substrate concentration is a factor on both x and y axes this method enhances inaccuracies which may occur due to pipetting errors (Voet et al., 2006). By comparing all three linear transformation methods with the extrapolation method used by Prism 5, the limitations of each method are taken into account.

4.3 Structural validation of lentivirus vectors containing *GLA* and *GFP*

Plasmid DNA was extracted from cultured STBL3 bacteria transformed with either *pRRL.cPPT.PGK-GLA.WPRE* or *pRRL.cPPT.PGK-GFP.WPRE* lentiviral plasmids. Restriction digest analysis compared fragment lengths with the reference sequence held on VectorNTI courtesy of Dr Conrad Vink (UCL GOSICH, London, UK) (Figure 4-1). Positions at which *Hin*dIII was predicted to cut the *GLA* lentiviral plasmid are shown in Figure 4-1C with reference to the structure shown in Figure 4-2. In both plasmids, the transgenes are contained within the second largest fragments, and so the results suggest both are approximately correct. However, within the *GLA* lentiviral plasmid there appears to be a large insert between the 3' LTR at position 2114 and just upstream of 5' LTR at position 5455.

To investigate the apparent insert further, the entire *pRRL.cPPT.PGK-GLA.WPRE* plasmid was sequenced. The resulting sequence was aligned with the reference plasmid model using Vector NTI software and mutations were identified at the positions shown in Figure 4-2. Additional sequencing was performed using plasmid DNA of *pRRL.cPPT.PGK-GFP.WPRE* to confirm whether the unexpected nucleotide differences in Figure 4-2 were also present in the *GFP* plasmid; results showed that all mutations were present except the 777 base insertion at position 5402, a finding consistent with the restriction digest results in Figure 4-1.

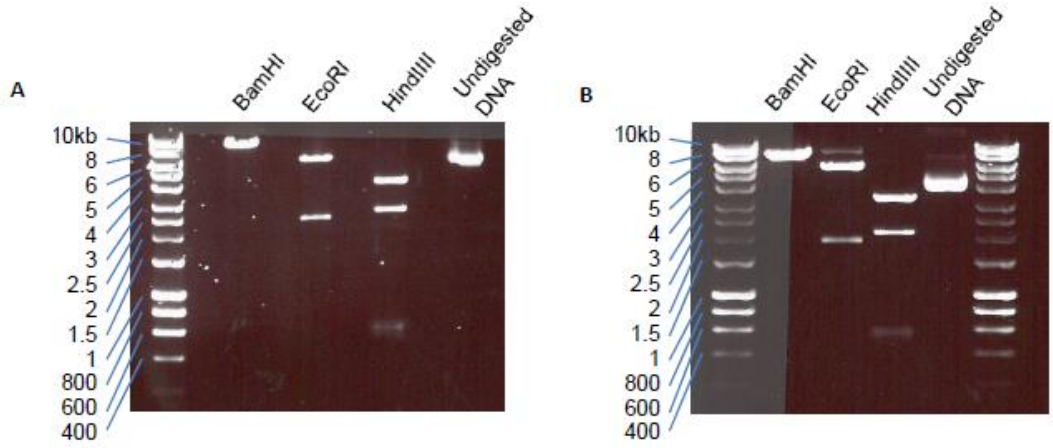

C

pRRL.cPPT.PGK-GLA.WPRE		pRRL.cPPT.PGK-GFP.WPRE
Fragment Position according to plasmid model	*Fragment length expected after HindIII digest*	*Fragment length expected after HindIII digest*
2114 – 5455	3341	3341
7407 – 2114	2648	2096
6324 - 6908	584	584
5768 - 6324	556	556
6908 - 7407	499	499
5455 - 5768	313	313

Figure 4-1: Gel electrophoresis of vector plasmid fragments following restriction digest

Gel electrophoresis of restriction digested plasmid DNA. (**A**) Plasmid *pRRL.cPPT.PGK-GLA.WPRE* was longer than expected according to the plasmid model, as shown by the largest fragment in the table. (**B**) Plasmid *pRRL.cPPT.PGK-GFP.WPRE* fragment sizes approximately agree with those expected. (**C**) Table show expected fragment lengths in number of nucleotide bases.

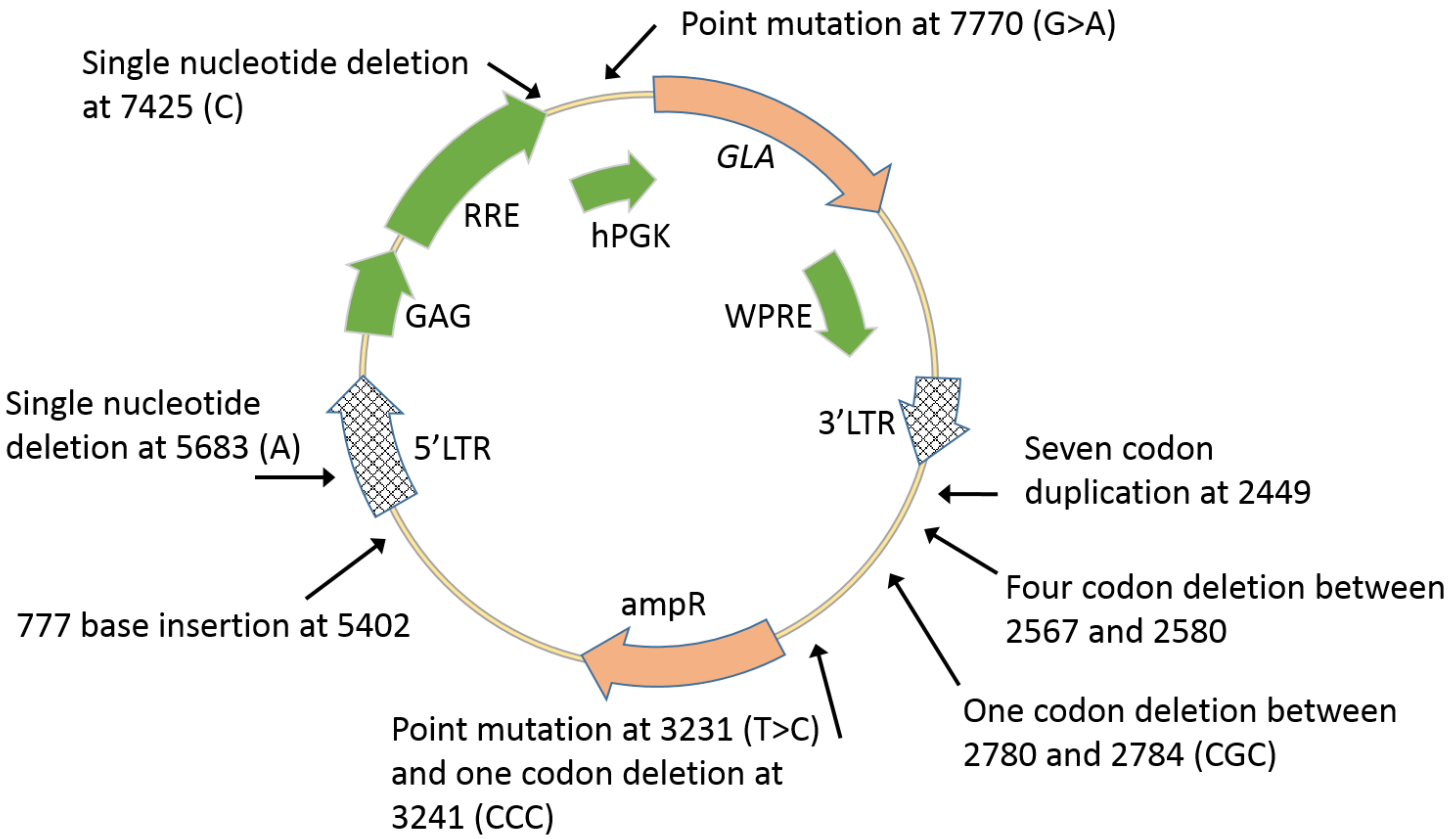

Figure 4-2: Location of mutations within the vector plasmid containing the *GLA* transgene

The mutations in the vector plasmids containing both *GLA* and *GFP* transgenes were found using restriction digest followed by SDS-PAGE and gene sequencing (Source Biosciences). The mutations in plasmid *pRRL.cPPT.PGK-GLA.WPRE* are shown with reference to the plasmid model. All mutations except the 777 base insertion at position 5402 were also present in plasmid *pRRL.cPPT.PGK-GFP.WPRE.*

4.4 Functional validation of the *GLA* lentivirus vector in the Jurkat human cell line

4.4.1 Dose-dependent over-expression and over-activity of α-gal A

To find out whether the mutations within the *pRRL.cPPT.PGK-GLA.WPRE* and *pRRL.cPPT.PGK-GFP.WPRE* DNA sequences were functionally deleterious, the plasmids were transfected, together with second generation packaging plasmids shown in Figure 1-18, into HEK-293T cells. The cells released self-inactivating lentivirus which was subsequently harvested, concentrated and the viral titre was measured to be 2.80×10^7 plaque forming units (pfu)/mL obtained in Jurkat cells using qPCR. In the previous chapter, the Jurkat human cell line was found to have low endogenous α-gal A activity relative to other human cell-types examined. Hence this cell line was transduced with various doses of lentivirus containing the *GLA* vector sequence within their transcriptome.

The level of expression of α-gal A and α-gal B was examined by Western blot as shown in Figure 4-3. The result showed that endogenous levels of both enzymes were undetectable, and expression of the A isoform, detected at approximately 50kDa, increased dependent upon the virus dose. A-gal B expression remained undetectable at the expected molecular size of 47kDa up to 0.45 virus genomes (vg)/cell. To ensure that the primary antibodies against the endogenous human enzymes were functional, strong expression of α-gal A was detected in untransduced HEK-293T cells as expected from characterisation of enzyme activity in Chapter 3. The positive control used by the manufacturers of the antibody to α-gal B was the human epidermoid carcinoma cell line A431. The expression of α-gal B in A431 cell homogenate shown in Figure 4-3 confirms that antibody was detecting the enzyme correctly, confirming that α-gal B expression was not influenced by *GLA*-overexpression.

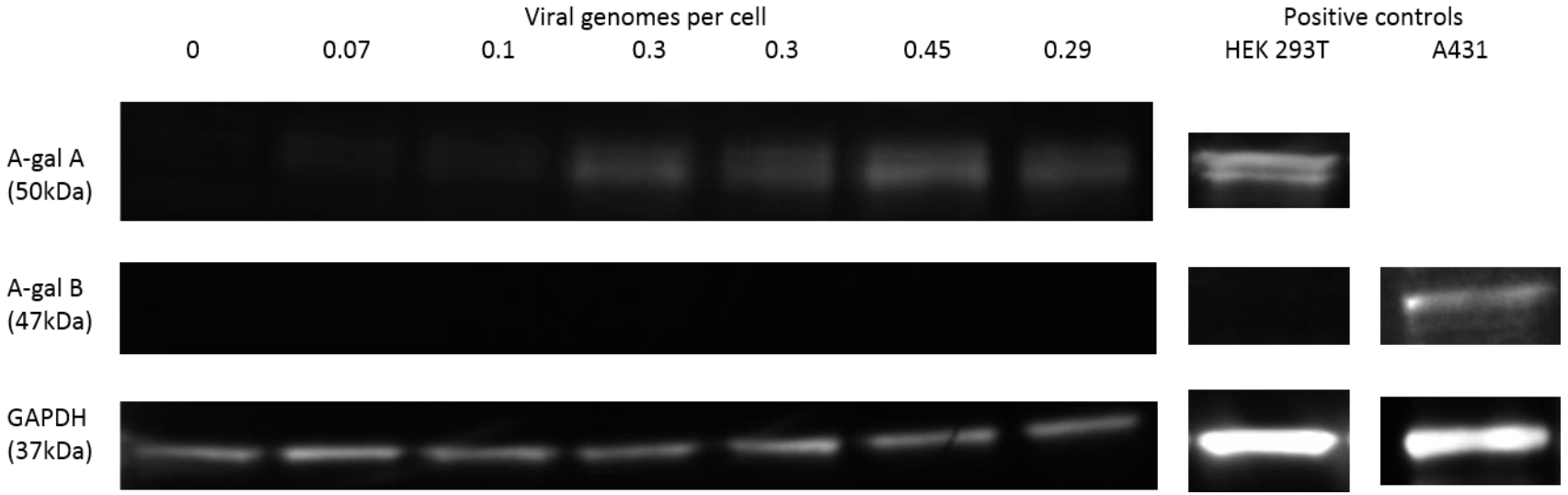

Figure 4-3: Western blot analysis of α-galactosidase isozymes A and B in total protein from *GLA*-Jurkats.

Alpha galactosidase A (α-gal A) expression was undetectable in wild type Jurkats but increased slightly in *GLA*-Jurkats dependent upon viral dose. Alpha galactosidase B (α-gal B) expression was undetectable in both wild-type and *GLA*-Jurkats. To show that the anti-α-gal A and anti-α-gal B antibodies were functioning correctly, a moderate expression is demonstrated in 293T cells and A431 cells respectively; the cell types were used as positive control by manufactures. Glyceraldehyde-6-phophate dehydrogenase (GAPDH) was used a positive control of sample viability and success of the assay. The number of viral genomes per cell were not presented linearly because doses were not fully quantified until after the Western blot was run.

Next, the intracellular α-gal A activity was measured in the transduced Jurkats and increased linearly dependent upon the dose of viral genome, and therefore *GLA* copy number, delivered to the cells as shown in Figure 4-4. There was no relationship between *GLA* transgene dose and activity found in β-galactosidase, total β-hexosaminidase or N-acetyl galactosaminidase (α-gal B), showing that the increase in α-gal A expression and activity with virus dose was specific to the enzyme and not due to general increase in lysosomal content or biogenesis. In order to confirm that *GLA* alone was responsible for this increase, and not another component of the vector plasmid, fresh Jurkats were transduced with lentivirus manufactured using the *pRRL.cPPT.PGK-GFP.WPRE* vector and containing the *GFP* transgene. The titre of lentivirus containing this transgene was measured to be $2.5x10^7$vg/mL, obtained in Jurkats using qPCR. Neither the activity of α-gal A nor β-galactosidase appeared to be effected by virus dose as shown in Figure 4-5, suggesting it is *GLA* over-expression that is causing increase in α-gal A activity.

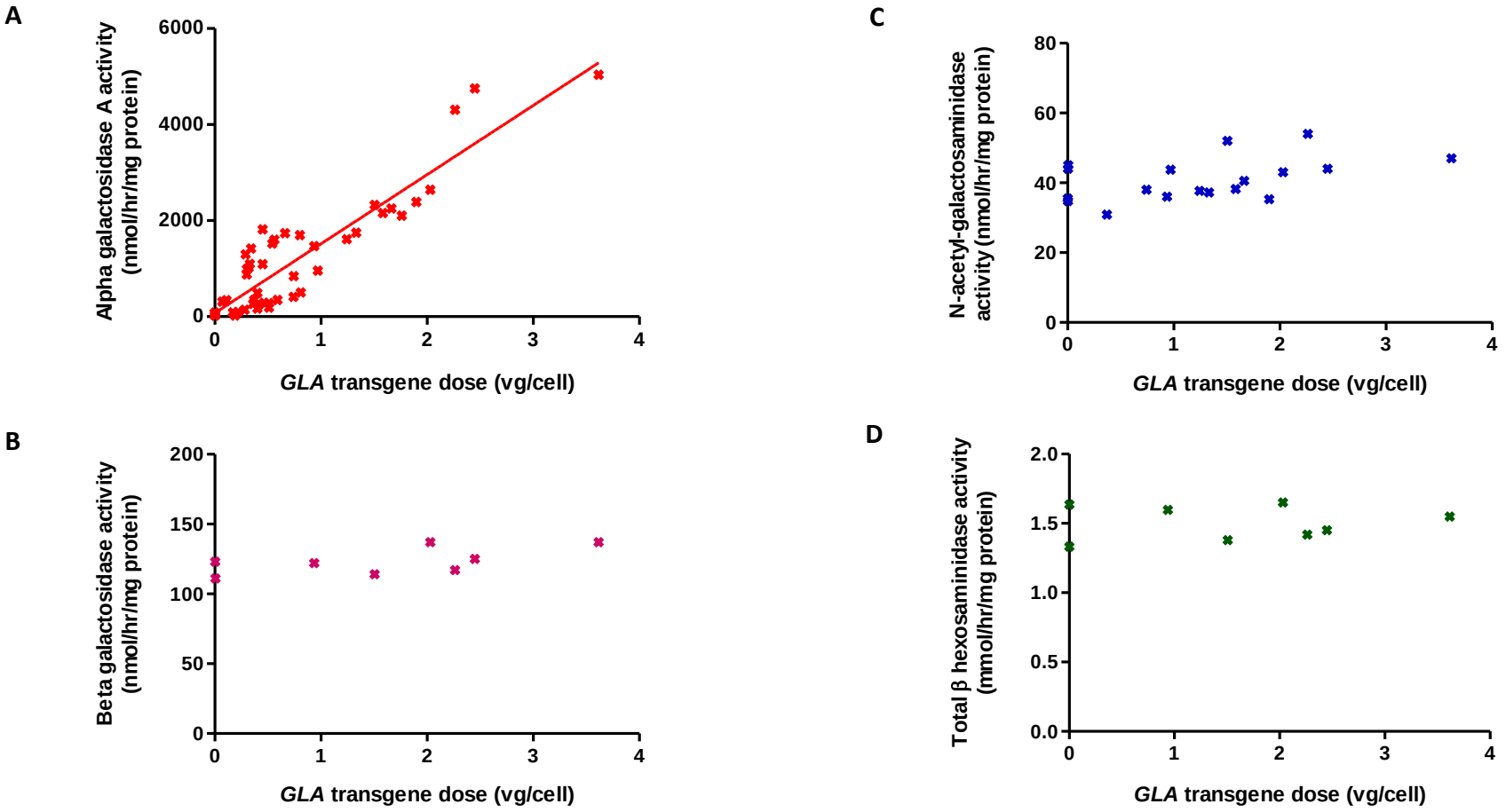

Figure 4-4: Activity of lysosomal hydrolytic enzymes α-gal A, α-gal B (on predominant substrate NAGA), β-gal and total β-hexosaminidase in GLA-Jurkats

Jurkats were transduced with lentivirus containing *GLA* (2.80×10^7 pfu/mL). (**A**) A-gal A activity increased with virus dose. Linear regression R^2=0.835, P<0.0001. (**B – D**) The activity of three other lysosomal enzymes were measured and show that correlation with virus dose was not statistically significant.

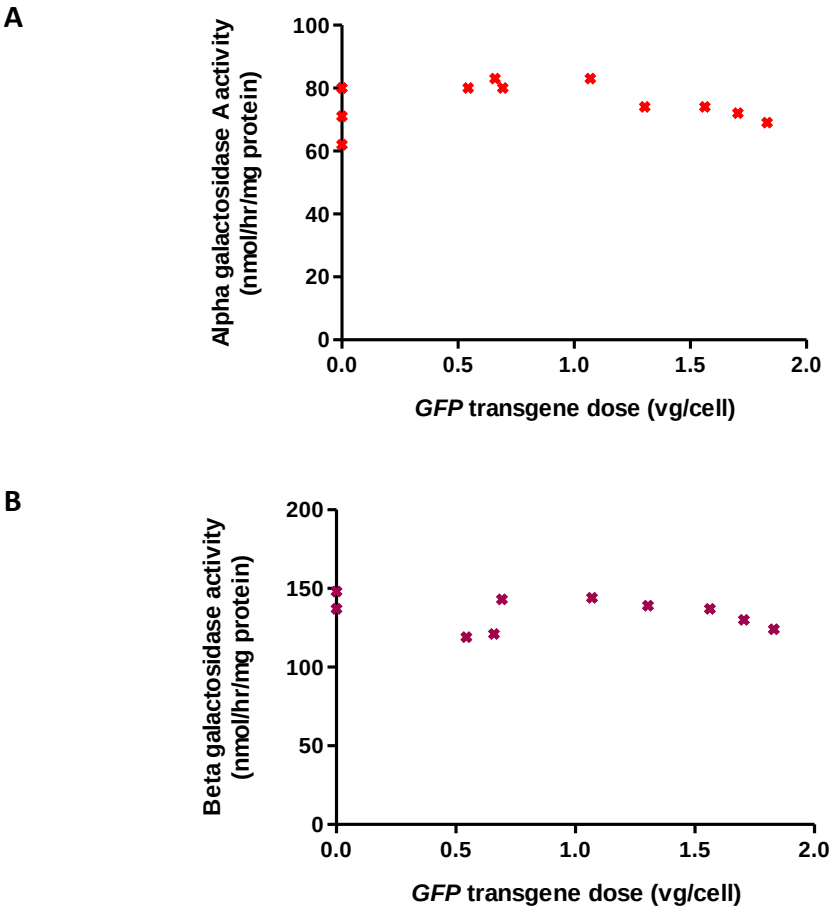

Figure 4-5: Activity of lysosomal hydrolytic enzymes α-gal A and β-gal in Jurkats transduced with lentivirus containing *GFP*

Jurkats were transduced with lentivirus containing the transgene encoding green fluorescent protein (*GFP*). Both α-galactosidase A (α-gal A) **(A)** and β-galactosidase (β-gal) activity **(B)** did not correlate with virus dose.

4.4.2 No evidence for *GLA* transgene cellular toxicity

To see whether the efficacy of lentivirus-mediated *GLA* delivery to Jurkats is diminished by cellular toxicity, fresh jurkats were transduced with lentivirus manufactured using the *pRRL.cPPT.PGK-GLA.WPRE* vector plasmid. The viral genome copy number within treated cells was measured by quantitative PCR. Approximately $3x10^5$ *GLA*-Jurkats were seeded and the number of live and dead cells counted every 24 hours for three days. This experiment was carried out in triplicate. Cell viability was calculated as:

$$Cell\ viability\ (\%) = 100 \times \frac{live\ cell\ count}{total\ number\ of\ live\ and\ dead\ cells}$$

The results, shown in Figure 4-6, show that the rate of cell growth over the three days reduced dependent upon the virus dose ($P<0.001$), but the cell viability remains over 90%, suggesting that the dosage of harvested lentivirus is not toxic to Jurkats up to 1.8vg/cells.

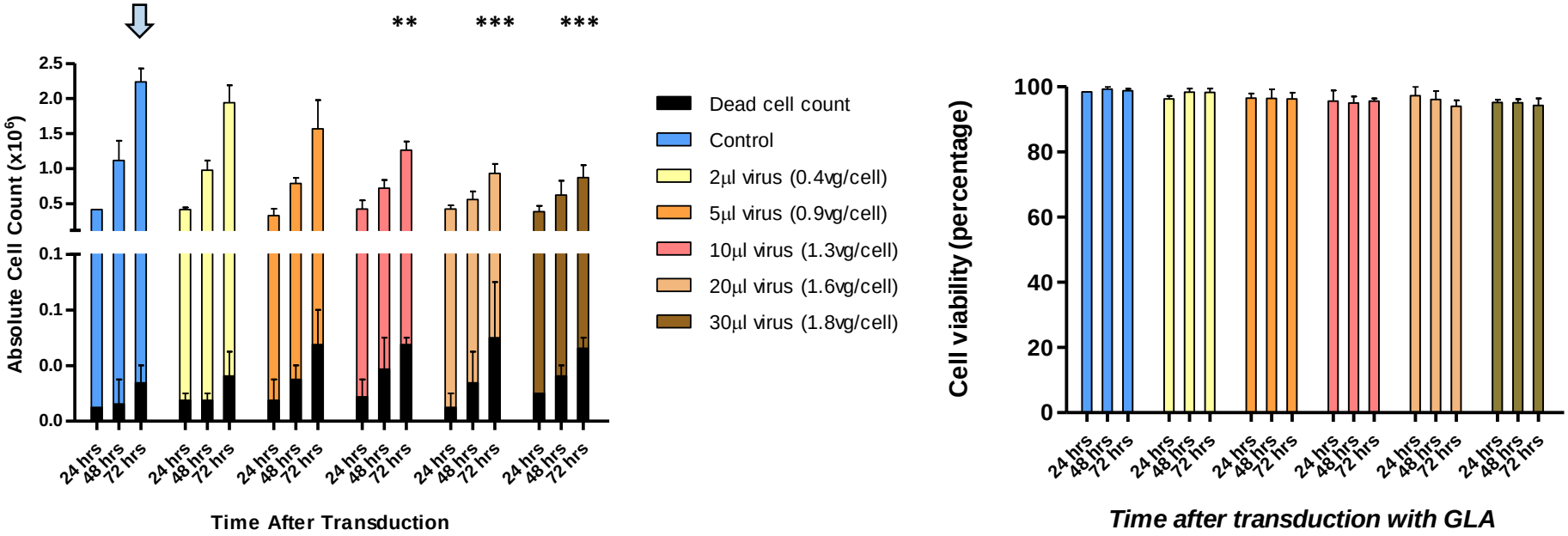

Figure 4-6: Cell growth and percentage viability in Jurkats during the first three days following transduction with lentivirus containing *GLA*.

Jurkats were transduced with lentivirus containing *GLA*. $3x10^5$ cells were seeded and live and dead cells were counted in triplicate every subsequent 24 hours up to three days. The bar chart of absolute cell count shows dead cell counts superimposed on the live cell counts. Two way ANOVA found the rate of cell proliferation was different across virus doses ($P<0.001$). After 72 hours incubation there was significant difference between live cell count in GLA-Jurkats containing ≥ 1.3vg/cell compared with controls ($P<0.01$). Cell viability was calculated as the percentage of total number of cells (live and dead) that were alive when counted. Two way ANOVA of transformed percentage cell viability data found that change in viability over time was not altered by virus dose.

4.5 Kinetic properties of α-galactosidase A in wild type and treated Jurkats

In order to evaluate the structure and catalytic mechanism of α-gal A in the Jurkat cell line, the relationship between the initial reaction velocity of the enzyme and the concentration of synthetic substrate 4MUG was examined. Since the enzyme's kinetic properties are specific to the substrate it reacts with, it is important to note that the substrate saturation curves produced here may not hold true for the natural substrates to α-gal A, predominately Gb3. However, by using 4MUG to measure α-gal A activity, any change in saturation curve parameters between wild type Jurkats and Jurkats transduced with *GLA* over a range of lentivirus doses, may suggest differences in the catalytic performance of the enzyme. This may have important implications for the design of future protocols for lentivirus-mediated delivery of therapeutic *GLA* to Fabry disease patient cells.

4.5.1 Michaelis Constant for intracellular α-gal A in wild type Jurkats using synthetic substrate 4MUG

The activity of α-gal A was measured from sonicate of wild type Jurkats at constant total protein concentration (15mg/ml) over a range of final substrate concentrations from 0.25M to 9M. Higher final concentrations (15M and 30M) were attempted but 4MUG precipitated from solution at 37^{o}C. A series of best-fit substrate saturation curves were plotted through the data using least-squares non-linear regression analysis obeying the Michaelis-Menton equation as shown in Figure 4-7.

Due to the asymptotic character of the curve in Figure 4-7 as reaction rate approaches Vmax, Km was estimated using four different methods: direct extrapolation of the substrate saturation curve as initial reaction rate tends to Vmax using Prism5 software, and three linear transformation methods for which results are shown in Figure 4-8 that allow direct measurement of Vmax and Km based upon the assumptions discussed earlier. The 95% confidence intervals for Km and Vmax estimated by each method was compared in Table 4-1 and show no statistical difference between methods for both kinetic parameters. Therefore all subsequent enzyme kinetic analysis in this chapter was carried out using non-linear regression analysis and extrapolation of substrate saturation curves to estimate Km in order to avoid skewing of results due to high Vmax.

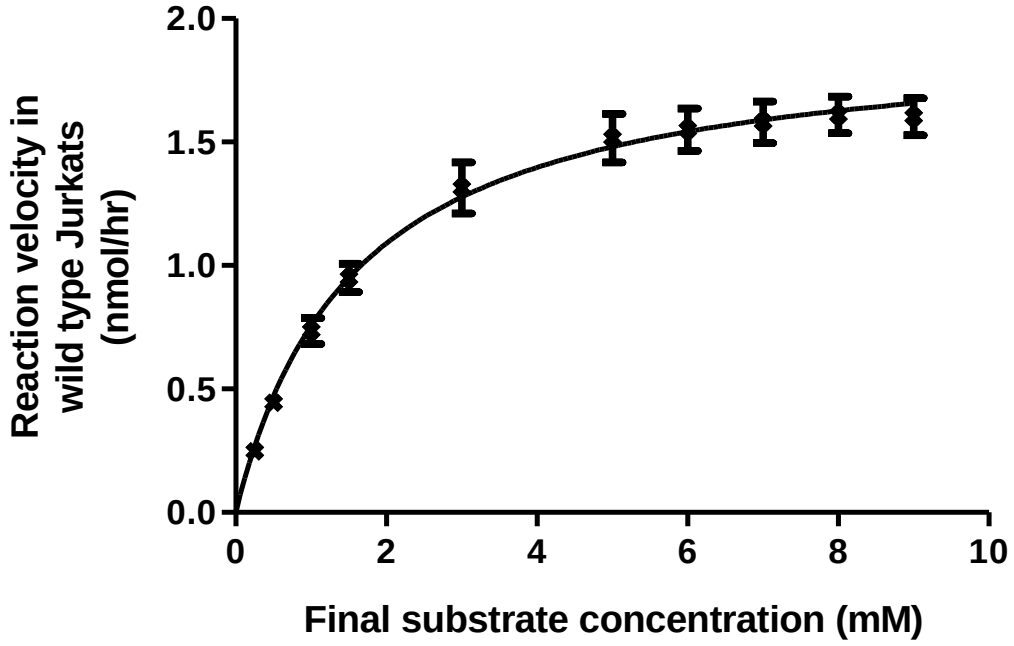

Figure 4-7: Substrate saturation curve for endogenous α-gal A from wild type Jurkats using the flurogenic synthetic substrate 4MUG

The data from experimental measurement (n=4) was plotted and non-linear regression analysis used to best fit to the Michaelis-Menton equation using Prism 5 statistical software (R^2 = 0.978). Estimation of maximum reaction velocity (Vmax), and consequently Michaelis constant (Km), requires extrapolation of the curve as substrate concentration tends to infinity because the curve is asymptotic to Vmax.

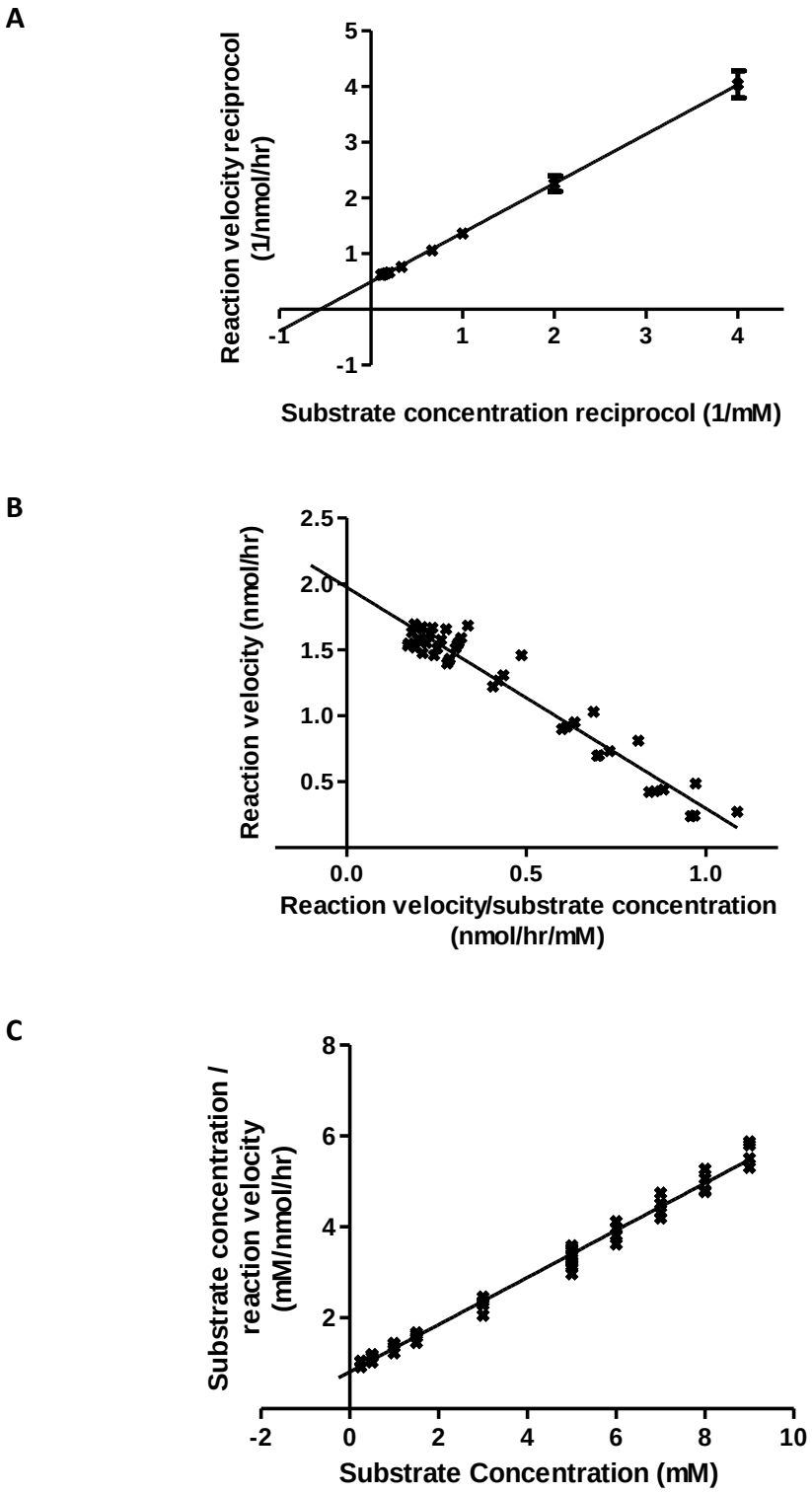

Figure 4-8: Linear transformations of the substrate saturation curve for endogenous α-gal A from wild type Jurkats using the synthetic substrate 4MUG

(**A**) Lineweaver-Burk plot showing $1/v_0$ versus 1/[S], R^2=0.993 (P<0.0001). (**B**) Eadie-Hofstee plot showing v_0 verses v_0/[S], R^2=0.942 (P<0.0001) (**C**) Hanes plot showing [S]/v_0 versus [S], R^2=0.987 (P<0.0001). 4MUG: 4-methylumbelliferyl-α-D-galactopyranoside; v_0: initial reaction rate (nmol/hr); [S]: substrate concentration (mM)

Table 4-1: Comparison of kinetic parameters, estimated by non-linear regression analysis of substrate saturation curves and three linear transformation methods, for endogenous α-gal A from wild type Jurkats using 4MUG as substrate

Substrate saturation curves (n=4) for α-gal A measured experimentally using 15µg total cell protein per assay were analysed by four methods in order to estimate kinetic parameters Km and Vmax for the enzyme from wild type Jurkats. The 95% confidence intervals for Km and Vmax are shown for the four methods. There is no statistical difference between methods. Km: Michaelis Constant; Vmax: maximum reaction rate; 4MUG: 4-methylumbelliferyl-α-D-galactopyranoside

Methods to analyse substrate saturation curves for α-gal A using 4MUG as substrate	Wild type Jurkat 95% confidence intervals	
	K_m *(mM)*	v_{max} *(nmol/hr)*
Extrapolation of Michaelis-Menten equation	1.355 to 1.788	1.872 to 2.021
Lineweaver-Burk plot	1.639 to 1.972	1.903 to 2.172
Eadie-Hofstee plot	1.549 to 1.808	1.904 to 2.046
Hanes plot	1.332 to 1.811	1.861 to 1.998

4.5.2 Over-expression of α-gal A may lead to decreased substrate affinity

Characterisation of the kinetic properties of endogenous α-gal A from wild type Jurkats in the previous section was next repeated for the enzyme produced by *GLA*-Jurkats following transduction with 10µL of the harvested lentivirus (titre 2.8 x 10^5 pfu/mL). The volume of virus used for this experiment equated to an expected multiplicity of infection (MOI) of 1pfu/cell. Jurkats were transduced in duplicate and the resulting virus copy numbers within the *GLA*-Jurkats were 1.5vg/cell and 2.0vg/cell. For both set of cells, α-gal A activity was measured (n=3) using final substrate concentrations from 0.25M to 9M. The resulting substrate saturation curves obeying the Michaelis-Menton equation are shown in Figure 4-9. Vmax and Km were estimated from the curves using the non-linear regression analysis and extrapolation method, consistent with the wild type analysis in the previous section, and shown in Table 4-2. Comparing the kinetics of α-gal A from wild type Jurkats and *GLA*-Jurkats shows that the Km was significantly increased in both 1.5vg/cell and 2.0vg/cell *GLA*-Jurkats. Vmax of α-gal A from the *GLA*-Jurkats were over 30 fold higher than for the enzyme from wild type Jurkats.

To check that high Vmax in *GLA*-Jurkats was not affecting the apparent rise in Km, fresh Jurkats were transduced again with virus dose of MOI 1pfu/cell resulting in *GLA*-Jurkats containing 1.8vg/cell. The total protein extracted from these cells was then diluted so that Vmax of α-gal A would approximate to the maximum reaction rate observed in the wild type Jurkats. The reaction rate of α-gal A was measured for substrate concentrations from 0.5M to 5M and the resulting substrate saturation curve (n=6) is shown in Figure 4-9. The kinetic parameters, estimated by extrapolation, are shown in Table 4-2 and confirm that the Km of α-gal A in *GLA*-Jurkats at the viral doses shown is increased, even when Vmax is reduced to wild type levels.

The results so far suggest that *GLA*-Jurkats transduced with over 1.5 copies of viral *GLA* per cell manufacture α-gal A with a higher Km against 4MUG than wild type Jurkats. In other words, lentivirus-mediated overexpression of α-gal A may increase the concentration of 4MUG required for maximal catalytic activity and reduce the

apparent affinity between enzyme and substrate. This raises the question whether at a lower virus dose the enzyme activity may be increased without a subsequent decline in overall catalytic efficiency. To explore this question Jurkats were transduced with the lentivirus at an MOI of 0.5pfu/cell, resulting in *GLA*-Jurkats containing 0.4vg/cell. Again, the substrate saturation curve for α-gal A was measured using from 0.5M to 9M 4MUG. The Michaelis-Menton equation was fit to the data-points and kinetic parameters Vmax and Km were estimated by extrapolation. The results are presented in Figure 4-9 and Table 4-2, and show that the Km of the enzyme in these cells was similar as in wild type Jurkats.

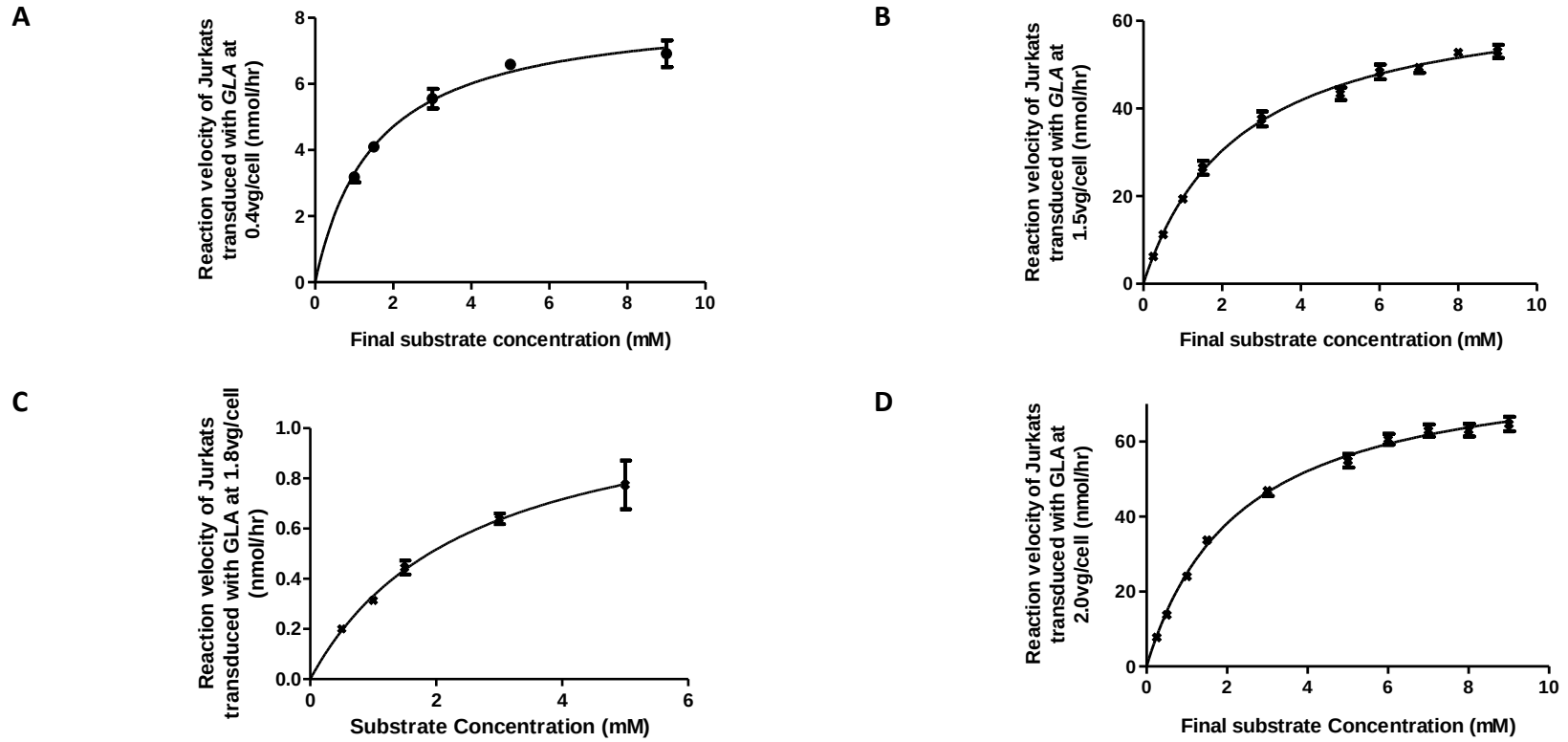

Figure 4-9: Substrate saturation curves for hydrolysis of 4MUG by α-gal A produced by Jurkats transduced with the *GLA* transgene

The Michaelis-Menten equation was fitted to the data points using non-linear regression analysis. Reaction velocity against substrate concentration is shown for *GLA*-Jurkats containing (**A**) 0.4vg/cell, R^2=0.972, n=3; (**B**) 1.5vg/cell, R^2=0.994, n=3; (**C**) 1.8vg/cell, R^2=0.957, n=6; and (**D**) 2.0vg/cell, R^2=0.995, n=3. The substrate saturation curve for α-gal A from *GLA*-Jurkats containing 1.8 vg/cell was measured after total protein content of assay was diluted so that the maximum reaction velocity (Vmax) was approximately equal to Vmax estimated in wild type Jurkats. Vg/cell: virus copy number per cell; 4MUG: 4-methylumbelliferyl-α-D-galactopyranoside

Table 4-2: Kinetic properties of α-gal A from wild type Jurkats and *GLA*-Jurkats, measured using 4MUG as substrate

Michaelis constant (Km) and maximum reaction rate (Vmax) was estimated by extrapolation of the Michaelis-Menton equation following non-linear regression analysis of experimental date. Km of α-gal A for *GLA*-Jurkats containing 1.8 vg/cell was estimated after total protein content of assay was diluted so that the maximum reaction velocity (Vmax) was approximately equal to Vmax estimated in wild type Jurkats. Vg/cell: virus copy number per cell; 4MUG: 4-methylumbelliferyl-α-D-galactopyranoside

	Wild type Jurkat (n=4)	*GLA*-transduced Jurkats			
		0.4vg/cell (n=3)	1.5vg/cell (n=3)	1.8vg/cell (n=6)	2.0vg/cell (n=3)
Km (mM)	1.572 +/- 0.107	1.527 +/- 0.130	2.429 +/- 0.121	2.531 +/- 0.287	2.305 +/- 0.102
Vmax (nmol/hr)	1.946 +/- 0.037	8.31 +/- 0.23	67.3 +/- 1.12	1.170 +/- 0.064	82.1 +/- 1.20
R^2	0.978	0.972	0.994	0.957	0.995

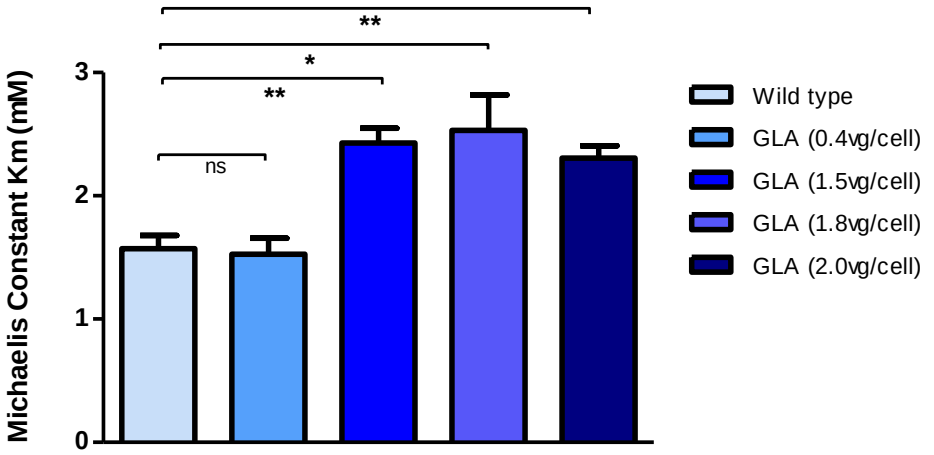

Figure 4-10: Michaelis Constants for α-gal A from wild type and *GLA*-Jurkats using 4MUG as substrate

This graph compares the Michaelis constants (Km) estimated for the hydrolysis of the florigenic substrate 4MUG by α-gal A produced from wild type (untreated) Jurkats and *GLA*-Jurkats containing a range of virus genomes per cell (vg/cell). The Km of 4MUG to α-gal A manufactured by *GLA*-Jurkats transduced with a low virus dose (0.4vg/cell) was the same as α-gal A from wild type Jurkats, but Km significantly increased in α-gal A produced by *GLA*-Jurkats transduced with high virus doses of 1.5 and 2.0 vg/cell ($P<0.01$). Km of α-gal A for *GLA*-Jurkats containing 1.8 vg/cell was estimated after total protein content of assay was diluted so that the maximum reaction velocity (Vmax) was approximately equal to Vmax estimated in wild type Jurkats. This was to ensure that significant differences were not due to large changes in Vmax. The Km of α-gal A using 4MUG was still significantly higher than wildtype ($P<0.05$). 4MUG: 4-methylumbelliferyl-α-D-galactopyranoside.

4.6 Conclusions

The overall aim of this chapter was to investigate the potential catalytic efficacy of virus-mediated overexpression of α-gal A by utilising a previously engineered lentivirus vector plasmid (Rajaraman, 2013) containing the complementary DNA sequence of *GLA* which encodes human mature α-gal A (Bishop et al., 1986). As both a negative and positive control for the work in this chapter, an identical lentivirus vector plasmid containing the *GFP* gene for green fluorescence protein in place of *GLA* was acquired from Dr Conrad Vink (UCL GOSICH, London, UK). Genetic verification of the structures of both vectors by gel electrophoresis and DNA sequencing (Source Biosciences, Nottingham, UK) revealed numerous minor deviations from the expected sequences (Rajaraman, 2013), but none were within the transgene region of the plasmids (Figure 4-2).

Successful transfection of 293T cells by the vector plasmids, and subsequent titration of lentiviruses containing the *GLA* transgene using Jurkat cells (2.80×10^7 vg/mL), confirmed that the genetic anomalies in Figure 4-2 did not interfere with the functionality of either vector. Jurkats, showed in the previous chapter to have a relatively low endogenous α-gal A activity, also showed increase in α-gal A expression (Figure 4-3) and activity (Figure 4-4), dependent upon the dose of lentiviral-*GLA* they contained. Furthermore, there was no evidence of cell toxicity resulting from lentivirus transduction or α-gal A overexpression in Jurkats (Figure 4-6).

These results suggest that the transgene was successfully translated by Jurkats into a precursor enzyme that matures into fully activated α-gal A within the lysosomal compartment. The process of cellular sorting of α-gal A for the lysosome is manose-6-phosphate-dependent, so the results shown here suggest the overexpressed enzyme is being appropriately modified post-translation within wild type Jurkats and *GLA*-Jurkats.

Investigations into the kinetic properties of α-gal A, both endogenous native to Jurkats and following lentivirus-mediated overexpression in Jurkats, revealed further important observations that qualify the above conclusions. First the Km value in wild

type Jurkats for the hydrolysis of the synthetic florigenic substrate 4MUG by α-gal A measured here (Km = 1.6mM) was compared with that seen in various human tissues (Km range from 1.6 to 2.9mM) reported in the literature and summarised in Table 4-2. A relatively low Km suggests the enzyme possesses high affinity with 4MUG and operates at maximal catalytic efficiency at low substrate concentrations. Table 4-3 shows that the Km derived from Jurkats is similar to that found in human tissues, suggesting that α-gal A from the various sources are of similar catalytic effectiveness and three-dimensional configuration. This gives confidence that the results herein are comparable with those reported by others.

Table 4-3: Comparison of Michaelis Constant estimated in wild type Jurkats, various human tissues and enzyme replacement therapies

The Km values given for human tissues and ERT are taken from previous research using purified α-gal A. ERT uses recombinant α-gal A produced in Chinese hamster ovary (CHO) cells (Replagal, Shire Pharmaceuticals, UK), and human foreskin fibroblasts (Fabrazyme, Sanofi Genzyme, USA). Km: Michaelis Constant; ERT: Enzyme Replacement Therapy.

Human cells or tissue	Jurkat	Plasma	Spleen	Liver	Placenta	ERT	
						Replagal	Fabrazyme
Km (mM)	1.6	1.9	2.5; 2.0	2.9	1.6	2.0	2.0; 4.0
Refs.	--	Desnick et al, 1979	Desnick et al, 1979; Bishop & Desnick, 1981	Dean & Sweeley, 1979	Kusiak et al, 1978	Sugawara et al, 2009	Lee et al, 2003

Secondly the enzyme kinetics of overexpressed α-gal A within *GLA*-Jurkats, which had been transduced with lentivirus containing the *GLA* transgene, suggested that the Km of the enzyme appeared to increase with transgene copy number. At a low virus dose (0.4vg/cell) the enzyme made by *GLA*-Jurkats showed equal affinity to the 4MUG substrate as that made by untreated wild type Jurkats, but at high virus doses (>1.5vg/cell), the enzyme produced in Jurkats has significantly higher Km, suggesting lower affinity to 4MUG. This observation was not an artefact of increased Vmax. Indeed, reducing total protein concentration so that the Vmax of α-gal A from *GLA*-

Jurkats (1.8vg/cell) was reduced to approximately the same as that from wild type Jurkats, resulted in even higher Km (Figure 4-10). A possible reason for this is that endogenous wild type α-gal A may be diluted out from the total protein since the majority of the enzyme will be manufactured from the transgene above 1vg/cell.

The Km of α-gal A manufactured from the transgene are consistent with the values reported in previous research reported by (Meghdari et al., 2015). The authors measured the kinetic properties of α-gal A purified from Pichia pastoris following electroporation of the yeast with plasmid containing the complementary DNA sequence, as reported by Bishop et al., (1986), that encodes mature human α-gal A. The sequence was confirmed as identical to the transgene used in the present thesis as explained earlier in this chapter. The Km of human α-gal A was 2.44 +/- 0.44 mM which agrees well with the Km of α-gal A manufactured by the transgene in Table 4-2. Meghdari et al, 2015 do not report the human *GLA* copy number and, since the authors used enzyme purified by double affinity chromatography and reported rate of hydrolysis of 4MUG in mmol/hr/mg, it is not possible to compare reaction rates or gene dosage.

So in conclusion, lentivirus-mediated overexpression of α-gal A within Jurkats leads to virus dose-dependent increase in enzyme activity, suggesting appropriate post-translational modifications and transportation to the lysosome. However, our kinetic studies show that the enzyme produced may have lower substrate affinity at high virus doses (from 1.5vg/cell upwards). These findings point to an important need to optimise virus dose in order to deliver maximum therapeutic benefit to Fabry disease patients.

Patterns of glycosylation of aspartate residues on α-gal A varies considerably between tissue types in humans (Hrebicek and Ledvinova, 2010) and other organisms including the yeast Pichia pastoris (Chen et al., 2000). The relative distribution of complex and high-mannose oligosaccharides attached to the enzyme are important for enzyme stability (Ioannou et al., 1998, Matsuura et al., 1998), uptake by cells (Bekri, 2006), half-life within humans (Desnick et al., 1979) and cellular trafficking to the lysosome for catalytic activation (Kornfeld, 1986). The variation in Km across

human tissue types (Table 4-3) may be in part due to differences in glycosylation (Hrebicek and Ledvinova, 2010). A similar variation in Km is seen here in Jurkats following lentivirus-mediated overexpression of α-gal A (Table 4-2). It is possible that increase in Km with increasing transgene dose may be due to cellular congestion leading to impaired post-translational modification and cellular sorting to the lysosome for complete enzyme activation (Lodish et al., 2000).

Two points limit the conclusions. Firstly Jurkats, as an immortalised cell line, are pseudo-diploid (ATCC, 2016). In calculations of viral transgene dose per cell it was assumed that on average the cells were diploid. Secondly, in order to compare *GLA*-Jurkats (1.8vg/cell) with wild type Jurkats after adjusting Vmax to wild type velocity, total protein to assay *GLA*-Jurkat was diluted from 15µg, used to measure intracellular α-gal A activity throughout this thesis, to 0.3µg. This total protein content was outside the range of assay linearity confirmed in chapter 3, but results indicate there was sufficient α-gal A to give similar reaction rates, given the same substrate concentration, as in wild type Jurkats. In order to confirm the kinetic parameters measured for *GLA*-Jurkats at 1.8vg/cell it would be important to check linearity at the lower total protein level from these cells. However there was insufficient protein after completion of substrate saturation experiments to check this.

Looking ahead, on translation α-gal A that evades capture by the golgi apparatus will be secreted, but may be recaptured by manose-6-phosphate receptors expressed on the plasma membrane, as long as the enzyme underwent the appropriate post-translational modifications before release (Lodish et al., 2000). So the results here raise the question whether any α-gal A is released from treated cells following lentivirus-mediated overexpression, and whether the released enzyme may be taken up by untreated cells. The process of release and uptake of lysosomal enzymes is termed cross-correction and is vital for the therapeutic efficacy of gene delivery to treat Fabry disease. These important research questions will be addressed in the next chapter.

Chapter 5 Cross-correction in the Jurkat human cell-line and the effect of inhibiting mitochondrial complex I

5.1 Introduction

The previous chapter of this thesis demonstrates the ability of human cells to overexpress α-gal A following transduction by a lentivirus vector containing *GLA*. Fabry disease is a multi-systemic disorder resulting from accumulation of Gb3 in many tissue types including vasculature, renal cell-types and peripheral neurons (Desnick et al., 2001). From a therapeutic perspective, it is impractical to consider transduction of all cells in order to increase their intracellular α-gal A activity and degrade Gb3 stores. This raises the question whether there is a mechanism by which the therapeutic benefit of gene delivery may be extended from transduced to untransduced cells

Landmark experiments in 1968 by Elizabeth Neufeld and colleagues were the first to demonstrate that a functional mechanism does exist by which lysosomal enzyme may transfer between cells with and without a functional allele of the enzyme-coding gene (Fratantoni et al., 1968). Cultured fibroblasts from patients with Hurlers and Hunters syndromes were used. These syndromes are genetically distinct lysosomal storage disorders effecting mucopolysaccharide (MPS) degradation and fibroblasts from patients accumulate intracellular MPS more than healthy cells. Co-culture of fibroblasts from either Hunters or Hurlers patients with healthy control fibroblasts resulted in reduction of rates of MPS accumulation within the disease cells to levels observed in the healthy cells. Even co-culture of fibroblasts from Hunters and Hurlers patients resulted in similar correction of MPS accumulation. It took two days of co-culture with healthy cells for accumulated stores of MPS within disease fibroblasts to degrade by 75% (Fratantoni et al., 1968). These results suggest that the specific enzyme deficit in diseased cells may be corrected by being grown in close proximity to cells with normal levels of that enzyme

Was the enzymatic correction observed by Neufeld and colleagues due to cell-cell fusion followed by genetic transfer of alleles, transfer of cytoplasmic material, or

transfer of functional enzyme through the culture medium? In 1974 Cantz and Kresse confirmed that it was the latter mechanism that was at work. Sandhoff disease is a lysosomal storage disorder of glycosphingolipid catalysis due to defective β-N-acetylhexosaminidase. Cells from patients with Sandhoff disease accumulate substrates including glycoaminoglycans. Cantz and Kresse extracted functional enzyme from urine and homogenized fibroblasts from healthy individuals. They found that adding the enzyme to the growth media of cultured skin fibroblasts from patients with Sandhoff disease resulted in dose dependent depletion of intracellular glycoaminoglycans (Cantz and Kresse, 1974). Similarly O'Brien and colleagues used α-acetylglucoaminidase isolated from human placenta to correct the metabolic deficit in MPS catabolism observed in cultured skin fibroblasts from Sanfilippo type B patients. Remarkably, purified enzyme added to culture media of the fibroblasts to give only 2% to 5% of normal intracellular activity was sufficient to clear 42% to 70% of stored keratin sulphate (O'Brien et al., 1970). Together these results show that only a small amount of transfer of functional enzyme between healthy and diseased cells in co-culture is necessary to significantly reduce substrate storage in the disease cells. Across the lysosomal storage diseases generally it is estimated that between 1% and 5% of normal intracellular activity is sufficient to correct the metabolic deficit in cells missing an enzyme (Desnick and Schuchman, 2012).

The transfer of specific proteins from replete to deficient cells has been termed metabolic cooperativity or cross-correction and depends upon a cells ability to secrete and take-up functional lysosomal enzymes (Medin et al., 1996, Takenaka et al., 1999a, Takenaka et al., 1999b, Yoshimitsu et al., 2007). This process is illustrated in Figure 5-1 and has been demonstrated in skin fibroblasts and immortalised B cells from Fabry disease patients following transduction of cells in culture with amphotropic retrovirus containing the human α-gal A gene. The treated patient fibroblasts showed ten-fold increase in intracellular α-gal A activity in patient fibroblasts above the activity observed in healthy control fibroblasts. In transformed patient B cells however, treatment only increased the enzyme activity to a similar level as seen in healthy control cells. Media collected from corrected patient fibroblasts and B cells showed ten-fold increase, and 50% increase respectively, in

extracellular α-gal A activity compared to media from untreated control cells, after 16 hours cell culture (Medin et al., 1996). The difference in secretion may reflect the difference in transduction efficiency of these cell types.

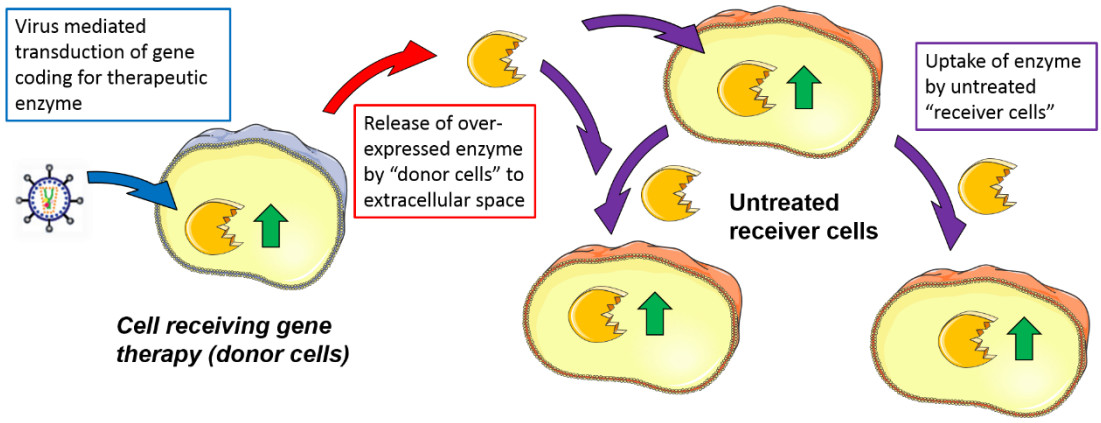

Figure 5-1: A schematic showing the process of cross correction of untreated cells by cells containing a therapeutic gene coding for a deficient enzyme following gene therapy

A therapeutic virus inserts a correct copy of a gene which overexpresses a functional enzyme which is otherwise missing into a patient's cells. Subsequently these cells act as enzyme donors to neighbouring untreated cells which receive the enzyme through a process of release and uptake. In the case of α-gal A, most cell-types take-up the enzyme via a manose-6-phosphate dependent pathway.

Uptake of functional α-gal A by untreated Fabry disease patient cells was assessed using culture media collected from the α-gal A-retrovirus-producer cell line. Patient fibroblasts incubated with this media for 3 hours showed manose 6 phosphate-dependent uptake of functional α-gal A. Similarly uptake was seen by patient B cells (Medin et al., 1996). From these results it is unclear whether some of the increase in enzyme activity in the untreated patient cells was due to transduction by virus in the virus-producer cell media rather than uptake of exogenous functional α-gal A alone. None-the-less this early work by Medin and colleagues was encouraging because it suggests that the benefit of functional enzyme expression by gene therapy may extend far beyond treated cells. This attribute of cross correction is essential for the therapeutic efficacy of gene therapy to treat multisystemic disorders such a Fabry disease.

As discussed in Chapter 1 Introduction, Fabry disease is a lysosomal storage disorder (Kolter and Sandhoff, 1999, Sweeley and Klionsky, 1963). The lysosome controls metabolic homeostasis (Settembre et al., 2013). Storage of Gb3 within lysosomes would therefore be expected to interrupt cellular response to energy demand and supply (Machann et al., 2011, Palecek et al., 2010). Central to this is the mitochondrion (Heales et al., 1996, Osellame et al., 2012). Fabry disease potentially disrupts mitochondrial function in a number of ways: impaired mitophagy (Liebau et al., 2013, Nelson et al., 2014), oxidative stress (Shen et al., 2008, Chimenti et al., 2015, Lenaz et al., 2002), and membrane lipid imbalance (Das and Naim, 2009). Consistent with this, Lücke et al (2004) observed reduction in the activity of respiratory chain complexes I, IV and V in skin fibroblasts from Fabry disease patients compared to controls (Lucke et al., 2004).

This raises a research question as to how damage to the mitochondrial respiratory chain in Fabry disease may affect the ability of cells to release and uptake functional α-gal A. The respiratory chain comprises five metaloenzyme complexes that are integral to the inner-mitochondrial membrane as shown in Figure 5-2. This system transfers high energy electrons from NADH to oxygen, releasing energy in a step-wise process which is harnessed to actively pump protons across the inner-mitochondrial membrane from the matrix, thereby creating an electrochemical proton gradient. Complex V is called ATP synthase and is not involved in electron transport but utilises passive translocation of protons back to the mitochondrial matrix to phosphorylate ADP (Osellame et al., 2012).

Metabolic control theory has shown that the majority of control over oxygen consumption in mitochondria from rat heart and brain was with complex I (Rossignol et al., 2000). The importance of complex I in metabolic flux control was also supported by similar research in synaptic mitochondria (Davey et al., 1998, Telford et al., 2009).

Complex I, called NADH-ubiquinone oxido-reductase, is a vital component of the respiratory chain. Firstly it recycles NADH through oxidation back to NAD+ which continually feeds the tricarboxylic acid cycle (TCA cycle) within the mitochondrial

matrix. Secondly, the liberated electron pair from NADH passes down the electron energy gradient, via the flavin mononucleotide (FMN) prosthetic group coupled to a chain of 7 iron-sulphur clusters, to reduce bound ubiquinone (Q_{10}) to ubiquinol ($Q_{10}H_2$). $Q_{10}H_2$ then transports the electron pair to complex III and the rest of the respiratory chain for final delivery to oxygen, thereby maintaining the electron energy gradient. Finally the free energy released from the electrons by complex I is used to pump four protons across the inner mitochondrial membrane from the matrix, allowing oxidative phosphorylation to proceed (Hirst and Roessler, 2016).

So, to address the research question raised in this chapter the following objectives were set:

- Examine ability of transduced Jurkat cells to secret functional enzyme into the surrounding culture media. This culture media taken from *GLA*-Jurkats is termed “donor media”.
- Examine ability of wild type Jurkat cells that are naive to treatment to take up exogenous enzyme from their surrounding media which comprises 75% donor media.
- Treat Jurkat cells with rotenone, to assess whether this complex I inhibitor effects transduction efficiency, α-gal A secretion and uptake by target cells.

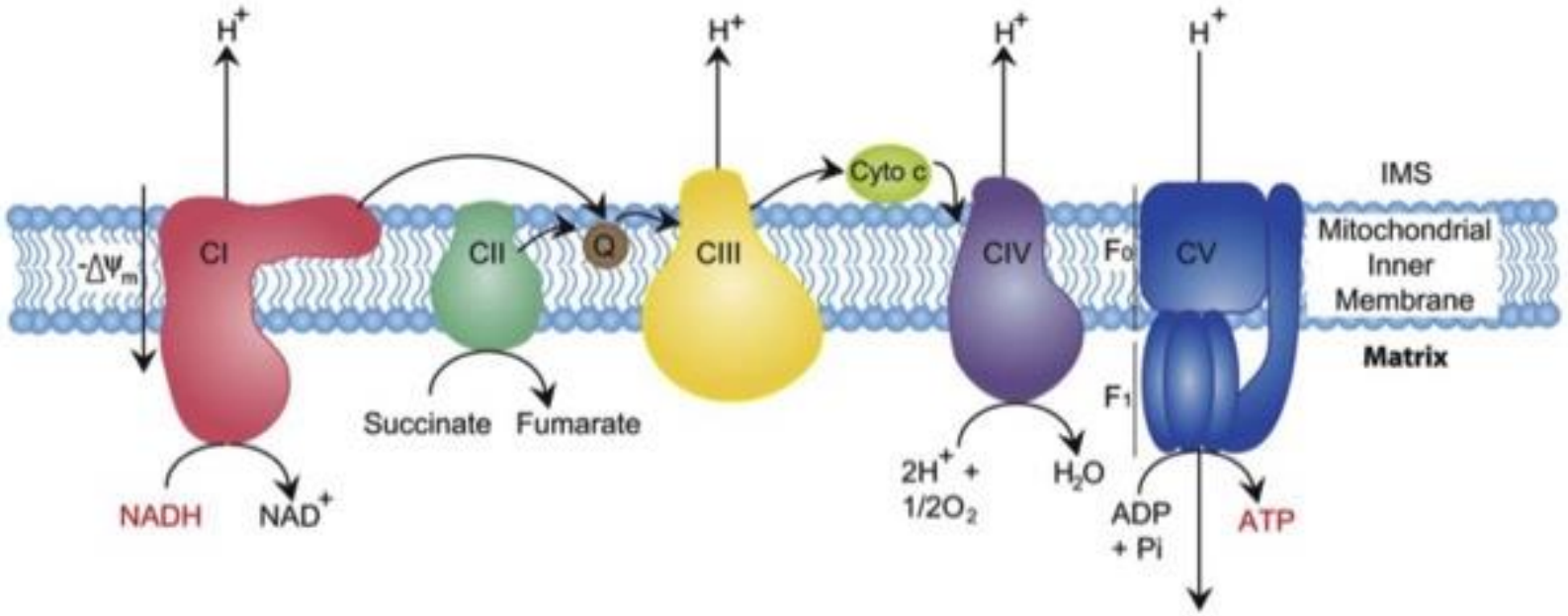

Figure 5-2: Mitochondrial respiratory chain

The respiratory chain comprises four metaloenzyme complexes that are integral to the inner mitochondrial membrane. Together they are responsible for step-wise transfer of high energy electrons from NADH, or succinate, to oxygen to form water. The energy released by complexes I, III and IV is used to pump protons from the mitochondrial matrix into the inter-membrane space, thus creating an electrochemical proton gradient across the inner membrane ($-\Delta\Psi_m$). ATP synthase is the fifth respiratory chain complex and contains a transmembrane channel (F_0) through which protons passively return down the gradient to the mitochondrial matrix. The flow of protons within the channel causes F_0 to rotate relative to a catalytic domain (F_1), causing conformational change in the binding site of F_1 leading to phosphorylation of ADP. This process is essential to aerobic cellular respiration and produces a rich harvest of energy in the form of ATP. CI, CII, CIII, CIV and CV represent Complex I (NADH-ubiquinone oxidoreductase), II (succinate-ubiquinone oxidoreductase), III (ubiquinol-cytochrome C oxidoreductase), IV (cytochrome C oxidase) and V (ATP synthase) respectively. Image sourced from (Osellame et al., 2012).

5.2 Methods

In secretion studies, transduced Jurkats were washed three times in PBS to remove any extracellular virus particles. Then cells were placed in fresh complete RPMI media for up to three days. Media samples were removed after zero, two and three days and centrifuged at 3,000rpm for 5 minutes. The supernatant was then collected and α-gal A and total β hex activities were measured in the supernatant from *GLA*-Jurkats using the supernatant assay described in Chapter 2 Materials and Methods. Since complete RMPI culture media made up half the reaction volume in the α-gal A assay, it was necessary to correct the measured activity for both auto-fluorescence and quenching effects of phenol red and foetal bovine serum. This was achieved for each sample of culture media using the 1nmol 4MU standards and blanks shown in Table 5-1.

Table 5-1: Content of standards and blanks used to measure alpha galactosidase in supernatant

	Standard blank	Standard	Sample blank	Sample
Substrate, standard or water	200µL H_2O	200µL standard (contains 1nmol 4MU)	100µL substrate	100µL substrate
Culture media from *GLA*-Jurkats (supernatant)	100µL	100µL	100µL (added after incubation period)	100µL
Stopping buffer (1M Glycine-NaOH)	900µL	900µL	1mL (added after the incubation period)	
Note	Corrected Standard = Standard – standard blank		---	---

Both sample and sample blank Eppendorf tubes were incubated at 30^0C for 2 hours and stopping buffer added to terminate hydrolysis. Sample was then added to the sample blank to take account of both auto-fluorescence of phenol red and foetal bovine serum within the culture media and their possible quenching effect on product fluorescence. The difference between standard and standard blank took

account of quenching and auto-fluorescence by culture media on the fluorescence emitted by 1nmol 4MU standard.

The collected donor media at the two-day point was mixed 3 in 4 with fresh RPMI media and then used to culture wild type Jurkats for two days. This ratio was consistent with that used by Neufeld's laboratory (Fratantoni et al., 1968). To take account of degradation of over-expressed enzyme in the growth media over this period, a sample of the mixed donor culture media was also incubated in the same way without cells as a control. The reduction in α-gal A activity measured in the control mixture was subtracted from the reduction measured in the similar mixture exposed to wild type Jurkats to quantify the enzyme uptake from the culture media. Intracellular activity within receiver cells was measured and compared with enzyme activity in untreated wild-type Jurkats.

To examine the effect of complex I inhibition on lentivirus-mediated transduction of Jurkats, and secretion and reuptake of overexpressed α-gal A, a rotenone (200μM) solution was prepared in absolute ethanol according to Aylett et al, 2013. The effect of 5μl rotenone solution on complex 1 and citrate synthase activities in $5x10^5$ cells wild type Jurkats suspended in 10mL complete RPMI (final rotenone concentration 100nM) was measured in the cells following two days incubation. Control cells were grown in the same volume of media with 5μl absolute ethanol to isolate the effect of rotenone alone on mitochondrial function. After 24 hours incubation at 37^{o}C the cells were harvested (Aylett et al., 2013).

In measuring complex I activity in the laboratory, potassium cyanide is used to inhibit complex IV, thereby preventing re-oxidation of ubiquinol to ubiquinone which would otherwise counteract the inhibitory effect of rotenone.

5.3 Secretion of alpha gal A by Jurkats overexpressing *GLA*

Since the plasma α-gal A assay (Chapter 2 Methods and Materials) requires a relatively large volume of culture media (100µl), it was necessary to find out whether phenol-red and foetal bovine serum in complete RPMI interfered with fluorescence emitted from the hydrolysed product. The activity of α-gal A was measured in fresh culture media, and the effects of quenching and auto-fluorescence are shown in Table 5-2.

Table 5-2: Baseline alpha-gal A fluorescence in culture media

Fresh complete RPMI culture media was assayed according to the protocol for α-gal A activity in supernatant. Comparing the difference between the standard with and without media shows that there was a small amount of quenching of fluorescence produced by 1nmol standard. The standard blank shows there is slight auto-fluorescence in complete RPMI, probably due to the phenol red and foetal bovine serum within the culture media.

	Standard without media	Standard blank	Substrate blank	Standard	Sample
Fluoresence due to α-gal A	392	1	14	383	15

The baseline activity of α-gal A in complete RPMI was calculated from the data in Table 5-2 to be very low at 0.01nmol/hr/ml media, suggesting that the effect of cross correction should be detectable in culture media. The interference identified in Table 5-2 was taken into account in subsequent experiments by continuing to use separate standards, standard blanks and substrate blanks for every supernatant sample analysed in this chapter.

This method was then used to see whether *GLA*-Jurkats were able to secret overexpressed α-gal A into the surrounding media. A fresh harvest of lentivirus containing the *GLA* transgene was again prepared and titred by transduction into Jurkats cells and measured to be 3.68 x 10^7pfu/mL using qPCR. The washed *GLA*-Jurkats, which ranged in transgene expression up to 0.8vg/cell were then grown in fresh media. The results in Figure 5-3 show that α-gal A activity increased in the

culture medium collected from the *GLA*-Jurkats compared with the baseline activity in complete RPMI. The increase in activity in the media was dependent upon both the intracellular α-gal A activity, and therefore *GLA* copy number, in the *GLA*-Jurkats and length of time in culture. There was a small increase in activity in supernatant from cells with increasing virus copy number, and this may be due to cell damage resulting in leakage of enzyme following centrifugation.

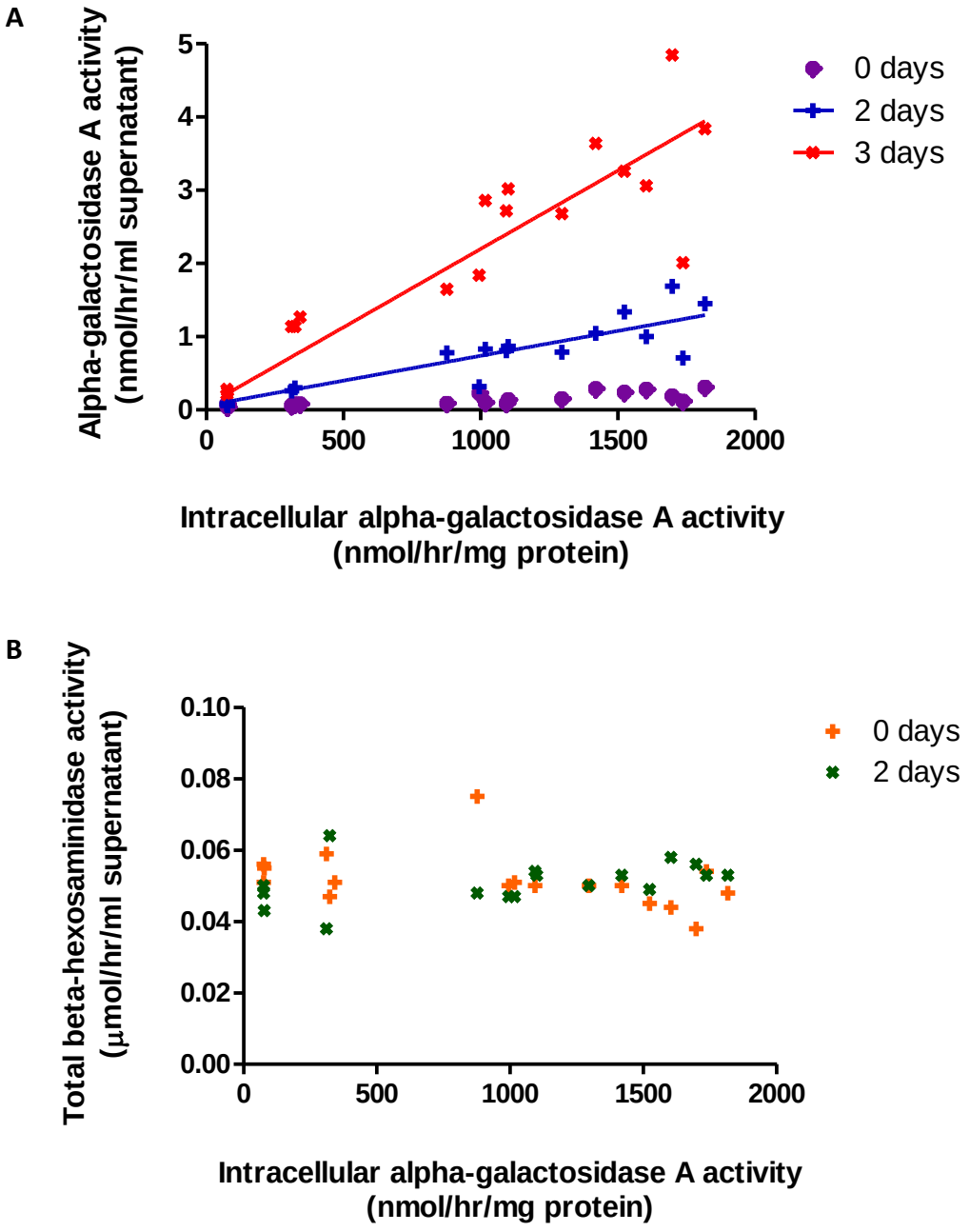

Figure 5-3: Secretion of α-gal A by *GLA* Jurkats

A-gal A (**A**) and total β-hexosaminidase (**B**) activity was measured in the culture media supernatant collected after zero, two and three days incubation at 37°C with *GLA*-Jurkats containing between zero and 0.8vg/cells. The extracellular activity in supernatant is plotted against intracellular activity within the *GLA*-Jurkats. Secretion of α-gal A activity into the surrounding media by *GLA*-Jurkats increased with both intracellular activity and duration of incubation. Linear regression found that at day 0, R^2=0.607 (P<0.001); day 2, R^2=0.786 (P<0.0001); and day 3, R^2=0.796 (P<0.0001). Total-β hex in supernatant did not change with either incubation time or intracellular α-gal A activity within the *GLA*-Jurkats, suggesting secretion was not non-specific due to cell damage following transduction.

5.4 Uptake of α-gal A by wild type Jurkats

Next, supernatant was collected from the *GLA* Jurkats after two days incubation. This time period was chosen because previous research found that lentivirus-mediated overexpression of α-gal A in Fabry disease patient fibroblasts resulted in clearance of stored Gb3 two days post-transduction (D'Costa et al., 2003). Figure 5-3 confirmed that two days incubation was sufficient for secretion of functional enzyme from *GLA* Jurkats to take place. The supernatant was mixed 3:1 with fresh complete RPMI to provide sufficient nutrients for cell growth. This is consistent with the method used by Neufeld and colleagues to demonstrate cross correction between fibroblasts taken from Hunters syndrome and from Hurlers syndrome patients (Fratantoni et al., 1968). The mixed media was then incubated with wild type Jurkats, termed receiver cells, for two days. Results in Figure 5-4 show that intracellular α-gal A activity increased with initial activity within the culture media, but intracellular total β-hex activity was unchanged. Quantitative PCR confirmed no contamination of the wild type Jurkats with lentivirus, suggesting that the increase in α-gal A activity observed was not due to virus contamination in the receiver cells leading to *GLA* overexpression. These results possibly suggest uptake of functional enzyme by the wild type Jurkats from the culture media.

Consistent with this, extracellular α-gal A activity decreased within the culture media following incubation with wild type Jurkats for two days, as shown in Figure 5-5A. During this incubation period, considerable degradation in enzyme activity within the culture media was observed (Figure 5-5B). However, after taking degradation into account there was slight but significant enzyme uptake from the culture media (Figure 5-6).

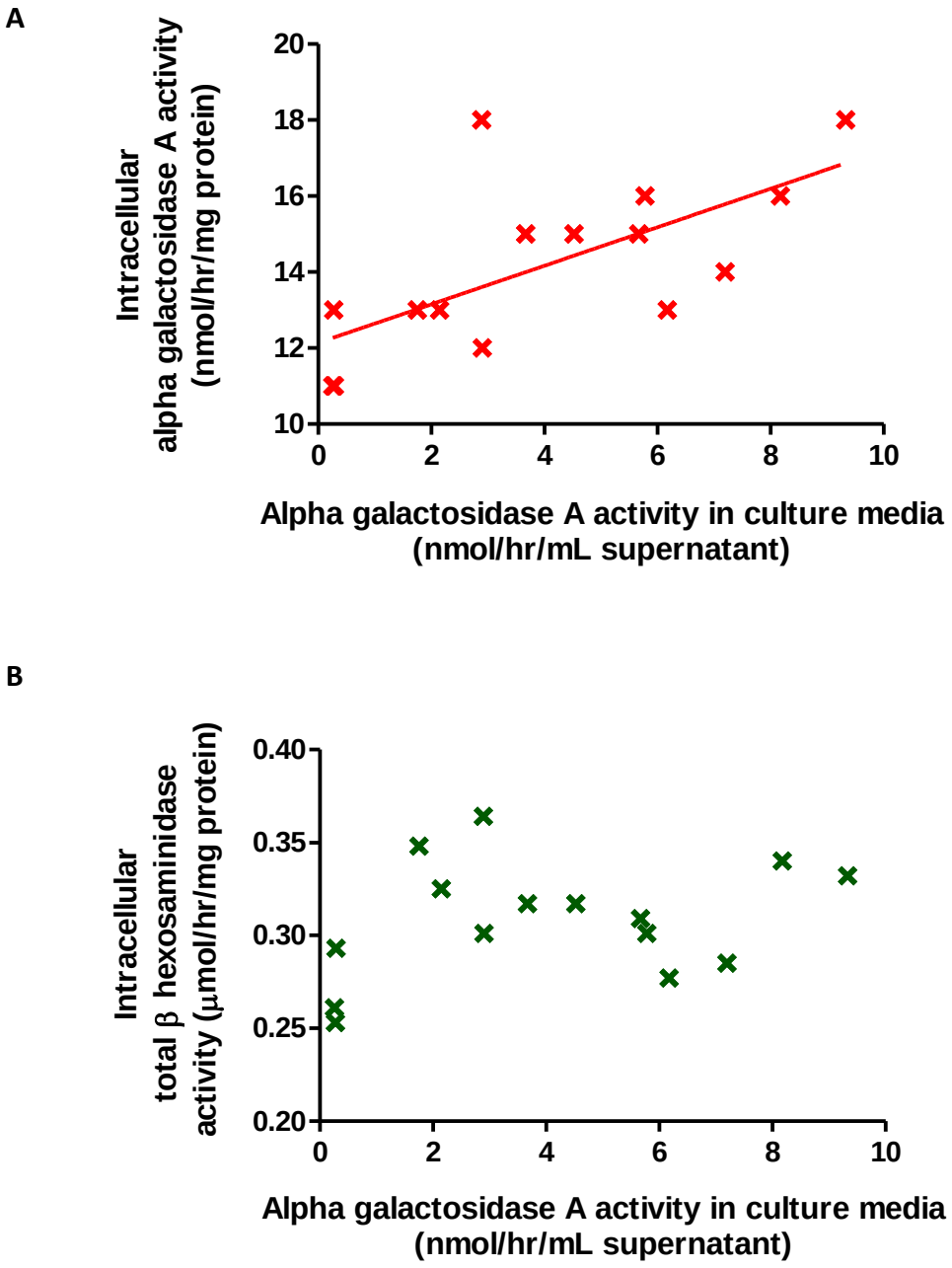

Figure 5-4: Uptake of alpha-galactosidase A and total beta hexosaminidase activity by wild type Jurkats from donor media overexpressing alpha galactosidase A

The donor media comprised one part fresh complete RPMI and three parts culture media taken from donor cells (*GLA*-Jurkats) after two days culture. The receiver cells (wild type Jurkats) were incubated for two days in the donor media. Intracellular α-galactosidase A (**A**) and total β-hexosaminidase (**B**) activity was plotted against the initial (day zero) α-gal A activity in donor media. There is slight but significant increase in α-gal A activity in the receiver cells with increasing donor media activity, linear regression R^2=0.450 (P<0.01), but no change in total β-hex activity.

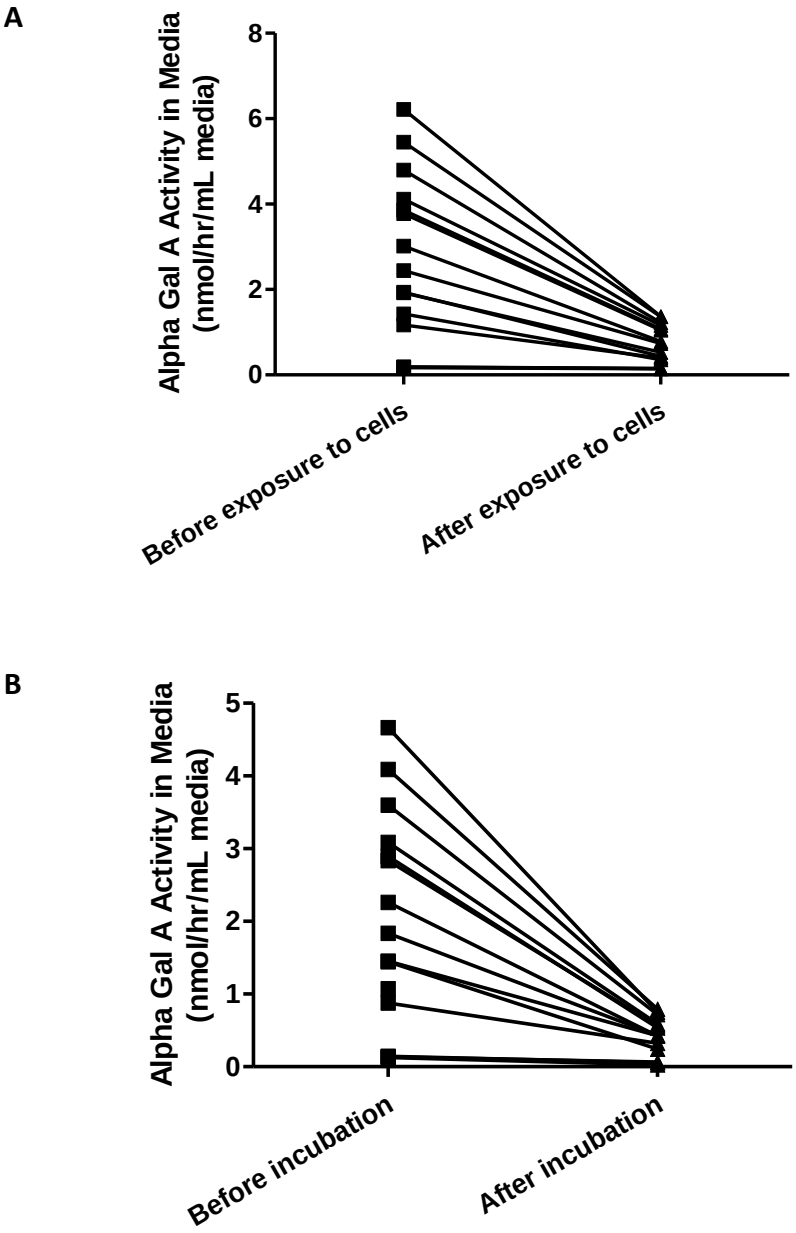

Figure 5-5: Reduction in α-gal A activity in media during 48 hours incubation with and without treatment-naive Jurkats present

A: Alpha-gal A activity in the donor media was measured before and after it was incubated with wild type Jurkats for two days. The graph presents the drop in activity observed. **B:** The drop in α-gal A activity in donor media measured before and activity incubation without cells present. This shows there is considerable degradation over two days incubation tending towards the baseline enzyme activity. The rate of degradation increases with initial enzyme activity in the donor media.

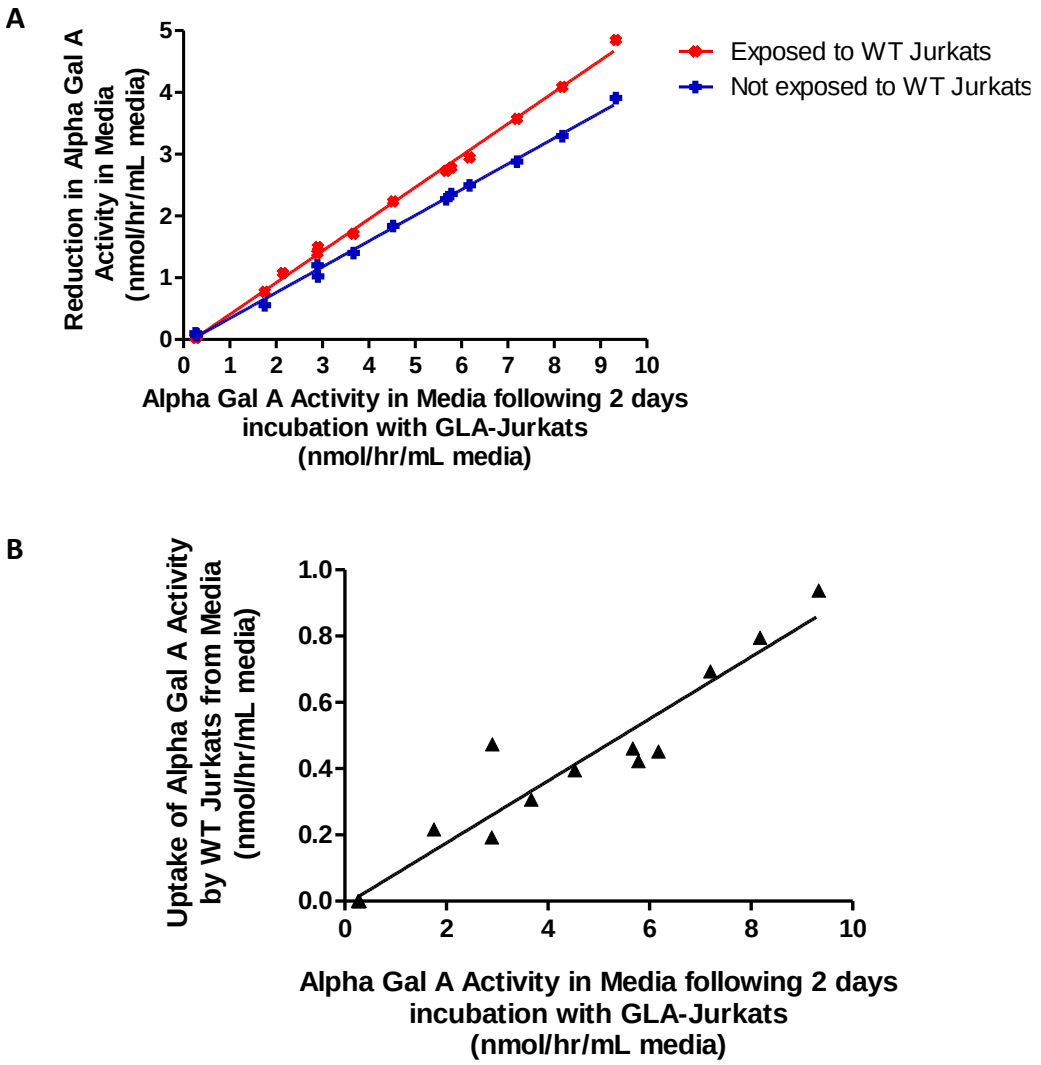

Figure 5-6: Uptake from donor media by wild type Jurkat (receiver cells)

A. Reduction in α-gal A activity in donor media over the incubation period was plotted against the initial α-gal A activity in the donor media before incubation. The red line shows the reduction in enzyme activity in the presence of wild type Jurkats (R^2=0.998); the blue line shows the degradation in enzyme activity over 48 hours incubation in the absence of Jurkats (R^2=0.997). There was a statistically significant difference between the slopes of the lines (P<0.0001), showing that the reduction in enzyme activity in media with cells is greater than without cells. **B**. The difference between red and blue data points in A equates to reduction in α-gal A activity in the culture media due to uptake of the enzyme by wild type Jurkats (R^2=0.917).

5.5 Effect of rotenone on cross-correction in Jurkats

Next, we sought to model the metabolic deficit observed in cultured skin fibroblasts from patients with Fabry disease, in order to observe its possible effect on the efficacy of lentivirus-mediated delivery of *GLA* to human cells and subsequent secretion and uptake of overexpressed α-gal A. Rotenone inhibits the mitochondrial respiratory chain complex I that oxidises NADH and reduces ubiquinone. Inhibition of complex I leads to ATP deficiency and oxidative stress because electrons transported by NADH cannot be delivered to oxygen. Therefore rotenone was used in a series of experiments to model ATP deficiency and oxidative stress in Jurkat cells.

Since the activity of complex I in whole cell homogenate will vary with mitochondrial content between cells, the activity of a second mitochondrial enzyme, citrate synthase, was analysed in Jurkats treated with and without rotenone for 24 hours. This treatment duration was based upon previous studies which used rotenone to inhibit Complex I (Aylett et al., 2013). Citrate synthase is a mitochondrial matrix enzyme that catalyses the rate limiting step in the TCA cycle. This enzyme speeds up the condensation reaction between acetyl coenzyme A, derived from pyruvate, amino acids or fatty acids, and oxaloacetate formed through the TCA cycle, to form citrate. Citrate synthase therefore enables continual hydrolysis of metabolic fuels.

Figure 5-7 shows the effect of 24 hours treatment with 100nM rotenone on complex I activity within Jurkats. Citrate synthase activity was also measured to normalise complex I activity for variation in mitochondrial content in wild type Jurkats.

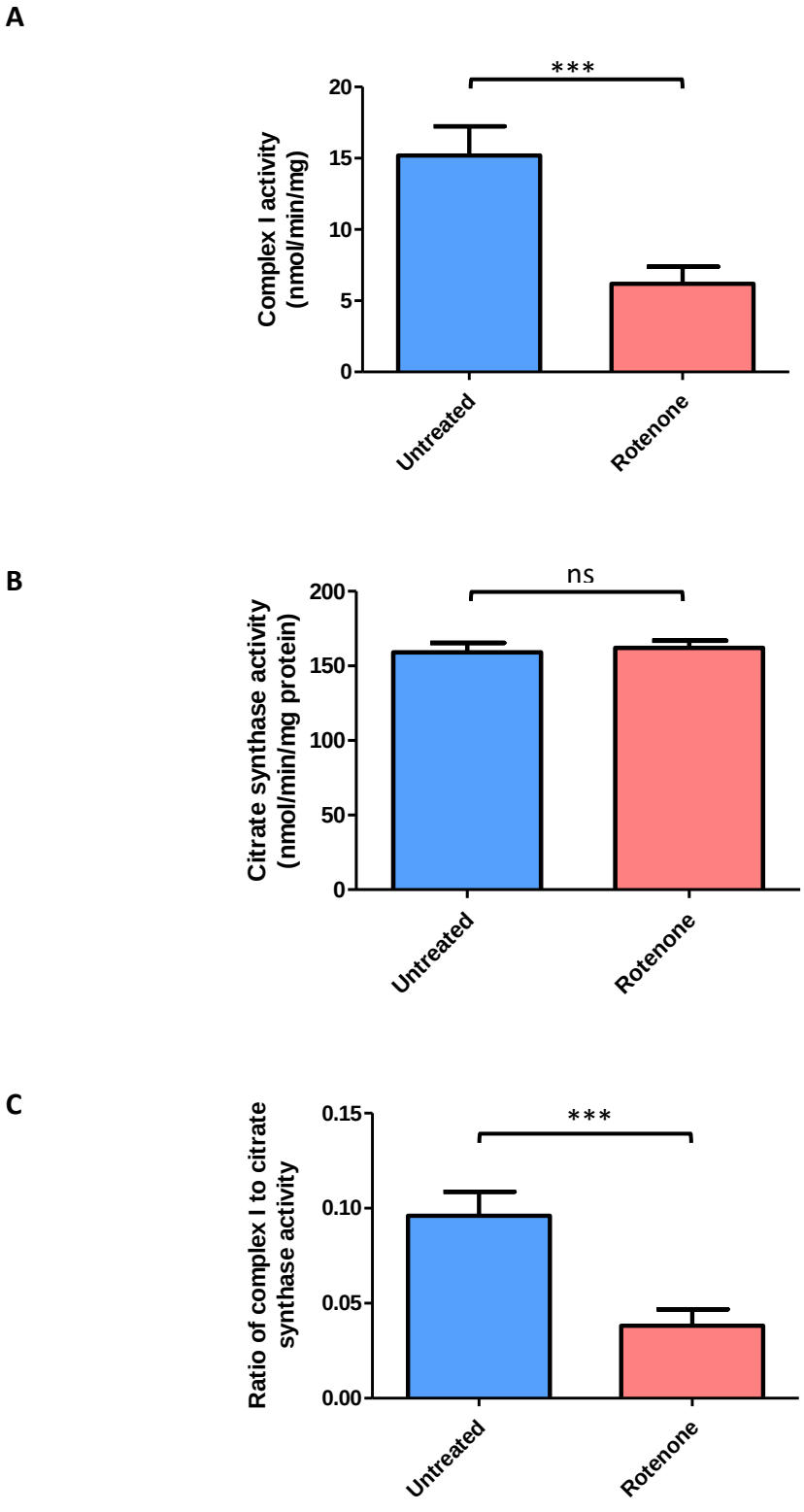

Figure 5-7: The effect of rotenone on mitochondrial complex I activity in wild type Jurkats

100nM rotenone halved complex I activity compared with untreated controls (**A**). There was no effect on citrate synthase activity (**B**). The ratio of complex I activity to citrate synthase activity takes account of variation in mitochondrial content between treated and untreated cells and shows a significant reduction in normalised complex I activity ($P<0.0001$) (**C**). n=3

5.5.1 Effect of rotenone on lentivirus-mediated *GLA* transduction efficiency

To examine the effect of mitochondrial complex I inhibition on the ability of human cells to be transduced by the lentivirus vector containing *GLA*, $3x10^5$ wild type Jurkats were incubated with virus (3.68×10^7pfu/mL, volumes from 0 - 5µL) with or without 100nM rotenone (final concentration in cell suspension) for 24 hours at 37°C. The cells were harvested and intracellular activity of α-gal A measured. Figure 5-8 shows there was no effect of 100nM rotenone on α-gal A activity compared with activity observed in untreated cells. Total β-hexosaminidase activity was also measured in the harvested cells and showed no change dependent on either virus load or rotenone treatment (Figure 5-9).

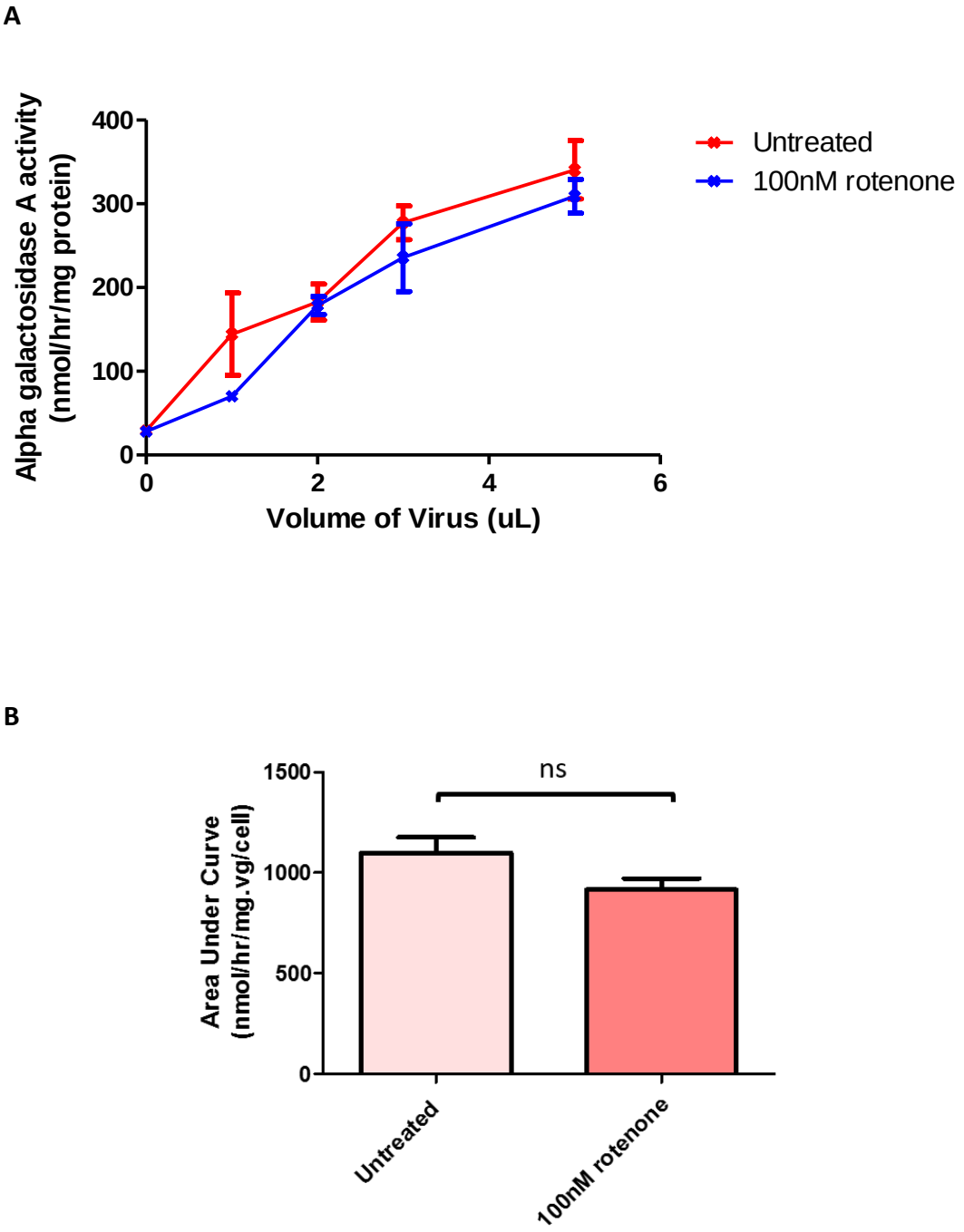

Figure 5-8: Efficiency of lentivirus-mediated overexpression of *GLA* with rotenone (n=3)

Human Jurkats were transduced with zero to 5µL lentivirus containing *GLA* (3.68 x 10^7viral particles per mL) in triplicate, with or without 100nM rotenone. **(A)** Shows α-gal A activity in cells following transduction with a range of virus volumes. Transduction with or without rotenone results in dose-dependent increase in the enzyme activity. **(B)** Area under the curve was calculated from the data and shows that inhibition of complex I does not affect the efficiency of lentivirus to transduce Jurkat cells.

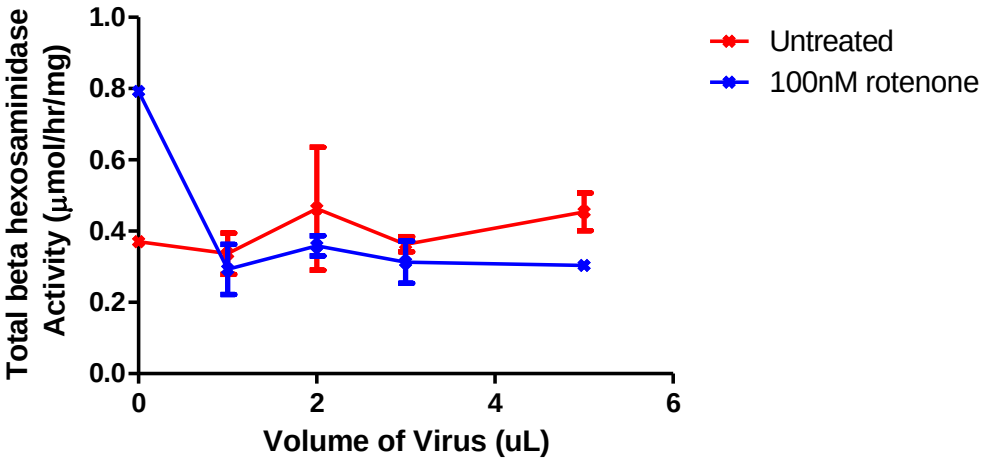

Figure 5-9: Effect of rotenone treatment on total β-hex activity in *GLA*-Jurkats (n=3)

There is no significant correlation between virus dose and enzyme activity in GLA-Jurkats with and without rotenone treatment. Using student t test to compare untreated and treated groups shows there is no statistical difference in activity relating to rotenone treatment.

5.5.2 Effect of rotenone on secretion of α-gal A by Jurkats overexpressing *GLA*.

The *GLA*-Jurkats that were transduced in the absence of rotenone in the previous experiment were washed three times in PBS to remove free lentivirus and ethanol. The donor cells were then re-suspended in fresh complete RPMI with or without 100nM or 50nM rotenone added. Culture media without rotenone treatment, was spiked with the same volume of absolute ethanol as the treated cells. The suspended cells were incubated for 24 hours at 37°C, after which the α-gal A activity within the media was measured.

The control in Figure 5-10 shows that, consistent with the previous experiments in Section 5.3, the secretion of intracellular enzyme into the surrounding media increased proportional to *GLA* overexpression within the donor cells. Rotenone treatment significantly reduced the amount of enzyme activity secreted over two days, but there was apparently no difference in secretion in the presence of 50nM compared with 100nM (final concentration) rotenone. There was no effect of either virus dose or rotenone dose on the activity of total β-hexosaminidase in the culture media (Figure 5-11).

A

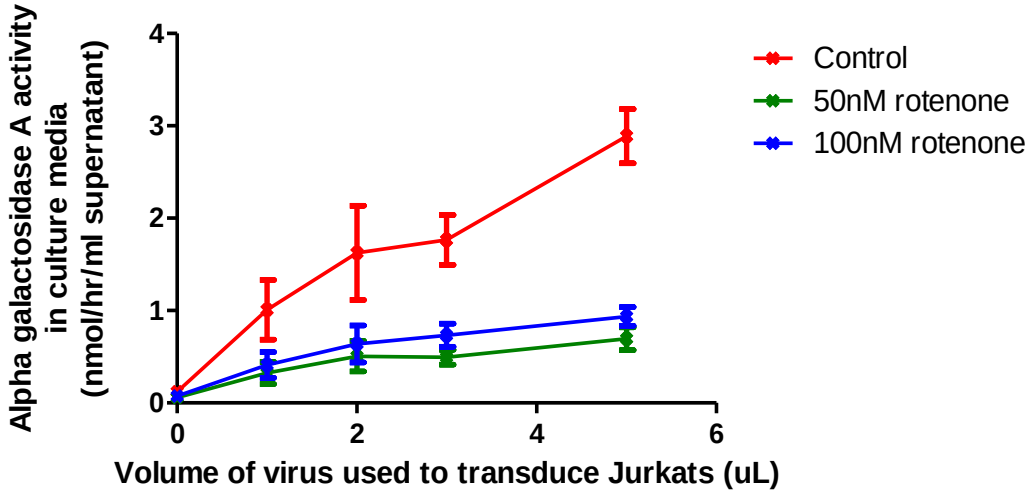

B

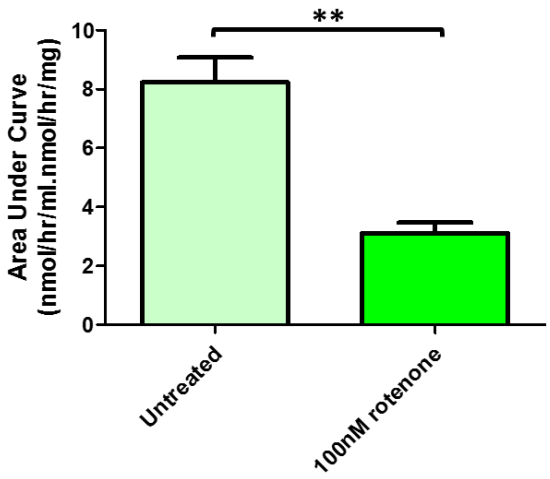

Figure 5-10: Effect of rotenone on secretion of alpha gal A into media by *GLA*-Jurkats

The activity of α-gal A was measured in the media of *GLA*-Jurkats after 24 hours incubation with or without treatment with rotenone 50nM and 100nM final concentrations. (**A**) Curves showing enzyme release from *GLA*-Jurkats with or without rotenone treatment. The enzyme activity in media increased with the virus dose used to transduce the *GLA*-Jurkats. The rate of increase was markedly lower in untreated media compared with untreated. Treatment with 100nM rotenone appeared to have the same effect on enzyme release as 50nM. (**B**) Difference in the enzyme release from *GLA*-Jurkats with or without 100nM rotenone treatment was assessed using area under the curve. There was a significant fall in α-gal A release with complex I inhibition ($P<0.001$).

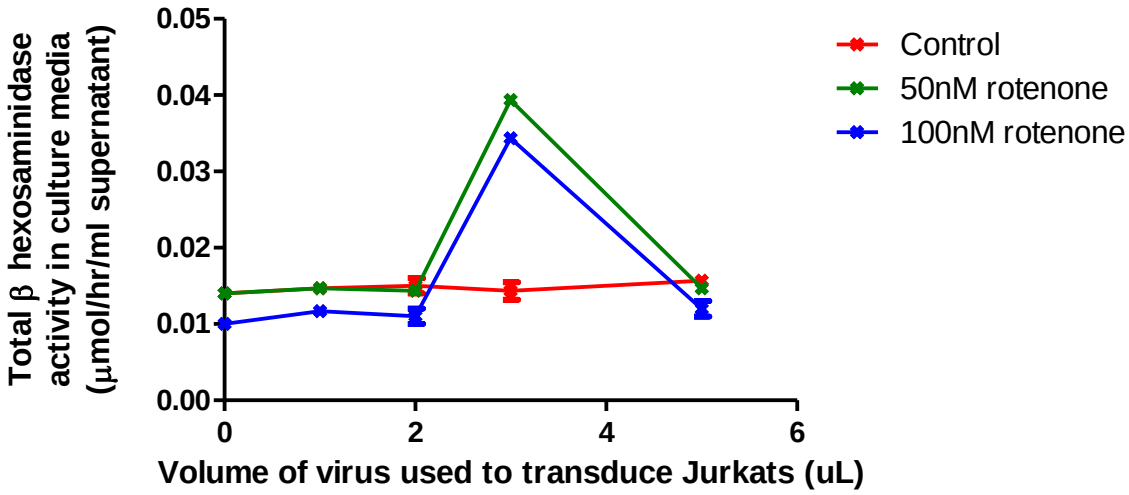

Figure 5-11: Secretion of total beta hex from GLA-Jurkats treated with rotenone

There was no correlation between enzyme secretion from GLA-Jurkats with virus dose. Using student t test to compare untreated and 100nM rotenone groups shows there is no statistical difference in activity relating to rotenone treatment.

5.5.3 Effect of rotenone on uptake of alpha gal A by wild type Jurkats.

Finally, the effect of complex I inhibition on uptake of overexpressed extracellular α-gal A by wild type Jurkats was examined. Control culture media from the previous secretion experiment, shown in section 5.5.2, was collected and mixed 3:1 with fresh complete RPMI, consistent with the uptake experiment in section 5.4. The initial α-gal A activity was measured in the mixed media before using it to incubate wild type Jurkats for 24 hours with/with-out 100nM rotenone. As a control, some of the mixed media was also incubated without cells for the same period of time. A volume of absolute ethanol was added to both the untreated cell group and the control group, equivalent to the volume of rotenone added to the treated group. After 24 hours the media was harvested and extracellular α-gal A activity was measured. In this way, the effect of rotenone alone was identified on enzyme uptake by wild-type (receiver) cells.

Similar to as shown in section 5.4, 24 hours incubation of media resulted in overall loss of α-gal A activity in receiver-Jurkat supernatant with or without rotenone. The natural degradation component of this loss was observed in the control medium which was not exposed to cells. In both the rotenone-treated and untreated groups, the difference between overall loss of enzyme activity in the presence of wildtype Jurkats and loss due to natural degradation was calculated. This difference may be due to uptake of functional α-gal A by wild type Jurkats. Figure 5-12A shows that there is no statistically significant difference in uptake by the cells treated with and without 100nM rotenone for 24 hours. The area under the two lines was calculated and shown in Figure 5-12B.

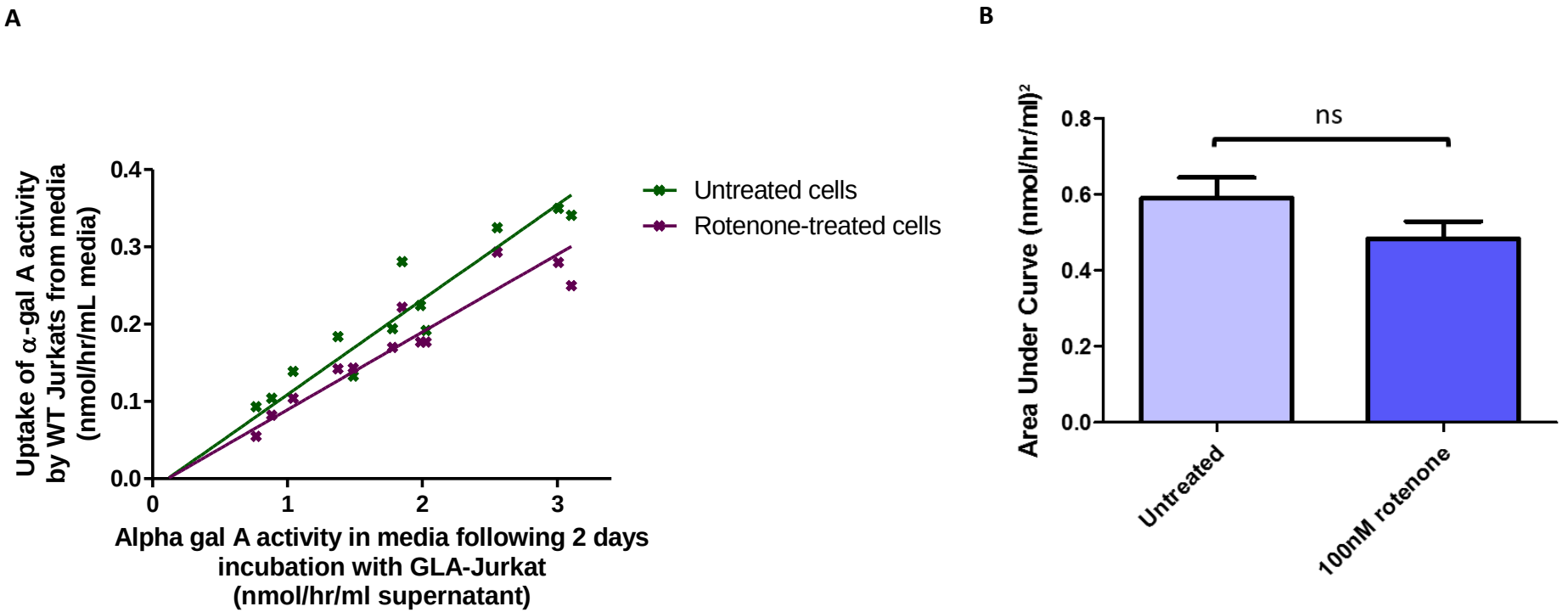

Figure 5-12: Effect of rotenone on uptake of α-gal A by wild type Jurkats from culture media.

Media taken from *GLA*-Jurkats was mixed 3 parts to 1 part fresh complete RPMI. The mixed media was added to wildtype Jurkats, with or without 100nM rotenone, and incubated for 24 hours. To take account of ethanol solvent used to dissolve rotenone, untreated cells were incubated with the equivalent volume of ethanol added to the media. **A**. The graph shows α-gal A activity in culture media supernatant from the wild type Jurkats, after media degradation was taken into account. There is no statistically significant difference between slopes for untreated and treated cells following linear regression analysis. Untreated cells R^2=0.917; Rotenone treated cells R^2=0.911. **B**. There was no difference in the area under the curve for uptake of α-gal A activity from treated and untreated media used to incubate wild type Jurkats.

5.6 Conclusions

The results in Figure 5-3 suggest that *GLA*-Jurkats are able to secrete functional α-gal A in both a time and virus dose dependent fashion. Although beyond three days the α-gal A activity within the culture media supernatant may continue to increase, it is possible that secretion reuptake by the *GLA*-Jurkats, and degradation of extracellular enzyme, may counteract any further rise. From Figure 5-3, two days appear to be sufficient for significant secretion of functional α-gal A. This agrees with previous research that found 48 hours was sufficient time for accumulated MPS to be significantly reduced in cells with either Hunters or Hurlers co-cultured with healthy cells (Fratantoni et al., 1968). Consequently, the uptake experiments shown in Figure 5-4 and Figure 5-5 were carried out using culture media previously incubated with *GLA*-Jurkats for two days.

The media used to incubate washed *GLA*-Jurkats for two days was re-incubated with wild type Jurkats for a further two days. Taking degradation of extracelluar enzyme activity during incubation into account, the results suggest significant evidence of uptake by wild type Jurkats (Figure 5-4 and Figure 5-6). This finding is supported by early research into using a lentivirus vector to deliver *GLA* to Fabry patient fibroblasts (Medin et al., 1996). This evidence is important because secretion and uptake of overexpressed α-gal A enzyme is essential for gene therapy to have therapeutic benefit against Fabry disease (Ruiz de Garibay et al., 2013).

Next, inhibition of complex I using rotenone (Figure 5-7) appeared not to block transduction efficiency of lentivirus into Jurkat cells and subsequent overexpression of enzyme being made. This suggests that Fabry disease does not prevent cells treated with gene therapy from manufacturing therapeutic enzyme and is an encouraging finding for development of future gene delivery for patients. However, inhibition of complex I appeared to significantly reduce secretion of α-gal A from treated Jurkats over 24 hours by 63% (Figure 5-10). This effect may be due to a number of factors. Firstly, ATP is necessary for the budding-off of enzyme-containing vesicles from the trans-golgi network following the secretory pathway (Salamero et al., 1990). So, ATP deficiency due to complex I inhibition may therefore decrease

secretion as observed. Secondly, reduced α-gal A secretion in response to complex I inhibition may also be due to oxidative stress. Complex I inhibition is both a cause and effect of oxidative stress on the mitochondrial respiratory chain (Ventura et al., 2002). If this is true, secretion of overexpressed α-gal A may therefore be enhanced by anti-oxidant treatments in combination with gene therapy. There may be great value in future work exploring the potential role of oxidative stress on inhibiting secretion.

Finally, the observation that complex I inhibition had no effect on enzyme uptake by receiver cells (Figure 5-12) suggests that, if release of α-gal A by donor cells is preserved, cross correction could still occur. Thus correction of the metabolic deficit may be of importance to optimise gene therapy for the future. Further work is now required to see if transduction corrects mitochondrial dysfunction in Fabry disease patient cells.

In conclusion, release of a-gal A from transfected cells has been demonstrated. Furthermore and consistent with the original cross contamination observations, uptake of enzyme by a target cell has been shown here. The finding that enzyme release is impaired when mitochondrial complex I is inhibited raises the possibility that cross correction could be compromised in Fabry disease. However, if enzyme replacement therapy or restoration of enzyme activity by gene transfer restores mitochondrial function then cross creation could proceed. Further work is now required to test this hypothesis.

Chapter 6 Alpha-galactosidase A activity in Fabry patient skin fibroblasts: efficiency of lentivirus-mediated overexpression

6.1 Introduction

The work presented so far in this thesis has been carried out in Jurkats. The reasons are firstly that, as an immortalised cell-line, Jurkats provide homogeneity between cultures, and relatively rapid and robust cell proliferation. They also exhibit low α-gal A activity relative to other cell-lines examined here, thus suggesting that this cell line may represent a useful model of enzyme deficiency and for examining the effects of α-gal A overexpression on cellular functions. Furthermore, as a lymphoblastic cell-line, Jurkats represent a good target for initial assessment of lentivirus-mediated gene delivery to haematopoietic cells. So the results reported thus far could hold important potential implications for the design of future gene delivery to treat Fabry disease.

The next stage is to begin to extend the work carried out in Jurkats using primary patient cells to see whether the findings so far hold true in a more clinically relevant cell type. Fabry disease is a multisystemic, metabolic disorder that effects nearly all cell types in humans, including fibroblasts of skin and heart, and myofibroblasts that support vascular smooth muscle. Some degree of Gb3 storage is typically seen in fibroblasts. Mitochondrial respiratory chain dysfunction was reported in skin fibroblasts from Fabry disease patients (Lucke et al., 2004). Fibroblasts are therefore potential participants in the pathophysiology of Fabry disease and clinically relevant targets for treatment. So, the overall aim of initial investigations is to assess whether fibroblasts from Fabry disease patients may be transduced by lentivirus made using the *pRRLSIN.cPPT.PGK-GLA.WPRE* vector plasmid.

6.2 Materials and Methods

All materials and methods were as described in Chapter 2 Materials and Methods, except for the following additions.

6.2.1 Human skin fibroblasts

The cells shown in Table 6-1 were purchased from the Coriell Institute for Medical Research, New Jersey, USA, and delivered as live cultures. All cell donors were Caucasian males.

Table 6-1: Human skin fibroblasts from Fabry disease patients and controls

The table shows the identity of cells purchased from the Coriell Institute for Medical Research (New Jersey, USA). Fabry disease patients GM00881 and GM02769 were reported to be hemizygous for a point mutation replacing cytosine with thymine at nucleotide 658 of the complementary DNA sequence of the *GLA* gene. This mutation results in a stop codon in place of a codon for arginine, leading to truncation of the α-gal A protein at position 220 of the amino acid sequence. NA: not applicable.

Cell ID	Tissue of origin	*GLA* genotype	Age of donor at sampling
GM00881	Primary skin fibroblasts from males with previously reported classical Fabry disease phenotype	c.658C>T	17
GM02769		c.658C>T	18
GM02775		Maternal 1st cousin of GM02769	16
GM23815	Primary skin fibroblasts from males, apparently healthy	NA	22
GM23964		NA	21
GM23973		NA	19
GM23975		NA	25
GM23976		NA	22

All members of the control group were reported to be clinically normal with no known medical or neurological signs of disease. Except for doner GM23815, each control had previously undergone magnetic resonance imaging of the brain, neurological and neuro-psychological examinations, and review of medical records. All these examinations confirmed the control group were apparently healthy. Members of the control group were selected for this study based upon similar ages to the group affected by Fabry disease.

Within the affected group, donor GM00881 displayed the phenotype for classical Fabry disease including undetectable α-gal A activity and lipid deposition in microvascular endothelium. Genetic analysis found a point mutation resulting in a premature stop codon within exon 5 of *GLA*. Donors GM02769 and GM02775 were within the same family. The proband, diagnosed first with classical Fabry disease, was GM02769 presented undetectable α-gal A activity and the same nonsense mutation within *GLA* as found in donor GM00881. Absent α-gal A activity was confirmed in donor GM02775.

6.2.2 Cell culture reagents

0.25% trypsin in EDTA	Life (Paisley, UK)
Hams F10 medium with 25mM HEPES and L-Glutamine (Hams)	Life (Paisley, UK)

6.2.3 Fibroblast culture methods

Apparently healthy control fibroblasts and fibroblasts from male Fabry disease patients shown in Table 6-1 were grown, according to suppliers instructions, in Hams medium, 14% FBS, 1% pen-strep at 37°C, 5% CO_2. The cells formed an adherent monolayer so 0.25% trypsin in EDTA was used to dissociate the cells for passaging 1:2 whenever the cells were confluent.

6.3 Results

6.3.1 Growth rate in skin fibroblasts from healthy controls and Fabry disease patients

Acquiring Fabry disease patient skin fibroblasts took considerable time. Two attempts to culture patient cells held in liquid nitrogen archives by the Department of Chemical Pathology, Great Ormond Street Hospital (London, UK) were unsuccessful. Cultured skin fibroblasts from Fabry disease patients and apparently healthy controls listed in Table 6-1 were eventually sourced from the Coriell Institute of Medical Research (New Jersey, USA). The cells were counted at two time points and the results are shown in Table 6-2, except for cells from Fabry disease patient donors GM02769 and GM02775, and control donor GM23975. Cells from these three donors grew very slowly and were quiescent after one month in culture. A second batch of cells from the same donors were purchased and cultured for experiments over three weeks, but cell growth data was not collected.

The live cell count data was used to estimate rate of growth for each donor culture in terms of time required for the number of cells to double, as shown in Table 6-2. The results may suggest a difference in rates of growth between control and patient cells, but there was an insufficient number of patients in the affected group to carry out statistical comparison. Further work is necessary to confirm whether there is a difference in rate of growth between control and patient fibroblasts.

Table 6-2: Live cell count and rate of growth of Fabry disease patient and healthy control skin fibroblasts in culture

Human skin fibroblasts were counted before transfer to T75 cell culture flasks for incubation according to the supplier's instructions over various periods of time. The cells were then counted again and approximate doubling time calculated. The data shown is the average of two independent counts of cells from the same culture flask from each patient or control. Statistical comparison was not possible because data was collected for cells from only one Fabry disease patient. The reason for this was that GM02769 and GM02775, as well as control cells GM23975, had stopped growing in this experiment.

Cell donor	Supplier's cell ID No:	Initial cell count ($x10^6$ cells)	Final cell count ($x10^6$ cells)	Duration of culture period (days)	Approximate doubling time (days)
Fabry disease patient	GM00881	0.8	1.6	10	10
Apparently health controls	GM23815	0.8	4.0	12	5
	GM23976	0.5	3.0	12	5
	GM23964	0.6	1.8	4	3
	GM23973	0.6	1.5	4	3

6.3.2 Alpha-galactosidase A activity is reduced in cultured skin fibroblasts from male patients with Fabry disease

Cultured skin fibroblasts from five healthy controls and three male patients shown in Table 6-1 were harvested and the activity of α-gal A, together with a second control lysosomal hydrolytic enzyme β-galactosidase, was measured. The results are shown in Figure 6-1 and confirm that the fibroblasts cultured from patients exhibit significantly lower α-gal A activity compared with healthy controls. In comparison there was no difference in β-galactosidase activity between the two groups, confirming that the difference in α-gal A activity was not due to cell viability or global differences in the cellular lysosomal content.

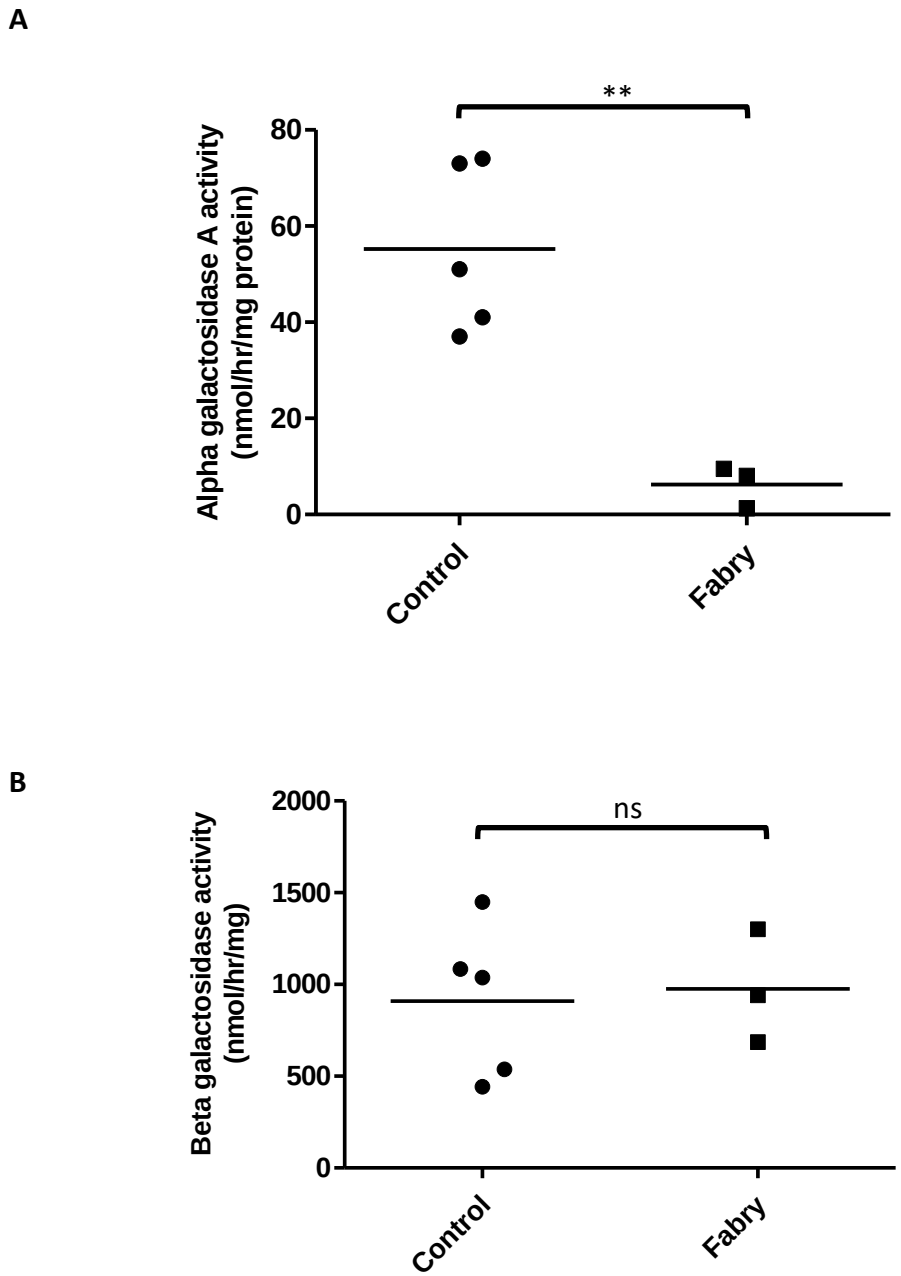

Figure 6-1: Activity of alpha and beta galactosidase enzymes in cultured skin fibroblasts

The activity of two hydrolytic lysosomal enzymes, β-gal acting as a control of both cell viability and lysosomal content, to assess α-gal A activity in fibroblast samples from healthy subjects and patients. **A**. Alpha-galactosidase A activity; there is a significant reduction in the activity of fibroblasts from patients compared to controls ($P<0.01$). **B.** Beta-galactosidase activity; there is no significant difference between the two groups.

6.3.3 Lentivirus-mediated overexpression of α-gal A in healthy control skin fibroblasts

The lentivirus preparation used for this experiment was previously titred in Jurkat cells and found to contain 3.68 x 10^7viral particles per mL, as used in Chapter 5. Approximately 3.0 x 10^5 fibroblasts were transduced with a volume of lentivirus equivalent to an MOI of 0.6 based on the titre. This volume was chosen because our earlier work in Chapter 4 suggested that cells containing 0.4vg/cell manufactured enzyme with similar affinity as wild type enzyme, but cells containing at least 1.5vg/cell overexpressed α-gal A with significantly less affinity to the synthetic substrate 4MUG. Based upon an idealised Poisson's distribution, an MOI of 0.6 would transduce 30% to 40% cells with at least one copy of the viral genome containing *GLA* (Fehse et al., 2004). So, at this virus copy number α-gal A was expected to exhibit the same substrate affinity as healthy control cells.

It is important to note that since titration and transduction were executed on different cell-types, it is not possible to make direct predictions of virus copy number within the transduced fibroblasts based upon the MOIs shown. However, the purpose of this experiment was not to assess enzyme activity in response to absolute virus doses, but to see the effect of *GLA* transgene delivery on intracellular α-gal A activity in healthy controls before and after transduction with lentivirus.

So, to that end, the skin fibroblasts from the healthy control group shown in Table 6-1 were transduced with 5µL lentivirus suspension (equivalent to MOI 0.6 in Jurkats), harvested and the intracellular activity of α-gal A measured. The activity was compared with the activity in untreated cells. The results, shown in Table 6-3, suggest that the lentivirus produced from the *pRRLSIN.cPPT.PGK-GLA.WPRE* vector plasmid is capable of infecting human skin fibroblasts to potentiate a highly significant increase in α-gal A activity.

Table 6-3: Lentivirus-mediated overexpression of alpha gal A in control human fibroblasts

Healthy human fibroblasts were transduced with 5µL lentivirus suspension (equivalent to MOI of 0.6 in Jurkats) and intracellular α-gal A activity was measured. There is a significant increase in activity (P<0.0001), suggesting that human skin fibroblasts may be successfully transduced with lentivirus produced from vector plasmid *pRRLSIN.cPPT.PGK-GLA.WPRE*. SD: standard deviation

	Control (n=5)	*GLA*-Control (n=5)
Mean activity +/- 1 SD (nmol/hr/mg protein)	55.2 +/- 17.5	9430 +/- 1577

6.3.4 Lentivirus-mediated expression of α-gal A in skin fibroblasts from Fabry disease patients

Next, attempts were made to transduce skin fibroblasts cultured from the Fabry disease patient group, shown in Table 6-1, with lentivirus containing *GLA*. After harvesting cells from the patient fibroblast cultures from the previous experiment shown in Section 6.3.2, there were insufficient cells from donor GM02775 to transduce. So results were only achieved for two of the three patient donors. In order to get some indication of relationship between relative transgene dose and α-gal A overexpression, 3.0 x 10^5 cells from each patient was treated with 3µL and 5µL lentivirus suspension (equivalent to MOIs of 0.4 and 0.6 in Jurkats). The results are shown in Table 6-4 and indicate a dose response in enzyme activity to amount of virus suspension delivered.

Table 6-4: Lentivirus-mediated overexpression of alpha gal A in Fabry disease patient skin fibroblasts

Dose-dependent increase in α-gal A activity in Fabry disease patient fibroblasts is shown in response to increasing volume of lentivirus suspension containing the *GLA* transgene (3µL and 5µL were equivalent to MOIs of 0.4 and 0.6 in Jurkats). Statistics not shown because each transduction has n=1 due to challenges of culturing the patient cells. SD: standard deviation

	Untreated patient fibroblasts (n=3)	Patient fibroblasts treated with:	
		3µL virus (n=1)	5µL virus (n=1)
Mean activity +/- 1SD (nmol/hr/mg protein)	6.3 +/- 4.4	1455	2241

Finally, the results from the above transduction experiment in Fabry disease patient fibroblasts were compared to those obtained with healthy control fibroblasts and the findings are shown in Figure 6-2. The activity of α-gal A within the Fabry patient cells treated with 5µL virus exceeded by nearly forty-fold the physiological levels found in the healthy control cells. Although statistical analysis was not possible due to the low n number in the Fabry disease patient group, visual observation suggests that the efficiency of transduction of patient cells is lower than in healthy controls at the same virus dose.

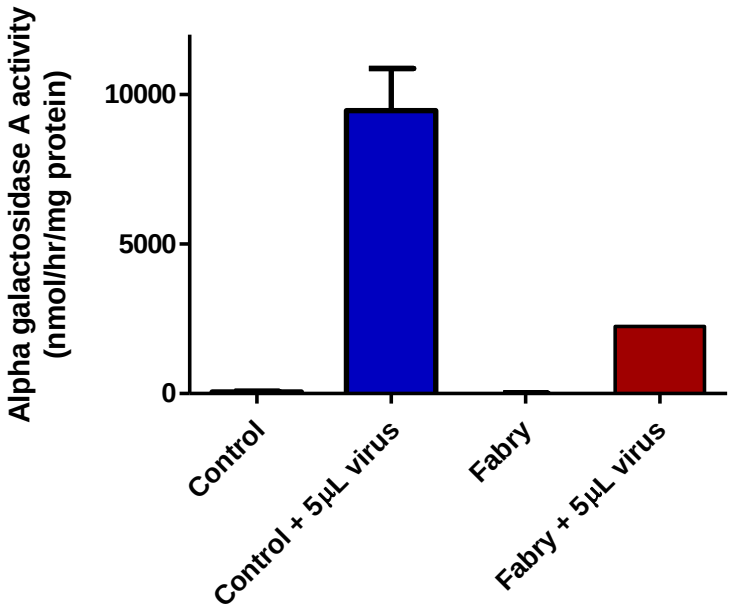

Figure 6-2: Comparison of transduction of efficiency in skin fibroblasts from Fabry disease patients and healthy controls

The overexpression of α-gal A in terms of activity was compared in skin fibroblasts from healthy controls (n=5) and a Fabry disease patient (n=1) following treatment with 5µL lentivirus suspension (volume equivalent to MOI 0.6 in Jurkats). The results suggest that transduction efficiency of the lentivirus may be lower in fibroblasts from Fabry disease patients than from healthy controls.

6.4 Conclusions

The intent was to begin to extend the work carried out in Jurkats and to generate initial data using fibroblasts from Fabry disease patients. Results suggested that growth rate of patient cells may be lower than in control cells, but this observation was based on only one patient and needs to be further investigated in future work. A possible mechanisms for reduced rate of growth in Fabry fibroblasts may be reduced activity of mitochondrial respiratory chain complexes leading to reduced ATP bioavailability (Lucke et al., 2004). However, despite significant Gb3 storage in Fabry fibroblasts, their function does not appear to be compromised since there is no evidence that wound healing is impaired (Elleder, 2010). Apparently in contradiction to this, fibrosis is observed in developed cases, suggesting that fibroblast activity may actually increase in Fabry disease patients (Nagano et al., 2016, Weidemann et al., 2013). *In vitro* cell culture does not provide fibroblasts with stimuli from the malleus of growth factors and cell-cell signalling which influence cell function *in vivo*. So future work investigating the effect of Fabry disease on fibroblast growth rates with higher n numbers should take this limitation into account.

Results also showed that patient fibroblasts exhibited lower α-gal A activity than in control cells, and primary skin fibroblasts were amenable to transduction by the lentivirus containing the *GLA* transgene. In patient fibroblasts the overexpression corrected enzyme deficiency to supra-physiological levels, but was not as great as in control cells transduced with the same virus dose. This suggests that transduction efficiency may be compromised in Fabry disease, based on a single culture from one patient. Further investigations using higher n numbers of viable fibroblast culture from Fabry disease patients are needed to explore this hypothesis. A possible mechanism for reduction in efficiency of lentivirus to transduce Fabry fibroblasts may be accumulation of Gb3 at the plasma membrane reducing the expression of glycoproteins recognised by the lentivirus for cell binding and infection (Lund et al., 2009, Ramkumar et al., 2009). Gb3 accumulation is known to reduce cholesterol content of cellular membranes, disrupting membrane fluidity and permeability (Das and Naim, 2009). This process may possibly influence virus endocytosis by target cells.

In conclusion, this preliminary work has raised questions regarding the effect of α-gal A deficiency on cell growth and ability to be transduced by therapeutic lentivirus. In the next chapter, these questions will be placed in the context of the overall thesis so that future work can be proposed which builds upon the understanding developed through this project.

Chapter 7 Discussion

7.1 General discussion

Fabry disease is a progressive, multi-systemic and heterogeneous metabolic disorder caused by mutations in the X-linked gene *GLA* (NCBI: NM_000169.2) that codes for the lysosomal acid hydrolase α-gal A (Bishop et al., 1986, Brady et al., 1967, Calhoun et al., 1985). The predominant natural substrate of α-gal A is the glycosphingolipid Gb3 (Dean and Sweeley, 1979a, Sweeley and Klionsky, 1963). Two aspartate residues within the enzyme's active site hydrolyses terminal galactose from Gb3 to produce lactosylceramide (Garman and Garboczi, 2004). This is an essential step in the sequential catalysis of globoside to ceramide within lysosomes (Kolter and Sandhoff, 1999).

Over the last three years the number of known pathogenic mutations detailed in the Human Gene Mutation Database in the *GLA* locus has increased from 600 to over 900 (Stenson et al., 2009). These mutations result in α-gal A deficiency leading to Gb3 accumulation in a wide variety of cell types. Notable sites of Gb3 storage in patients include endothelium, peripheral neurons, cardiomyocytes and renal podocytes (Desnick et al., 2001, Elleder, 2010, Hozumi et al., 1990). The reasons for the apparent instability of the *GLA* locus is unknown. Possibly, mutations in *GLA* may confer some evolutionary advantage against pathogens because Gb3 plays an important role in immunity (Darmoise et al., 2010). Gb3 is the cell surface marker CD77 which is the sole receptor for Escherichia *coli* verotoxins (Tetaud et al., 2003), and natural resistance factor against HIV infection (Lund et al., 2009, Ramkumar et al., 2009).

Though a single gene disorder, the phenotypic consequences of *GLA* mutations are complex. Symptoms of classical Fabry disease are devastating and life-threatening. They begin in early childhood and progress to effect cerebrovascular, cardiovascular and renal systems. There are non-classical variants of the disease which tend to be later-onset, milder and focused on one or more of these systems (Ko et al., 1996). Certain *GLA* mutations have been linked with classical and non-classical variants of the disease (Schiffmann et al., 2016), but generally genotype and phenotype do not

correlate (Gal, 2010); family members carrying the same mutation may present very different symptoms in different organs and cell-types (Ries and Gal, 2006).

From the genetic and clinical picture it was logical to hypothesise that cell-types vary in terms of susceptibility to pathology resulting from *GLA* mutation and α-gal A deficiency. The present work therefore commenced with characterisation of α-galactosidase activity in different human cell-types. Alpha-gal A activity, standardised for variation in lysosomal content, was significantly higher in the transformed embryonic kidney (293T) cell-line compared with primary fibroblasts and a hepatocarcinoma (Hu-H7) cell-line. Proteinuria is one of the early signs of FD in which glomeruli and distal tubules become major sites of Gb3 storage (Desnick et al., 2001, Hozumi et al., 1990). Gb3 clearance from renal podocytes in response to ERT is limited (Weidemann et al., 2013) and end-stage kidney failure is a notable cause of mortality amongst patients (Germain, 2010). Lyso-Gb3 stimulated release of fibrogenic cytokine TGF-β1 and other mediators of increased extracullular matrix production in cultured human podocytes (Sanchez-Nino et al., 2011). So kidney has important relevance, whereas liver and fibroblasts have lower relevance, in the pathophysiology of FD. In liver, Gb3 accumulation is low and limited to hepatocytes which do not show major signs of pathology. Gb3 accumulation in fibroblasts is significant but without signs of subsequent cell dysfunction in either wound healing or extracellular matrix production (Elleder, 2010). This may be because lyso-Gb3 does not stimulate fibroblast proliferation (Aerts et al., 2008), which suggests secondary mediators of tissue injury are not promoting pathogenic processes in fibroblasts (Weidemann et al., 2013).

The evidence in support of the hypothesis is limited by the finding in skin fibroblasts of reduced respiratory chain enzyme activity in FD (Lucke et al., 2004), which may be due to Gb3 accumulation disrupting lipid composition of cellular membranes (Das and Naim, 2009). A further limitation is that the results here were in human immortalised cell-lines rather than primary cells. The transformation of cell-lines, whilst improving standardisation between cultures, may effect *GLA* expression and alter α-gal A activity. The morphology of human cell-lines are often different from their tissue of origin. To address this limitation, induced human pluripotent stem (iPS)

cells may be reprogrammed into relevant cell-types for further investigation (Raval et al., 2015).

In wild type male CD1 mice, the standardised ratio of α-gal A against β-gal was significantly higher in murine skeletal muscle than brain, lung, liver, kidney, heart and spleen. Skeletal muscle shows limited clinical manifestations of FD. Although cases of osteopenia and osteoporosis have been identified in various studies of FD, it was unclear whether results were skewed by undetected vitamin D deficiencies (Germain, 2010). Any involvement of skeletal muscle in FD is considerably less than cerebrovascular, cardiovascular and renal tissues (Elleder, 2010). So there is an apparent reversal of relationship between standardised ratio for α-gal A activity and susceptibility to Fabry disease in man and mouse.

The murine model of Fabry disease in which *GLA* is knocked out, exhibits absent α-gal A activity and Gb3 accumulation in various tissues, yet none of the clinical symptoms observed in patients (Ohshima et al., 1997, Ohshima et al., 1999). Perhaps the loss or reversal of tissue susceptibility suggested here in wild type mice relates to the absence of clinical phenotype reported in the *GLA* knock-out mouse. In considering this possibility it should be noted that the lysosomal enzyme assays used in the present work were only fully validated for human cells and tissues. To study lysosomal enzymes in murine tissues in detail, the assay should be re-evaluated.

On diagnosis of Fabry disease, there are currently two forms of treatment available to patients: enzyme replacement therapy (ERT) (Schiffmann et al., 2001, Eng et al., 2001) and small molecule chaperone therapy (Markham, 2016). In some cases, but not all, the clinical response to ERT may be a poor return for the psycho-social and physical burden of biweekly intravenous administration of recombinant protein that ERT imposes on patients. In comparison chaperone therapy is administered orally but is only applicable for amenable mutations which account for 35% - 50% of pathogenic mutations in *GLA* (Hughes et al., 2016, Markham, 2016). So, at least half of all Fabry disease patients will not benefit from this mode of treatment.

Alternative therapies are therefore urgently required to treat Fabry disease. Substrate reduction therapy, an orally administered glucosylceramide synthase

inhibitor, has recently completed its first early-stage clinical trial in patients receiving ERT (Guerard et al., 2017). Another option is to address the root cause of the disorder by inserting a correct copy of *GLA* into patient cells to enable synthesis of functional α-gal A for long-term therapeutic benefit. This is the rationale behind gene therapy (Friedmann and Roblin, 1972).

Since Fabry disease is due to monogenic loss-of-function mutations, it is a good candidate for gene therapy (Friedmann and Roblin, 1972). Lentivirus offers a potent method of gene delivery to both dividing and non-dividing cells with high transduction efficiency and clinical safety (Sakuma et al., 2012). So the work reported next explored the impact of lentivirus-mediated α-gal A overexpression in order to improve understanding of this important therapeutic option on the cellular level.

A third generation lentivirus vector plasmid (*pRRLSIN.cPPT.PGK-GLA.WPRE*), containing a transgene encoding mature human α-gal A regulated by the human phosphoglycerate kinase promoter, was constructed at UCL GOSICH (London, UK) (Rajaraman, 2013). The vector was then transfected into a packaging cell-line to harvest concentrated lentivirus supernatant containing 2.8 x 10^7 pfu/mL in Chapter 4 and 3.68 x 10^7 pfu/mL in Chapters 5 and 6.

The characterisation of α-galactosidase in human cell types showed that the B-lymphoblastic leukaemia cell-line called Jurkat exhibited low endogenous α-gal A activity relative to other cell-types tested. Furthermore, as a cell-line originating from transformed haematopoietic progenitors, Jurkats may have some relevance to *ex-vivo* gene therapy. Transduction of Jurkats by the lentivirus harvest resulted in a dose-dependent increase in both the expression and activity of intracellular α-gal A, with no evidence of cell toxicity up to 1.8vg/cell. This is consistent with many previous studies that showed engineered vectors containing cDNA encoding human α-gal A can generate therapeutic *GLA* transgene expression in transduced target cells (Huang et al., 2017, Jung et al., 2001, Medin et al., 1996, Pacienza et al., 2012, Park et al., 2003, Sharma et al., 2015, Sugimoto et al., 1995, Takenaka et al., 1999a, Takenaka et al., 2000, Takiyama et al., 1999, Yoshimitsu et al., 2006, Yoshimitsu et al., 2007, Yoshimitsu et al., 2004).

Enzyme kinetic studies were used to explore the catalytic efficacy of therapeutic enzyme produced as a result of transgene delivery. The findings suggested that as virus dose increases in transduced cells from 0.4vg/cell to 1.5vg/cell, the affinity of α-gal A to synthetic substrate 4MUG reduced, as indicated by increased Km. This appears to be the first study exploring the kinetic properties of α-gal A produced by transduced cells. The findings may point to need to optimise virus dose in order to deliver maximum therapeutic benefit to patients.

The observed increase in Km, and corresponding decrease in affinity, with increasing transgene dose may be due to impaired cellular sorting because of congested lysosomal trafficking. For evidence to support this hypothesis, Lysotracker may be used with live-cell imaging to study the intracellular trafficking of fluorescence-labelled α-gal A (Chazotte, 2011). The cells can be transduced by a lentivirus containing a hybrid transgene incorporating *GLA* and *GFP*. In this way the effect of various degrees of enzyme overexpression on lysosomal trafficking can be explored. Congested lysosomal trafficking may lead to impaired cellular sorting because of glycosylation defects. Glycosylation patterns are cell type-specific and may regulate tissue/plasma distribution, proportion of enzyme targeted for secretion, and dose-response to ERT (Garman and Garboczi, 2004).

As a haematopoietic progenitor, Jurkats are a highly relevant cell-line for investigation of gene therapy for Fabry disease. HSCs have been proposed as ideal targets for *ex vivo* gene delivery due to their ability to self-renew and to differentiate to give rise to all the cell-types of blood and tissue macrophages (Karlsson, 1991). Enzymatic correction of macrophages is important because they accumulate high levels of Gb3 through digesting globoside from within the plasma membranes of redundant, damaged or senescent erythrocytes (Dawson and Sweeley, 1970). Blood cells may subsequently cross correct parenchymal and stromal cells throughout the body (Fratantoni et al., 1968, Karlsson, 1991).

Cross correction between transduced and treatment-naive cells in the development gene therapy for Fabry disease needs to be explored since Gb3 accumulation is widely distributed throughout patients and effects multiple organs (Desnick et al., 2001,

Elleder, 2010, Germain, 2010). This need is urgent because a clinical trial application for a “first in the world” gene therapy trial for Fabry disease using *ex vivo* lentivirus-mediated transgene delivery to HSCs was recently accepted (Huang et al., 2017). So, here Jurkat cells were transduced with the harvested lentivirus containing the *GLA* transgene. They showed virus dose- and time-dependent release of α-gal A activity out into their culture media during 3 days incubation. Media collected after two days incubation was collected and used to incubate treatment-naive Jurkats for a further two days, during which time the cells specifically took up α-gal A from the media. Together this demonstrated cross correction between Jurkats as observed previously in fibroblasts (Takenaka et al., 1999b) and immortalised lymphoblasts derived from Fabry disease patients (Medin et al., 1996).

Fabry disease is known to interrupt energy metabolism in cardiomyocytes (Machann et al., 2011, Nagano et al., 2016, Palecek et al., 2010) and brain tissue (Itoh et al., 2001). Furthermore, the activity of mitochondrial respiratory chain complexes is reduced in skin fibroblasts from patients (Lucke et al., 2004). In view of these affects, rotenone was used to inhibit the mitochondrial respiratory chain complex I in Jurkats. Complex I helps control ATP biosynthesis and its inhibition may model metabolic deficit with relevance to FD (Davey et al., 1998, Rossignol et al., 2000, Telford et al., 2009). Here it was shown that Complex I inhibition had no effect on the transduction efficiency of the lentivirus on Jurkats. However, the ability of transduced Jurkats to secrete overexpressed α-gal A out into their surrounding media was reduced. No effect was observed on the ability of wild-type Jurkats to take up enzyme from collected media. These results hold implications since they suggest that the uptake of ERT into cells from plasma and interstitial fluid is not abrogated by mitochondrial dysfunction.

Reduced secretion of α-gal A may be attributable to the low ATP bioavailability or increased oxidative stress resulting from Complex I inhibition (Osellame et al., 2012). ATP may be required to induce lysosomal enzyme release from polymophonuclear leukocytes (Becker and Henson, 1975). Oxidative stress accumulates during aging, resulting in increased size and number of lysosomes in cells (Hohn et al., 2017). There is evidence that secretion of lysosomal enzymes may decline with age (Carmona-

Gutierrez et al., 2016), as suggested in polymophonuclear leucocytes (Suzuki et al., 1983).

Expanding this study to fibroblasts cultured from Fabry disease patients, cell culture data suggested the growth rate of fibroblasts cultured from Fabry disease patients may be slower than apparently healthy controls. If mitochondrial function in patient fibroblasts were measured, the findings here would be consistent with the possibility of respiratory chain defects within patient cells because the mitochondria regulates cell growth, division and death (Osellame et al., 2012). Lentivirus appeared to be less efficient at cellular transduction. Whilst a degree of caution needs to be applied when considering this preliminary result, it is of interest to note that rotenone treatment of Jurkat cells had no significant effect on transduction efficacy. Such a finding may suggest that complex I inhibition alone is not sufficient to impair transduction and that other factors, occurring in Fabry cells, need to be considered, e.g. multiple respiratory chain inhibition (Lucke et al., 2004), substrate accumulation (Sweeley and Klionsky, 1963) and oxidative stress (Shen et al., 2008). Confirmation of this finding may indicate that consideration of impaired transduction may be required when considering the efficacy of gene therapy in patients with Fabry disease.

In summary, the hypothesis based on results in human cell-lines and murine tissues is illustrated in Figure 7-1. Due to their relatively low endogenous α-gal A activity, the Jurkat human cell-line was carried forward for transduction experiments using an engineered lentivirus to overexpress α-gal A. Figure 7-2A shows kinetic studies which suggest the substrate affinity of overexpressed α-gal A reduces with increasing virus dose. Cross-correction, which is important for the efficacy of gene therapy, may be disrupted by mitochondrial deficits reported previously in Fabry disease. Cross-correction occurs between transduced and naïve Jurkats (Figure 7-2B), so the effect of respiratory chain complex I inhibition on cross-correction is shown in Figure 7-2C. Finally, preliminary experiments carried out to extend this thesis into patient skin fibroblasts raised further hypotheses illustrated in Figure 7-3. The hypotheses made in this thesis lead to research questions, highlighted in red in Figure 7-1, Figure 7-2 and Figure 7-3 to drive future work.

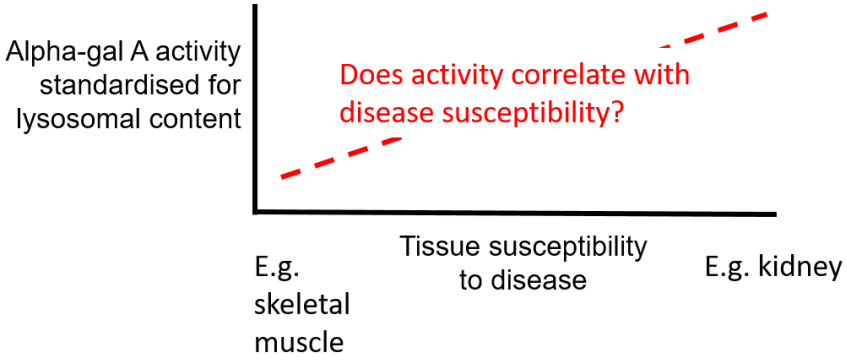

Figure 7-1: Hypothesised relationship between a-gal A and tissue susceptibility

Characterisation of α-gal A in human cell-lines and murine tissues lead to the hypothesis that the activity of α-gal A, following standardisation for variations in lysosomal content between cell and tissue types, may positively correlate with involvement in the pathophysiology of Fabry disease. Findings were not conclusive but the research question, shown in red, was carried forward for future work.

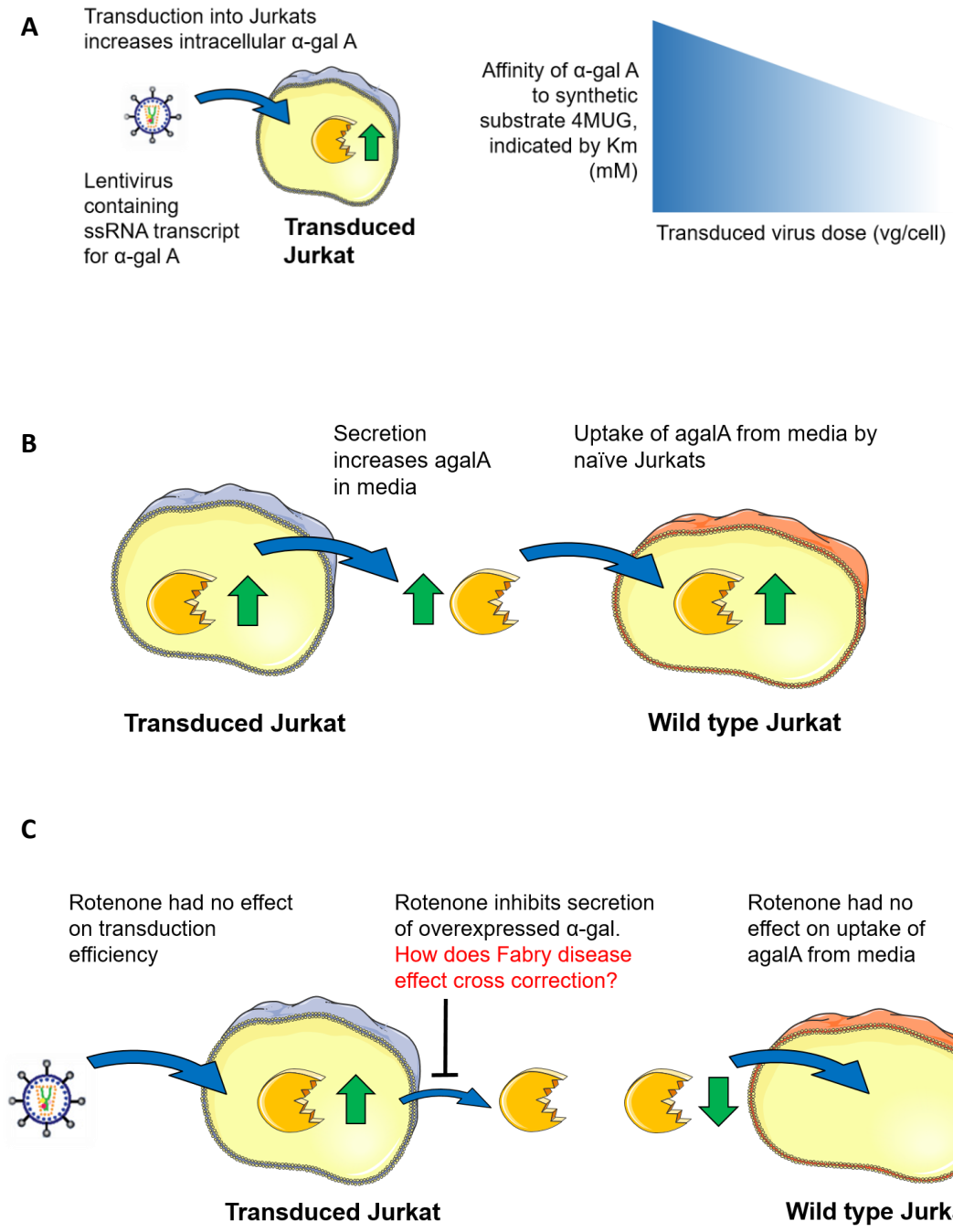

Figure 7-2: Summary of results in Jurkat human B-lymphoblastic leukaemia cell-line

A. Kinetic studies of overexpressed α-gal A using the synthetic substrate 4MUG following transduction of Jurkats found that Km, and therefore affinity with the substrate, declined with higher virus doses. This suggested that lower doses of gene therapy may be more clinically effective. **B**. Cross correction between transduced Jurkats and treatment-naïve wild type Jurkats. **C**. Mitochondrial deficiency, reported previously in Fabry disease, was modelled in Jurkats using the respiratory chain complex I-inhibitor Rotenone. Rotenone reduced cross-correction in Jurkats by inhibiting release of α-gal A by transduced cells.

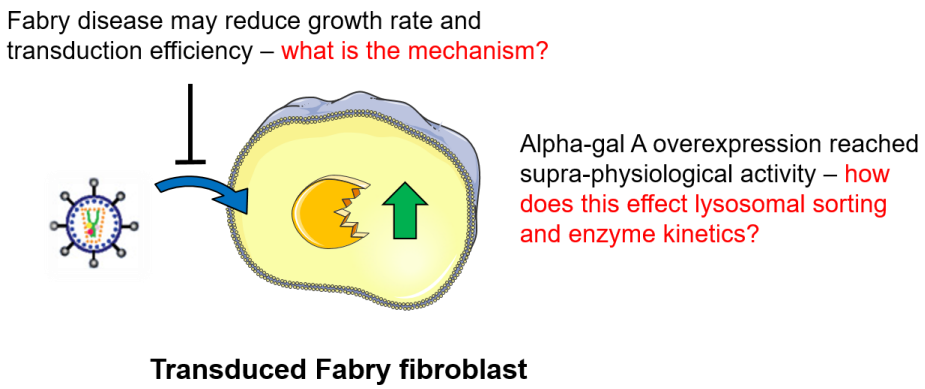

Figure 7-3: Lentivirus-mediated α-gal A overexpression in skin fibroblasts cultured from patient with Fabry disease.

Summary of hypotheses made based upon preliminary results in patient fibroblasts. Growth rate data suggested Fabry disease inhibited cell division. Transduction efficiency may be lower in Fabry patients compared with control, raising questions about possible interactions between lentivirus and the natural enzyme substrate Gb3. Lentivirus-mediated α-gal A overexpression in patient fibroblasts resulted in super-physiological enzyme activity. Since the earlier work found that substrate affinity reduced with high levels of overexpression, this raises questions about the possible effect of overexpression on lysosomal sorting and posttranslational enzyme modifications and maturation.

7.2 Future work

The thesis raises a number of points requiring further investigation. These were broken down into three key research questions shown in Figure 7-4.

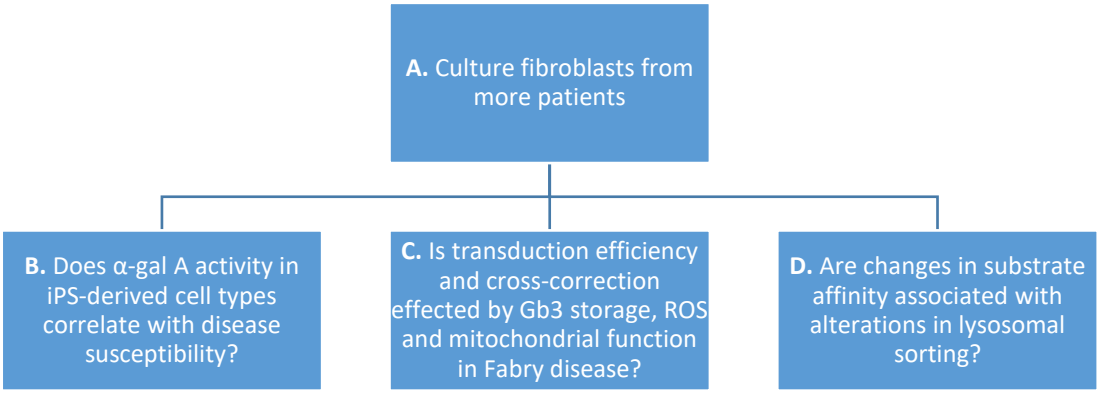

Figure 7-4: Research questions arising from this thesis which directs future work
The future work is split into three pathways with a common starting point which is to procure and grow fibroblasts cultured from a larger cohort of patients with Fabry disease. Each pathway is driven by a research question which the current thesis has raised.

Addressing the research questions shown in Figure 7-4 depends upon first procuring and growing fibroblast from more patients. All these work items are detailed in the following list:

A. To overcome the low number of Fabry disease patients donating skin fibroblasts for results reported herein, more cultures must be purchased. This will enable any significant differences in growth rate and transduction efficiency to be identified. To overcome the challenges encountered in culturing fibroblasts, basic fibroblast growth factor may be used according to Abdian et al (2015) (Abdian et al., 2015).

B. There is a need to investigate further the hypothesis that standardised ratio for α-gal A activity may correlate with tissue susceptibility in humans. To address this a range of relevant cell types may be derived from iPS cells grown from patient fibroblasts, e.g. cardiomyocytes, endothelium, neurons and podocytes (Raval et al., 2015).

C. Results here suggested α-gal A deficiency may cause reduced transduction efficiency in patient fibroblasts. This raises the research question whether reduced lentivirus efficacy is linked with Gb3 accumulation, oxidative stress and mitochondrial dysfunction; and whether these factors impact cross-correction. The following research is required to answer this question:

   - The lentivirus harvested in this study should be re-titred in fibroblasts from patients and controls in order to calculate accurate average virus dosing per cell. This would also enable direct comparison of transduction efficiency in Jurkats and fibroblasts.

   - Measure the activity of respiratory chain enzymes and identify links with Gb3 expression and markers of oxidative stress in fibroblasts from patients and controls, before and after transduction. Accumulation of Gb3 disrupts the lipid and cholesterol composition of cellular membranes which is important for permeability, integrity and membrane–associated processes such as the mitochondrial respiratory chain (Das and Naim, 2009). Gb3 storage in the lysosomal-endosomal compartments of vascular endothelium increases production of reactive oxygen species (ROS) which cause oxidative stress (Shen et al., 2008). Both Gb3 and ROS may affect global mitochondrial function with far wider implications for cellular metabolism than modelled in Jurkats by complex I inhibition (Lucke et al., 2004).

   - Correlate Gb3 expression with transduction efficacy. Gb3 is a natural resistance factor to HIV infection (Lund et al., 2009, Ramkumar et al., 2009). Possibly, as lentivirus is based upon the HIV virus structure, the low transduction efficiency in Fabry fibroblasts is due to Gb3 accumulation.

   - To see whether Fabry disease effects the ability of patient cells to cross-correct, investigate whether cross-correction may occur between transduced and treatment-naïve fibroblasts from patients and controls. Subsequently link outcomes with the mitochondrial function data collected in item b. Results in Jurkats suggested release of α-gal A by transduced cells was reduced by complex I inhibition. Comparison between fibroblasts and Jurkats must take account of differences in virus dose and transduction efficiency.

D. Examine the kinetic properties of α-gal A in transduced fibroblasts. The very high overexpression observed in transduced fibroblasts may not be producing enzyme of equal affinity to substrate as in untreated fibroblasts. Use cell imaging to explore the hypothesis that high transduction levels in Jurkats (above 0.4vg/cell) alters enzyme kinetics on 4MUG because of impaired cellular sorting due to congestion of lysosomal trafficking pathways. LysoTracker probes will allow study of enzyme trafficking to lysosomes in live cells before and after transduction with various doses of the lentivirus (Chazotte, 2011).

7.3 Conclusion

This thesis has provided data that may impact on our understanding of the efficacy of ERT and gene therapy for Fabry Disease. Alpha-gal A activity may help predict susceptibility to enzyme deficiency. Through further study using iPS cells from patient fibroblasts to derive various tissue types of relevance to the disease pathophysiology, enzyme activity could potentially inform personalised targeting of therapy.

Kinetic studies showed that at high virus dose the affinity of α-gal A to the synthetic substrate 4MUG decreases, suggesting a low dosage may have more clinical effectiveness. However the disease appears to lower the transduction efficiency of lentivirus to patient cells. Gene therapy dosage should therefore be optimised with consideration to these potential factors. Cross correction may possibly be enhanced by pre-treating patients with diets/agents that enhance mitochondrial function and antioxidant capacity, e.g. ketogenic diets prior to gene therapy.

Through the proposed future work, it is hoped that the encouraging potential of lentivirus-mediated gene delivery shown here can be realised in clinical practice to improve outcomes for patients with this devastating and life-threatening disease.

Chapter 8 The thesis in three minutes

This thesis was presented in three minutes to a potentially world-wide audience through the 2016 UK Three Minute Thesis (3MT) competition. The 3MT concept was developed by The University of Queensland, Australia, where the first competition was held in 2008. Since 2011 the competition has grown in popularity and spread internationally to over 600 universities (The University of Queensland, 2017).

The aim of a 3MT presentation was to clearly convey to the general public, in an accessible and engaging style, my doctoral research and its potential impact for society. The competition rules required the presentation was spoken without props accept one static slide that was to be on display throughout the talk without animations, sound or video. The slide developed to help communicate my thesis is shown in Figure 8-1. Figure 8-2 is a quick response (QR) code for access to an online video of my talk available on the internet to all. My progress through the UCL and UK national competitions is shown in Figure 8-3.

The lysosome was conceptualised as the “wheelie bin” of the cell. The audience was asked to imagine a situation arising if the waste removal company went permanently on strike: waste would accumulate in bins resulting in anxiety, illness and death to the householder. My talk explained that on a cellular level this situation is similar to Fabry disease in which enzyme deficiency results from mutations in *GLA* leading to accumulation of waste in lysosomes. Hence it was proposed that gene therapy, which inserts a correct copy of the *GLA* gene into patient cells using a virus vector, may be a good treatment. Investigating this possibility, the talk explained the results of my research shown in Figure 8-1. Gene delivery produced a dose-dependent increase in enzyme activity in target cells. A low dose produced an enzyme equally efficient at breaking down waste as in healthy cells, but a high dose produced an enzyme significantly less efficient. Importantly, these results were placed back into the context of the waste removal company, to help the audience appreciate the potential relevance of these findings for patients. A low dose gene therapy may be thought of as a single workman, focused on his job and efficient at clearing waste from bins. A high dose delivery is like a team of workman distracted by arguing and talking with

each other so that they can't work efficiently. This point was summarised with the take home message that "less may be more". The talk concluded with on-going work studying the potential of gene therapy to repair damage to the "power supply" of the cell, the mitochondria, in patient cells. The potential impact of this future work was highlighted by explaining that, if gene therapy could repair mitochondrial damage, this may be equivalent to giving back "cellular mojo" to enable cells to repair and save the lives of Fabry disease patients.

My presentation won the 2016 UCL Final and came runner-up in the 2016 Vitae 3MT UK National Final that was held as part of the annual Vitae Career Researchers international conference (Figure 8-3). Participation in the 3MT competition not only improved my presentation and communication skills but inspired me in public engagement, teaching activities, and a successful grant application to the National Institute of Health Research (NIHR) Biomedical Research Centre at Great Ormond Street Institute of Child Health that funded Chapter 6 of this thesis.

What is Fabry disease?

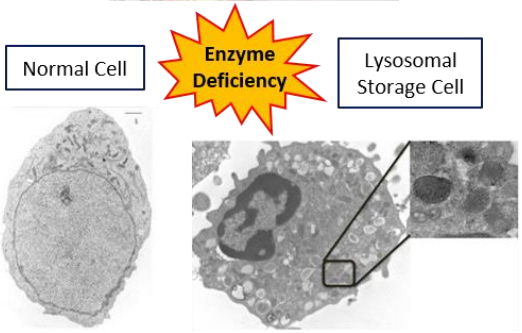

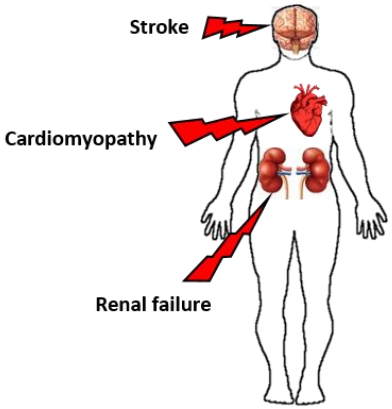

What is gene therapy?

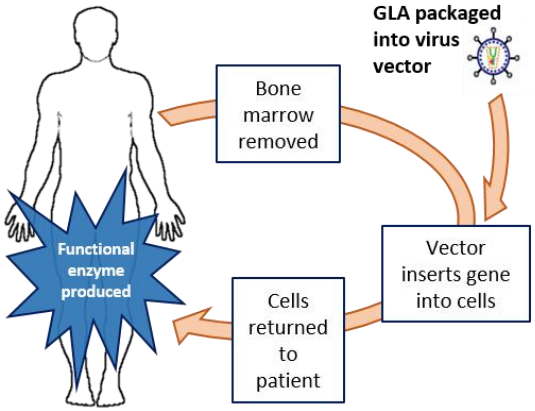

Efficacy of gene therapy for Fabry disease?

Measured in leukaemia cells

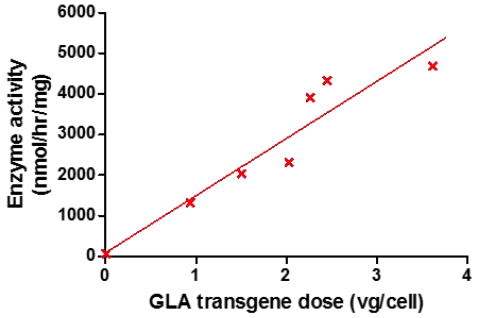

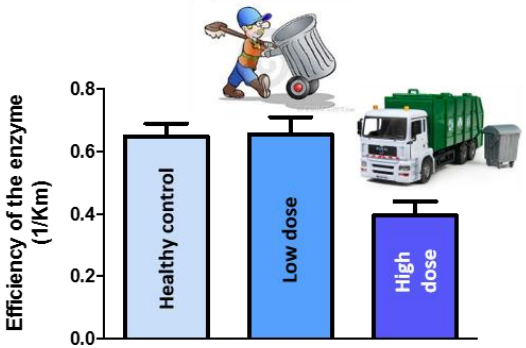

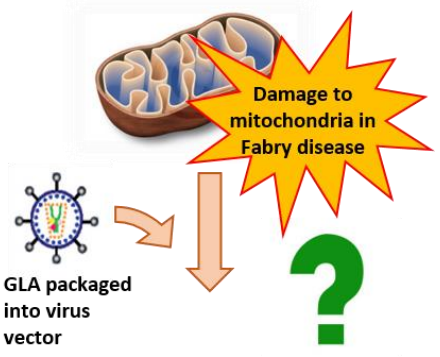

Figure 8-1: The slide used in the UK Three Minute Thesis competition 2016

A single slide, without animation, sound or video, was allowed to support a three minute presentation of the PhD thesis. Adaptations of this slide were subsequently used in a public engagement talk at the Biomedical Research Centre (BRC) Great Ormond Street Institute of Child Health (GOSICH) open day 2016 which was targeted to families and children.

Figure 8-2: QR code to access a video of the UCL Three Minute Thesis 2016 competition

The video was submitted for the UK national 3MT semi-final competition. As a result I was one of six selected for the UK national final held in Manchester in September 2016, at which I was a runner-up. The website accessed by the code is:
https://www.youtube.com/watch?v=poyot209O_k&amp=&feature=youtu.be

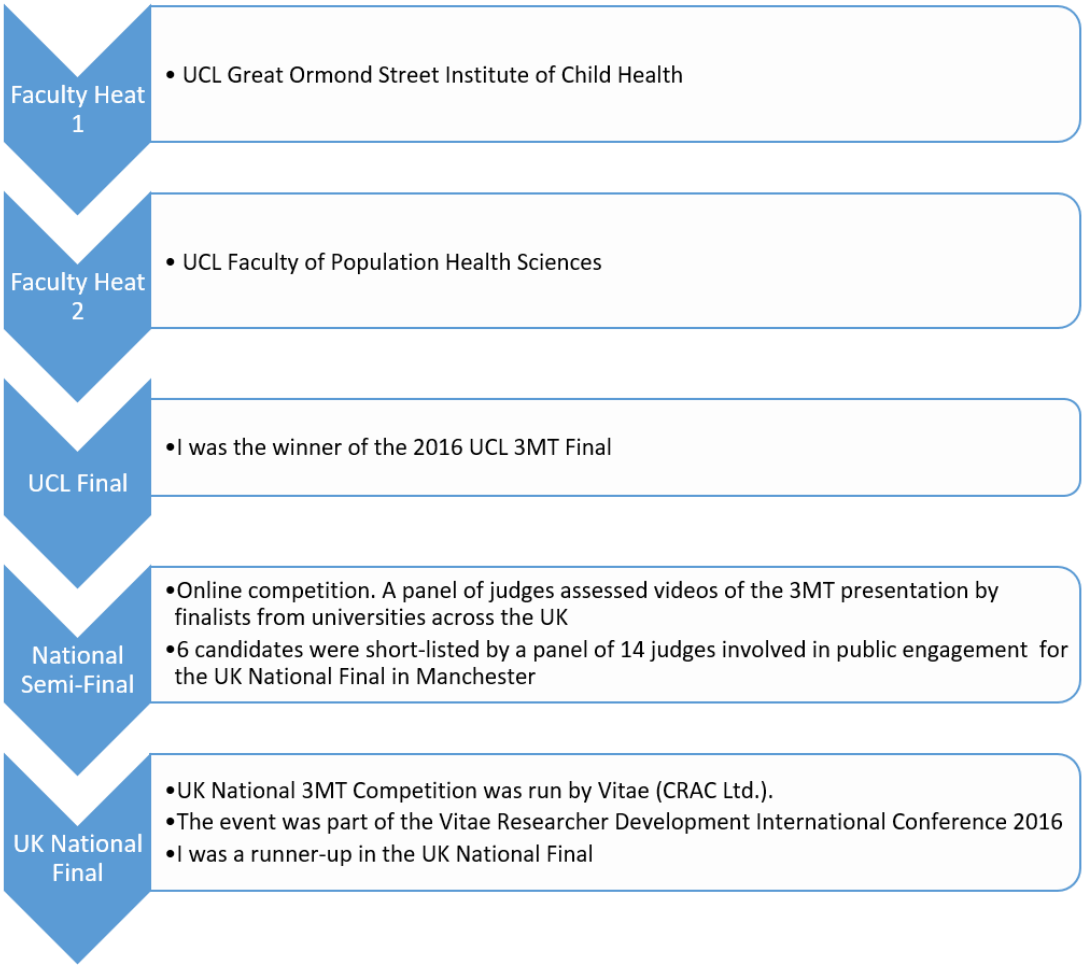

Figure 8-3: Rounds of the 2016 UCL and Vitae UK National Three Minute Thesis competition

There were five rounds of competition. The first three were within UCL and participants were judged following their live presentations before an audience of students, researchers and academics. As winner of the 2016 UCL Final I went through to the UK Nationals which were organised by Vitae, part of Careers Research Advisory Centre (CRAC) Ltd. The Semi-Final was an on-line round in which a panel of judges selected 6 Finalists based upon video presentations by 56 winners from participating universities. The UK National Final was held live in Manchester at the Vitae Researcher Development International Conference.

References

ABDIAN, N., GHASEMI-DEHKORDI, P., HASHEMZADEH-CHALESHTORI, M., GANJI-ARJENAKI, M., DOOSTI, A. & AMIRI, B. 2015. Comparison of human dermal fibroblasts (HDFs) growth rate in culture media supplemented with or without basic fibroblast growth factor (bFGF). *Cell Tissue Bank,* 16**,** 487-95.

ABM, I. 2015. *The Lentivirus - An Introduction* [Online]. https://www.abmgood.com/marketing/knowledge_base.php: Applied Biological Materials Inc. [Accessed 25th November 2017].

AERTS, J. M., GROENER, J. E., KUIPER, S., DONKER-KOOPMAN, W. E., STRIJLAND, A., OTTENHOFF, R., VAN ROOMEN, C., MIRZAIAN, M., WIJBURG, F. A., LINTHORST, G. E., VEDDER, A. C., ROMBACH, S. M., COX-BRINKMAN, J., SOMERHARJU, P., BOOT, R. G., HOLLAK, C. E., BRADY, R. O. & POORTHUIS, B. J. 2008. Elevated globotriaosylsphingosine is a hallmark of Fabry disease. *Proc Natl Acad Sci U S A,* 105**,** 2812-7.

ANDERSON, W. 1898. A case of angiokeratoma. *Br J Dermatology,* 1**,** 4.

ARENZ, C. 2017. Recent advances and novel treatments for sphingolipidoses. *Future Med Chem,* 9**,** 1685-1698.

ATCC. 2016. *Jurkat, Clone E6-1 (ATCC TIB-152)* [Online]. https://www.lgcstandards-atcc.org/products/all/TIB-152.aspx?geo_country=gb#characteristics: LGC Standards. [Accessed 26th October 2016].

AURAY-BLAIS, C., BLAIS, C. M., RAMASWAMI, U., BOUTIN, M., GERMAIN, D. P., DYACK, S., BODAMER, O., PINTOS-MORELL, G., CLARKE, J. T., BICHET, D. G., WARNOCK, D. G., ECHEVARRIA, L., WEST, M. L. & LAVOIE, P. 2015. Urinary biomarker investigation in children with Fabry disease using tandem mass spectrometry. *Clin Chim Acta,* 438**,** 195-204.

AURAY-BLAIS, C., NTWARI, A., CLARKE, J. T., WARNOCK, D. G., OLIVEIRA, J. P., YOUNG, S. P., MILLINGTON, D. S., BICHET, D. G., SIRRS, S., WEST, M. L., CASEY, R., HWU, W. L., KEUTZER, J. M., ZHANG, X. K. & GAGNON, R. 2010. How well does urinary lyso-Gb3 function as a biomarker in Fabry disease? *Clin Chim Acta,* 411**,** 1906-14.

AVERY, O. T., MACLEOD, C. M. & MCCARTY, M. 1944. Studies on the Chemical Nature of the Substance Inducing Transformation of Pneumococcal Types : Induction of Transformation by a Desoxyribonucleic Acid Fraction Isolated from Pneumococcus Type Iii. *J Exp Med,* 79**,** 137-58.

AYLETT, S. B., NEERGHEEN, V., HARGREAVES, I. P., EATON, S., LAND, J. M., RAHMAN, S. & HEALES, S. J. 2013. Levels of 5-methyltetrahydrofolate and ascorbic acid in cerebrospinal fluid are correlated: implications for the accelerated degradation of folate by reactive oxygen species. *Neurochem Int,* 63**,** 750-5.

BECKER, E. L. & HENSON, P. M. 1975. Biochemical characteristics of ATP-induced secretion of lysosomal enzymes from rabbit polymorphonuclear leukocytes. *Inflammation,* 1**,** 71-84.

BEIRAO, I., CABRITA, A., TORRES, M., SILVA, F., AGUIAR, P., LARANJEIRA, F. & GOMES, A. M. 2017. Biomarkers and Imaging Findings of Anderson-Fabry Disease-What We Know Now. *Diseases,* 5.

BEKRI, S. 2006. Importance of glycosylation in enzyme replacement therapy. *In:* MEHTA, A., BECK, M. & SUNDER-PLASSMANN, G. (eds.) *Fabry Disease: Perspectives from 5 Years of FOS.* Oxford.

BENJAMIN, E. R., DELLA VALLE, M. C., WU, X., KATZ, E., PRUTHI, F., BOND, S., BRONFIN, B., WILLIAMS, H., YU, J., BICHET, D. G., GERMAIN, D. P., GIUGLIANI, R., HUGHES, D., SCHIFFMANN, R., WILCOX, W. R., DESNICK, R. J., KIRK, J., BARTH, J., BARLOW, C., VALENZANO, K. J., CASTELLI, J. & LOCKHART, D. J. 2017. The validation of pharmacogenetics for the identification of Fabry patients to be treated with migalastat. *Genet Med,* 19**,** 430-438.

BERTHET, J., BERTHET, L., APPELMANS, F. & DE DUVE, C. 1951. Tissue fractionation studies. II. The nature of the linkage between acid phosphatase and mitochondria in rat-liver tissue. *Biochem J,* 50**,** 182-9.

BEUTLER, E., GUINTO, E. & KUHL, W. 1973. Variability of -galactosidase A and B in different tissues of man. *Am J Hum Genet,* 25**,** 42-6.

BEUTLER, E. & KUHL, W. 1972. Biochemical and electrophoretic studies of -galactosidase in normal man, in patients with Fabry's disease, and in Equidae. *Am J Hum Genet,* 24**,** 237-49.

BIFFI, A. 2016. Gene therapy for lysosomal storage disorders: a good start. *Hum Mol Genet,* 25**,** R65-75.

BISHOP, D. F., CALHOUN, D. H., BERNSTEIN, H. S., HANTZOPOULOS, P., QUINN, M. & DESNICK, R. J. 1986. Human alpha-galactosidase A: nucleotide sequence of a cDNA clone encoding the mature enzyme. *Proc Natl Acad Sci U S A,* 83**,** 4859-63.

BOUTIN, M. & AURAY-BLAIS, C. 2015. Metabolomic discovery of novel urinary galabiosylceramide analogs as Fabry disease biomarkers. *J Am Soc Mass Spectrom,* 26**,** 499-510.

BOUTIN, M., LAVOIE, P., ABAOUI, M. & AURAY-BLAIS, C. 2016. Tandem Mass Spectrometry Quantitation of Lyso-Gb3 and Six Related Analogs in Plasma for Fabry Disease Patients. *Curr Protoc Hum Genet,* 90**,** 17 23 1-9.

BRADY, R. O. 2010. Fabry disease - An Overview. *In:* ELSTEIN, D., ALTARESCU, G. & BECK, M. (eds.) *Fabry Disease.* Springer.

BRADY, R. O., GAL, A. E., BRADLEY, R. M., MARTENSSON, E., WARSHAW, A. L. & LASTER, L. 1967. Enzymatic defect in Fabry's disease. Ceramidetrihexosidase deficiency. *N Engl J Med,* 276**,** 1163-7.

BRAKCH, N., DORMOND, O., BEKRI, S., GOLSHAYAN, D., CORREVON, M., MAZZOLAI, L., STEINMANN, B. & BARBEY, F. 2010. Evidence for a role of sphingosine-1 phosphate in cardiovascular remodelling in Fabry disease. *Eur Heart J,* 31**,** 67-76.

BRETT, E. M., ELLIS, R. B., HAAS, L., IKONNE, J. U., LAKE, B. D., PATRICK, A. D. & STEPHENS, R. 1973. Late onset GM2-gangliosidosis. Clinical, pathological, and biochemical studies on 8 patients. *Arch Dis Child,* 48**,** 775-85.

BYRNE, B. J., FALK, D. J., CLEMENT, N. & MAH, C. S. 2012. Gene therapy approaches for lysosomal storage disease: next-generation treatment. *Hum Gene Ther,* 23**,** 808-15.

CAETANO, F., BOTELHO, A., MOTA, P., SILVA, J. & LEITAO MARQUES, A. 2014. Fabry disease presenting as apical left ventricular hypertrophy in a patient carrying the missense mutation R118C. *Rev Port Cardiol,* 33**,** 183 e1-5.

CALHOUN, D. H., BISHOP, D. F., BERNSTEIN, H. S., QUINN, M., HANTZOPOULOS, P. & DESNICK, R. J. 1985. Fabry disease: isolation of a cDNA clone encoding human alpha-galactosidase A. *Proc Natl Acad Sci U S A,* 82**,** 7364-8.

CANTZ, M. & KRESSE, H. 1974. Sandhoff disease: defective glycosaminoglycan catabolism in cultured fibroblasts and its correction by beta-N-acetylhexosaminidase. *Eur J Biochem,* 47**,** 581-90.

CARMONA-GUTIERREZ, D., HUGHES, A. L., MADEO, F. & RUCKENSTUHL, C. 2016. The crucial impact of lysosomes in aging and longevity. *Ageing Res Rev,* 32**,** 2-12.

CHABAS, A., COLL, M. J., APARICIO, M. & RODRIGUEZ DIAZ, E. 1994. Mild phenotypic expression of alpha-N-acetylgalactosaminidase deficiency in two adult siblings. *J Inherit Metab Dis,* 17**,** 724-31.

CHAZOTTE, B. 2011. Labeling lysosomes in live cells with LysoTracker. *Cold Spring Harb Protoc,* 2011**,** pdb prot5571.

CHEN, Z. Y., HUANG, A. J., HE, C., LU, C. L. & WU, X. F. 2000. [Expression of human GDNF in methyltrophic yeast Pichia pastoris and silkworm larvae]. *Sheng Wu Gong Cheng Xue Bao,* 16**,** 561-5.

CHEVRIER, M., BRAKCH, N., CELINE, L., GENTY, D., RAMDANI, Y., MOLL, S., DJAVAHERI-MERGNY, M., BRASSE-LAGNEL, C., ANNIE LAQUERRIERE, A. L., BARBEY, F. & BEKRI, S. 2010. Autophagosome maturation is impaired in Fabry disease. *Autophagy,* 6**,** 589-99.

CHIMENTI, C., SCOPELLITI, F., VULPIS, E., TAFANI, M., VILLANOVA, L., VERARDO, R., DE PAULIS, R., RUSSO, M. A. & FRUSTACI, A. 2015. Increased oxidative stress contributes to cardiomyocyte dysfunction and death in patients with Fabry disease cardiomyopathy. *Hum Pathol,* 46**,** 1760-8.

CHOI, L., VERNON, J., KOPACH, O., MINETT, M. S., MILLS, K., CLAYTON, P. T., MEERT, T. & WOOD, J. N. 2015. The Fabry disease-associated lipid Lyso-Gb3 enhances voltage-gated calcium currents in sensory neurons and causes pain. *Neurosci Lett,* 594**,** 163-8.

CLARK, N. E. & GARMAN, S. C. 2009. The 1.9 a structure of human alpha-N-acetylgalactosaminidase: The molecular basis of Schindler and Kanzaki diseases. *J Mol Biol,* 393**,** 435-47.

COUTINHO, M. F., PRATA, M. J. & ALVES, S. 2012. Mannose-6-phosphate pathway: a review on its role in lysosomal function and dysfunction. *Mol Genet Metab,* 105**,** 542-50.

COX, T. M. & CACHON-GONZALEZ, M. B. 2012. The cellular pathology of lysosomal diseases. *J Pathol,* 226**,** 241-54.

D'COSTA, J., HARVEY-WHITE, J., QASBA, P., LIMAYE, A., KANESKI, C. R., DAVIS-WARREN, A., BRADY, R. O., BANKIEWICZ, K. S., MAJOR, E. O. & ARYA, S. K. 2003. HIV-2 derived lentiviral vectors: gene transfer in Parkinson's and Fabry disease models in vitro. *J Med Virol,* 71**,** 173-82.

DARMOISE, A., TENEBERG, S., BOUZONVILLE, L., BRADY, R. O., BECK, M., KAUFMANN, S. H. & WINAU, F. 2010. Lysosomal alpha-galactosidase controls the generation of self lipid antigens for natural killer T cells. *Immunity,* 33**,** 216-28.

DAS, A. M. & NAIM, H. Y. 2009. Biochemical basis of Fabry disease with emphasis on mitochondrial function and protein trafficking. *Advances in Clinical Chemistry,* 49**,** 14.

DAVEY, G. P., PEUCHEN, S. & CLARK, J. B. 1998. Energy thresholds in brain mitochondria. Potential involvement in neurodegeneration. *J Biol Chem,* 273**,** 12753-7.

DAWSON, G. & SWEELEY, C. C. 1970. In vivo studies on glycosphingolipid metabolism in porcine blood. *J Biol Chem,* 245**,** 410-6.

DE DUVE, C. 1963. General properties of lysosomes: the lysosome concept. *In:* DE REUCK, A. V. S. & CAMERON, M. P. (eds.) *Lysosomes.* Ciba Foundation.

DE DUVE, C. 2005. The lysosome turns fifty. *Nat Cell Biol,* 7**,** 847-9.

DEAN, K. J. & SWEELEY, C. C. 1979a. Studies on human liver alpha-galactosidases. I. Purification of alpha-galactosidase A and its enzymatic properties with glycolipid and oligosaccharide substrates. *J Biol Chem,* 254**,** 9994-10000.

DEAN, K. J. & SWEELEY, C. C. 1979b. Studies on human liver alpha-galactosidases. II. Purification and enzymatic properties of alpha-galactosidase B (alpha-N-acetylgalactosaminidase). *J Biol Chem,* 254**,** 10001-5.

DESNICK, R. J., DEAN, K. J., GRABOWSKI, G., BISHOP, D. F. & SWEELEY, C. C. 1979. Enzyme therapy in Fabry disease: differential in vivo plasma clearance and metabolic effectiveness of plasma and splenic alpha-galactosidase A isozymes. *Proc Natl Acad Sci U S A,* 76**,** 5326-30.

DESNICK, R. J., IOANNOU, Y. A. & ENG, C. M. 2001. Alpha-galactosidase A deficiency: Fabry disease. *In:* SCRIVER, C. R., BEAUDET, A. T., SLY, W. S., VALLE, D., CHILDS, B., KINZLER, K. W. & VOGELSTEIN, B. (eds.) *The metabolic and molecular basis of inherited disease.* New York: McGraw Hill.

DESNICK, R. J. & SCHUCHMAN, E. H. 2012. Enzyme replacement therapy for lysosomal diseases: lessons from 20 years of experience and remaining challenges. *Annu Rev Genomics Hum Genet,* 13**,** 307-35.

DONNAI, P., DONNAI, D., HARRIS, R., STEPHENS, R., YOUNG, E. & CAMPBELL, S. 1981. Antenatal diagnosis of Niemann-Pick disease in a twin pregnancy. *J Med Genet,* 18**,** 359-61.

DUPONT, F. O., GAGNON, R., BOUTIN, M. & AURAY-BLAIS, C. 2013. A metabolomic study reveals novel plasma lyso-Gb3 analogs as Fabry disease biomarkers. *Curr Med Chem,* 20**,** 280-8.

DUVE, C. D., PRESSMAN, B. C., GIANETTO, R., WATTIAUX, R. & APPELMANS, F. 1955. Tissue Fractionation Studies .6. Intracellular Distribution Patterns of Enzymes in Rat-Liver Tissue. *Biochemical Journal,* 60**,** 604-617.

EL DIB, R., GOMAA, H., CARVALHO, R. P., CAMARGO, S. E., BAZAN, R., BARRETTI, P. & BARRETO, F. C. 2016. Enzyme replacement therapy for Anderson-Fabry disease. *Cochrane Database Syst Rev,* 7**,** CD006663.

ELLEDER, M. 2010. Subcellular, Cellular and Organ Pathology of Fabry Disease. *In:* ELSTEIN, D., BECK, M. & ALTARESCU, G. (eds.) *Fabry Disease.* Springer.

ENDO, Y., TSURUGI, K., YUTSUDO, T., TAKEDA, Y., OGASAWARA, T. & IGARASHI, K. 1988. Site of action of a Vero toxin (VT2) from Escherichia coli O157:H7 and of Shiga toxin on eukaryotic ribosomes. RNA N-glycosidase activity of the toxins. *Eur J Biochem,* 171**,** 45-50.

ENG, C. M. & DESNICK, R. J. 1994. Molecular basis of Fabry disease: mutations and polymorphisms in the human alpha-galactosidase A gene. *Hum Mutat,* 3**,** 103-11.

ENG, C. M., GUFFON, N., WILCOX, W. R., GERMAIN, D. P., LEE, P., WALDEK, S., CAPLAN, L., LINTHORST, G. E., DESNICK, R. J. & INTERNATIONAL COLLABORATIVE FABRY DISEASE STUDY, G. 2001. Safety and efficacy of recombinant human alpha-galactosidase A--replacement therapy in Fabry's disease. *N Engl J Med,* 345**,** 9-16.

ENG, C. M., RESNICK-SILVERMAN, L. A., NIEHAUS, D. J., ASTRIN, K. H. & DESNICK, R. J. 1993. Nature and frequency of mutations in the alpha-galactosidase A gene that cause Fabry disease. *Am J Hum Genet,* 53**,** 1186-97.

ESSNER, E. & NOVIKOFF, A. B. 1961. Localization of Acid Phosphatase Activity in Hepatic Lysosomes by Means of Electron Microscopy. *Journal of Biophysical and Biochemical Cytology,* 9**,** 773-&.

FABRY, H. 2002. Angiokeratoma corporis diffusum--Fabry disease: historical review from the original description to the introduction of enzyme replacement therapy. *Acta Paediatr Suppl,* 91**,** 3-5.

FABRY, J. 1898. Ein Beitrag zur Kanntnis der Purpura haemaorrhagica nodularis (Purpura papulosa haemaorrhagica Hebrae). *Arch Dermatol Syph,* 43**,** 4.

FAN, J. Q., ISHII, S., ASANO, N. & SUZUKI, Y. 1999. Accelerated transport and maturation of lysosomal alpha-galactosidase A in Fabry lymphoblasts by an enzyme inhibitor. *Nat Med,* 5**,** 112-5.

FEHSE, B., KUSTIKOVA, O. S., BUBENHEIM, M. & BAUM, C. 2004. Pois(s)on - It's a question of dose ... *Gene Therapy,* 11**,** 879-881.

FELDT-RASMUSSEN, U., GIUGLIANI, R., GERMAIN, D. P., HUGHES, D. A., WILCOX, W. R., SCHIFFMANN, R., BICHET, D. G., JOVANOVIC, A., BRATKOVIC, D., CASTELLI, J. P., YU, J. L., SKUBAN, N. & BARTH, J. A. 2017. Efficacy and safety of migalastat, an oral pharmacologic chaperone for Fabry disease: results from two randomized phase 3 studies, FACETS and ATTRACT. *Molecular Genetics and Metabolism,* 120**,** S45-S46.

FERREIRA, S., AURAY-BLAIS, C., BOUTIN, M., LAVOIE, P., NUNES, J. P., MARTINS, E., GARMAN, S. & OLIVEIRA, J. P. 2015. Variations in the GLA gene correlate with globotriaosylceramide and globotriaosylsphingosine analog levels in urine and plasma. *Clin Chim Acta,* 447**,** 96-104.

FILOCAMO, M. & MORRONE, A. 2011. Lysosomal storage disorders: molecular basis and laboratory testing. *Hum Genomics,* 5**,** 156-69.

FLOTTE, T. R., AFIONE, S. A. & ZEITLIN, P. L. 1994. Adeno-associated virus vector gene expression occurs in nondividing cells in the absence of vector DNA integration. *Am J Respir Cell Mol Biol,* 11**,** 517-21.

FORSTERMANN, U. & MUNZEL, T. 2006. Endothelial nitric oxide synthase in vascular disease: from marvel to menace. *Circulation,* 113**,** 1708-14.

FOX, M. F., DUTOIT, D. L., WARNICH, L. & RETIEF, A. E. 1984. Regional localization of alpha-galactosidase (GLA) to Xpter----q22, hexosaminidase B (HEXB) to 5q13----qter, and arylsulfatase B (ARSB) to 5pter----q13. *Cytogenet Cell Genet,* 38**,** 45-9.

FRATANTONI, J. C., HALL, C. W. & NEUFELD, E. F. 1968. Hurler and Hunter syndromes: mutual correction of the defect in cultured fibroblasts. *Science,* 162**,** 570-2.

FRIEDMANN, T. & ROBLIN, R. 1972. Gene therapy for human genetic disease? *Science,* 175**,** 949-55.

FURUKAWA, K., YOKOYAMA, K., SATO, T., WIELS, J., HIRAYAMA, Y., OHTA, M. & FURUKAWA, K. 2002. Expression of the Gb3/CD77 synthase gene in megakaryoblastic leukemia cells: implication in the sensitivity to verotoxins. *J Biol Chem,* 277**,** 11247-54.

FUTERMAN, A. H. & VAN MEER, G. 2004. The cell biology of lysosomal storage disorders. *Nat Rev Mol Cell Biol,* 5**,** 554-65.

GAL, A. 2010. Molecular genetics of Fabry disease and genotype-phenotype correlation. *In:* ELSTEIN, D., ALTARESCU, G. & BECK, M. (eds.) *Fabry Disease.* Springer.

GAL, A., HUGHES, D. A. & WINCHESTER, B. 2011. Toward a consensus in the laboratory diagnostics of Fabry disease - recommendations of a European expert group. *J Inherit Metab Dis,* 34**,** 509-14.

GARMAN, S. C. & GARBOCZI, D. N. 2004. The molecular defect leading to Fabry disease: structure of human alpha-galactosidase. *J Mol Biol,* 337**,** 319-35.

GASPAROTTO, N., TOMANIN, R., FRIGO, A. C., NIIZAWA, G., PASQUINI, E., BLANCO, M., DONATI, M. A., KEUTZER, J., ZACCHELLO, F. & SCARPA, M. 2009. Rapid diagnostic testing procedures for lysosomal storage disorders: alpha-glucosidase and beta-galactosidase assays on dried blood spots. *Clin Chim Acta,* 402**,** 38-41.

GERMAIN, D. P. 2010. Fabry disease. *Orphanet J Rare Dis,* 5**,** 30.

GERMAIN, D. P., GIUGLIANI, R., BICHET, D. G., WILCOX, W. R., HUGHES, D. A., AMARTINO, H. M., SCHIFFMANNG, R., VIERECK, C., SKUBAN, N., CASTELLI, J. P. & BARTH, J. A. 2017a. Efficacy of migalastat in a cohort of male patients with the classic Fabry phenotype in the FACETS phase 3 study. *Molecular Genetics and Metabolism,* 120**,** S52-S52.

GERMAIN, D. P., HUGHES, D. A., BICHET, D. G., SCHIFFMANN, R., WILCOX, W. R., HOLDBROOK, F., VIERECK, C., YU, J., SKUBAN, N., CASTELLI, J. P. & BARTH, J. A. 2017b. Effects of treatment with migalastat on the combined endpoint of kidney globotriaosylcermide accumulation and diarrhea in patients with Fabry disease: results from the phase 3 FACETS study. *Molecular Genetics and Metabolism,* 120**,** S52-S52.

GERMAIN, D. P., HUGHES, D. A., NICHOLLS, K., BICHET, D. G., GIUGLIANI, R., WILCOX, W. R., FELICIANI, C., SHANKAR, S. P., EZGU, F., AMARTINO, H., BRATKOVIC, D., FELDT-RASMUSSEN, U., NEDD, K., SHARAF EL DIN, U., LOURENCO, C. M., BANIKAZEMI, M., CHARROW, J., DASOUKI, M., FINEGOLD, D., GIRALDO, P., GOKER-ALPAN, O., LONGO, N., SCOTT, C. R., TORRA, R., TUFFAHA, A., JOVANOVIC, A., WALDEK, S., PACKMAN, S., LUDINGTON, E., VIERECK, C., KIRK, J., YU, J., BENJAMIN, E. R., JOHNSON, F., LOCKHART, D. J., SKUBAN, N., CASTELLI, J., BARTH, J., BARLOW, C. & SCHIFFMANN, R. 2016. Treatment of Fabry's Disease with the Pharmacologic Chaperone Migalastat. *N Engl J Med,* 375**,** 545-55.

GONCALVES, M. A. 2005. Adeno-associated virus: from defective virus to effective vector. *Virol J,* 2**,** 43.

GRIFFITH, F. 1928. The Significance of Pneumococcal Types. *J Hyg (Lond),* 27**,** 113-59.

GUERARD, N., ODER, D., NORDBECK, P., ZWINGELSTEIN, C., MORAND, O., WELFORD, R. W., DINGEMANSE, J. & WANNER, C. 2017. Lucerastat, an Iminosugar for Substrate Reduction Therapy: Tolerability, Pharmacodynamics, and Pharmacokinetics in Patients With Fabry Disease on Enzyme Replacement. *Clin Pharmacol Ther*.

HADJIMICHAEL, E., THOMAS, A. S., MEHTA, A. & HUGHES, D. 2013. Relationship of serum HIF1a, VEGF-A and TGF-a to clinical severity in Fabry disease. *Molecular Genetics and Metabolism,* 108**,** 2.

HAMLER, R., BRIGNOL, N., BOYD, R. E., BICHET, D. G., GERMAIN, D. P., GIUGLIANI, R., HUGHES, D. A., SCHIFFMANN, R., WILCOX, W. R., WILLIAMS, H. N., YU, J., BARTH, J., CASTELLI, J., VALENZANO, K. J. & BENJAMIN, E. R. 2015. Accurate quantitation of plasma globotriaosylsphingosine (lyso-Gb(3)) in normal individuals and Fabry disease patients by liquid chromatography-tandem mass spectrometry (LC-MS/MS). *Molecular Genetics and Metabolism,* 114**,** S51-S51.

HEALES, S. J., BOLANOS, J. P., BRAND, M. P., CLARK, J. B. & LAND, J. M. 1996. Mitochondrial damage: an important feature in a number of inborn errors of metabolism? *J Inherit Metab Dis,* 19**,** 140-2.

HELTIANU, C., COSTACHE, G., AZIBI, K., POENARU, L. & SIMIONESCU, M. 2002. Endothelial nitric oxide synthase gene polymorphisms in Fabry's disease. *Clin Genet,* 61**,** 423-9.

HERS, H. G. 1963. alpha-Glucosidase deficiency in generalized glycogenstorage disease (Pompe's disease). *Biochem J,* 86**,** 11-6.

HIRST, J. & ROESSLER, M. M. 2016. Energy conversion, redox catalysis and generation of reactive oxygen species by respiratory complex I. *Biochim Biophys Acta,* 1857**,** 872-83.

HOHN, A., WEBER, D., JUNG, T., OTT, C., HUGO, M., KOCHLIK, B., KEHM, R., KONIG, J., GRUNE, T. & CASTRO, J. P. 2017. Happily (n)ever after: Aging in the context of oxidative stress, proteostasis loss and cellular senescence. *Redox Biol,* 11**,** 482-501.

HOZUMI, I., NISHIZAWA, M., ARIGA, T. & MIYATAKE, T. 1990. Biochemical and clinical analysis of accumulated glycolipids in symptomatic heterozygotes of angiokeratoma corporis diffusum (Fabry's disease) in comparison with hemizygotes. *J Lipid Res,* 31**,** 335-40.

HREBICEK, M. & LEDVINOVA, J. 2010. Biochemistry of Fabry Disease. *In:* ELSTEIN, D., BECK, M. & ALTARESCU, G. (eds.) *Fabry Disease.* Springer.

HUANG, J., KHAN, A., AU, B. C., BARBER, D. L., LOPEZ-VASQUEZ, L., PROKOPISHYN, N. L., BOUTIN, M., ROTHE, M., RIP, J. W., ABAOUI, M., NAGREE, M. S., DWORSKI, S., SCHAMBACH, A., KEATING, A., WEST, M. L., KLASSEN, J., TURNER, P. V., SIRRS, S., RUPAR, C. A., AURAY-BLAIS, C., FOLEY, R. & MEDIN, J. A. 2017. Lentivector Iterations and Pre-Clinical Scale-Up/Toxicity Testing: Targeting Mobilized CD34(+) Cells for Correction of Fabry Disease. *Mol Ther Methods Clin Dev,* 5**,** 241-258.

HUGHES, A. K., ERGONUL, Z., STRICKLETT, P. K. & KOHAN, D. E. 2002. Molecular Basis for High Renal Cell Sensitivity to the Cytotoxic Effects of Shigatoxin-1: Upregulation of Globotriaosylceramide Expression. *Journal of the American Society of Nephrology,* 13**,** 2239-2245.

HUGHES, D., BICHET, D. G., GERMAIN, D. P., GIUGLIANI, R., SCHIFFMANN, R., WILCOX, W., CASTELLI, J. P., BENJAMIN, E., SKUBAN, N. & BARTH, J. 2016. Phenotype of Fabry disease in patients with mutations amenable to migalastat. *Molecular Genetics and Metabolism,* 117**,** S58-S59.

HUGHES, D. A., DEEGAN, P. B., MILLIGAN, A., WRIGHT, N., BUTLER, L. H., JACOBS, A. & MEHTA, A. B. 2013. A randomised, double-blind, placebo-controlled, crossover study to assess the efficacy and safety of three dosing schedules of agalsidase alfa enzyme replacement therapy for Fabry disease. *Mol Genet Metab,* 109**,** 269-75.

HWU, W. L., CHIEN, Y. H., LEE, N. C., CHIANG, S. C., DOBROVOLNY, R., HUANG, A. C., YEH, H. Y., CHAO, M. C., LIN, S. J., KITAGAWA, T., DESNICK, R. J. & HSU, L. W. 2009. Newborn screening for Fabry disease in Taiwan reveals a high incidence of the later-onset GLA mutation c.936+919G>A (IVS4+919G>A). *Hum Mutat,* 30**,** 1397-405.

IOANNOU, Y. A., ZEIDNER, K. M., GRACE, M. E. & DESNICK, R. J. 1998. Human alpha-galactosidase A: glycosylation site 3 is essential for enzyme solubility. *Biochem J,* 332 (Pt 3)**,** 789-97.

ISHII, S., NAKAO, S., MINAMIKAWA-TACHINO, R., DESNICK, R. J. & FAN, J. Q. 2002. Alternative splicing in the alpha-galactosidase A gene: increased exon inclusion results in the Fabry cardiac phenotype. *Am J Hum Genet,* 70**,** 994-1002.

ITOH, Y., ESAKI, T., COOK, M., QASBA, P., SHIMOJI, K., ALROY, J., BRADY, R. O., SOKOLOFF, L. & MOORE, D. F. 2001. Local and global cerebral blood flow and glucose utilization in the alpha-galactosidase A knockout mouse model of Fabry disease. *J Neurochem,* 79**,** 1217-24.

JUNG, S. C., HAN, I. P., LIMAYE, A., XU, R., GELDERMAN, M. P., ZERFAS, P., TIRUMALAI, K., MURRAY, G. J., DURING, M. J., BRADY, R. O. & QASBA, P. 2001. Adeno-associated viral vector-mediated gene transfer results in long-term enzymatic and functional correction in multiple organs of Fabry mice. *Proc Natl Acad Sci U S A,* 98**,** 2676-81.

KANG, J. J., SHU, L., PARK, J. L., SHAYMAN, J. A. & BODARY, P. F. 2014. Endothelial nitric oxide synthase uncoupling and microvascular dysfunction in the mesentery of mice deficient in alpha-galactosidase A. *Am J Physiol Gastrointest Liver Physiol,* 306**,** G140-6.

KARLSSON, S. 1991. Treatment of genetic defects in hematopoietic cell function by gene transfer. *Blood,* 78**,** 2481-92.

KARR, W. J., JR. 1959. Fabry's disease (angiokeratoma corporis diffusum universale). An unusual syndrome with multisystem involvement and unique skin manifestations. *Am J Med,* 27**,** 829-35.

KHINE, A. A., FIRTEL, M. & LINGWOOD, C. A. 1998. CD77-dependent retrograde transport of CD19 to the nuclear membrane: functional relationship between CD77 and CD19 during germinal center B-cell apoptosis. *J Cell Physiol,* 176**,** 281-92.

KIETADISORN, R., JUNI, R. P. & MOENS, A. L. 2012. Tackling endothelial dysfunction by modulating NOS uncoupling: new insights into its pathogenesis and therapeutic possibilities. *Am J Physiol Endocrinol Metab,* 302**,** E481-95.

KO, Y. H., KIM, H. J., ROH, Y. S., PARK, C. K., KWON, C. K. & PARK, M. H. 1996. Atypical Fabry's disease. An oligosymptomatic variant. *Arch Pathol Lab Med,* 120**,** 86-9.

KODAMA, T., TSUKIMURA, T., KAWASHIMA, I., SATO, A., SAKURABA, H. & TOGAWA, T. 2017. Differences in cleavage of globotriaosylceramide and its derivatives accumulated in organs of young Fabry mice following enzyme replacement therapy. *Mol Genet Metab,* 120**,** 116-120.

KOJIMA, Y., FUKUMOTO, S., FURUKAWA, K., OKAJIMA, T., WIELS, J., YOKOYAMA, K., SUZUKI, Y., URANO, T., OHTA, M. & FURUKAWA, K. 2000. Molecular cloning of globotriaosylceramide/CD77 synthase, a glycosyltransferase that initiates the synthesis of globo series glycosphingolipids. *J Biol Chem,* 275**,** 15152-6.

KOLTER, T. & SANDHOFF, K. 1999. Sphingolipids - Their metabolic pathways and the pathobiochemistry of neurodegenerative diseases. *Angewandte Chemie-International Edition,* 38**,** 1532-1568.

KORNFELD, S. 1986. Trafficking of lysosomal enzymes in normal and disease states. *J Clin Invest,* 77**,** 1-6.

LANDER, E. S., LINTON, L. M., BIRREN, B., NUSBAUM, C., ZODY, M. C., BALDWIN, J., DEVON, K., DEWAR, K., DOYLE, M., FITZHUGH, W., FUNKE, R., GAGE, D., HARRIS, K., HEAFORD, A., HOWLAND, J., KANN, L., LEHOCZKY, J., LEVINE, R., MCEWAN, P., MCKERNAN, K., MELDRIM, J., MESIROV, J. P., MIRANDA, C., MORRIS, W., NAYLOR, J., RAYMOND, C., ROSETTI, M., SANTOS, R., SHERIDAN, A., SOUGNEZ, C., STANGE-THOMANN, Y., STOJANOVIC, N., SUBRAMANIAN, A., WYMAN, D., ROGERS, J., SULSTON, J., AINSCOUGH, R., BECK, S., BENTLEY, D., BURTON, J., CLEE, C., CARTER, N., COULSON, A., DEADMAN, R., DELOUKAS, P., DUNHAM, A., DUNHAM, I., DURBIN, R., FRENCH, L., GRAFHAM, D., GREGORY, S., HUBBARD, T., HUMPHRAY, S., HUNT, A., JONES, M., LLOYD, C., MCMURRAY, A., MATTHEWS, L., MERCER, S., MILNE, S., MULLIKIN, J. C., MUNGALL, A., PLUMB, R., ROSS, M., SHOWNKEEN, R., SIMS, S., WATERSTON, R. H., WILSON, R. K., HILLIER, L. W., MCPHERSON, J. D., MARRA, M. A., MARDIS, E. R., FULTON, L. A., CHINWALLA, A. T., PEPIN, K. H., GISH, W. R., CHISSOE, S. L., WENDL, M. C., DELEHAUNTY, K. D., MINER, T. L., DELEHAUNTY, A., KRAMER, J. B., COOK, L. L., FULTON, R. S., JOHNSON, D. L., MINX, P. J., CLIFTON, S. W., HAWKINS, T., BRANSCOMB, E., PREDKI, P., RICHARDSON, P., WENNING, S., SLEZAK, T., DOGGETT, N., CHENG, J. F., OLSEN, A., LUCAS, S., ELKIN, C., UBERBACHER, E., FRAZIER, M., et al. 2001. Initial sequencing and analysis of the human genome. *Nature,* 409**,** 860-921.

LAVOIE, P., BOUTIN, M. & AURAY-BLAIS, C. 2013. Multiplex analysis of novel urinary lyso-Gb3-related biomarkers for Fabry disease by tandem mass spectrometry. *Anal Chem,* 85**,** 1743-52.

LEE, C. J., FAN, X., GUO, X. & MEDIN, J. A. 2011. Promoter-specific lentivectors for long-term, cardiac-directed therapy of Fabry disease. *J Cardiol,* 57**,** 115-22.

LEE, M. H., CHOI, E. N., JEON, Y. J. & JUNG, S. C. 2012. Possible role of transforming growth factor-beta1 and vascular endothelial growth factor in Fabry disease nephropathy. *Int J Mol Med,* 30**,** 1275-80.

LEJEUNE, N., THINES-SEMPOUX, D. & HERS, H. G. 1963. Tissue fractionation studies. 16. Intracellular distribution and properties of alpha-glucosidases in rat liver. *Biochem J,* 86**,** 16-21.

LENAZ, G., BOVINA, C., D'AURELIO, M., FATO, R., FORMIGGINI, G., GENOVA, M. L., GIULIANO, G., MERLO PICH, M., PAOLUCCI, U., PARENTI CASTELLI, G. & VENTURA, B. 2002. Role of mitochondria in oxidative stress and aging. *Ann N Y Acad Sci,* 959**,** 199-213.

LENDERS, M., KARABUL, N., DUNING, T., SCHMITZ, B., SCHELLECKES, M., MESTERS, R., HENSE, H. W., BECK, M., BRAND, S. M. & BRAND, E. 2015. Thromboembolic events in Fabry disease and the impact of factor V Leiden. *Neurology,* 84**,** 1009-16.

LIEBAU, M. C., BRAUN, F., HOPKER, K., WEITBRECHT, C., BARTELS, V., MULLER, R. U., BRODESSER, S., SALEEM, M. A., BENZING, T., SCHERMER, B., CYBULLA, M. & KURSCHAT, C. E. 2013. Dysregulated autophagy contributes to podocyte damage in Fabry's disease. *PLoS One,* 8**,** e63506.

LINGWOOD, C. A. 2011. Glycosphingolipid functions. *Cold Spring Harb Perspect Biol,* 3.

LODISH, H., BERK, A., ZIPURSKY, L., MATSUDAIRA, P., BALTIMORE, D. & DARNELL, J. 2000. *Molecular Cell Biology,* New York, W. H. Freeman.

LUCKE, T., HOPPNER, W., SCHMIDT, E., ILLSINGER, S. & DAS, A. M. 2004. Fabry disease: reduced activities of respiratory chain enzymes with decreased levels of energy-rich phosphates in fibroblasts. *Mol Genet Metab,* 82**,** 93-7.

LUKAS, J., GIESE, A. K., MARKOFF, A., GRITTNER, U., KOLODNY, E., MASCHER, H., LACKNER, K. J., MEYER, W., WREE, P., SAVIOUK, V. & ROLFS, A. 2013. Functional characterisation of alpha-galactosidase a mutations as a basis for a new classification system in fabry disease. *PLoS Genet,* 9**,** e1003632.

LUND, N., OLSSON, M. L., RAMKUMAR, S., SAKAC, D., YAHALOM, V., LEVENE, C., HELLBERG, A., MA, X. Z., BINNINGTON, B., JUNG, D., LINGWOOD, C. A. & BRANCH, D. R. 2009. The human P(k) histo-blood group antigen provides protection against HIV-1 infection. *Blood,* 113**,** 4980-91.

MAALOUF, K., JIA, J., RIZK, S., BROGDEN, G., KEISER, M., DAS, A. & NAIM, H. Y. 2010. A modified lipid composition in Fabry disease leads to an intracellular block of the detergent-resistant membrane-associated dipeptidyl peptidase IV. *J Inherit Metab Dis,* 33**,** 445-9.

MACHANN, W., BREUNIG, F., WEIDEMANN, F., SANDSTEDE, J., HAHN, D., KOSTLER, H., NEUBAUER, S., WANNER, C. & BEER, M. 2011. Cardiac energy metabolism is disturbed in Fabry disease and improves with enzyme replacement therapy using recombinant human galactosidase A. *Eur J Heart Fail,* 13**,** 278-83.

MALONEY, M. D., BINNINGTON-BOYD, B. & LINGWOOD, C. A. 1999. Globotriaosyl ceramide modulates interferon-alpha-induced growth inhibition and CD19 expression in Burkitt's lymphoma cells. *Glycoconj J,* 16**,** 821-8.

MANGENEY, M., RICHARD, Y., COULAUD, D., TURSZ, T. & WIELS, J. 1991. CD77: an antigen of germinal center B cells entering apoptosis. *Eur J Immunol,* 21**,** 1131-40.

MANWARING, V., BOUTIN, M. & AURAY-BLAIS, C. 2013. A metabolomic study to identify new globotriaosylceramide-related biomarkers in the plasma of Fabry disease patients. *Anal Chem,* 85**,** 9039-48.

MARCHESAN, D., COX, T. M. & DEEGAN, P. B. 2012. Lysosomal delivery of therapeutic enzymes in cell models of Fabry disease. *J Inherit Metab Dis,* 35**,** 1107-17.

MARCUS, D. M., KUNDU, S. K. & SUZUKI, A. 1981. The P blood group system: recent progress in immunochemistry and genetics. *Semin Hematol,* 18**,** 63-71.

MARKHAM, A. 2016. Migalastat: First Global Approval. *Drugs,* 76**,** 1147-52.

MATSUURA, F., OHTA, M., IOANNOU, Y. A. & DESNICK, R. J. 1998. Human alpha-galactosidase A: characterization of the N-linked oligosaccharides on the intracellular and secreted glycoforms overexpressed by Chinese hamster ovary cells. *Glycobiology,* 8**,** 329-39.

MAUER, M., SOKOLOVSKIY, A., BARTH, J. A., CASTELLI, J. P., WILLIAMS, H. N., BENJAMIN, E. R. & NAJAFIAN, B. 2017. Reduction of podocyte globotriaosylceramide content in adult male patients with Fabry disease with amenable GLA mutations following 6 months of migalastat treatment. *J Med Genet,* 54**,** 781-786.

MAYES, J. S., SCHEERER, J. B., SIFERS, R. N. & DONALDSON, M. L. 1981. Differential assay for lysosomal alpha-galactosidases in human tissues and its application to Fabry's disease. *Clin Chim Acta,* 112**,** 247-51.

MEDIN, J. A., TUDOR, M., SIMOVITCH, R., QUIRK, J. M., JACOBSON, S., MURRAY, G. J. & BRADY, R. O. 1996. Correction in trans for Fabry disease: expression, secretion and uptake of alpha-galactosidase A in patient-derived cells driven by a high-titer recombinant retroviral vector. *Proc Natl Acad Sci U S A,* 93**,** 7917-22.

MEDINA, D. L., FRALDI, A., BOUCHE, V., ANNUNZIATA, F., MANSUETO, G., SPAMPANATO, C., PURI, C., PIGNATA, A., MARTINA, J. A., SARDIELLO, M., PALMIERI, M., POLISHCHUK, R., PUERTOLLANO, R. & BALLABIO, A. 2011. Transcriptional activation of lysosomal exocytosis promotes cellular clearance. *Dev Cell,* 21**,** 421-30.

MEGHDARI, M., GAO, N., ABDULLAHI, A., STOKES, E. & CALHOUN, D. H. 2015. Carboxyl-terminal truncations alter the activity of the human alpha-galactosidase A. *PLoS One,* 10**,** e0118341.

MEHTA, A. & HUGHES, D. A. 2002. Fabry Disease. *In:* PAGON, R. A., ADAM, M. P., ARDINGER, H. H., WALLACE, S. E., AMEMIYA, A., BEAN, L. J. H., BIRD, T. D., DOLAN, C. R., FONG, C. T., SMITH, R. J. H. & STEPHENS, K. (eds.) *GeneReviews(R).* Seattle (WA): University of Washington.

MEIKLE, P. J., HOPWOOD, J. J., CLAGUE, A. E. & CAREY, W. F. 1999. Prevalence of lysosomal storage disorders. *JAMA,* 281**,** 249-54.

MILLS, K., JOHNSON, A. & WINCHESTER, B. 2002. Synthesis of novel internal standards for the quantitative determination of plasma ceramide trihexoside in Fabry disease by tandem mass spectrometry. *FEBS Lett,* 515**,** 171-6.

MORGAN, S. H., RUDGE, P., SMITH, S. J., BRONSTEIN, A. M., KENDALL, B. E., HOLLY, E., YOUNG, E. P., CRAWFURD, M. D. & BANNISTER, R. 1990. The neurological complications of Anderson-Fabry disease (alpha-galactosidase A deficiency)--investigation of symptomatic and presymptomatic patients. *Q J Med,* 75**,** 491-507.

MOTABAR, O., LIU, K., SOUTHALL, N., MARUGAN, J. J., GOLDIN, E., SIDRANSKY, E. & ZHENG, W. 2010a. High throughput screening for inhibitors of alpha-galactosidase. *Curr Chem Genomics,* 4**,** 67-73.

MOTABAR, O., SIDRANSKY, E., GOLDIN, E. & ZHENG, W. 2010b. Fabry disease - current treatment and new drug development. *Curr Chem Genomics,* 4**,** 50-6.

NAGANO, T., NAKATSUKA, S., FUJITA, S., KANDA, T., UEMATSU, M., IKEDA, Y., ISHIBASHI-UEDA, H. & YUTANI, C. 2016. Myocardial fibrosis pathology in Anderson-Fabry disease: Evaluation of autopsy cases in the long- and short-term enzyme replacement therapy, and non-therapy case. *Ijc Metabolic & Endocrine,* 12**,** 46-51.

NELSON, M. P., BOUTIN, M., TSE, T. E., LU, H., HALEY, E. D., OUYANG, X., ZHANG, J., AURAY-BLAIS, C. & SHACKA, J. J. 2017. The lysosomal enzyme alpha-Galactosidase A is deficient in Parkinson's disease brain in association with the pathologic accumulation of alpha-synuclein. *Neurobiol Dis,* 110**,** 68-81.

NELSON, M. P., TSE, T. E., O'QUINN, D. B., PERCIVAL, S. M., JAIMES, E. A., WARNOCK, D. G. & SHACKA, J. J. 2014. Autophagy-lysosome pathway associated neuropathology and axonal degeneration in the brains of alpha-galactosidase A-deficient mice. *Acta Neuropathol Commun,* 2**,** 20.

NIEMANN, M., ROLFS, A., STORK, S., BIJNENS, B., BREUNIG, F., BEER, M., ERTL, G., WANNER, C. & WEIDEMANN, F. 2014. Gene mutations versus clinically relevant phenotypes: lyso-Gb3 defines Fabry disease. *Circ Cardiovasc Genet,* 7**,** 8-16.

NOVIKOFF, A. B., BEAUFAY, H. & DE DUVE, C. 1956. Electron microscopy of lysosomerich fractions from rat liver. *J Biophys Biochem Cytol,* 2**,** 179-84.

NOWAK, A., MECHTLER, T. P., DESNICK, R. J. & KASPER, D. C. 2017. Plasma LysoGb3: A useful biomarker for the diagnosis and treatment of Fabry disease heterozygotes. *Mol Genet Metab,* 120**,** 57-61.

NUDELMAN, E., KANNAGI, R., HAKOMORI, S., PARSONS, M., LIPINSKI, M., WIELS, J., FELLOUS, M. & TURSZ, T. 1983. A glycolipid antigen associated with Burkitt lymphoma defined by a monoclonal antibody. *Science,* 220**,** 509-11.

O'BRIEN, J. S., OKADA, S., CHEN, A. & FILLERUP, D. L. 1970. Tay-sachs disease. Detection of heterozygotes and homozygotes by serum hexosaminidase assay. *N Engl J Med,* 283**,** 15-20.

OHSHIMA, T., MURRAY, G. J., SWAIM, W. D., LONGENECKER, G., QUIRK, J. M., CARDARELLI, C. O., SUGIMOTO, Y., PASTAN, I., GOTTESMAN, M. M., BRADY, R. O. & KULKARNI, A. B. 1997. alpha-Galactosidase A deficient mice: a model of Fabry disease. *Proc Natl Acad Sci U S A,* 94**,** 2540-4.

OHSHIMA, T., SCHIFFMANN, R., MURRAY, G. J., KOPP, J., QUIRK, J. M., STAHL, S., CHAN, C. C., ZERFAS, P., TAO-CHENG, J. H., WARD, J. M., BRADY, R. O. & KULKARNI, A. B. 1999. Aging accentuates and bone marrow transplantation ameliorates metabolic defects in Fabry disease mice. *Proc Natl Acad Sci U S A,* 96**,** 6423-7.

OPITZ, J. M., STILES, F. C., WISE, D., RACE, R. R., SANGER, R., VON GEMMINGEN, G. R., KIERLAND, R. R., CROSS, E. G. & DE GROOT, W. P. 1965. The Genetics of Angiokeratoma Corporis Diffusum (Fabry's Disease) and Its Linkage Relations with the Xg Locus. *Am J Hum Genet,* 17**,** 325-42.

ORTIZ, A., ABIOSE, A., BICHET, D. G., CABRERA, G., CHARROW, J., GERMAIN, D. P., HOPKIN, R. J., JOVANOVIC, A., LINHART, A., MARUTI, S. S., MAUER, M., OLIVEIRA, J. P., PATEL, M. R., POLITEI, J., WALDEK, S., WANNER, C., YOO, H. W. & WARNOCK, D. G. 2016. Time to treatment benefit for adult patients with Fabry disease receiving agalsidase beta: data from the Fabry Registry. *J Med Genet,* 53**,** 495-502.

OSELLAME, L. D., BLACKER, T. S. & DUCHEN, M. R. 2012. Cellular and molecular mechanisms of mitochondrial function. *Best Pract Res Clin Endocrinol Metab,* 26**,** 711-23.

PACIENZA, N., YOSHIMITSU, M., MIZUE, N., AU, B. C., WANG, J. C., FAN, X., TAKENAKA, T. & MEDIN, J. A. 2012. Lentivector transduction improves outcomes over transplantation of human HSCs alone in NOD/SCID/Fabry mice. *Mol Ther,* 20**,** 1454-61.

PALECEK, T., BULTAS, J., HAJEK, M., KARETOVA, D., KUCHYNKA, P., KAUTZNER, J., ELLEDER, M. & LINHART, A. 2010. Association between cardiac energy metabolism and gain of left ventricular mass in Fabry disease. *Int J Cardiol,* 144**,** 337-9.

PALLESEN, G. & ZEUTHEN, J. 1987. Distribution of the Burkitt's lymphoma-associated antigen (BLA) in normal human tissue and malignant lymphoma as defined by immunohistological staining with monoclonal antibody 38.13. *J Cancer Res Clin Oncol,* 113**,** 78-86.

PARK, J., MURRAY, G. J., LIMAYE, A., QUIRK, J. M., GELDERMAN, M. P., BRADY, R. O. & QASBA, P. 2003. Long-term correction of globotriaosylceramide storage in Fabry mice by recombinant adeno-associated virus-mediated gene transfer. *Proc Natl Acad Sci U S A,* 100**,** 3450-4.

PARK, J. L., WHITESALL, S. E., D'ALECY, L. G., SHU, L. & SHAYMAN, J. A. 2008. Vascular dysfunction in the alpha-galactosidase A-knockout mouse is an endothelial cell-, plasma membrane-based defect. *Clin Exp Pharmacol Physiol,* 35**,** 1156-63.

PENATI, R., FUMAGALLI, F., CALBI, V., BERNARDO, M. E. & AIUTI, A. 2017. Gene therapy for lysosomal storage disorders: recent advances for metachromatic leukodystrophy and mucopolysaccaridosis I. *J Inherit Metab Dis,* 40**,** 543-554.

PEREIRA, C. S., SA-MIRANDA, C., DE LIBERO, G., MORI, L. & MACEDO, M. F. 2016. Globotriaosylceramide inhibits iNKT-cell activation in a CD1d-dependent manner. *Eur J Immunol,* 46**,** 147-53.

PINTO, L. L., VIEIRA, T. A., GIUGLIANI, R. & SCHWARTZ, I. V. 2010. Expression of the disease on female carriers of X-linked lysosomal disorders: a brief review. *Orphanet J Rare Dis,* 5**,** 14.

PLOTEGHER, N. & DUCHEN, M. R. 2017. Mitochondrial Dysfunction and Neurodegeneration in Lysosomal Storage Disorders. *Trends Mol Med,* 23**,** 116-134.

PRABAKARAN, T., NIELSEN, R., LARSEN, J. V., SORENSEN, S. S., FELDT-RASMUSSEN, U., SALEEM, M. A., PETERSEN, C. M., VERROUST, P. J. & CHRISTENSEN, E. I. 2011. Receptor-mediated endocytosis of alpha-galactosidase A in human podocytes in Fabry disease. *PLoS One,* 6**,** e25065.

PRABAKARAN, T., NIELSEN, R., SATCHELL, S. C., MATHIESON, P. W., FELDT-RASMUSSEN, U., SORENSEN, S. S. & CHRISTENSEN, E. I. 2012. Mannose 6-phosphate receptor and sortilin mediated endocytosis of alpha-galactosidase A in kidney endothelial cells. *PLoS One,* 7**,** e39975.

PRYOR, P. R. & LUZIO, J. P. 2009. Delivery of endocytosed membrane proteins to the lysosome. *Biochim Biophys Acta,* 1793**,** 615-24.

RABINOWITZ, J. D. & WHITE, E. 2010. Autophagy and metabolism. *Science,* 330**,** 1344-8.

RAJARAMAN, S. 2013. Developing lentiviral vectors for gene therapy of Fabry disease. University College London.

RAMKUMAR, S., SAKAC, D., BINNINGTON, B., BRANCH, D. R. & LINGWOOD, C. A. 2009. Induction of HIV-1 resistance: cell susceptibility to infection is an inverse function of globotriaosyl ceramide levels. *Glycobiology,* 19**,** 76-82.

RAVAL, K. K., TAO, R., WHITE, B. E., DE LANGE, W. J., KOONCE, C. H., YU, J., KISHNANI, P. S., THOMSON, J. A., MOSHER, D. F., RALPHE, J. C. & KAMP, T. J. 2015. Pompe disease results in a Golgi-based glycosylation deficit in human induced pluripotent stem cell-derived cardiomyocytes. *J Biol Chem,* 290**,** 3121-36.

RECZEK, D., SCHWAKE, M., SCHRODER, J., HUGHES, H., BLANZ, J., JIN, X., BRONDYK, W., VAN PATTEN, S., EDMUNDS, T. & SAFTIG, P. 2007. LIMP-2 is a receptor for lysosomal mannose-6-phosphate-independent targeting of beta-glucocerebrosidase. *Cell,* 131**,** 770-83.

RIES, M. & GAL, A. 2006. Genotype-phenotype correlation in Fabry disease. *In:* MEHTA, A., BECK, M. & SUNDER-PLASSMANN, G. (eds.) *Fabry disease: Perspectives from 5 years of FOS.* Oxford, UK: Oxford PharmaGenesis.

ROGERS, S. 1966. Shope papilloma virus: a passenger in man and its significance to the potential control of the host genome. *Nature,* 212**,** 1220-2.

ROGERS, S., LOWENTHAL, A., TERHEGGEN, H. G. & COLUMBO, J. P. 1973. Induction of arginase activity with the Shope papilloma virus in tissue culture cells from an argininemic patient. *J Exp Med,* 137**,** 1091-6.

ROHARD, I., SCHAEFER, E., KAMPMANN, C., BECK, M. & GAL, A. 2008. Association between polymorphisms of endothelial nitric oxide synthase gene (NOS3) and left posterior wall thickness (LPWT) of the heart in Fabry disease. *J Inherit Metab Dis,* 31 Suppl 2**,** S349-56.

ROLFS, A., FAZEKAS, F., GRITTNER, U., DICHGANS, M., MARTUS, P., HOLZHAUSEN, M., BOTTCHER, T., HEUSCHMANN, P. U., TATLISUMAK, T., TANISLAV, C., JUNGEHULSING, G. J., GIESE, A. K., PUTAALA, J., HUBER, R., BODECHTEL, U., LICHY, C., ENZINGER, C., SCHMIDT, R., HENNERICI, M. G., KAPS, M., KESSLER, C., LACKNER, K., PASCHKE, E., MEYER, W., MASCHER, H., RIESS, O., KOLODNY, E., NORRVING, B. & STROKE IN YOUNG FABRY PATIENTS, I. 2013. Acute cerebrovascular disease in the young: the Stroke in Young Fabry Patients study. *Stroke,* 44**,** 340-9.

ROMBACH, S. M., DEKKER, N., BOUWMAN, M. G., LINTHORST, G. E., ZWINDERMAN, A. H., WIJBURG, F. A., KUIPER, S., VD BERGH WEERMAN, M. A., GROENER, J. E., POORTHUIS, B. J., HOLLAK, C. E. & AERTS, J. M. 2010. Plasma globotriaosylsphingosine: diagnostic value and relation to clinical manifestations of Fabry disease. *Biochim Biophys Acta,* 1802**,** 741-8.

ROMBACH, S. M., SMID, B. E., BOUWMAN, M. G., LINTHORST, G. E., DIJKGRAAF, M. G. & HOLLAK, C. E. 2013. Long term enzyme replacement therapy for Fabry disease: effectiveness on kidney, heart and brain. *Orphanet J Rare Dis,* 8**,** 47.

ROSENBERG, S. A., AEBERSOLD, P., CORNETTA, K., KASID, A., MORGAN, R. A., MOEN, R., KARSON, E. M., LOTZE, M. T., YANG, J. C., TOPALIAN, S. L. & ET AL. 1990. Gene transfer into humans--immunotherapy of patients with advanced melanoma, using tumor-infiltrating lymphocytes modified by retroviral gene transduction. *N Engl J Med,* 323**,** 570-8.

ROSENBERG, S. A., ANDERSON, W. F., BLAESE, M., HWU, P., YANNELLI, J. R., YANG, J. C., TOPALIAN, S. L., SCHWARTZENTRUBER, D. J., WEBER, J. S., ETTINGHAUSEN, S. E. & ET AL. 1993. The development of gene therapy for the treatment of cancer. *Ann Surg,* 218**,** 455-63; discussion 463-4.

ROSSIGNOL, R., LETELLIER, T., MALGAT, M., ROCHER, C. & MAZAT, J. P. 2000. Tissue variation in the control of oxidative phosphorylation: implication for mitochondrial diseases. *Biochem J,* 347 Pt 1**,** 45-53.

RUIZ DE GARIBAY, A. P., SOLINIS, M. A. & RODRIGUEZ-GASCON, A. 2013. Gene therapy for fabry disease: a review of the literature. *BioDrugs,* 27**,** 237-46.

SACHDEV, B. & ELLIOTT, P. M. 2002. Isolated cardiac manifestations in Fabry disease: the UK experience. *Acta Paediatr Suppl,* 439**,** 2.

SAFTIG, P. & KLUMPERMAN, J. 2009. Lysosome biogenesis and lysosomal membrane proteins: trafficking meets function. *Nat Rev Mol Cell Biol,* 10**,** 623-35.

SAKUMA, T., BARRY, M. A. & IKEDA, Y. 2012. Lentiviral vectors: basic to translational. *Biochem J,* 443**,** 603-18.

SAKURABA, H., OSHIMA, A., FUKUHARA, Y., SHIMMOTO, M., NAGAO, Y., BISHOP, D. F., DESNICK, R. J. & SUZUKI, Y. 1990. Identification of point mutations in the alpha-galactosidase A gene in classical and atypical hemizygotes with Fabry disease. *Am J Hum Genet,* 47**,** 784-9.

SALAMERO, J., SZTUL, E. S. & HOWELL, K. E. 1990. Exocytic transport vesicles generated in vitro from the trans-Golgi network carry secretory and plasma membrane proteins. *Proc Natl Acad Sci U S A,* 87**,** 7717-21.

SAMIE, M. A. & XU, H. 2014. Lysosomal exocytosis and lipid storage disorders. *J Lipid Res,* 55**,** 995-1009.

SANCHEZ-NINO, M. D., SANZ, A. B., CARRASCO, S., SALEEM, M. A., MATHIESON, P. W., VALDIVIELSO, J. M., RUIZ-ORTEGA, M., EGIDO, J. & ORTIZ, A. 2011. Globotriaosylsphingosine actions on human glomerular podocytes: implications for Fabry nephropathy. *Nephrol Dial Transplant,* 26**,** 1797-802.

SARDIELLO, M., PALMIERI, M., DI RONZA, A., MEDINA, D. L., VALENZA, M., GENNARINO, V. A., DI MALTA, C., DONAUDY, F., EMBRIONE, V., POLISHCHUK, R. S., BANFI, S., PARENTI, G., CATTANEO, E. & BALLABIO, A. 2009. A gene network regulating lysosomal biogenesis and function. *Science,* 325**,** 473-7.

SCHAPIRA, A. H., COOPER, J. M., DEXTER, D., CLARK, J. B., JENNER, P. & MARSDEN, C. D. 1990. Mitochondrial complex I deficiency in Parkinson's disease. *J Neurochem,* 54**,** 823-7.

SCHIFFMANN, R., FULLER, M., CLARKE, L. A. & AERTS, J. M. F. G. 2016. Is it Fabry disease? *Genetics in Medicine,* 18**,** 1181-1185.

SCHIFFMANN, R., KOPP, J. B., AUSTIN, H. A., 3RD, SABNIS, S., MOORE, D. F., WEIBEL, T., BALOW, J. E. & BRADY, R. O. 2001. Enzyme replacement therapy in Fabry disease: a randomized controlled trial. *JAMA,* 285**,** 2743-9.

SEMENZA, G. L. 2011. Hypoxia-inducible factor 1: regulator of mitochondrial metabolism and mediator of ischemic preconditioning. *Biochim Biophys Acta,* 1813**,** 1263-8.

SETTEMBRE, C. & BALLABIO, A. 2014a. Cell metabolism: autophagy transcribed. *Nature,* 516**,** 40-1.

SETTEMBRE, C. & BALLABIO, A. 2014b. Lysosomal adaptation: how the lysosome responds to external cues. *Cold Spring Harb Perspect Biol,* 6.

SETTEMBRE, C., DI MALTA, C., POLITO, V. A., GARCIA ARENCIBIA, M., VETRINI, F., ERDIN, S., ERDIN, S. U., HUYNH, T., MEDINA, D., COLELLA, P., SARDIELLO, M., RUBINSZTEIN, D. C. & BALLABIO, A. 2011. TFEB links autophagy to lysosomal biogenesis. *Science,* 332**,** 1429-33.

SETTEMBRE, C., FRALDI, A., MEDINA, D. L. & BALLABIO, A. 2013. Signals from the lysosome: a control centre for cellular clearance and energy metabolism. *Nat Rev Mol Cell Biol,* 14**,** 283-96.

SETTEMBRE, C., ZONCU, R., MEDINA, D. L., VETRINI, F., ERDIN, S., ERDIN, S., HUYNH, T., FERRON, M., KARSENTY, G., VELLARD, M. C., FACCHINETTI, V., SABATINI, D. M. & BALLABIO, A. 2012. A lysosome-to-nucleus signalling mechanism senses and regulates the lysosome via mTOR and TFEB. *EMBO J,* 31**,** 1095-108.

SHARMA, R., ANGUELA, X. M., DOYON, Y., WECHSLER, T., DEKELVER, R. C., SPROUL, S., PASCHON, D. E., MILLER, J. C., DAVIDSON, R. J., SHIVAK, D., ZHOU, S., RIEDERS, J., GREGORY, P. D., HOLMES, M. C., REBAR, E. J. & HIGH, K. A. 2015. In vivo genome editing of the albumin locus as a platform for protein replacement therapy. *Blood,* 126**,** 1777-84.

SHAYMAN, J. A. 2010. Experimental studies in mice on the vasculopathy of Fabry disease. *In:* ELSTEIN, D., ALTARESCU, G. & BECK, M. (eds.) *Fabry Disease.* Springer.

SHEN, J. S., MENG, X. L., MOORE, D. F., QUIRK, J. M., SHAYMAN, J. A., SCHIFFMANN, R. & KANESKI, C. R. 2008. Globotriaosylceramide induces oxidative stress and up-regulates cell adhesion molecule expression in Fabry disease endothelial cells. *Mol Genet Metab,* 95**,** 163-8.

SHEPHERD, D. & GARLAND, P. B. 1969. The kinetic properties of citrate synthase from rat liver mitochondria. *Biochem J,* 114**,** 13.

SHU, L. & SHAYMAN, J. A. 2007. Caveolin-associated accumulation of globotriaosylceramide in the vascular endothelium of alpha-galactosidase A null mice. *J Biol Chem,* 282**,** 20960-7.

SIRKA, E., HEYWOOD, W. E., ZHANG, X. K. K., LIU, L., CHUANG, W. L., DOYKOV, I., BURKE, D., HEALES, S., VELLODI, A., CLEARY, M., GRUNEWALD, S., FOOTITT, E., GISSEN, P., HUGHES, D. & MILLS, K. 2015. The development of a rapid, multiplexed UPLC-MS/MS assay for quantitation of lyso-Gb3 and Gb3 in dried blood spots. *Molecular Genetics and Metabolism,* 114**,** S107-S107.

SMITH, P. K., KROHN, R. I., HERMANSON, G. T., MALLIA, A. K., GARTNER, F. H., PROVENZANO, M. D., FUJIMOTO, E. K., GOEKE, N. M., OLSON, B. J. & KLENK, D. C. 1985. Measurement of protein using bicinchoninic acid. *Analytical Biochemistry,* 150**,** 76-85.

SONG, W., WANG, F., SAVINI, M., AKE, A., DI RONZA, A., SARDIELLO, M. & SEGATORI, L. 2013. TFEB regulates lysosomal proteostasis. *Hum Mol Genet,* 22**,** 1994-2009.

SPADA, M., PAGLIARDINI, S., YASUDA, M., TUKEL, T., THIAGARAJAN, G., SAKURABA, H., PONZONE, A. & DESNICK, R. J. 2006. High incidence of later-onset fabry disease revealed by newborn screening. *Am J Hum Genet,* 79**,** 31-40.

STENSON, P. D., MORT, M., BALL, E. V., HOWELLS, K., PHILLIPS, A. D., THOMAS, N. S. & COOPER, D. N. 2009. The Human Gene Mutation Database: 2008 update. *Genome Medicine.* BIOBASE Corporation.

STOKA, V., TURK, V. & TURK, B. 2016. Lysosomal cathepsins and their regulation in aging and neurodegeneration. *Ageing Res Rev,* 32**,** 22-37.

SUGIMOTO, Y., AKSENTIJEVICH, I., MURRAY, G. J., BRADY, R. O., PASTAN, I. & GOTTESMAN, M. M. 1995. Retroviral coexpression of a multidrug resistance gene (MDR1) and human alpha-galactosidase A for gene therapy of Fabry disease. *Hum Gene Ther,* 6**,** 905-15.

SUZUKI, K., SWENSON, C., SASAGAWA, S., SAKATANI, T., WATANABE, M., KOBAYASHI, M. & FUJIKURA, T. 1983. Age-related decline in lysosomal enzyme release from polymorphonuclear leukocytes after N-formyl-methionyl-leucyl-phenylalanine stimulation. *Exp Hematol,* 11**,** 1005-13.

SWEELEY, C. C. & KLIONSKY, B. 1963. Fabrys Disease - Classification as a Sphingolipidosis and Partial Characterization of a Novel Glycolipid. *Journal of Biological Chemistry,* 238**,** 3148-&.

SZYBALSKA, E. H. & SZYBALSKI, W. 1962. Genetics of human cess line. IV. DNA-mediated heritable transformation of a biochemical trait. *Proc Natl Acad Sci U S A,* 48**,** 2026-34.

TAKENAKA, T., HENDRICKSON, C. S., TWOREK, D. M., TUDOR, M., SCHIFFMANN, R., BRADY, R. O. & MEDIN, J. A. 1999a. Enzymatic and functional correction along with long-term enzyme secretion from transduced bone marrow hematopoietic stem/progenitor and stromal cells derived from patients with Fabry disease. *Exp Hematol,* 27**,** 1149-59.

TAKENAKA, T., MURRAY, G. J., QIN, G., QUIRK, J. M., OHSHIMA, T., QASBA, P., CLARK, K., KULKARNI, A. B., BRADY, R. O. & MEDIN, J. A. 2000. Long-term enzyme correction and lipid reduction in multiple organs of primary and secondary transplanted Fabry mice receiving transduced bone marrow cells. *Proc Natl Acad Sci U S A,* 97**,** 7515-20.

TAKENAKA, T., QIN, G., BRADY, R. O. & MEDIN, J. A. 1999b. Circulating alpha-galactosidase A derived from transduced bone marrow cells: relevance for corrective gene transfer for Fabry disease. *Hum Gene Ther,* 10**,** 1931-9.

TAKIYAMA, N., DUNIGAN, J. T., VALLOR, M. J., KASE, R., SAKURABA, H. & BARRANGER, J. A. 1999. Retrovirus-mediated transfer of human alpha-galactosidase A gene to human CD34+ hematopoietic progenitor cells. *Hum Gene Ther,* 10**,** 2881-9.

TELFORD, J. E., KILBRIDE, S. M. & DAVEY, G. P. 2009. Complex I is rate-limiting for oxygen consumption in the nerve terminal. *J Biol Chem,* 284**,** 9109-14.

TETAUD, C., FALGUIERES, T., CARLIER, K., LECLUSE, Y., GARIBAL, J., COULAUD, D., BUSSON, P., STEFFENSEN, R., CLAUSEN, H., JOHANNES, L. & WIELS, J. 2003. Two distinct Gb3/CD77 signaling pathways leading to apoptosis are triggered by anti-Gb3/CD77 mAb and verotoxin-1. *J Biol Chem,* 278**,** 45200-8.

THE UNIVERSITY OF QUEENSLAND. 2017. *Three Minute Thesis* [Online]. https://threeminutethesis.uq.edu.au/about: The University of Queensland. [Accessed 17 November 2017].

THOMAIDIS, T., RELLE, M., GOLBAS, M., BROCHHAUSEN, C., GALLE, P. R., BECK, M. & SCHWARTING, A. 2009. Downregulation of alpha-galactosidase A upregulates CD77: functional impact for Fabry nephropathy. *Kidney Int,* 75**,** 399-407.

THOMAS, A. S. & MEHTA, A. B. 2013. Difficulties and barriers in diagnosing Fabry disease: what can be learnt from the literature? *Expert Opin Med Diagn,* 7**,** 589-99.

TOGAWA, T., KODAMA, T., SUZUKI, T., SUGAWARA, K., TSUKIMURA, T., OHASHI, T., ISHIGE, N., SUZUKI, K., KITAGAWA, T. & SAKURABA, H. 2010. Plasma globotriaosylsphingosine as a biomarker of Fabry disease. *Mol Genet Metab,* 100**,** 257-61.

TOMASIC, I. B., METCALF, M. C., GUCE, A. I., CLARK, N. E. & GARMAN, S. C. 2010. Interconversion of the specificities of human lysosomal enzymes associated with Fabry and Schindler diseases. *J Biol Chem,* 285**,** 21560-6.

VAN DER TOL, L., SMID, B. E., POORTHUIS, B. J., BIEGSTRAATEN, M., DEPREZ, R. H., LINTHORST, G. E. & HOLLAK, C. E. 2014. A systematic review on screening for Fabry disease: prevalence of individuals with genetic variants of unknown significance. *J Med Genet,* 51**,** 1-9.

VENTURA, B., GENOVA, M. L., BOVINA, C., FORMIGGINI, G. & LENAZ, G. 2002. Control of oxidative phosphorylation by Complex I in rat liver mitochondria: implications for aging. *Biochim Biophys Acta,* 1553**,** 249-60.

VOET, D., VOET, J. G. & PRATT, C. W. 2006. *Fundermentals of Biochemistry*, John Wiley & Sons.

WANG, R. Y., LELIS, A., MIROCHA, J. & WILCOX, W. R. 2007. Heterozygous Fabry women are not just carriers, but have a significant burden of disease and impaired quality of life. *Genet Med,* 9**,** 34-45.

WEIDEMANN, F., SANCHEZ-NINO, M. D., POLITEI, J., OLIVEIRA, J. P., WANNER, C., WARNOCK, D. G. & ORTIZ, A. 2013. Fibrosis: a key feature of Fabry disease with potential therapeutic implications. *Orphanet J Rare Dis,* 8**,** 116.

WHYBRA, C., KAMPMANN, C., WILLERS, I., DAVIES, J., WINCHESTER, B., KRIEGSMANN, J., BRUHL, K., GAL, A., BUNGE, S. & BECK, M. 2001. Anderson-Fabry disease: clinical manifestations of disease in female heterozygotes. *J Inherit Metab Dis,* 24**,** 715-24.

WILLIAMS, D. A., LEMISCHKA, I. R., NATHAN, D. G. & MULLIGAN, R. C. 1984. Introduction of new genetic material into pluripotent haematopoietic stem cells of the mouse. *Nature,* 310**,** 476-80.

WINCHESTER, B. 2012. Classification of Lysosomal Storage Diseases. *In:* MEHTA, A. & WINCHESTER, B. (eds.) *Lysosomal Storage Disorders: A practical guide.* Wiley-Blackwell.

WINCHESTER, B. 2014. Lysosomal diseases: diagnostic update. *J Inherit Metab Dis,* 37**,** 599-608.

WIRTH, T., PARKER, N. & YLA-HERTTUALA, S. 2013. History of gene therapy. *Gene,* 525**,** 162-9.

WU, X., KATZ, E., DELLA VALLE, M. C., MASCIOLI, K., FLANAGAN, J. J., CASTELLI, J. P., SCHIFFMANN, R., BOUDES, P., LOCKHART, D. J., VALENZANO, K. J. & BENJAMIN, E. R. 2011. A pharmacogenetic approach to identify mutant forms of alpha-galactosidase A that respond to a pharmacological chaperone for Fabry disease. *Hum Mutat,* 32**,** 965-77.

YANG, Y. P., HU, L. F., ZHENG, H. F., MAO, C. J., HU, W. D., XIONG, K. P., WANG, F. & LIU, C. F. 2013. Application and interpretation of current autophagy inhibitors and activators. *Acta Pharmacol Sin,* 34**,** 625-35.

YANG, Y. P., LIANG, Z. Q., GU, Z. L. & QIN, Z. H. 2005. Molecular mechanism and regulation of autophagy. *Acta Pharmacol Sin,* 26**,** 1421-34.

YOSHIMITSU, M., HIGUCHI, K., DAWOOD, F., RASAIAH, V. I., AYACH, B., CHEN, M., LIU, P. & MEDIN, J. A. 2006. Correction of cardiac abnormalities in fabry mice by direct intraventricular injection of a recombinant lentiviral vector that engineers expression of alpha-galactosidase A. *Circ J,* 70**,** 1503-8.

YOSHIMITSU, M., HIGUCHI, K., RAMSUBIR, S., NONAKA, T., RASAIAH, V. I., SIATSKAS, C., LIANG, S. B., MURRAY, G. J., BRADY, R. O. & MEDIN, J. A. 2007. Efficient correction of Fabry mice and patient cells mediated by lentiviral transduction of hematopoietic stem/progenitor cells. *Gene Ther,* 14**,** 256-65.

YOSHIMITSU, M., SATO, T., TAO, K., WALIA, J. S., RASAIAH, V. I., SLEEP, G. T., MURRAY, G. J., POEPPL, A. G., UNDERWOOD, J., WEST, L., BRADY, R. O. & MEDIN, J. A. 2004. Bioluminescent imaging of a marking transgene and correction of Fabry mice by neonatal injection of recombinant lentiviral vectors. *Proc Natl Acad Sci U S A,* 101**,** 16909-14.

YOUNG, E., MILLS, K., MORRIS, P., VELLODI, A., LEE, P., WALDEK, S. & WINCHESTER, B. 2005. Is globotriaosylceramide a useful biomarker in Fabry disease? *Acta Paediatr Suppl,* 94**,** 51-4; discussion 37-8.

YOUNG, I. D., YOUNG, E. P., MOSSMAN, J., FIELDER, A. R. & MOORE, J. R. 1987. Neuraminidase deficiency: case report and review of the phenotype. *J Med Genet,* 24**,** 283-90.

ZANTA-BOUSSIF, M. A., CHARRIER, S., BRICE-OUZET, A., MARTIN, S., OPOLON, P., THRASHER, A. J., HOPE, T. J. & GALY, A. 2009. Validation of a mutated PRE sequence allowing high and sustained transgene expression while abrogating WHV-X protein synthesis: application to the gene therapy of WAS. *Gene Ther,* 16**,** 605-19.

ZINDER, N. D. & LEDERBERG, J. 1952. Genetic exchange in Salmonella. *J Bacteriol,* 64**,** 679-99.

Publications

Talks:

- "Gene therapy for Fabry disease: less is more". GOSH Metabolic meeting, February 2017.
- "Investigating the efficacy of lentivirus mediated gene delivery to treat Fabry disease". UCL GOSICH Genetics and Genomic Medicine program seminar, November 2016.
- "Characterization of α-galactosidase A: towards understanding the biochemistry of Fabry-Anderson disease". GOSH Chemical Pathology departmental seminar, April 2015.
- "Characterization of α-galactosidase A: towards understanding the biochemistry of Fabry disease". UK National Collaborative Diagnostic Laboratories meeting, June 2015.
- "Investigating the pathophysiology of Fabry Anderson disease". UCL GOSICH Inflammation, Immunity of Immunology program seminar, July 2014.

Posters:

- "Characterization of α-galactosidase A: towards understanding the biochemistry of Fabry disease", presented at the UCL GOSICH open day, November 2014.
- "Lentivirus-mediated overexpression of alpha-galactosidase A increases N-acetyl galactosaminidase activity: relevance to Fabry disease?" Lambert, Jonathan; Burke, Derek; Howe, Steven & Heales, Simon (2015). Annual conference of the British Society of Gene and Cell Therapy, Volume 26, A35-A35.
- "Characterization of α-galactosidase A: towards understanding the biochemistry of Fabry disease", presented at the UCL GOSICH open day, November 2015.
- "Efficacy of lentivirus-mediated gene delivery to treat Fabry disease". J R A Lambert, D G Burke, S J Howe, A A Rahim, S J R Heales (2016). Presented as a poster at the Society for the Study of In-born Errors of Metabolism (SSIEM) annual symposium in Rome, Italy, September 2016. Journal of Inherited Metabolic Diseases, Volume 39, S24-S24 (P-515). The same poster won second prize in the poster competition as part of the UCL GOSICH open day, November 2016.

UK National 3MT competition:

- "Fabry disease: can gene therapy clear the waste and revive cellular mojo?" presented in the UCL and UK National Three Minute Thesis competitions 2016. A video of the talk was also published in the MPS magazine (www.mpssociety.org.uk), Autumn 2016.

Public Engagement

Talks were given at the National Institute of Health Research Biomedical Research Centre GOSH open days held of UCL GOSICH, targeted to the general public, especially young families:

- "Cells: keeping from clean and tidy in a messy world", October 2015
- "Fabry disease: can gene therapy help tidy up cells from a very messy situation", given as part of a series of talks entitled "Three Spotlights on current PhD research", October 2016.

Teaching

The material in this thesis has led to several teaching opportunities:

- "Gene therapy for metabolic disorders", part of the MSc Gene and Cell Therapies course offered at UCL in January 2015, 2016 and 2017.
- "Lysosomes, lysosomal storage diseases and treatment" delivered to third year undergraduates on the BSc Biomedical Science course at Anglia Ruskin University. This lecture was part of their Medical Genetics module taught during the spring semester, 2016.